Group 14 -, 15 -, 16 - Element in the Periphery of Trovacene : New Derivatives to study Electronic Communication in Di- and Trinuclear Complexes

Dissertation
zur Erlangung des Doktorgrades
der Naturwissenschaften
(Dr. ret. nat)

vorgelegt
dem Fachbereich Chemie
der Philipps-Universität Marburg

von
Feng LU
aus China

Marburg/Lahn 2001

Vom Fachbereich Chemie der Philipps-Univeristät Marburg/Lahn
als Dissertation angenommen am 15, Oct., 2001

Erstgutachter: Herr Prof. Dr. Ch. Elschenbroich
Zweitgutachter: Herr Prof. Dr. J. Sundermeyer

Tag der mündlichen Prüfung am 04, Feb., 2002

Table of Contents

Abbreviations

A	acceptor
a, A	isotropic, anisotropic hyperfine coupling constant (EPR)
$A_{\parallel}$	hyperfine coupling parallel to the symmetry axis
$A_{\perp}$	hyperfine coupling perpendicular to a symmetry axis
Cp	cyclopentadienyl
CV	cyclic voltammetry
D	donor
D	zero field splitting tensor
DME	1,2-dimethoxyethane
DMF	dimethylformamid
$E_{1/2}$	redox potential
$\Delta E_{1/2}$	redox splitting
E_{pa}	anodic potential
E_{pc}	cathodic potential
EPR	Electron Paramagnetic Resonance
Et	ethyl
ET	electron transfer
f	frequency
F	Faraday constant
Fc	ferrocene
g	electron g-factor
g_e	free spin g factor (2.0023)
G	Gauss
G	Gibbs free energy
h	Planck constant
H	magnetic field
H	Hamiltonian operator
HOMO	highest occupied molecular orbital
i	current
I	quantum number for nuclear spin angular momentum
J	electron exchange interaction constant
k	Boltzmann constant / rate constant
l	quantum number for the electron orbital angular momentum
L	total orbital angular momentum quantum number
LUMO	lowest unoccupied molecular orbital
Me	methyl
M_L	electron orbital angular momentum quantum number
M_S	electron spin angular momentum quantum number
MS	mass spectrum
Ph	phenyl
PE	petroleum ether (40-60°C)
R	organic group
r.t.	room temperature
S	singlet
T	triplet
T	absolute temperature (Kelvin)
TMEDA	1,2 - bis(dimethylamino)ethane
THF	tetrahydrofuran

TVC	(η^7-tropylium)vanadium(η^5-cyclopentadienyl) or Trovacene
α	spin function for $m_s = \frac{1}{2}$
β	Bohr magneton
ψ	wave function
μ	magnetic moment
θ	Weiss constant
χ	molar magnetic susceptibility

Numbered Compounds

1	Bis(pentaammineruthenium)pyrazine
2	Biferrocene
3	Bisfulvalenediiron
4[.]	Bis(benzene)vanadium
5	Bis(benzene)chromium
6[.]	(η^7-Cycloheptatrienyl)(η^5-cyclopentadienyl)vanadium, Trovacene
7[..]	μ-(η^6: η^6-biphenyl)-bis[(η^6-biphenyl)vanadium]
8	Bis[μ-(η^6: η^6-biphenyl)]dichromium
9	μ-(η^6: η^6-biphenyl)-bis[(η^6-biphenyl)chromium]
10[..]	[5,5]bitrovacene
11[..]	Mesityldi([5]trovacenyl)borane
12[..]	Z-2,3-Di([5]trovancenyl)-2-butene
13[..]	E-2,3-Di([5]trovancenyl)-2-butene
14	4, 4´- dithiobipyridine
15[..]	Di([5]trovacenyl)peroxide
16[..]	Di([5]trovacenyl)sulfide
17	1,2,3-trithia[3]ferrocenophane
18[..]	Di([5]trovacenyl)disulfide
19[.]	lithium [5]trovacenythiolate
20[..]	Di([5]trovacenylthio)methane
21[.]	[5]Trovacenylthiol
22[.]	Benzyl([5]trovacenyl)thioether
23[.]	Methyl([5]trovacenyl)thioether
24[..]	Di([5]trovacenylthio)dimethyltin
25[..]	Di([5]trovacenyl)diselenide
26[..]	Di([5]trovacenyl)ditelluride
27[.]	Trimethylsiloxy[5]trovacene
28[.]	[5]Trovacenol / Hydroxytrovacene
29[...]	Tri([5]trovacenylthio)antimony
30[...]	Tri([5]trovacenylthio)bismuth
31	1,1´-Ferrocenyldicarboxylic acid
32[.]	[5]Trovacenylcarboxylic acid
33	1,1´-Diferrocenediol
34	Ferrocenol
35	(Hydroxy-η^5-cyclopendienyl)manganese tricarbonyl
36	(Hydroxy-η^5-cyclopendienyl)tungsten tricarbonyl
37[.]	Diphenyl(trovacenyl)phosphane
38[..]	Bis[(diphenylphosphano-η^5-cyclopentadienyl)(η^7-cycloheptatrienyl)vanadium]tetra carbonylchromium
39[.]	Amino[5]trovacene
40[.]	(Dimethylamino)[5]trovacene
41[..]	Di([5]trovacenyl)-phenyl-phosphane
42[...]	Tri([5]trovacenyl)phosphane
43[..]	Di([5]trovacenyl)chloroarsane
44[..]	Di([5]trovacenyl)-butyl-arsane
45[..]	Di([5]trovacenyl)arsane
46[..]	Di([5]trovacenyl)arsinous acid
47[...]	Tri([5]trovacenyl)arsane

1. Introduction

1.1 Electron Transfer

1.1.1 Fundamentals

Electron transfer (ET) is an important topic which covers the areas of chemistry and biology. Until now, two chemists have obtained the **Nobel Prize** for their contributions to ET; H. Taube for his work on ET processes, mixed valence and N_2 complexes (1983),[1] and R. A. Marcus for his theory of outer-sphere ET mechanism (1992).[2]

In general, ET can be divided into two classic types; outer-sphere and inner-sphere mechanisms.[3] Outer-sphere ET mechanism means simply no intermediate formation of a chemical bond (1-1).

$$D + A \rightarrow D^+ + A^- \quad \Delta G^0 < 0 \text{ (exergonic)} \tag{1-1}$$
D: donor; A: acceptor; ΔG^0: the Gibbs standard free-energy change.
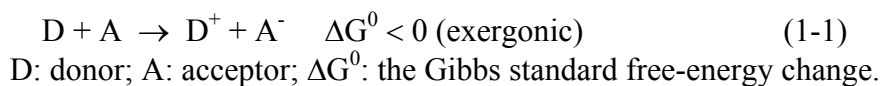
Inner-sphere ET mechanism describes the transfer process involving a bridging ligand between donor and acceptor (1-2).[4]

$$D^{+m}\text{-}L\text{-}A^{+n} \rightarrow D^{+m+1}\text{-}L\text{-}A^{+n-1} \rightarrow \text{Products} \tag{1-2}$$
L: bridging ligand
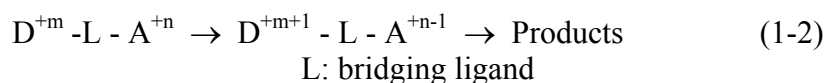
As for the outer-sphere ET mechanism, the Frank-Condon principle implies that the position of the atoms and the interatomic distances remain unchanged during the process of ET. Marcus pointed out the relationship between the kinetic barrier $\Delta G^{\neq}$ and the activation barrier ΔG^0 (1-3) (1-4).[5]

$$\Delta G^{\neq} = Z_D Z_A e^2 f / \varepsilon\, r_{DA} + (\lambda / 4)(1 + \Delta G^{'0} /\lambda)^2 \tag{1-3}$$
$$\Delta G^{'0} = \Delta G^0 + (Z_D - Z_A - 1) e^2 f / \varepsilon\, r_{DA} \tag{1-4}$$

Z_D, Z_A: the number of charges of the donor and acceptor; e: charge of the electron;
f: ionic strength factor; λ: reorganization energy for a zero driving force;
ε: dielectric constant of the solvent; r_{DA}: radii of donor and acceptor;
$\Delta G^{'0}$: the free-energy change.

For Donor-Bridge-Acceptor molecules, it is widely demonstrated that the covalent linkages between donor and acceptor units play the key role in the ET processes. Meanwhile, it has been proved that **hydrogen-bonded** linkage and **non-bonded interaction** are also involved in the electron transfer mechanism.[6]

In addition, ET can also be divided into thermally-induced ET and photo-induced ET. Here, we mainly focus on studying the inner-sphere electron transfer and thermally-induced ET processes.

1.1.2 Inner-Sphere Electron Transfer

Inner-sphere electron transfer always occur via a bridge which can have various types. Inner-sphere ET reactions have various mechanisms, for example, a rate-limiting chemical reaction preceded or followed the ET (EC, or CE mechanisms).[7] ET between redox centers can be induced thermally or by light. A mixed-valence complex [8] is the satisfactory model for studying the mechanism of inner-sphere ET. It is fundamental for understanding other more complicated systems. **1** is the first synthesized binuclear mixed-valence complex - the famous Creutz-Taube ion.

$$[(NH_3)_5RuN \bigcirc N\ Ru(NH_3)_5]^{5+}$$

1
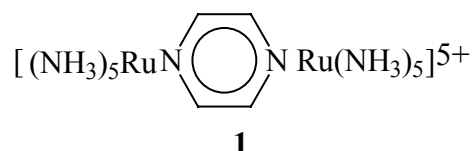
Robin and Day [9] have classified the mixed-valence complexes in 1967 and described them as follows. The nature of the bridging ligand plays a crucial role in determining the classification of complexes.[10]

Class I:

$\Delta G^{\neq} \gg RT$
No interaction between redox centers
No electron transfer
Isolated redox centers
UV

Class II:

$\Delta G^{\neq} \cong RT$
Weak interaction between redox centers
Electron transfer
Localized (Trapped)
VIS

Class III:

$\Delta G^{\neq} \ll RT$
Strong interaction between redox centers
Electron transfer
Delocalized (Detrapped)
N-IR

There are several techniques available to distinguish class II and III.[11] Sometimes different physical technique will lead to contradictory results, because of the difference between the ET rate and the time scales of investigation. For example, the IR time scale is 10^{-13} s , but for EPR, the time scale is 10^{-7}-10^{-9} s.

Information of inter- or intra-molecular communication between redox centers can be obtained from: a) the redox splitting $\Delta E_{1/2}$ (Cyclic Voltammetry); b) the magnitudes of the hyperfine interaction a(^{51}V), and the exchange coupling constant J (EPR),[12] c) shifts of ν (C-H) or B-H etc. in the vibrational spectra.[13] There are also other efficient physical methods available to investigate the mixed-valence communication, such as, IR (including Near-IR), magnetic measurements, Mössbauer spectroscope etc.

1.2. EPR (Electron Paramagnetic Resonance)

Electron paramagnetic resonance (EPR or ESR) is a powerful tool to study the electronic structures of materials with unpaired electrons. It has been extensively used to investigate the interaction between metals containing unpaired electrons.[14]

(η^7-Tropylium)vanadium(η^5-cyclopentadienyl) (TVC or Trovacene) is an ideal paramagnetic building block containing one unpaired electron, because of its electron configuration $e_{2g}^4 a_{1g}^1 e_{1g}^0$, the ground state $^2A_{1g}$ and the 99.75% abundance of the nucleus ^{51}V with I = 7/2.

Monomeric paramagnetic TVC molecules show in liquid solution an EPR spectrum consisting of a Lorenzian shaped lines with splitting of -6.98mT, and a line width of 1.6mT. The splitting is due to the interactions between the unpaired electron (S=1/2) and nucleus, the metal nuclear spin I(^{51}V) = 7/2.[15]

For binuclear or polynuclear paramagnetic complexes, the interaction between the unpaired electrons are important. In case of binuclear systems, the interactions can be expressed by the Spin-Hamiltonian (1-5):[16]

$$\mathbf{H} = g\beta_e B[(S(1) + S(2)] + a[(S(1)\cdot I(1) + S(2)\cdot I(2)] + J [S(1)\cdot S(2)] \qquad (1-5)$$
$$\text{Zeemann effect} \qquad \text{hyperfine interaction} \qquad \text{exchange interaction}$$

g: g factor; β_e: Bohr magneton; B: magnetic field; a: hyperfine coupling constant;
S: electron spin operator; I: nuclear spin operator; J: electron exchange interaction constant

For binuclear complex containing two ^{51}V nuclei (I = 7/2), there are 256 spin states to be considered (S, M_S, I_1, $m_I(1)$, I_2, $m_I(2)$). In order to obtain the energies and wave functions, a 256×256 matrix must be diagonalized. In a first order calculation, the simplified 4×4 matrix gives the magnetic fields for the allowed EPR transitions and intensities as follow:[16]

$$B_1 = B_0 + [J + R - A\{m_I(1) + m_I(2)\}]/2g\beta_e \qquad S$$
$$B_2 = B_0 + [J - R - A\{m_I(1) + m_I(2)\}]/2g\beta_e \qquad T$$
$$B_3 = B_0 - [J + R + A\{m_I(1) + m_I(2)\}]/2g\beta_e \qquad S$$
$$B_4 = B_0 - [J - R + A\{m_I(1) + m_I(2)\}]/2g\beta_e \qquad T$$

$$R = \{J^2 + A^2(\Delta m)^2\}^{1/2}, \Delta m = m_I(1) - m_I(2)$$
$$B_1 = B_3 = (R - J)/4R, B_4 = B_2 = (R + J)/4R$$

According to the *J/A* values, the characteristic properties, such as the line positions and the intensities can be obtained. Some simulated spectra for a vanadium (IV) dimer are shown in Figure 1.1.

1) If $|J| = 0$, the spectrum is corresponding to a monomer; which shows only 8 lines.
2) If $|J| \gg |A|$, a strong interaction or a rapid exchange exhibit a characteristic 15 lines spectrum based on the rules of (2nI + 1) (for ^{51}V, I = 7/2).
3) For $|J| \sim |A|$, complicated multi-line spectrum is observed.

Figure 1.1. Simulated EPR spectra for various $|J|/|A|$ values of a two vanadium(IV)-center complex

(a) $|J|/|A| = 0$

(b) $|J|/|A| = 2$

(c) $|J|/|A| = 4$

(d) $|J|/|A| = 10$

(e) $|J|/|A| = 30$

(f) $|J|/|A| = 50$

(g) $|J|/|A| = 100$

(h) $|J|/|A| = 1000$

From the simulation of the spectra, characteristic information can be obtained. The line width (ΔB) is one of the important parameters.[17] In the limit of very rapid exchange ($|J| > |A|$), the expression for the line-width in the dimer[18] can be described as follows (1-6) :

$$\Delta B = a + b\{m_I(1) + m_I(2)\} + c \{m_I(1) + m_I(2)\}^2 + d \{m_I(1) - m_I(2)\}^2 \quad (1\text{-}6)$$

In which, the term d $\{m_I(1) - m_I(2)\}^2$ is responsible for the alteration of the amplitudes. Parameter d contains the information about the fluctuation of the exchange relative to its static value J and the correlation time of the fluctuation.

There are two kinds of exchange between two nuclei contributing to the value of J. First, the two centers interact directly which is expressed as the j (direct) division, or *through space* interaction; the second is the so-called, *through bond* interaction,[19a] which can be divided into delocalization and polarization.

$$J = j \text{ (direct)} + j \text{ (delocalization)} + j \text{ (polarization)}$$
$$\text{through space} \qquad\qquad \text{through bond}$$

In fact, until now, no research results about the interaction between two metals, or the exchange between binuclear complex, have given the detailed characteristic quantitative description about J value. Despite there are many reports making use of empirical, or semi-empirical methods to calculate the J value, many factors have been minimized or neglected during the course. It is well know that the interaction between two metals, simply saying, is the interaction between their electronic sphere through space (direct) and through bond (polarization), and the whole electronic environment should not be neglected.

There are many factors which determine the value of J, such as the distance of the two centers, the angle of the configuration, etc. Even for the very simple model - two nuclei connected by a single atomic bridge, there is still no detailed explanation available, for example, for Fe-O-Fe systems, according to the angular overlap model (AOM), Güdel [19b] gave:

$$J_{model} = 4/25 \ [e'_{p\pi}{}^2 (1 + \cos^2\varnothing) + (e'_{s\sigma}\text{-}e'_{p\sigma}(\text{-}\cos^2\varnothing))^2 + 2e'_{p\sigma}e'_{p\pi}(\sin\varnothing)^2] \ f^2(r_1) \ f^2(r_2)$$
$$= 4/25 \ G(\varnothing)F(r_1, r_2)$$

or

$$J_{model} = 1.337 \times 10^{\,8} \ (3.536 + 2.488 \cos\varnothing + \cos^2\varnothing) \ \exp(\text{-}7.909r)$$

$\varnothing$: angle of Fe-O-Fe; r_1, r_2: Fe-O distance; $e'_{p\pi}$, $e'_{s\sigma}$, $e'_{p\sigma}$: ligand-field parameters
$G(\varnothing)$: angular function; $F(r_1, r_2)$: radial function

This model neglects, such as the direct metal -metal interaction, and the influence from the supporting bridging ligand.

1.3. Magnetochemistry

1.3.1. Fundamentals

Magnetic susceptibility measurement is another efficient method to measure the value and sign of J directly.[20] The susceptibilities of matter can be defined by the following equation (1-7):

$$M = \chi \, H \qquad (1\text{-}7)$$

M: magnetization (magnetic moment per unit of volume);
χ: susceptibility; H: the magnetic field strength.

In principle, χ is the algebraic sum of two contributions χ^D and χ^P:

$$\chi = \chi^D + \chi^P \qquad (1\text{-}8)$$

χ^D, χ^P represent the diamagnetic and paramagnetic susceptibilities, respectively. The former is negative and the latter is positive. Diamagnetic susceptibilities are temperature independent or the strength of the applied field, but paramagnetic susceptibilities depend on the temperature of the sample. For binuclear or polynuclear substance, it will be a more complex situation than for monomers.

Because some paramagnetic transition metal ions also have filled shells, the susceptibilities also contain diamagnetic contributions, although there are negative and rather small. Indeed, compared with the large value of paramagnetic susceptibility even at low temperature (10^2 ~ $10^4 \times 10^{-6}$ emu/mol), the diamagnetic susceptibility (-1 ~ -100 $\times$ 10^{-6} emu/mol) could be often neglected.

Paramagnetic susceptibilities are temperature dependent , their susceptibility χ varies inversely with temperature (Curie Law) (1-9):

$$\chi = C \, / \, T \qquad (1\text{-}9)$$

χ: measured susceptibility; C: Curie constant; T: absolute temperature.
Curie constant C: $N \, g^2 \, \mu_B^2 \, S \, (S + 1) \, / \, 3k;$

Similar to the ideal gas law, Curie´s law are not suitable to describe many actual situations. Therefore, a modification should be considered to correct the Curie Law. This lead to the Curie-Weiss Law (1-10) (Figure 1.2):

$$\chi = C \, / \, (T - \theta) \qquad (1\text{-}10)$$

Weiss constant (or temperature) θ: $z \, J \, S \, (S+1) \, / \, 3k$

The correction term θ has the unit of temperature. When θ is negative, it is called *antiferromagnetic*, on the contrary, when θ is positive, it is called *ferromagnetic*.

6

Figure 1.2. χ^{-1} versus temperature plot for an assembly of molecules obeying the Curie-Weiss law.
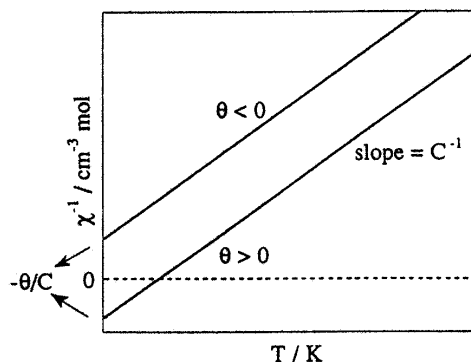
1.3.2. Magnetic susceptibility of binuclear compounds

The representative example for binuclear compounds are the copper(II) ions. Two metal centers noted A and B are in the same molecule, in which a ligand is connecting the two interacting centers. Magnetic susceptibility measurements are used to investigate the interaction between two the metal centers.

The local spin is $S_A = S_B = \frac{1}{2}$, if S = 0, it is named singlet, if S = 1, it is called triplet, the separation between the energy level of singlet and triplet is defined to be J, the isotropic interaction parameter. If S = 0 is the ground state, the interaction is said to be antiferromagnetic, J < 0. If S = 1 is the ground state, it is ferromagnetic, and J > 0.
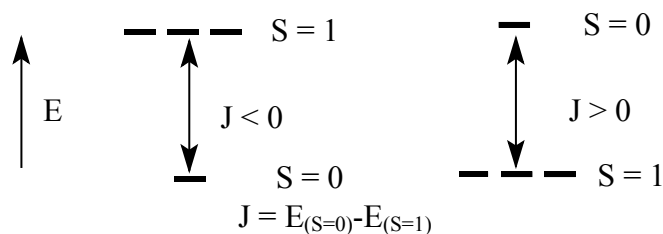
The magnetic susceptibility can be expressed in the following equation which was derived for the first time by Bleaney and Bowers:[21]

$$\chi = 2N\,g^2\,\beta^2 / kT\,[3 + \exp(-J/kT)] \qquad (1\text{-}11)$$

The χ versus T plot is shown in Figure 1.3.

If J < 0, there is maximum for the magnetic susceptibility. The susceptibility tends to zero when T approaches zero. The presence of a maximum is a signature of an antiferromagnetic interaction. The relation between J and temperature T_{max} is described as follow (1-12);

$$|J| / k\,T_{max} = 1.599 \qquad (1\text{-}12)$$

If J > 0, a ferromagnetic interaction has been defined, with decreasing temperature and below the Curie temperature, the χ increases rapidly.

7

Figure 1.3. χ versus T curves for binuclear compound with J = 0, ±100 cm^{-1}
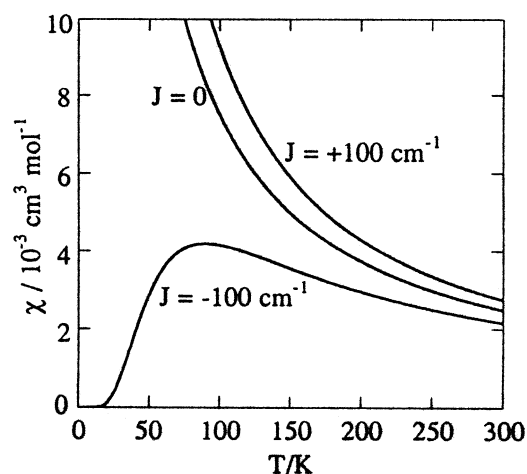
The coupling between two local spins where S_A and S_B are the spin operators of the individual electrons can be described by the Heisenberg-Dira-Van Vleck Hamiltonian (1-13):

$$H = -J\, S_A\, S_B \qquad (1\text{-}13)$$

A modification of χ has been given for a non-coupled species (1-14):[20a]

$$\chi = 2N\, g^2\, \beta^2\, (1\text{-}\rho) / kT\, [3 + \exp(-J/kT)] + 2N\, g^2\, \beta^2\, \rho / 2\, kT \qquad (1\text{-}14)$$

$$\rho: \text{molar fraction}$$

1.4. Cyclic Voltammetry (CV)

1.4.1. Fundamentals

Cyclic voltammetry has been used as an efficient and popular tool to investigate the interaction between metals for many years,[22] it can give much thermodynamic and kinetic information about the electron transfer within molecules (Figure 1.4).

The separation of redox potential of two or more metal centers which are apparently in chemically identical environments is a manifestation of the metal-metal interaction. The interaction may be expressed as a comproportionation constant (K_c) (1-15):

$$K_c = \exp(F\, \Delta E / R\, T) = \exp(\Delta E / 25.69) \qquad (1\text{-}15)$$

$$\Delta E: \text{redox splitting}$$

For example:

$$M^{n+}\text{-}M^{n+} + e^- \;\underset{}{\overset{E_{1/2}1}{\rightleftharpoons}}\; M^{(n-1)+}\text{-}M^{n+} + e^- \;\underset{}{\overset{E_{1/2}2}{\rightleftharpoons}}\; M^{(n-1)+}\text{-}M^{(n-1)+}$$

$$\Delta E_{1/2} = E_{1/2}1 - E_{1/2}2$$
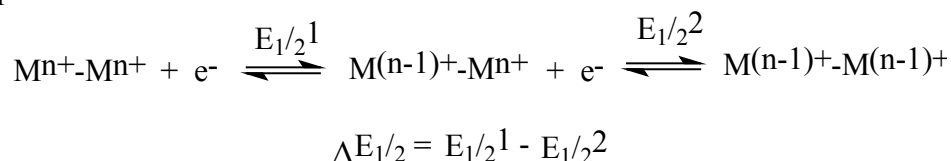
In CV, the potential of an electrode pair which is immersed in a stationary solution is cycled. Diffusion is the main driving force for the mass transport between the working electrode and

8

the bulk of the solution. The supporting electrolyte is dissolved in the solution, and the resulting current is measured. The electrode potential is scanned linearly as a function of time from an initial potential E_i (no electrode reaction) to a predetermined limit potential E_λ where the scan is reversed.[23] The current response as a function of applied potential can be recorded, and the changes of repetitive cycles are recorded as an important key to learn about the reaction mechanism.

Three electrodes are immersed into the solution, the working electrode (such as platium, glassy carbon, etc.), the reference electrode (such as saturated calomel electrode SCE, etc.) and the auxiliary electrode.[24] In order to insure that the migration current is coming from the supporting electrolyte and not from the studied compound, large excess of electroinactive supporting electrolyte is added to a non-aqueous solvent, for this purpose tetrabutylammonium tetrafluoroborate or hexafluorophosphate ($TBABF_4$ or $TBAPF_6$) is currently used.[25]

Figure 1.4. Cyclic voltammogram
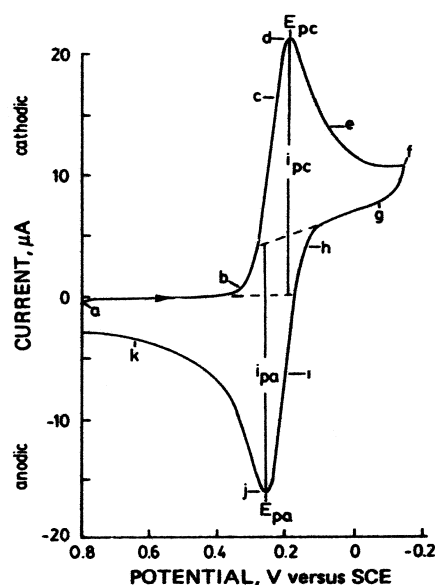
E_{pa}: anodic peak potential; E_{pc}: cathodic peak potential; i_{pa}: anodic peak current; i_{pc}: cathodic peak potential; $E_{1/2}$: half-peak potential; ΔE_p: separation between peaks

Different electron transfer rates correspond to various characteristics, see also Figure 1.5.[26] ($k°$: standard heterogeneous electron-transfer rate constant)

1) Reversible charge-transfer, $k° > 10^{-1}$ cm·s^{-1}
Criteria:

Formal reduction potential; $E°' = (E_{pa} + E_{pc}) / 2$
Separation between peaks; $\Delta E_p = E_{pa} - E_{pc} \cong 0.059/n$ V (25°C)
Peak current;
$i_p = (2.69 \times 10^5) n^{3/2} A D^{1/2} C v^{1/2}$
n: electron stoichiometry; A: electrode area (cm^2); D: diffusion coefficient (cm^2/s); C : concentration (mol/cm^3); v: scan rate (V/s).
$i_{pa} / i_{pc} = 1$
E_{pa} E_{pc} independent of scan rate

9

2) Quasi-reversible charge-transfer, $10^{-5} < k° < 10^{-1}$ cm·s^{-1}
Criteria:

$E_{pa} - E_{pc} > 0.059/n$ V
I_p linear with $v^{1/2}$
$i_{pa} / i_{pc} = 1$ ($\alpha = 0.5$)
Variation of E_{pa} E_{pc} with scan rate

3) Irreversible charge-transfer $k° < 10^{-5}$
Criteria:

$\Delta E_p / \Delta \log(v) = -30mV/n\alpha$
i_p linear with $v^{1/2}$

It is important to make sure that an uncompensated ohmic drop is not responsible for a ΔE_p. The ΔE_p value would become somewhat larger than the correct value for a fast ET rate (59mV for n=1), although uncompensated ohmic drop is influencing the ΔE_p value in some cases.

Figure 1.5. Cyclic voltammograms for reversible (a), quasi-reversible (b) and irreversible (c)
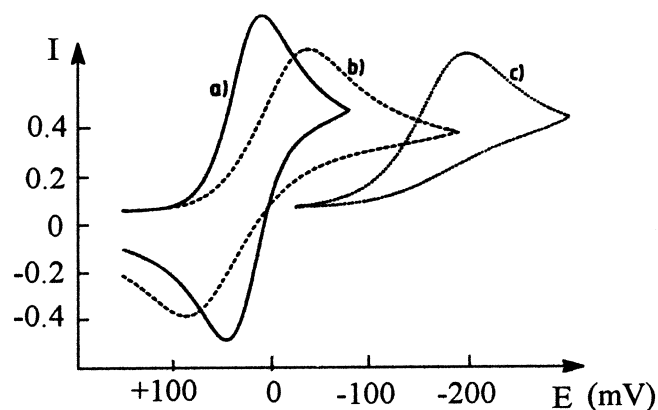
1.4.2. $\Delta E_{1/2}$

The mean potential between the cathodic and anodic peak potentials corresponds to half-wave potential. $\Delta E_{1/2}$ which is the separation of the midpoint potential of two redox centers, has been used widely to investigate the metal-metal interaction of metallocene systems. Normally, different separations indicate some variation of the interaction between metals, as Figure 1.6 shown. For Robin-Day class I systems, a rather small separation is observed, which means no electronic interaction between two redox centers. The electrochemical properties only exhibit the isolated redox center in each redox state. As for class II or III, a larger and measurable $\Delta E_{1/2}$ value is observed. For example, for class II system, $\Delta E_{1/2} < 200$ mV indicates the weak interaction between redox centers. The larger $\Delta E_{1/2}$ value of class III system corresponding to stronger interaction, which exhibits a delocalized or average-valence property.

Figure 1.6.

$\Delta E_{1/2} = 330$ mV $\Delta E_{1/2} = 590$ mV

2   **3**
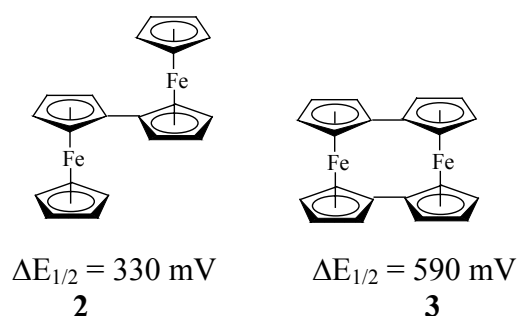
$\Delta E_{1/2}$ depends on the separation between the metal centers and the degree of conjugation in the bridge linking the two metallocene. It should be noted that there will be different $\Delta E_{1/2}$ value in different solvents and for different measuring conditions.[27]

1.5. Infrared Spectroscopy

For mixed-valence complexes, infrared spectroscopy often gives definitive information about electronic delocalization.[28] The infrared time scale is 10^{-11}- 10^{-12}s. Infrared localized systems show the bands of separated metallocenes for oligomers, whereas delocalized species show a new band of the averaged valence (metallocene)$^{0.5+}$ unit. For example, for ferrocene based mixed valent systems a band assigned to a C-H bonding vibration of the cyclopentadienyl ring has been shown to reflect the iron oxidation state. The C-H bend of ferrocene is found at 815 cm^{-1}, at 851cm^{-1} for ferrocenium triiodide (KBr).[29] {[2.2]ferrocenophane-1,13-diyne}$^+$ I$_3^-$ shows a single band at 830cm^{-1},[30] while a localized species, [Fv{Fe(C$_5$H$_4$I)}$_2$]$^+$I$_3^-$ has bands at 822 and 849cm^{-1}.[31] It means that a trapped mixed-valence complex would show a perpendicular C-H bending vibration for two oxidation state, one band for detrapped valences.[32a]

In general, IR studies in this spectral region have been confined to solid-state samples, which means mixed-valent systems had to be separated and purified in order to obtain useful information about detrapped or trapped states. Recently, a new thin layer spectro-electrochemical technique[32b] was developed to reduced the possibility of separation of the unstable or sensitive mixed-valent intermediate.

1.6. Previous Studies

Bis(benzene)vanadium (**4·**) or bis(benzene)chromium (**5**) as ideal parent compounds have been investigated for some time.

4·   **5**   **6·**
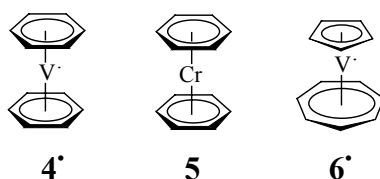
The metal-metal interaction between redox centers have been studied in detail by CV, EPR etc. Some examples are given below: (**7··**,[32c] **8**$^{++··}$ [32d] and **9**$^{++··}$ [32e])

$$7^{\cdot\cdot} \qquad 8^{++\cdot\cdot} \qquad 9^{++\cdot\cdot}$$
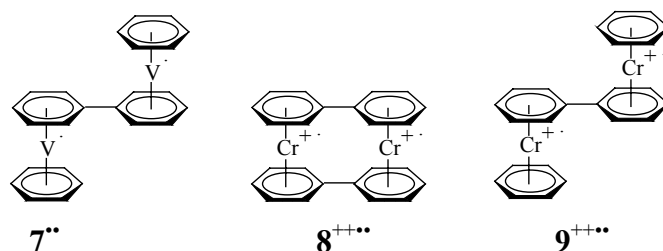
Recently, paramagnetic trovacene ($6^{\cdot}$) as an ideal parent complex has attracted attention. The considerably easy lithiation of the cyclopentadienyl ring of trovacene provides the chance to synthesize various binuclear or polynuclear complexes, which offer simultaneously the possibility to study magnetic exchange interactions by magnetic susceptibility, EPR spectroscopic measurements and investigation of electronic interactions by cyclic voltammetry.

Some new trovacene derivatives have been synthesized and studied by our research group (below $10^{\cdot\cdot}$,[12] $11^{\cdot\cdot}$,[71] $12^{\cdot\cdot}$ [92] and $13^{\cdot\cdot}$ [92]).

$$10^{\cdot\cdot} \qquad\qquad\qquad 11^{\cdot\cdot}$$

$$12^{\cdot\cdot} \qquad\qquad\qquad 13^{\cdot\cdot}$$
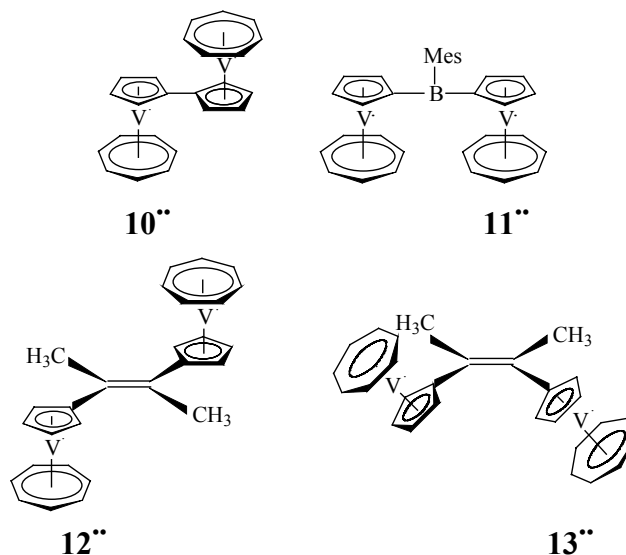
1.7. Research Objectives

The goals of this work are:
1) synthesizing new group 14, 15, 16 derivatives of trovacene which contain oligo-atom bridging units, and termetallocene derivative;
2) investigating the electronic communication among the redox centers by CV, EPR and magnetic susceptibility measurements.

The interaction could occur though space if the centers are close together or through bond if the redox centers are linked by a bridge which is formed by covalent bonds.

In complexes, generally, the *d*- electrons of metals in *d*(π) orbital enter into the formation of bonds with bridging atoms or overlap with the π-acceptor ligands. To some extent, the d-electrons delocalize between metals across the conjugated bridge or saturated covalent bonds

which normally play a very important role in ET. There are varieties of factors which would influence the ET, such as, the separation between redox centers, molecule conformation, etc.. New derivatives of trovacene are generally characterized by mass spectra, elemental analysis, and/or X-ray diffraction. Additionally, they are investigated by cyclic voltammetry, electron spin resonance, and/or magnetic susceptibility measurements. Due to their air-sensitive and thermally unstable properties, the melting points/decomposition points of them have not been measured in general.

2. Group 16 Derivatives

2.1. Introduction

Metal-metal interaction in linked metallocenes have been studied for many years since the discovery of ferrocene - an ideal redox center in 1951. In the past few years, much of the research interest related to linked metallocenes has been focused on the developing new materials, such as, molecular electronics,[33] nano-structured materials,[34] liquid crystalline organometallic polymers,[35] etc., and elucidating the mechanism in biochemistry, e. g., light energy collection and conversion,[36] etc.. The metal-metal interaction of organometallic complexes in which 16 group element are used as bridges, have scarcely been systematically investigated. Most of the previous works have focused on the synthesis of group 16 bridging species. For example, FcEFc, and FcEEFc (E = S, Se, Te).[37]

Previously, some studies on Creutz-Taube salts containing group 16 bridges have been reported. For example, the disulfide bridge of 4,4′-dithiobipyridine (**14**) effectively mediates the metal-metal interaction ($K_c = 8 \times 10^4$),[38] in contrast, the analogous $[\{Ru(NH_3)_5\}_2(\mu\text{-dps})]^{5+}$ in which di(4-pyridyl)sulfide linked as the bridge ($K_c = 158$) exhibits a relatively weak interaction between metals, the former is mainly due to the strong $p(\pi)\text{-}d(\pi)$ interaction between pyridyl rings and their sulfur substitutent, and the strong $d(\pi)\text{-}d(\pi)$ overlap between the sulfur atoms.
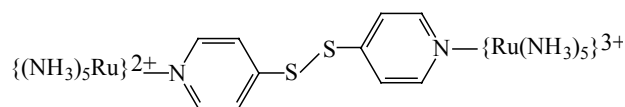
14

Meanwhile, as for the saturated bridged complexes, $\{Ru(NH_3)_5\}_2(\mu\text{-L})]^{5+}$(L as below described),[39] weak metal-metal interaction can occur through the hyper-conjugated orbital[40] provided by the overlap of p-orbital on the S and C atoms of the bridging ligand.
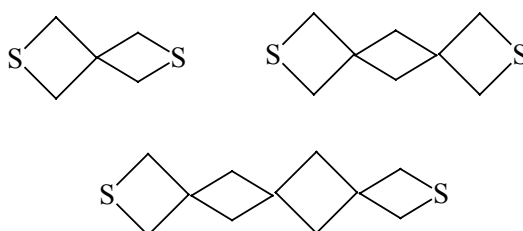
In this case the weak interaction between two metal fragments is also ascribed to long-range electron tunneling across the σ -framework of the bridging ligand.[41] The rigidity of spiro-fused rings leads to a fixed metal-metal distance. These cases indicate that S atom as bridge linked the binuclear redox centers can mediate effectively the interaction between the metals.

Therefore, in order to systematically investigate the influence of the bridge to the electron transfer for chemical and biological systems, various group 16 trovacene derivatives are prepared and studied in this work by CV, EPR and/or magnetic susceptibility measurements.

2.2. Synthetic Methods

First of all, the feasibility of the synthesis for various group 16 atom links to trovacene is evaluated. Although various synthetic methods related to ferrocene derivatives have been reported, these methods which are summarized below, probably are not suitable for the synthesis of air-sensitive organometallic species. Since a peroxo bridge is expected to cause decomposition via an intramolecular redox process, di([5]trovacenyl)peroxide (**15··**) was not considered for synthesis.

15··
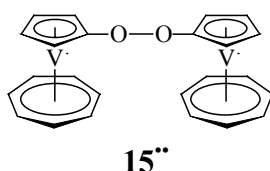
Organic disulfides and respective thiols have been fully studied. In general, disulfides can be prepared via oxidation of respective thiol by various oxidizing agent, e.g. halogen, hydrogen peroxide, oxygen (air).[42] However, these methods are limited to synthesize organometallic disulfides, in particularly, regarding the formation of cyclopentadienyl-substituted sulfur compounds due to their unstable property.

Until now, only few organometallic disulfide have been reported, such as, diferrocenyldisulfide and diruthenocenyldisulfide.[43] Pauson[44] obtained diferrocenyldisulfide from ferrocenylthiol with the help of oxygen. Herberhold[45] reported the formation of diferrocenyldisulfide as a result of acidification of lithium-ferrocenthiolate. It was surprisingly not to obtain ferrocene-1,1'-dithiol. But the disulfide has not been characterize by X-ray diffraction analysis.

E = S; Se, Te
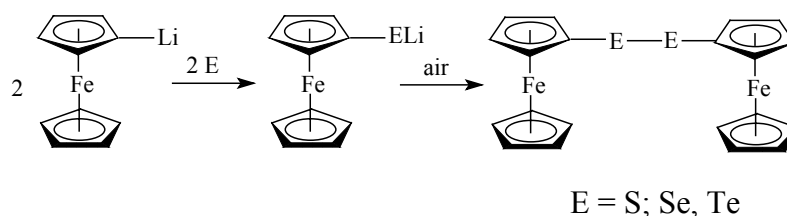
Recently, Kataeva et al.[46] reported the synthesis of $(CO)_3MnC_5H_4SSC_5H_4Mn(CO)_3$ with the help of air and its crystal structure. In addition, FcSeSeFc [37a] could be prepared from the reaction of FcHgCl and $Cu(SeCN)_2$. It should be mentioned that FcSeSeFc with amino group derivatives [47] as a mimetic for glutathione peroxidase have been studied,[48] in which a dramatic increase in the peroxidase activity could be observed. The synthesis of FcTeTeFc is similar to that of FcSeSeFc.

Furthermore, mono-chalkogenide bridged binuclear complexes have also been described, e.g., Fc_2Se can be synthesized by reaction of Fc_2Hg with $SeCl_2$,[49] or the reaction of FcHgCl with FcSeCN.[50] Several routes have been reported to synthesize diferrocenylsulfide, for example, the reaction of ferrocenylthiol with iodoferrocene in the presence of freshly activated copper bronze, or the reaction of diferrocenyldisulfide with lithioferrocene in a low yield. In addition, SCl_2 had ever been utilized to prepare the sulfide.
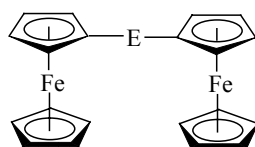
E = S; Se, Te

Unfortunately, since most of the cyclopentadienyl-type organometallic compounds are sensitive to air, those methods described above probably are not suitable for the unstable organometallic disulfide, which also can be used as a versatile intermediate to convert into organometallic thiol. But they give us a hint; whether the sulfur can be used as a medium oxidation regent to attain the goal or not. Therefore, we turned our interest to study the oxidation ability of sulfur, because sulfur lies in the same column as oxygen in the periodic table.

We successfully develop a novel and effective method to synthesize REER (E = S, Se, Te, R = trovacene) *via* oxidation of TVC-ELi by elemental powder of sulfur, selenium and tellurium, respectively. This is the first time to effectively modify the synthesis method of dichalkogenide. Meanwhile, this method also may be used to prepare other air-sensitive organometallic dichalkogenide which need a further study.

2.3. Trovacenylthiolate Derivatives

2.3.1. Synthesis of di([5]trovacenyl)sulfide (16··)

16··
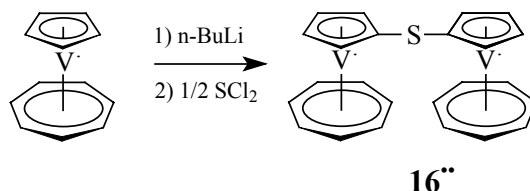
SCl_2 was chosen as the convenient reagent to afford **16··** in a satisfactory yield. Half equiv. of freshly distilled SCl_2 (58-60°C) in Et_2O was added dropwise over 1h to the ether solution of lithiotrovacene at 0°C, much pale green precipitate was formed. Filtration and extraction by benzene, then filtration through Celite and isolation by chromatography (eluted by toluene) afforded di(trovacenyl)sulfide as dark green solid. Recrystallization from benzene/PE gave analytically pure **16··** as dark violet needles in 14% yield. Di([5]trovacenyl)sulfide has been characterized by mass spectra, elemental analysis (see experimental part) and X-ray diffraction analysis. It has a good solubility in polar solvent, and is relatively stable in the air for several minutes.

In addition, the above noted dark green solid isolated by chromatography always contained some di([5]trovacenyl)disulfide, which is difficult to separate by chromatography completely. Therefore, the purity of SCl_2 is relative important.

2.3.2. X-ray Crystal Structure Analysis of 16[¨]

Dark violet needle-like crystals of di([5]trovacenyl)sulfide suitable for X-ray diffraction were generated from benzene/PE at 8°C. The molecular structure of **16**[¨] is depicted in Figure 2.1. Selected bonds, angles and torsion angles are summarized in Table 2.1 and 2.2, respectively.

The stereoview of the complex shows that some of the two molecule adopt a nearly square conformation, although they do not link, and the axes of opposite trovacene units are parallel.
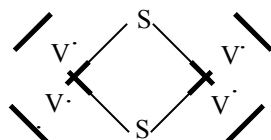
Detailed analysis of the bond lengths reveals that S-C bonds (S-C(13) = 1.765(7) Å, S-C(1) = 1.772(7) Å) are slightly longer than those of **16**[¨] (S-C(mean) = 1.754(7) Å). All carbon atoms of the Cp rings are almost coplanar, and the S atom is nearly coplanar with the respective two linked Cp rings, based on the torsion angle S(1)-C(1)-C(2)-C(3) (-179.53(16)°) and S(1)-C(13)-C(14)-C(15) (178.54(16)°). The dihedral angle of two Cp rings is 82.41(14)°.

Figure 2.1. Molecular structure and stereoview of **16**[¨]
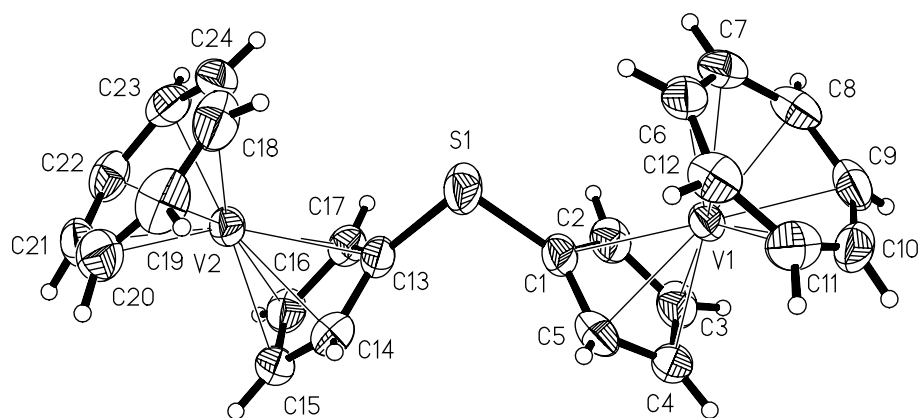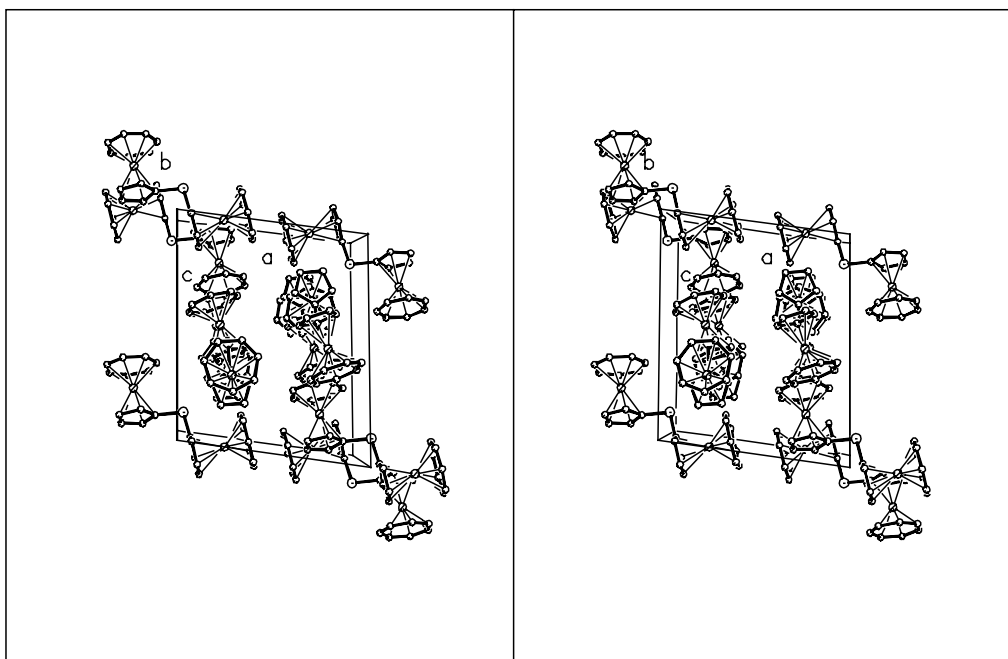
Due to steric hindrance, the two trovacene units arrange with an obtuse angle. The S atom is bridging the two trovacene groups with an angle of 98.96(10)°. V-V distance is 6.9937(0) Å, which is between the value of [5,5]ditrovacene (5.501(1) Å) and **18··** (8.0781(45) Å). This may be the main reason for the strong metal-metal interaction in solid relative to disulfide **18··**, when considering the results of electrochemistry, too.

Table 2.1. Selected bond lengths [Å] of **16··**

S(1)-C(1)	1.772(2)	V(1) - C(6)	2.186(2)
S(1) - C(13)	1.765(2)	V(1) - C(7)	2.189(2)
S(1) - C(mean)	1.7685(2)	V(1) - C(8)	2.187(2)
V(1) - C(1)	2.250(2)	V(1) - C(9)	2.182(2)
V(1) - C(2)	2.268(2)	V(1) - C(10)	2.186(2)
V(1) - C(3)	2.271(2)	V(1) - C(11)	2.179(3)
V(1) - C(4)	2.250(2)	V(1) - C(12)	2.173(2)
V(1) - C(5)	2.243(2)	**V(1)-C_7 Ring (mean)**	2.183(2)
V(1)-C_5 Ring (mean)	2.256(2)	**V(1)-C_7 (centroid)**	1.466(1)
V(1)-C_5 (centroid)	1.911(1)	C(6) - C(7)	1.401(3)
C(1) - C(2)	1.417(3)	C(6) - C(12)	1.401(4)
C(1) - C(5)	1.410(4)	C(7) - C(8)	1.406(3)
C(2) - C(3)	1.404(4)	C(8) - C(9)	1.399(4)
C(3) - C(4)	1.395(4)	C(9) - C(10)	1.404(4)
C(4) - C(5)	1.428(4)	C(10) - C(11)	1.411(4)
C-C (mean for C_5)	1.411(4)	C(11) - C(12)	1.416(4)
V(1) - V(2)	6.9937(0)	**C-C (mean for C_7)**	1.405(4)

Table 2.2. Selected angles and torsion [°] of **16**[**··**]

C(13)-S(1)-C(1)	98.96(10)	C(13)-S(1)-C(1)-C(5)	-84.2(2)
C(5)-C(1)-S(1)	126.38(19)	C(13)-S(1)-C(1)-C(2)	94.9(2)
C(2)-C(1)-S(1)	125.9(2)	C(1)-S(1)-C(13)-C(14)	85.8(2)
C(14)-C(13)-S(1)	126.48(19)	C(1)-S(1)-C(13)-C(17)	-92.2(2)
C(17)-C(13)-S(1)	125.87(18)	S(1)-C(1)-C(5)-C(4)	179.58(17)
C(2)-C(1)-C(5)	107.7(2)	S(1)-C(1)-C(2)-C(3)	-179.53(16)
C(17)-C(13)-C(14)	107.4(2)	S(1)-C(13)-C(14)-C(15)	-178.54(16)
		S(1)-C(13)-C(17)-C(16)	178.44(15)
Torsion C$_5$ ring (mean)	**0.1(3)**	**Torsion C$_7$ ring (mean)**	**0.0(4)**

2.3.3. Synthesis of di([5]trovacenyl)disulfide (18[··])

18[**··**]
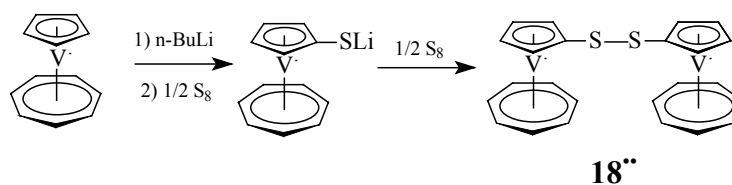
Lithiotrovacene reacted with elemental sulfur in diethylether in a stepwise fashion to give di(trovacenyl)disulfide (**18**[**··**]), despite excess sulfur reacted with dilithioferrocene to afford trisulfide (**17**).
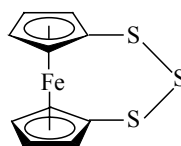
17

Because metalation [51] of trovacene stops at 50% conversion with one equiv. of n-BuLi, half equiv. molecule small particle of elemental sulfur was added to the concentrated solution of lithiotrovacene in Et$_2$O at -20°C with stirring for 1h, then the mixture was warmed to 0°C and stirred for 1h and at r.t. with further 1h, to afford a pale red-brown suspension (small amount of precipitate). After addition of another half equiv. molecule sulfur powder and stirring for 3h at r.t., a large amount of green precipitates formed. Filtration and washing by PE gave crude **18**[**··**]. Analytically pure di([5]trovacene)disulfide was obtained by chromatography (Al$_2$O$_3$) after elution with toluene as green solid in ~50% yield based on TVC.

Some factors should influence the formation of disulfide, such as, the solution volume of lithiotrovacene, the reaction temperature, the choice of solvent and the addition of sulfur in the last step. At high temperature, e. g., r.t., lithiotrovacene would not react effectively with elemental sulfur to result in TVC-SLi. The reduced volume would cause the disulfide as precipitate in high yield. When the reaction of lithiotrovacene with sulfur was performed in THF, no disulfide was formed, despite the other reaction condition were not changed. If toluene was used as the solvent, a poor yield was obtained. The stepwise addition of sulfur is

crucial important, if the equiv. sulfur was added at once to the solution of lithiotrovacene in Et$_2$O, no disulfide was observed as green precipitate.

The disulfide **18$^{¨}$** has been characterized by EI-MS; elemental analysis and X-ray structural analysis. Red-violet crystals suitable for X-ray diffraction were obtained from diffusion of PE to benzene solution at 8°C within 24 h. It has a good solubility in polar solvent, such as benzene, THF etc.. It is to some extent stable in the air for a short time (several minutes or longer).

Alternatively, S$_2$Cl$_2$ has been used to react with lithiotrovacene in Et$_2$O, but no molecular ion peak of disulfide from EI-MS (70eV) could be observed, despite S$_2$(C$_5$Me$_5$)$_2$ can be prepared by reaction of S$_2$Cl$_2$ with Li(C$_5$Me$_5$).[52]

2.3.4. X-ray Crystal Structure Analysis of 18$^{¨}$

The X-ray structure is exhibited in Figure 2.2. Selected bonds, selected angles and torsional angles are summarized in Table 2.3, and 2.4, respectively. The crystal contains a molecule of benzene in the crystal lattice.

The geometry around the S-S is not coplanar, but adopts cis- bent conformation, this is determined by the sum of the bond angles of the sulfur atoms, and the torsional angle of C-S-S-C.
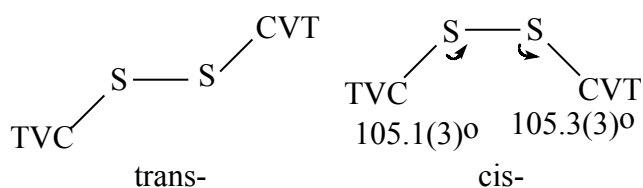
Two trovacene units are twisted around the central S-S bond by 105.1(3) and 105.3(3)°. Due to the steric hindrance, the angle C-S-S-C adopts a distorted geometry with almost vertical angle (92.5(3)°), in which two trovacene fragments arrange around the S-S axis toward two directions. The angle between S-S bond and the plane of Cp ring is 70.7(3)°.
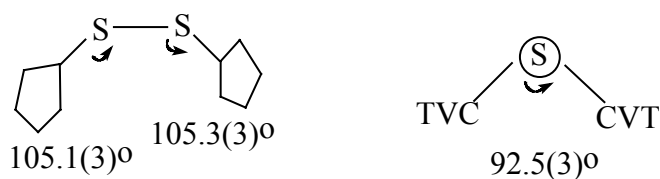
Two S atoms adopt a staggered conformation and are nearly coplanar with the corresponding linked cyclopentadienyl rings. The two cyclopentadienyl rings are not parallel, but have a dihedral angle of 29.8(4)°. Whereas within the two cyclopentadienyl rings, the carbon atoms lie nearly coplanar with small torsion angles, e.g. C(2)-C(1)-C(5)-C(4), -0.2(8)°; C(8)-C(9)-C(10)-C(11), 4.5(11)°.

Fig. 2.2 Molecular structure and stereoview of **18**[**]
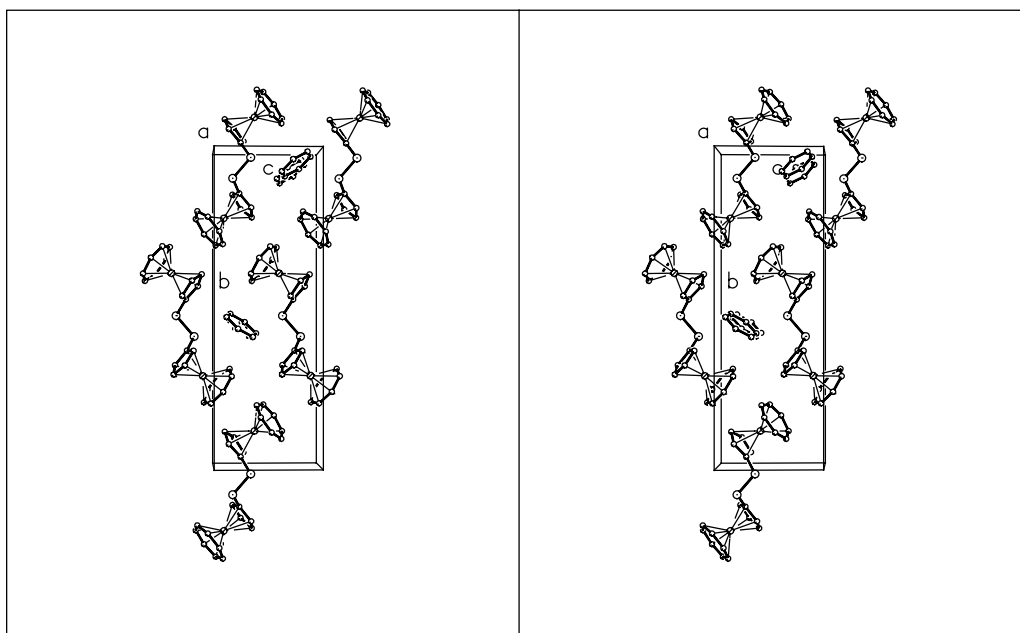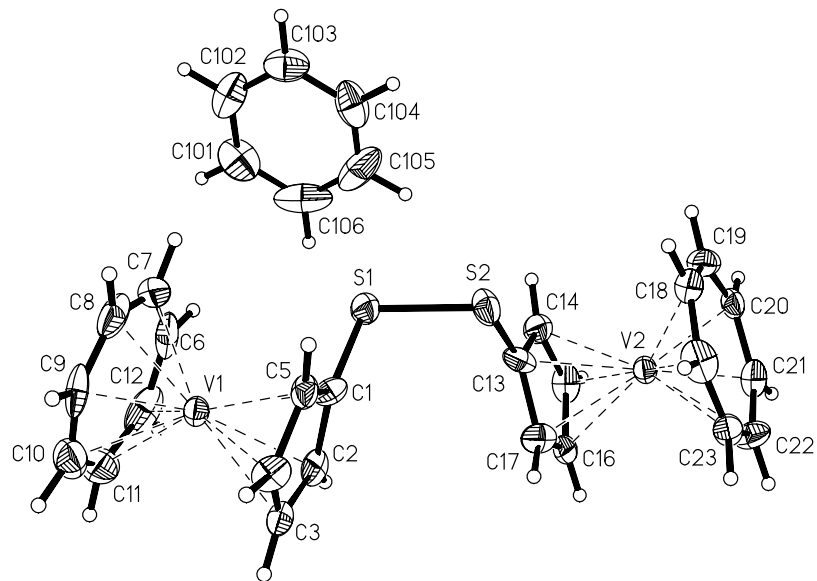
The S-S length is 2.076(3)Å close to that of $(CO)_3MnC_5H_4SSC_5H_4Mn(CO)_3$ (2.066(1)Å).[46] The C-S bonds in the C-S-S-C bridge are of equal lengths within statistical error (mean 1.755Å). The V-C distances associated with the cyclopentadienyl and the cycloheptatrienyl ring rang from 2.240(8) to 2.285(7)Å and 2.156(9) to 2.196(8) Å, respectively.

One important point, which should be mentioned, is that the single crystals suitable for X-ray diffraction happened to be twin crystals. The crystals contain one molecule of benzene in the crystal lattice.

Table 2.3. Selected bond lengths [Å] of **18**··

S(1)-C(1)	1.758(7)	V(1) - C(6)	2.162(7)
S(2) - C(13)	1.750(7)	V(1) - C(7)	2.165(6)
S(1) - C(mean)	1.754(7)	V(1) - C(8)	2.162(7)
S(1) - S(2)	2.076(3)	V(1) - C(9)	2.156(9)
V(1) - C(1)	2.240(8)	V(1) - C(10)	2.184(9)
V(1) - C(2)	2.248(7)	V(1) - C(11)	2.188(8)
V(1) - C(3)	2.278(6)	V(1) - C(12)	2.173(8)
V(1) - C(4)	2.285(7)	**V(1)-C₇ Ring (mean)**	2.170(8)
V(1) - C(5)	2.260(7)	**V(1)-C₇ (centroid)**	1.466(1)
V(1)-C₅ Ring (mean)	2.262(7)	C(6) - C(7)	1.418(13)
V(1)-C₅ (centroid)	1.913(3)	C(6) - C(12)	1.402(11)
C(1) - C(2)	1.410(8)	C(7) - C(8)	1.401(14)
C(1) - C(5)	1.428(10)	C(8) - C(9)	1.359(12)
C(2) - C(3)	1.395(10)	C(9) - C(10)	1.407(11)
C(3) - C(4)	1.430(9)	C(10) - C(11)	1.343(12)
C(4) - C(5)	1.422(10)	C(11) - C(12)	1.425(14)
C-C (mean for C₅)	1.417(9)	**C-C (mean for C₇)**	1.394(12)
V(1) - V(2)	**8.0781(45)**		

Table 2.4. Selected angles and torsion [°] of **18**··

C(1)-S(1)-S(2)	105.1(3)	C(1)-S(1)-S(2)-C(13)	92.5(3)
C(13)-S(2)-S(1)	105.3(3)	S(2)-S(1)-C(1)-C(5)	88.8(6)
C(5)-C(1)-S(1)	124.6(4)	S(2)-S(1)-C(1)-C(2)	-96.8(6)
C(2)-C(1)-S(1)	127.5(5)	S(1)-C(1)-C(2)-C(3)	-175.4(6)
C(14)-C(13)-S(1)	125.4(4)	S(1)-S(2)-C(13)-C(17)	-95.0(6)
C(17)-C(13)-S(1)	126.8(6)	S(1)-S(2)-C(13)-C(14)	92.3(7)
C(2)-C(1)-C(5)	107.7(6)	S(2)-C(13)-C(14)-C(15)	174.4(6)
C(14)-C(13)-C(17)	107.5(6)	S(2)-C(13)-C(17)-C(16)	-175.6(6)
Torsion C₅ ring (mean)	**0.1(8)**	**Torsion C₇ ring (mean)**	**-0.1(16)**

2.3.5. Synthesis of Di([5]trovacenylthio)methane (20··)

19·   **20··**
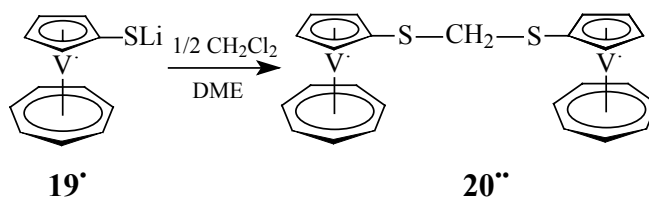
TVC-SLi (**19·**) was obtained by reaction of lithiotrovacene with half equiv. molecule S powder at ambient temperature (vide infra). Because **19·** has a good solubility in DME, half equiv. CH_2Cl_2 was added dropwise to the solution of **19·** in DME, and the mixture was stirred at r.t. overnight. Then all the volatiles were removed in vacuo and the residue was extracted by toluene. The analytically pure **20··** was obtained by chromatography (Al_2O_3) as violet solid in 20% yield, and recrystallized from benzene/PE to form dark violet needle-like crystals which were suitable for X-ray diffraction analysis. **20··** has a good solubility in common organic solvents. The characterization of **20··** is established by mass spectra, elemental analysis and X-ray diffraction analysis.

The reactivity of **19·** has also been confirmed by metathetical reactions with different electrophilic chloro-substituted reagents (vide infra, see 2.3.13). It should be noted that we have attempted to synthesize (TVC-S)₃CH by treatment of **19·** with CHI_3 under the same reaction condition as for **20··**, however, only complicated mixture was obtained without any information of the expected product (TVC-S)₃CH according to the result of mass spectroscopy.
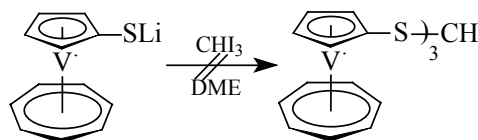
2.3.6. X-ray Crystal Structure Analysis of 20··

The X-ray structure of **20··** is shown in Figure 2.3, and the selected bonds and angles are summarized in Table 2.5 and 2.6. Due to introduction of CH_2 between the S-S bond, the geometry of the molecule is tetrahedral similar to CH_4, which leads to a shorter V-V distance(7.4889Å) than that of **18··** (8.0781(45)Å).

The angle S(1)a-C(13)-S(1) (116.7(2)°) is close to the ideal tetrahedral angle (109.28° of CH_4). The S atoms are nearly coplanar with respective Cp ring (mean, 178.43(19)°). The bond length of C(1)-S(1) (1.768(3)Å) is slightly shorter than that of S(1)-C(13) (1.816(2)Å) and is close to that of **18··** (1.754(7)Å). The angle of C(1)-S(1)-C(13) is 100.34(9)°. The molecule of **20··** also crystallize, similar to **18··**, as twin in the crystal.

23

Figure 2.3. Molecular structure and stereoview of **20**[··]
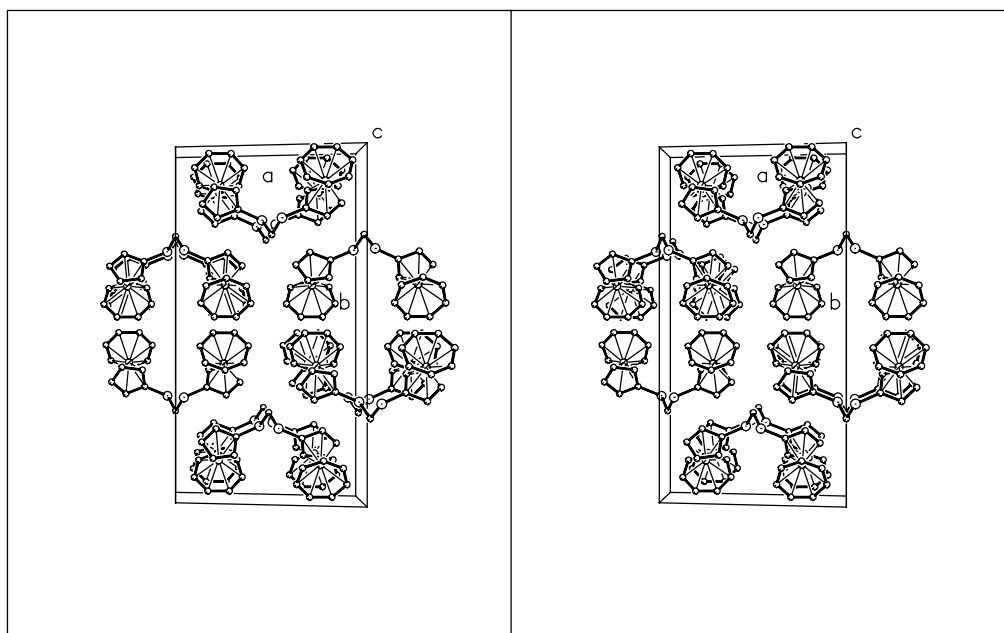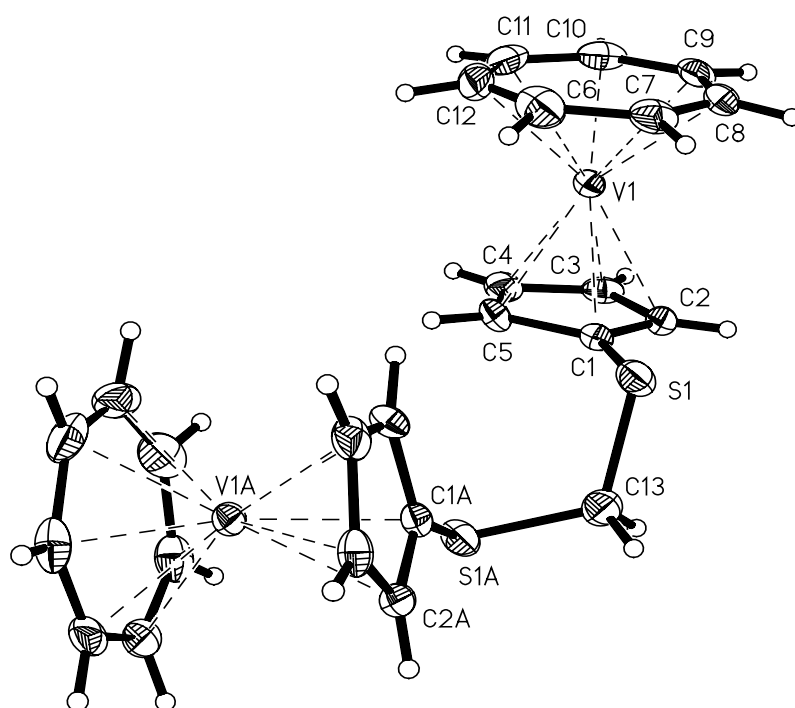
Table 2.5. Selected bond lengths [Å] of **20**¨

S(1)-C(1)	1.768(3)	V(1) - C(6)	2.183(3)
S(1) - C(13)	1.816(2)	V(1) - C(7)	2.183(3)
C(13) - S(1)a	1.816(2)	V(1) - C(8)	2.189(3)
V(1) - C(1)	2.251(2)	V(1) - C(9)	2.199(3)
V(1) - C(2)	2.270(3)	V(1) - C(10)	2.197(3)
V(1) - C(3)	2.273(3)	V(1) - C(11)	2.176(3)
V(1) - C(4)	2.262(3)	V(1) - C(12)	2.179(3)
V(1) - C(5)	2.254(3)	**V(1)-C$_7$ Ring (mean)**	2.186(3)
V(1)-C$_5$ Ring (mean)	2.262(3)	**V(1)-C$_7$ (centroid)**	1.468(1)
V(1)-C$_5$ (centroid)	1.917(4)	C(6) - C(7)	1.411(4)
C(1) - C(2)	1.413(4)	C(6) - C(12)	1.404(4)
C(1) - C(5)	1.425(4)	C(7) - C(8)	1.406(4)
C(2) - C(3)	1.406(4)	C(8) - C(9)	1.404(4)
C(3) - C(4)	1.415(4)	C(9) - C(10)	1.404(4)
C(4) - C(5)	1.400(4)	C(10) - C(11)	1.407(4)
C-C (mean for C$_5$)	1.412(4)	C(11) - C(12)	1.406(5)
V(1) - V(2)	**7.4889**	**C-C (mean for C$_7$)**	1.406(4)

Table 2.6. Selected angles and torsion [°] of **20**¨

C(1)-S(1)-C(13)	100.34(9)	C(13)-S(1)-C(1)-C(2)	-100.5(2)
C(2)-C(1)-S(1)	126.0(2)	C(13)-S(1)-C(1)-C(5)	80.9(2)
C(5)-C(1)-S(1)	126.2(2)	S(1)-C(1)-C(2)-C(3)	-178.34(19)
S(1)a-C(13)-S(1)	116.7(2)	S(1)-C(1)-C(5)-C(4)	178.53(19)
C(2)-C(1)-C(5)	107.8(2)	C(1)-S(1)-C(13)-S(1)a	-70.83(9)
C(9)-C(8)-C(7)	129.1(3)	**Torsion C$_5$ ring (mean)**	**0.0(3)**
S(1)a-C(13)-H(13)	106.7(14)	**Torsion C$_7$ ring (mean)**	**0.0(5)**
S(1)-C(13)-H(13)	111.4(15)		

2.3.7. Results of Cyclic Voltammetry (16¨, 18¨ and 20¨)

The cyclic voltammograms of **16**¨, **18**¨ and **20**¨ are shown in Figure 2.4. Their redox potentials are summarized in Table 2.7.

Based on the relation between the current height and the number of electron transfer,[53] electrochemistry of complex **16**¨ shows two successive reversible one-electron oxidation waves at 360mV ($E_{1/2}(0/+)$) and 447mV ($E_{1/2}(+/2+)$) with a redox separation of 87mV ($\Delta E_{1/2}(0/+)(+/2+)$), the first wave is close to the second oxidation of [5,5]bitrovacene (**10**¨) ($E_{1/2}(+/2+)=364$mV). It is significantly more difficult to remove the second electron than the first one from the metal centers.

Meanwhile, two successive reversible one-electron reduction wave at -2.358 V and -2.492 V are presented with a splitting of 134 mV. The second reduction potential is close to the first reduction potential of **10**¨ ($E_{1/2}(0/-)=-2.484$V).

On the contrary to the electron-donating feature of trovacenyl unit, for example, **10**¨ led to a cathodic shift of the redox potential $E_{1/2}(0/+)$ (217mV) relative to the parent trovacene

(260mV). The electron-withdrawing nature of trovacenylthio substituent (TVC-S) results in an anodic shift ($E_{1/2}(0/+)=360$mV) relative to trovacene. Therefore, reduction of **16**$^{\cdot\cdot}$ ($E_{1/2}(0/-)$ = -2.358 V) is easier than that of trovacene (-2.55 V), and analogue **10**$^{\cdot\cdot}$ (-2.484 V).

For complex **18**$^{\cdot\cdot}$ and **20**$^{\cdot\cdot}$, a reversible two-electron oxidation potential are observed at 392mV and 378mV, respectively, due to two S atoms′ strong polarizability. The large ΔE_p value indicates that the overlap of two one-electron oxidation waves and the small redox splitting ($\Delta E_{1/2}(0/+)(+/2+) \leq 70$mV) occurred.

While, for **18**$^{\cdot\cdot}$, a reversible two-electron reduction couple at -2.84 V is given, it does not has an anodic shift rather than a more cathodic shift relative to that of TVC. The lack in parallelism of the shifts pertaining to oxidation and reduction may be due to the increase of the S-S bond; weak electron-delocalization effect and the strong $d(\pi)$-$d(\pi)$ overlap between the sulfur atoms. This behavior is similar to that of TVC-Se-Se-TVC (**25**$^{\cdot\cdot}$) and TVC-Te-Te-TVC (**26**$^{\cdot\cdot}$) (vide infra).

Owing to the same electron-withdrawing effect of the thiolate unit (TVC-S), introduction of saturated CH_2 group between S-S bond of disulfide (**18**$^{\cdot\cdot}$) has a similar pronounced effect on the redox potential. Two successive reduction waves are observed at -2.387V and -2.782V, with a redox splitting of 395mV. The first reduction is close to that of **16**$^{\cdot\cdot}$ which is consistent with the anodic shift due to binding an electron-withdrawing group. However, the second reduction is similar to that of **18**$^{\cdot\cdot}$ with a high cathodic shift relative to TVC.

For the first reduction, due to the introduction of saturated CH_2, which prevents the two lone electron from pairing together, thus, the electron-withdrawing effect dominates, compared to the effect of lone electron pair of S atom. But, when **20**$^{\cdot\cdot}$ was reduced further, it is difficult and this indicates that the lone electron pairing effect would dominate in respect to electron-withdrawing effect.

Although introduction of methylene group would increase the distance of two redox metal centers by addition of two S-C bonds, and the *through-bond* metal-metal interaction should be decreased generally. Since CH_2 group prefers to build a tetrahedral structure, it could decrease spatially the distance between two redox metal center. Therefore, two contrary effects work together, in other words, the *through bond* interaction decreased, but the *through space* interaction increased.

As for the analogue ferrocene derivatives, FcSFc, FcSSFc and FcSCH$_2$SFc, only two oxidation potential separation of FcSFc was observed by 290mv (in CH_2Cl_2),[54] the systematic studies about the metal-metal interaction still have not been reported. Furthermore, electrochemical studies of Fc$_2$Se and FcSeSeFc showed two oxidation separation by 220 mV and 140 mV (in CH_3CN), respectively,[33e] which could exemplify that with the length increasing, the metal-metal interaction decreased. In the related Fc-E-Fc-E-E-Fc-E-Fc (E = S, Se, Te, below),[33c] three oxidation waves at around 0.46, 0.75 and 0.87 V were observed.

The electrochemical behavior suggests that the ease of oxidation of **16**$^{\cdot\cdot}$, **18**$^{\cdot\cdot}$ and **20**$^{\cdot\cdot}$ increase with the chain length, as the tendency of **20**$^{\cdot\cdot}$ ($E_{1/2}(0/2+)_{SCS} = 378$mV) < **18**$^{\cdot\cdot}$ ($E_{1/2}(0/2+)_{SS} = 392$mV)< **16**$^{\cdot\cdot}$ ($E_{1/2}(+/2+)_S = 447$mV).
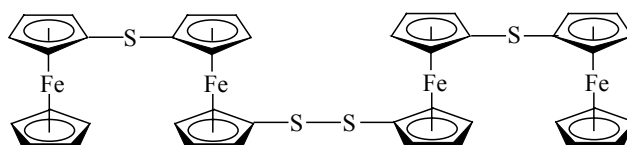
The electrochemical behavior could be rationalized as follows: 1), The strong $p(\pi)$-$d(\pi)$ conjugation interaction between the cyclopentadienyl occupied π orbital with sulfur lone pairs; 2), the strong $d(\pi)$-$d(\pi)$ overlap between the sulfur atoms; 3), the hyperconjugation by the overlap of p-orbital on the S and C atoms of CH_2. The related 1,n-dithio-(n)ferrocenophanes, through-bond conjugation between the 1,n-dithiamethylene bridge and the cyclopentadienyl π orbital had been demonstrated by photoelectron spectroscopy.[55]
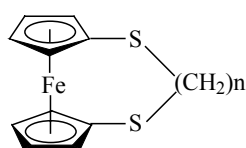
The large redox separation value of **10$^{••}$** suggests a higher degree of metal-metal interaction than those of other bridging bitrovacenyl complexes. The result of cyclic voltammetry also reveals that there is a considerable stronger interaction of **16$^{••}$** than that of S-S bridging **18$^{••}$** and S-C-S bridging **20$^{••}$**. In conclusion, with the distance between two redox metal centers increasing like the trend of $d_s < d_{scs} < d_{ss}$, the metal-metal interaction, either through bond or through space, decreased.

Table 2.7. Cyclic Voltammetry Data for **16$^{••}$, 18$^{••}$, 20$^{••}$**

	16$^{••}$		**18$^{••}$**	**20$^{••}$**
$E_{1/2}(0/+)$	360mV	$E_{1/2}(0/2+)$	392mV	378mV
ΔE_p	68mV	ΔE_p	96mV	148mV
I_{pa}/I_{pc}	1	I_{pa}/I_{pc}	1	1
$E_{1/2}(+/2+)$	447mV	$\Delta E_{1/2}(0/+)(+/2+)$	≤ 70mV	≤ 70mV
ΔE_p	58mV	$E_{pa}(2+/3+)$	1.038V	1.136V
I_{pa}/I_{pc}	1	$E_{1/2}(0/2-)$	-2.840V	
$\Delta E_{1/2}(0/+)(+/2+)$	87mV	ΔE_p	104mV	
$E_{1/2}(2+/3+)$	1.030V	I_{pa}/I_{pc}	1	
$E_{1/2}(0/-)$	-2.358V	$E_{1/2}(0/-)$		-2.387V
ΔE_p	88mV	ΔE_p		134mV
I_{pa}/I_{pc}	1	I_{pa}/I_{pc}		0.54
$E_{1/2}(-/2-)$	-2.492V	$E_{1/2}(-/2-)$		-2.782V
ΔE_p	100mV	ΔE_p		120mV
I_{pa}/I_{pc}	1	I_{pa}/I_{pc}		0.80
$\Delta E_{1/2}(0/-)(-/2-)$	134mV	$\Delta E_{1/2}(0/-)(-/2-)$		395mV

Figure 2.4. Cyclic voltammograms for **16**[¨], **18**[¨] and **20**[¨] in DME/TBAP at -40°C, v=100mV/s

16[¨]

18[¨]

20[¨]

mA

-3.0   -2.0   -1.0   [V]   0.0   1.0   1.6
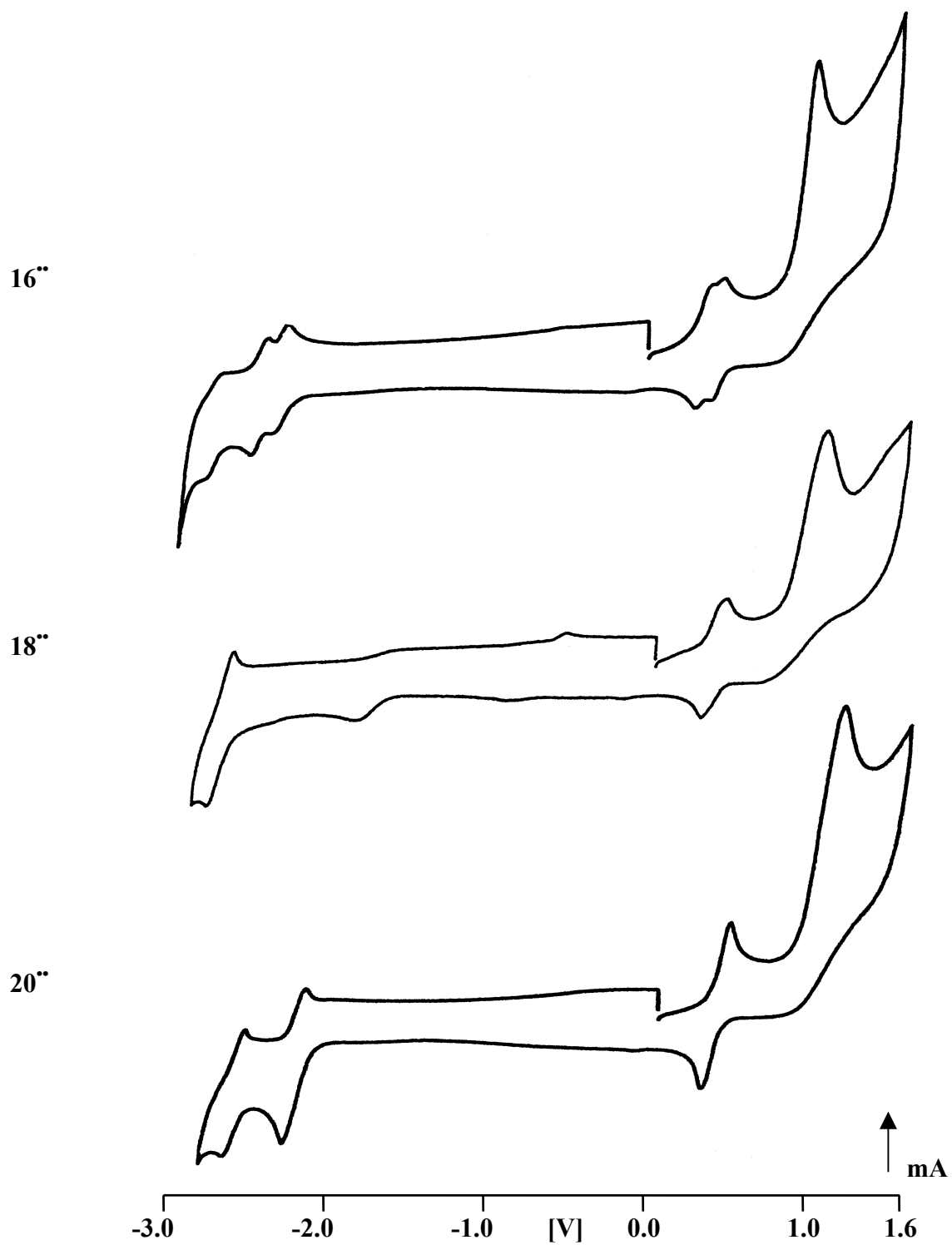
2.3.8. EPR Spectra (16··, 18··, and 20··)

The EPR spectra of **16··**, **18··**, and **20··** are shown in Figure 2.5, 2.6 and 2.7, respectively. The spectroscopic parameters are summarized in Table 2.8.

All the three complexes display the typical binuclear 15-line pattern in accord with the 2nI+1 rule, which indicate that the unpaired electrons couple with both of the vanadium nuclei. On the EPR time scale, the unpaired electrons are delocalized between the two trovacene units. The magnitude of the ^{51}V splitting are close to each other in value and near one-half of that of trovacene. The coupling constant ($A_{iso}(^{51}V)$) of **16··**, **18··**, and **20··** are 7.215mT, 7.22mT and 7.22mT. The strong polarizability of the S atom, the conjugation between cyclopentadienyl p_π orbital and the S atom d_π orbital, and/or additional d_π - d_π conjugation from S-S, contribute to spin-spin interaction. For **20··**, the introduction of CH_2 group between S-S bridge and the sp^3 hybrid of C atom would attenuate the coupling between two nucleus, the probably spatial orbital overlap between two nucleus would lead to the contrary effect, J value reflects it.

Spectra simulation furnished the exchange coupling constant of **16··** $J \cong$ -2.80 cm^{-1}, the largest among the three binuclear complexes, it also represents nearly double time of J value in [5]bitrovacene. Whereas, the exchange coupling constant J of **18··** is 0.65 cm^{-1}, only 23% of that of **16··** in value. The exchange coupling constant J of **20··** is the smallest among them, only 4% of that of **16··**. Based on the relative confident of the J value from simulation, it can be inferred that the interaction between metals of **16··** is the strongest among them which is consist with the result of electrochemistry.

So, it is apparent that the introduction of the saturated CH_2 and the increasing distance between two metals attenuate the metal-metal interaction. It also can be inferred that if the bridge were S-S-S, three S atoms between two trovacene units, the metal-metal interaction were very weak and probably eight-line pattern would be observed. Therefore, it can be concluded that the S atoms could not be used as an efficient molecular wire component.

Figure 2.5. EPR spectra of **16··** in fluid solution and rigid solution (toluene); at 293K, ν = 9.2462GHz, A) experimental, B) simulated; experimental C) 330K, ν = 9.2462GHz; D) 250K, ν = 9.2464GHz; E) 210K, ν = 9.2472GHz; F) 126K, ν = 9.2511GHz.
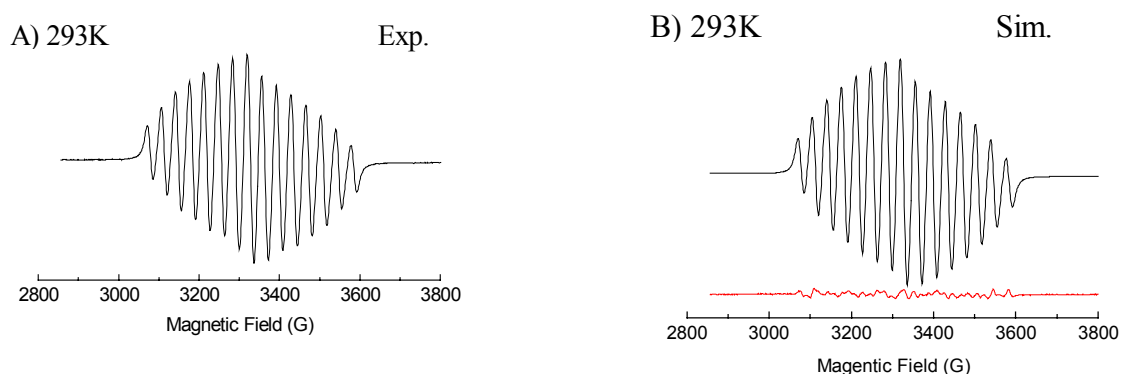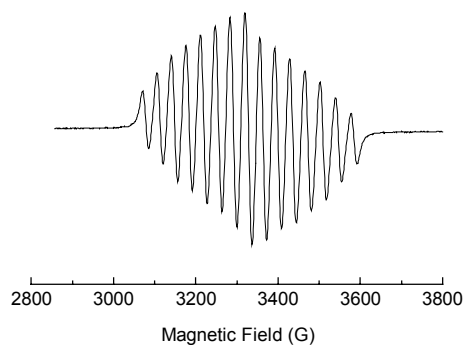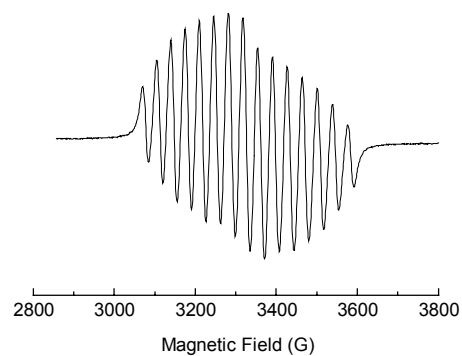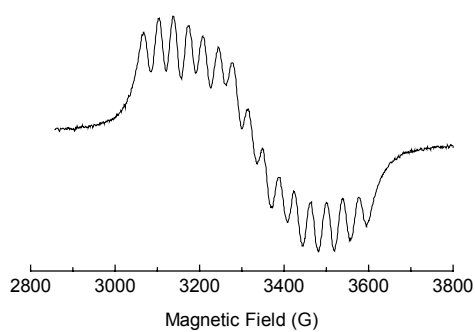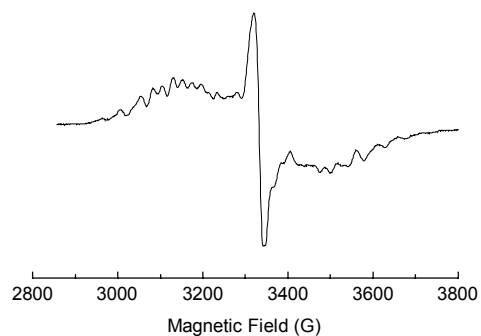
Figure 2.6 EPR spectra of **18**¨ in fluid solution (toluene) and rigid solution (toluene); 340K, ν = 9.24547GHz, A) experimental; B) simulated; experimental C) 320K, ν = 9.24496GHz, D) 360K, ν = 9.24548GHz.

C) 320K

D) 360K
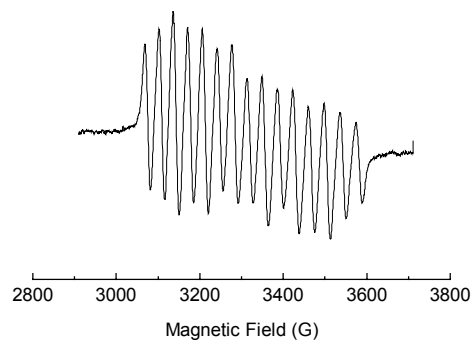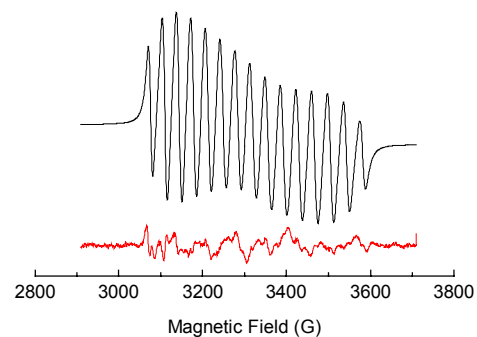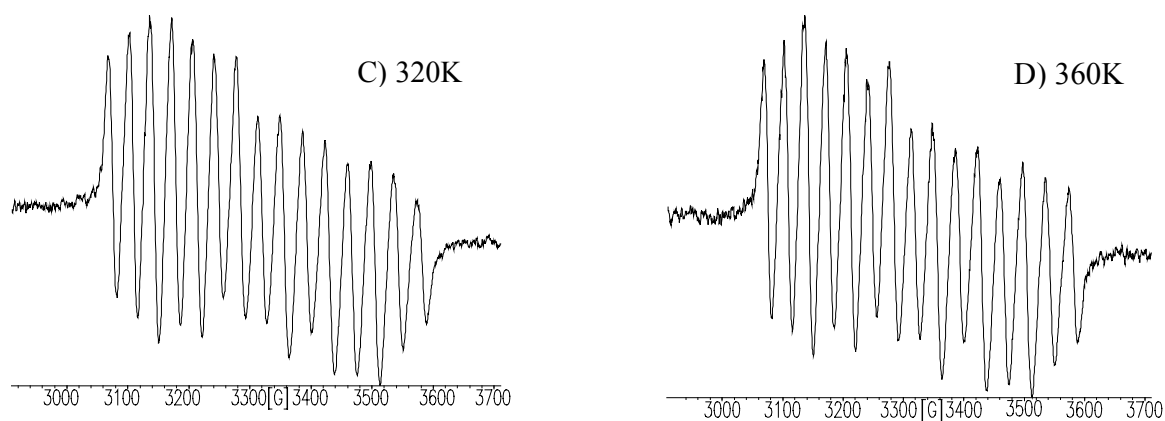
Figure 2.7. Experimental fluid solution spectra (toluene) of **20·**; A) 350K, ν = 9.24435GHz, B) 320K, ν = 9.24472GHz, C) 300K, ν = 9.24309GHz, D) 260K, ν = 9.24553GHz; and E) experimental rigid solution (toluene) spectra at 117K, ν = 9.24792GHz.

A) 350K

B) 320K

C) 300K

D) 260K

E) 117K

31
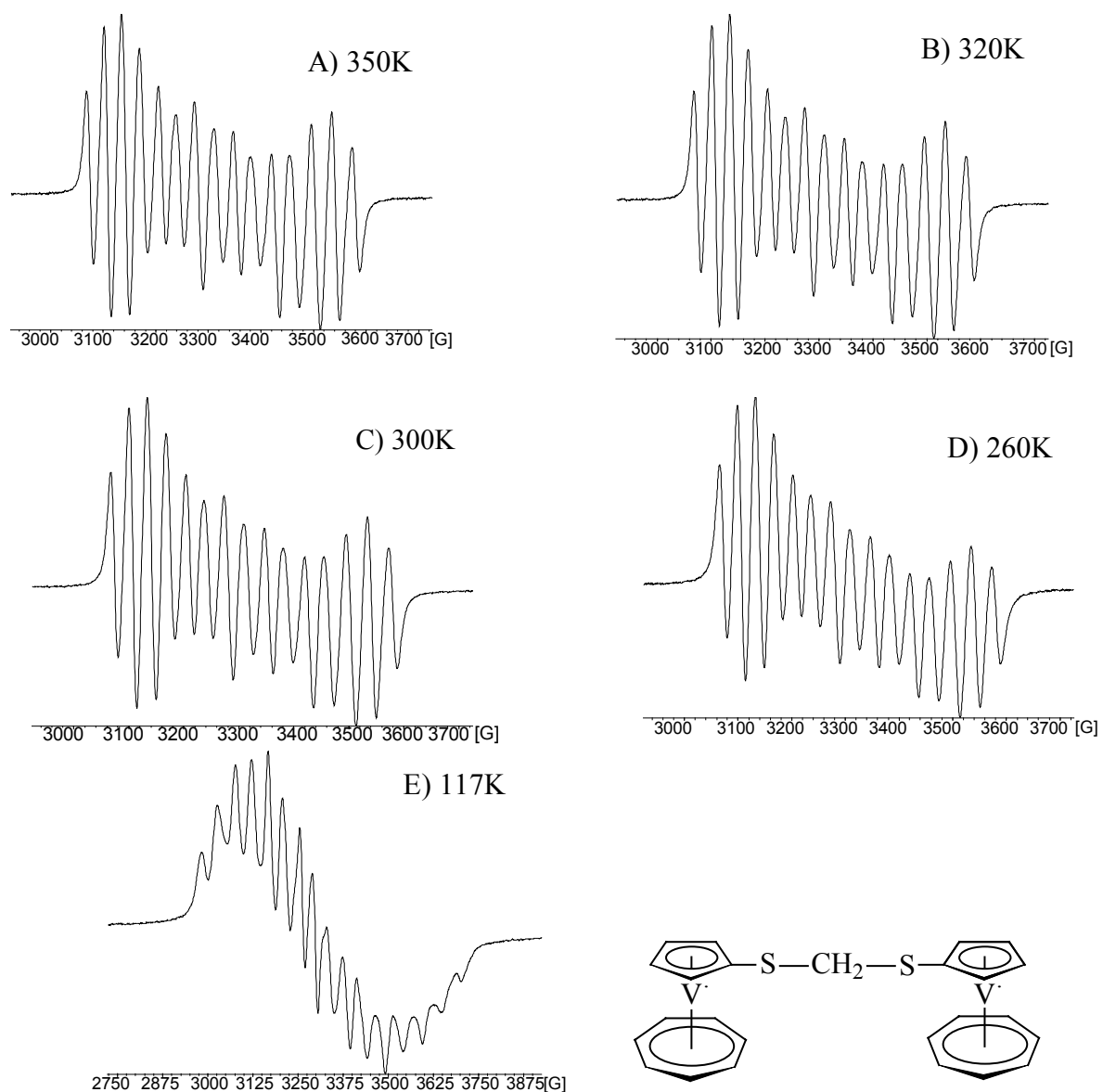
Table 2.8. EPR Data of **16**``, **18**`` and **20**``.

	A(^{51}V)$_{iso}$	g$_{iso}$	J	α	β	γ	ΔB
16``	7.215mT	1.9834	2.80 cm^{-1}	-0.125	-0.086	0.111	22.8G
18``	7.220mT	1.9826	0.65 cm^{-1}	-0.47	-0.140	1.02	29.1G
20``	7.22mT	1.9874	0.11 cm^{-1}	-0.443	-0.100	0.434	29.3G

2.3.9. Magnetic Susceptibility (16``, 18``, and 20``)

In order complement the J value from the simulation of EPR spectroscope, magnetic susceptibility of crystals of **16**``, **18**``, and **20**`` were measured on a SQUID magnetometer (Figure 2.8).

The Bleaney-Bowers type equation as following described, proposed by Prof. Dr. Pebler, was fitted to the experimental data of the three dinuclear complexes, and the data are summarized in Table 2.9.

$$\chi_m = 2\frac{N\mu_B g^2}{3kT}\cdot\frac{3\exp(\frac{2J}{kT})}{1+3\exp(\frac{2J}{kT})}\cdot\frac{T}{T-\Theta}$$

Table 2.9. Magnetic Susceptibility of **16**``, **18**`` and **20**``

	J/k [K]	Θ [K]	J'/k [K]	g	μ$_v$ [μ$_B$]
16``	-2.0(1)	-5.0(2)	1.0	1.999	1.55(5)
18``	-1.95(5)	-3.3(1)	0.7	1.999	1.51(5)
20``	-2.0(1)	-6.7(2)	1.5	1.999	1.52(5)

J/k [K]: intramolecular exchange constant; Θ [K]: paramagnetic Curie-temperature; intermolecular interaction J'/k = |Θ| /(zS(S+1)) z = 6; μ$_v$: magnetic moment.

Table 2.10. J values and V-V distances of **16**``, **18**`` and **20**``

	J* [cm^{-1}]	J** [cm^{-1}]	D [Å]
16``	-1.39	2.80	6.99
18``	-1.36	0.65	8.08
20``	-1.39	0.11	7.49

J* [cm^{-1}]: Magnetic simulation; J** [cm^{-1}]: EPR simulation; D: V-V distance.

Based on Table 2.9, it is apparent that the three dinuclear complexes are antiferromagnetic metal-metal interaction. The exchange constant J/k of the three species **16**``, **18**`` and **20**``are -2.0(1) K, -1.95(5) K and -2.0(1) K, respectively, which are corresponding to -1.355 cm^{-1}, -1.39(46) cm^{-1} and -1.39(46) cm^{-1}, respectively. Meanwhile, the intermolecular interaction are 0.49 cm^{-1}, 0.70 cm^{-1} and 1.04 cm^{-1}, respectively.

Together with the V-V distances of the three compounds (Table 2.10), therefore, it could be concluded that the metal - metal interaction are decrease as **18¨** < **16¨** = **20¨**. It is surprising to learn that the interaction of **20¨** is nearly the same as that of **16¨** above on the magnetic simulation which are different from the EPR simulation. This may be attributed to the fact that the introduction of CH_2 which is performed a tetrahedron conformation would reduce the V-V distance directly.

Thus, despite it could be inferred the tendency that with the length of bridge increasing, the metal-metal interaction decreased, in order to fully investigate the magnitude of J changing with the length of S bridge, an additionally detailed comparison from the analogue of S-S-S bridging complex **78¨** should be provided in the further study.

78¨
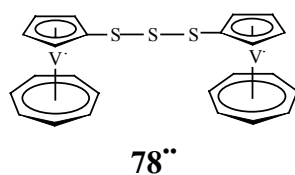
Figure 2.8. χ_m versus T curves for **16¨**, **18¨** and **20¨**.

33
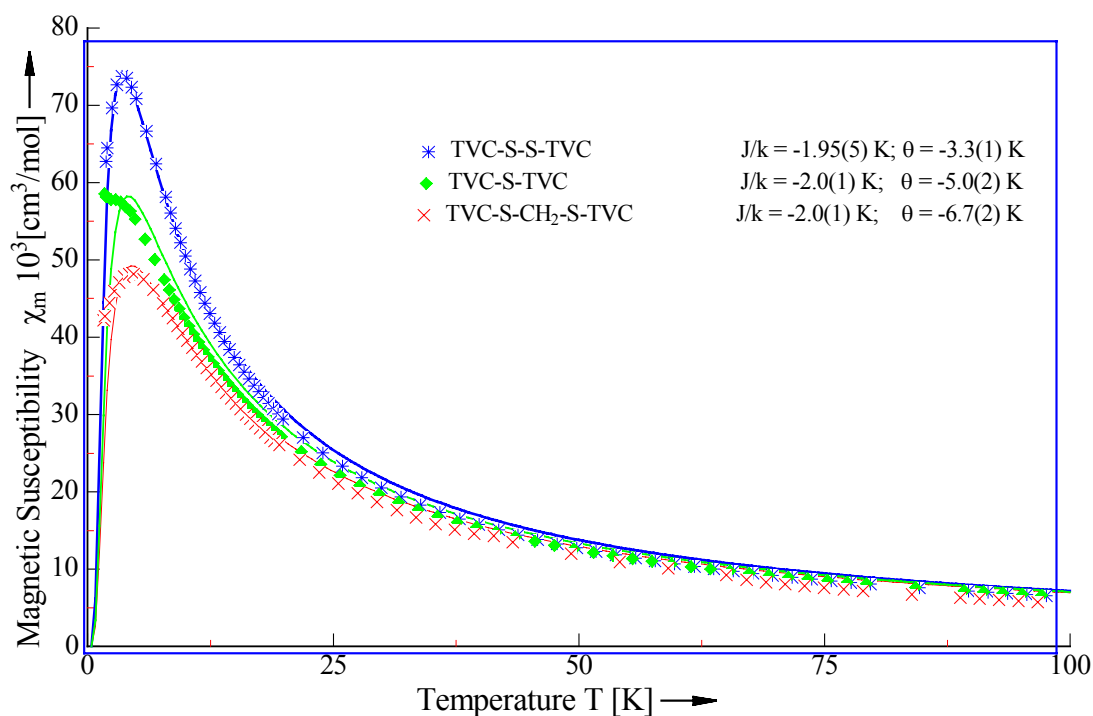
2.3.10. Synthesis of [5]Trovacenylthiol (21˙)

Two efficient and versatile methods have been performed to synthesize **21˙** (below). Previous work [56] also reported one tedious multiple-step method to prepare the analogous ferrocenylthiol. We had attempted to synthesize **21˙** according to it, but without obtaining characterized results.

Method **a**.
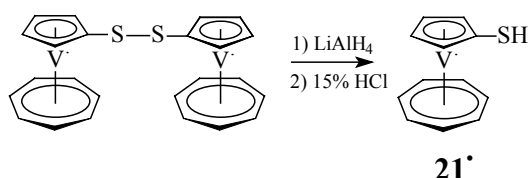
Method **b.**
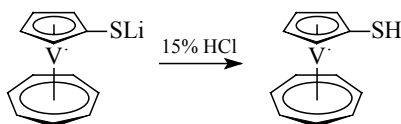
Method a) involves the reduction of **18˙˙** by LiAlH$_4$ in DME and subsequent hydrolysis by HCl (15%) to afford **21˙** as purple solid in quantitative yield. Method b) is making use of direct acidification of **19˙** with 15% HCl giving **21˙** in 45% yield. **21˙** is strongly air sensitive and it is very easy to oxidize and converted to disulfide **18˙˙**.
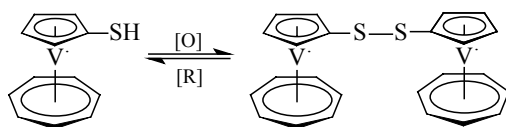
21˙ obtained according to the above described two methods are characterized by mass spectroscopy and elemental analysis. It has a good solubility in common organic solvent, such as PE and benzene, in contrast to the sulfide (**16˙˙**) and disulfide (**18˙˙**).

2.3.11. Results of Cyclic Voltammetry of 21˙

Cyclic voltammetry of **21˙** is shown in Figure 2.9, and the data are summarized in Table 2.11. Surprisingly, at -40 °C, two barely resolved oxidation and reduction peaks were observed, but at room temperature, only one broad coupled oxidation and reduction were obtained.

The oxidation potential (E$_{1/2}$(0/+) = 324mV) exhibits an anodic shift relative to trovacene (260mV), due to electron-withdrawing group SH directly linked to the cyclopentadienyl ring. This behavior is different from that of TVC-OH (vide infra). Wherein TVC-OH shows a

significant cathodic shift relative to trovacene because of the electron-donating effect of OH and intermolecular hydrogen bond. The second oxidation peak is at 470 mV and the corresponding reversible reduction peak is at 390 mV.

The first reduction ($E_{1/2}(0/-)$ = -2.494V) exists a slightly anodic shift relative to that of trovacene (-2.55V). On the contrary, the second reduction potential shows a cathodic shift. Assignment of the second reduction coupled peaks is yet uncertain. Therefore, it is obvious that the interaction between p_π electrons of SH and the π -system of the Cp ring will determine the electrochemical behavior of **21˙**.

Although the actual reason of the second oxidation and reduction waves are still unknown, a probable mechanism is proposed as following described. Due to its lability, **21˙** may convert to disulfide during the electrochemical process, in which the formed small amount of disulfide was measured by CV too. The comparison between the second oxidation (430mV) and reduction (-2.780V) potential of **21˙** and the corresponding redox potential (392mV, -2.840V) of **16¨** may provide a confident evidence.
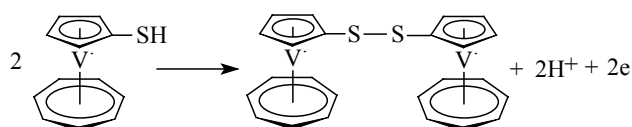
Table 2.11. Cyclic Voltammetry Data for **21˙**

	21˙
$E_{1/2}(0/+)$	324mV
ΔE_p	72mV
I_{pa}/I_{pc}	3.5
E_{pa1}	470mV
E_{pc1}	390mV
E_{pa2}	989mV
$E_{1/2}(0/-)$	-2.494V
ΔE_p	80mV
I_{pa}/I_{pc}	1
E_{pc2}	-2.834V
E_{pa3}	-2.734V

Figure 2.9. Cyclic voltammograms for **21**⋅ in DME/TBAP at -40°C, v = 100mV/s
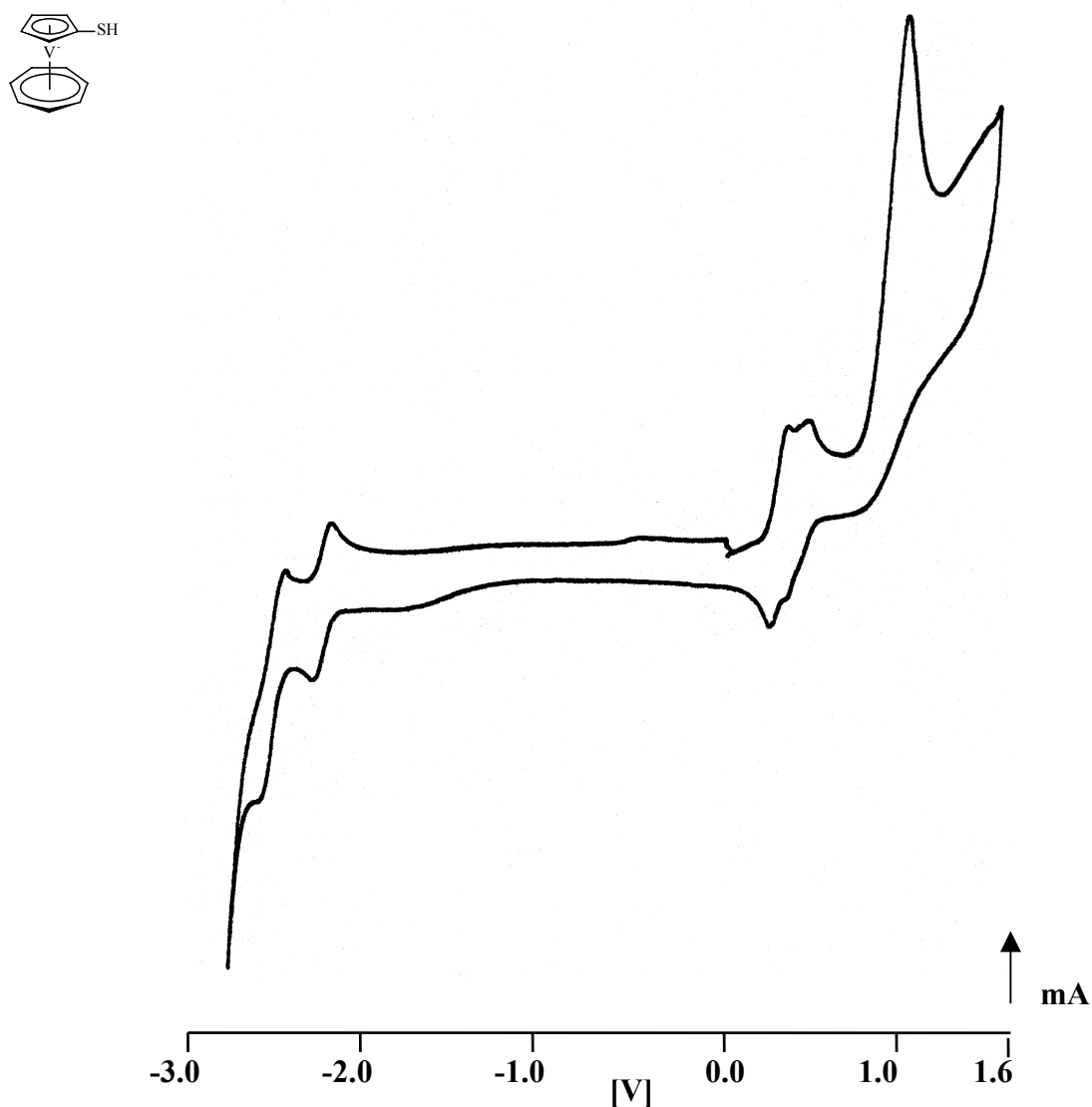
2.3.12. EPR Spectra (21⋅)

The EPR spectra of [5]trovacenylthiol (**21**⋅) in fluid and rigid solution (toluene) are depicted in Figure 2.10, and the parameters are summarized in Table 2.12.

The hyperfine pattern indicaties unpaired electron coupling to one vanadium nucleus, giving a typical monomer 8-line spectrum. The coupling constant ($A_{iso}(^{51}V)$ = 7.23 mT) is larger than that of trovacene.

Table 2.12. EPR Data of **21**⋅

$A(^{51}V)_{iso}$	g_{iso}	ΔB
7.23 mT	1.9841	1.2 mT

Figure 2.10. EPR spectra of **21˙** in fluid solution and rigid solution (toluene); A) experimental and B) simulated at 220K, ν = 9.2451GHz; C) experimental and D) simulated at 133K, ν = 9.2463GHz; experimental E) 295K, ν = 9.2452GHz; F) 260K, ν = 9.2445GHz.
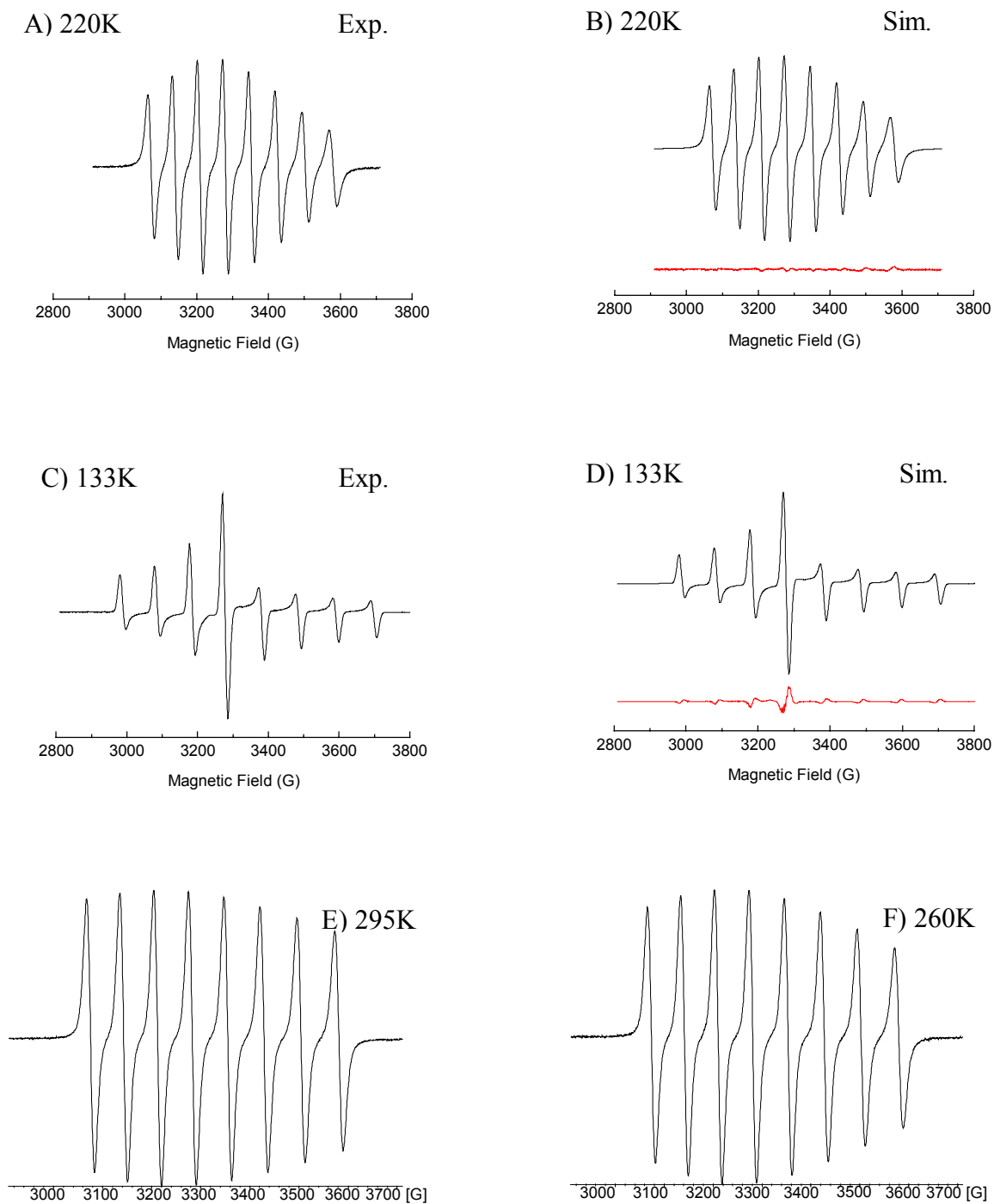
2.3.13. Lithium trovacenylthiolate (19˙)

2.3.13.1. Reactivity of trovacenylthiolate (19˙)

The reactivity of trovacenylthiolate (**19˙**) has already been demonstrated by the reaction with CH_2Cl_2. Furthermore, treatment of **19˙** with 14 group electrophiles, such as, Me_2SiCl_2, Me_2SnCl_2, Me_3SiCl, resulted in corresponding TVC-SSiMe$_3$ (**75˙˙**), (TVC-S)$_2$SiMe$_2$ (**79˙˙**) and (TVC-S)$_2$SnMe$_2$ (**24˙˙**), which have been characterized by mass spectra (EI) and/or unsatisfactory result of elemental analysis.

M = Si, **79˙˙**, Sn, **24˙˙**
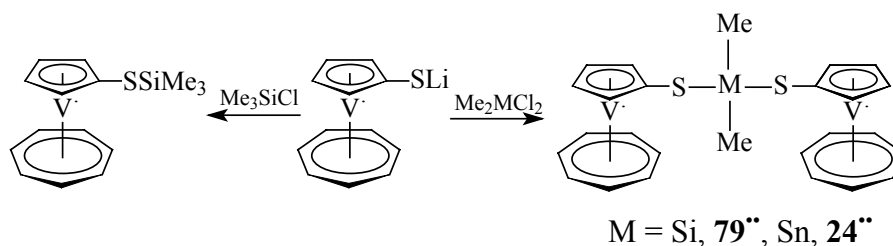
Treatment of **19˙** with group 15 electrophiles, PCl_3, $AsCl_3$, afforded uncertain pale-yellow solids, and no information of parent trovacene was observed from mass spectra. However, **19˙** reacted with heavier homologues $SbCl_3$ and $BiCl_3$ [57] to give corresponding green (TVC-S)$_3$Sb (**29˙˙˙**) and red-brown (TVC-S)$_3$Bi (**30˙˙˙**) in fair yield, which have been characterized by mass spectra and elemental analysis. It should be noted that the mass spectral results did not show the corresponding molecular ion peak, rather than a peak at 238 (TVC-S$^+$) as the basic peak intensity. Another method utilizing Bi[N(SiMe$_3$)$_2$]$_3$ to react with **20˙** have been attempted and given the same results as the reaction of **19˙** with $BiCl_3$.

29˙˙˙ has a good solubility in benzene and toluene. However, **30˙˙˙** only has a poor solubility in hot toluene, it can not dissolve in other common organic solvent, such as Et$_2$O, THF, PE, benzene. This character limits its purification. However, analogous M(EC$_6$H$_2$R′$_3$-2,4,6)$_3$ (M = Sb, Bi, E = S, Se, R′= Me, Pr^i, Bu^t) had been reported by Bochmann [58] and Sb(SC$_6$H$_2$R′$_3$-2,4,6)$_3$ had been characterized by X-ray diffraction.

21˙   **30˙˙˙**
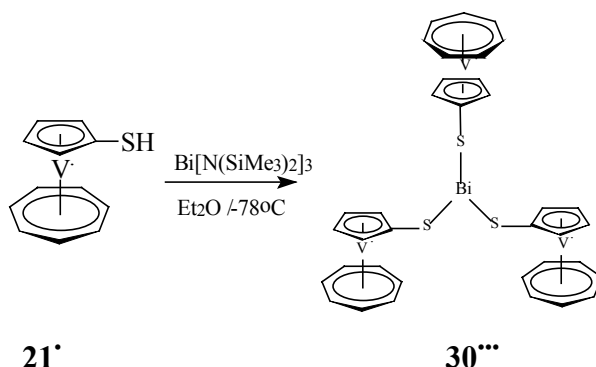
Treatment of **19˙** with different metal salts, for instance, $ZnCl_2$, $CoCl_2$, $PbCl_2$, $MoCl_4(CH_3CN)_2$, did not form the corresponding complexes as expected (TVC-S)$_n$M (n = 2, M= Zn, Pb, Co; n = 4, M = Mo), with exception of some dark brown or black powder which can not dissolve in general organic solvent, such as, DME, CH_3CN, toluene, DMSO, and water.
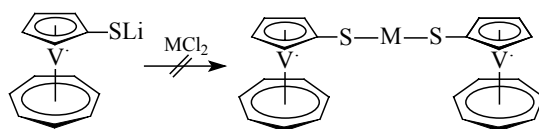
These dark brown or black powder was characterized to be of low carbon content by elemental analysis, it seems to be inorganic salts. Although sometimes, the result of mass spectra would show the signal of trovacene at 207/206 or TVC-S fragment at 238, after washed by organic solvent many times, these peaks would disappear and were replaced by a very small molecular peak at ~<50. However, an exception is the reaction of thiolate with $SnCl_2$, the molecular peak of expected $(TVC-S)_2Sn$ was observed (see experimental part), further isolation and studies have not been performed.

Therefore, in view of the formation of **18··** and **20··**, **19·** is a useful precursor for the synthesis of various trovacenylthiolate derivatives.

2.3.13.2. Synthesis of trovacenylthioether
(Benzyl([5]trovacenyl)thioether (22·), Methyl([5]trovacenyl)thioether) (23·)
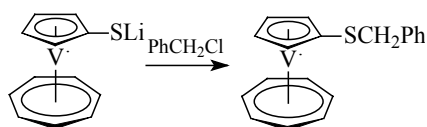
Two different methods have been performed to synthesize aryl- and alkyl- thioether. One way is to utilize **19·** which react with corresponding chloro-substituted reagents in DME. Here, the solvent plays an important role, if THF was used as solvent, **18··** was always the main product. Another route is lithiotrovacene as nucleophilic reagent to react with dialkyldisulfide, for example, **23·**.

23·
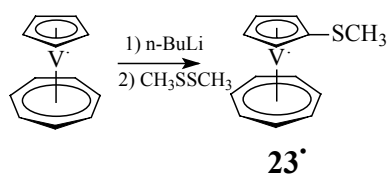
Both of the analytically pure **22·** and **23·** were obtained by chromatography (Al_2O_3) as violet solids in 40% and 36% yield, respectively, and characterized by mass spectra and elemental analysis. A good solubility in general organic solvent, such as PE and benzene, is their common property.

The main reason to prepare **23·**, is to synthesize the binuclear complex (**24··**) by the reaction of $(nbd)Mo(CO)_4$ with **23·**, according to the similar reported synthesis [59] and modified method as literature described,[60] and study the metal-metal interaction *via* S-Mo-S bridge. But no positive results from mass spectroscopy and chromatography (Al_2O_3) have been obtained.

SCH$_3$ (nbd)Mo(CO)$_4$ ⇸ PE, r.t or reflux Me S Me S Mo (CO)$_4$

80
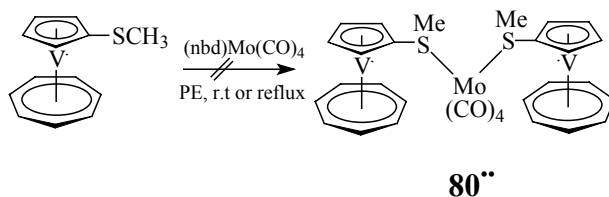
Recently, more attention has been directed to the synthesis of supermolecular ferrocenyl thiolates. For example, Sato [61] has reported that a metal-metal interaction between Fe atom and Pt(II)/Pd(II) center of tetrathia[5,5]ferrocenophane complexes (see below).

$$[\; \cdots \;]^{2+} \; (BF_4^-)_2$$

M = Pt, Pd
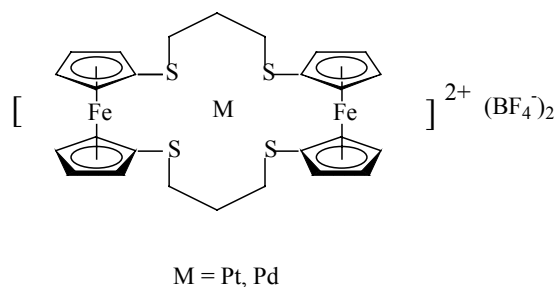
The interaction seems to be due to induced effect or the field effect of the Pt(II) or Pd(II) atom through the coordination of the S atom to the metal site. A small interaction between the two ferrocene units probably through the Pd(II) atom, has been inferred, according to the oxidation waves separation (redox splitting 130mV).

2.3.13.3 Results of Cyclic Voltammetry (22˙ and 23˙)

Figure 2.11 shows the cyclic voltammograms of **22˙** and **23˙**. The data are summarized in Table 2.13. Figure 2.11 exhibits an oxidation wave at 355mV with a large difference in reduction and oxidation peak potential (ΔE_p = 162mV), and with a significant anodic shift relative to TVC. Although in **22˙**, the phenyl group is distant from the trovacene moiety, and it exerts sufficient electron-withdrawal *via* the carbon and sulfur atoms. The σ-π hyperconjugation from the electron pair of S and π- system lead to an anodic shift. It is interesting to compare the results with TVC-Ph ($E_{1/2}(0/+)$ = 297 mV).[12]

Simultaneously, for **22˙**, two irreversible reduction peak potentials, at -2.394 V and -2.854 V, which did not display directly associated response in the reverse scan, were observed. This is different from other trovacenylthiolate complexes. The thioether did not decompose during the electrochemical measurements.

The aryl- thioether, **23˙** also shows a slightly anodic oxidation shift at 282 mV (ΔE_p = 152 mV) relative to TVC. It has been testified that the large difference in reduction and oxidation peak potential of **22˙** and **23˙** were not due to the uncompensated solution resistance.

One-electron reduction of **23˙** was observed at -2.438 V which is close to that of TVC, and greatly differ from the reduction of **22˙**. These behavior reveal that the SMe has a very little electron-withdrawing effect compared with that of SPh.

Figure 2.11. Cyclic voltammograms for **22˙** and **23˙** in DME/TBAP at -40°C, v = 100mV/s

22˙

23˙

↑ **mA**

| -2.9 | -2.0 | -1.0 | **[V]** | 0.0 | 1.0 | 1.6 |
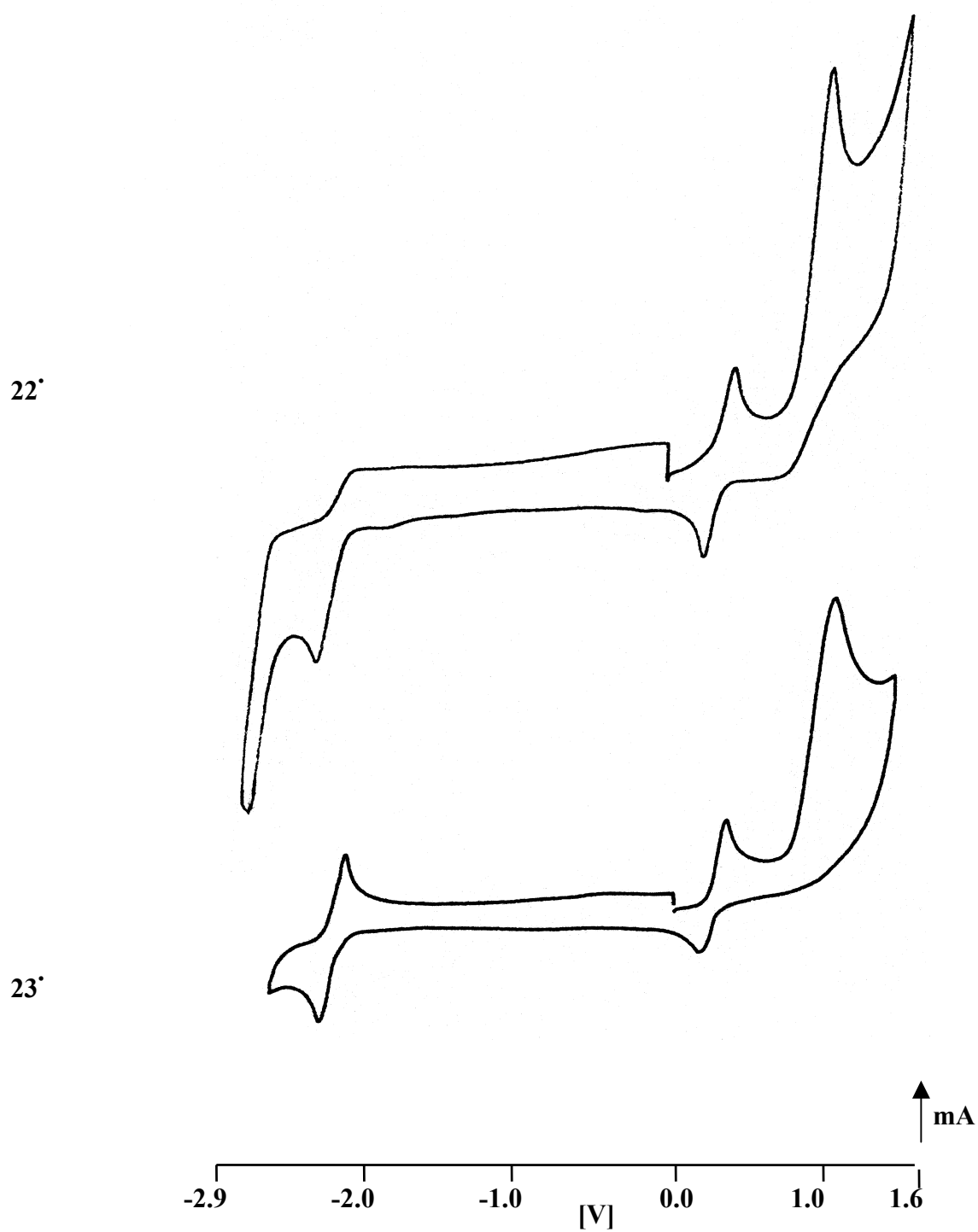
Table 2.13. Cyclic Voltammetry Data for **22·** and **23·**

	22·	**23·**
$E_{1/2}(0/+)$	355mV	282mV
ΔE_p	162 mV	152mV
I_{pa}/I_{pc}	0.92	0.52
$E_{1/2}(+/2+)$	1.036V	1.136V
$E_{1/2}(0/-)$		-2.438
ΔE_p		152mV
I_{pa}/I_{pc}		0.93
$E_{pc\ 1}$	-2.394V	
$E_{pc\ 2}$	-2.854V	

2.1.13.4. EPR Spectra (22·)

The EPR spectra of **22·** in fluid and rigid solution (toluene) are shown in Figure 2.12, and the parameters are exhibited in Table 2.14.

A typical monomer 8-line exists, along with a slightly large coupling constant ($a(^{51}V) = 71.87$ G) relative to the parent trovacene. Similar to its analog TVC-Ph, the electron-withdrawing character of SPh group and the p_π-d_π-p_π conjugation among cyclopentadienyl, S atom and phenyl should be responsible for the behavior. The rigid solution shows $A_\perp(^{51}V) = 100.82$ G and $A_\parallel(^{51}V) = 13.97$ G.

Figure 2.12. Experimental fluid solution (toluene) spectra of **22·**; (A) 295K, ν = 9.245936GHz, (B) experimental rigid solution (toluene) at 116K, ν = 9.24804GHz.

Table 2.14. EPR Data of **22·**

$\langle g \rangle$	$a(^{51}V)$	$A_\perp(^{51}V)$	$A_\parallel(^{51}V)$	$g_\perp$	$g_\parallel$
1.9905	7.187mT	100.82 G	13.97 G	1.9738	2.0239

2.4. Di([5]trovacenyl)diselenide (25··) and Di([5]trovacenyl)ditelluride (26··)

2.4.1. Synthesis

E = Se, **25··**; Te, **26··**
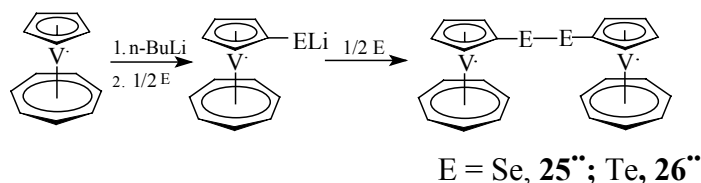
On the basis of the formation of **18··**, selenium or tellurium were used as the oxidzing reagents to yield the TVC-SeLi or TVC-TeLi, respectively, and afforded the expected diselenium - **25··**, or ditellurium - complex **26··**. This is the first report of the novel, simple, and effective method for synthesis of organometallic complexes REER (E = S, Se, Te) when R is sensitive to air.

Concentrated solution of lithiotrovacene in Et_2O reacted with half stoichiometric amounts of elemental selenium powder at ambient temperature for 3h (-20°/1h; 0°/1h; r.t./1h) to afford $(C_7H_7)V(C_5H_4SeLi)$. Then another half equiv. selenium was added. After stirred at r.t. overnight, a large amount of pale green precipitate - the crude product was formed. The analytically pure **25··** was obtained by column chromatography (Al_2O_3) eluted with THF as green solid in moderate yield (34%).

The synthesis of **26··** is similar to that of **25··** as described above. The only exception is that: after addition of second half equiv. elemental tellurium powder and stirred overnight, almost no precipitate was formed, except small amount of unreacted tellurium powder as black solid. Thus, another half equiv. sulfur powder was added to the red-violet suspension and stirred at r.t. overnight again. Then much pale yellow-green precipitate was formed. Analytically pure **26··** was obtained as yellow-green powder in 44% yield after recrystallization. The weak oxidation ability of Te relative to S and Se was probably responsible for the synthesis of **26··**. Based on the result of EI-MS, S did not insert into the Te-Li bonds to give TVC-Te-S-Te-CVT.
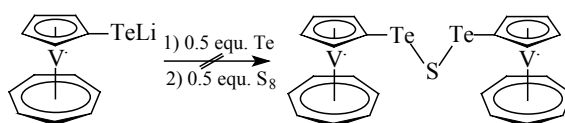
Herberhold[37a] had reported that E (E=S, Se, Te) was inserted into Te-Li bonds to give $Fe(C_5HeTe)_2E$ (E=S, Se, Te) in air with the excess of chalcogen E (S, Se, Te).

E = S, Se, Te

43
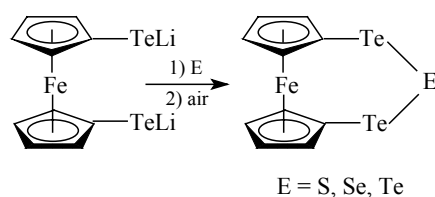
Similar to the synthesis of **18**$^{\cdot\cdot}$, the solvent, Et$_2$O, also plays an important role. The addition of selenium or tellurium in portions is another key process. **25**$^{\cdot\cdot}$ and **26**$^{\cdot\cdot}$ have been characterized by mass spectra and elemental analysis. Both of them have good solubility in polar solvent.

2.4.2. Results of Cyclic Voltammetry

The electrochemistry of **25**$^{\cdot\cdot}$ and **26**$^{\cdot\cdot}$ are illustrated in Figure 2.13, and the results are summarized in Table 2.15.

According to the cyclic voltammograms, both of **25**$^{\cdot\cdot}$ and **26**$^{\cdot\cdot}$ undergo a two-electron oxidation at 382 mV and 358 mV, respectively. Similar to disulfide, the large ΔE_p indicates that the overlap of the two one-electron oxidation waves and a small redox splitting ($\Delta E_{1/2}(0/+)(+/2+) \leq 70mV$). Significant anodic shifts relative to parent TVC were observed. Comparing to that of disulfide **18**$^{\cdot\cdot}$, with the increase of the atomic numbers or atom radii, S < Se < Te, or with decrease of the electronic polarity, the anodic shifts are slightly decreasing ranging from 392 mV to 382mV and 358 mV. This indicates that the electron - withdrawal effect decrease, on the other hand, the ease of oxidation increases with the atom radii increasing.

Similar to the reduction of **18**$^{\cdot\cdot}$, **25**$^{\cdot\cdot}$ and **26**$^{\cdot\cdot}$ also present a reversible two-electron reduction at -2.778 V and -2.718 V, respectively, because the ratios of the wave height of oxidation to reduction is close 1:1. The same trend of reduction was observed for oxidation: $E_{1/2}(0/2\text{-})_{TeTe} < E_{1/2}(0/2\text{-})_{SeSe} < E_{1/2}(0/2\text{-})_{SS}$ (Figure 2.14).

Figure 2.14. Redox potential of **18**$^{\cdot\cdot}$, **25**$^{\cdot\cdot}$ and **26**$^{\cdot\cdot}$
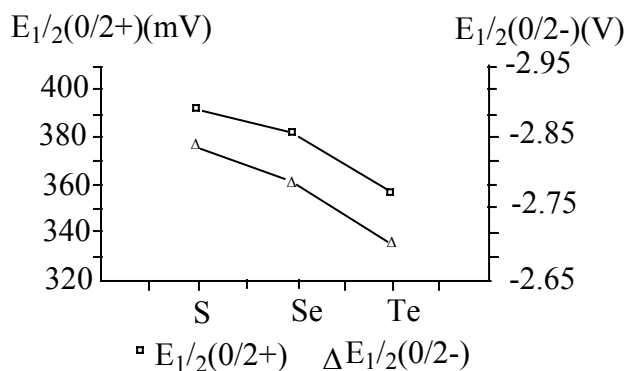
Due to the identical reason with **18**$^{\cdot\cdot}$, a large cathodic shift was exhibited relative to trovacene. With the radius of chalcogen atom increase, and the length of C-Se (C-Te) and Se-Se (Te-Te) bond increase, the distance between metal centers increase. The lone electron pair of the two chalcogen atom bridge (E-E) and electron-withdrawing effect contributes to the significant cathodic shift. The relatively long C-Se (C-Te) and Se-Se (Te-Te) bonds might eliminate the metal-metal interaction either through bond or through space.

On the contrary, the voltammogram of analog FcSeSeFc [62, 37e, 37f] showed a redox splitting of 0.14 V, similar to FcSeFc (0.22 V), the metal-metal interaction was most likely due to inductive (σ bond) effects, in which the more polarizable selenium transmits more efficiently. It has been reported that diferrocenyldichalcogenide complexes behaved as communicating sites to exhibit two separate one-electron oxidations.[37c]

Therefore, it is suggested that, for trovacene units, dichalcogen bridges substantially quench the interaction between the trovacene moiety, this limits the use of an effective transmitting bridge enabling the interaction between two redox centers.

Figure 2.13. Cyclic voltammograms for **25··** and **26··** in DME/TBAP at -40°C, v = 100mV/s
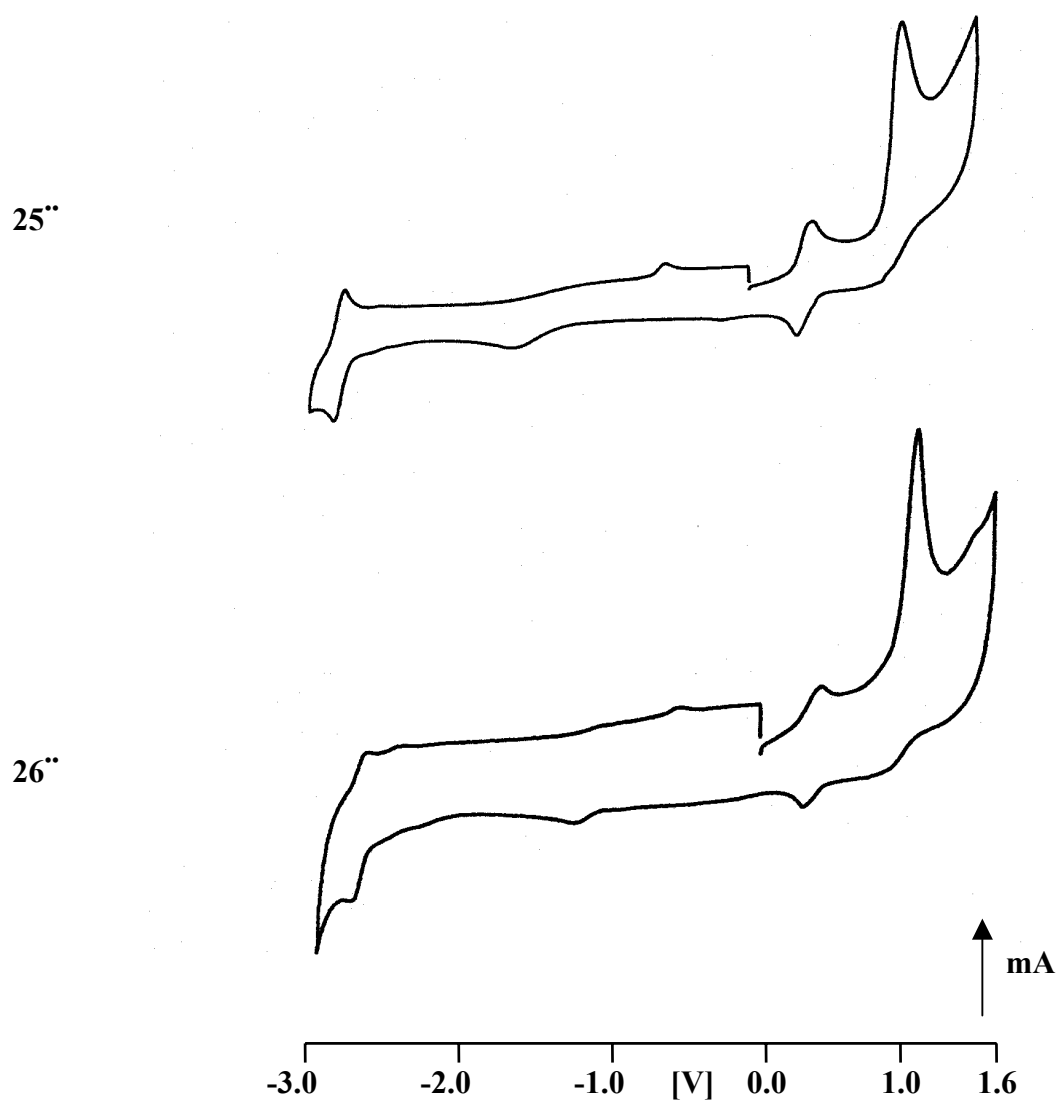
Table 2.15. Cyclic Voltammetry Data of **25**[¨] and **26**[¨]

	25[¨]	**26**[¨]
$E_{1/2}(0/2+)$	382 mV	358 mV
ΔE_p	120 mV	76 mV
I_{pa}/I_{pc}	0.9	1
$\Delta E_{1/2}(0/+)(+/2+)$	≤ 70mV	≤ 70mV
$E_{1/2}(2+/3+)$	1.086 V	1.046 V
$E_{1/2}(0/2-)$	-2.778 V	-2.717 V
ΔE_p	86 mV	78 mV
I_{pa}/I_{pc}	0.9	1

2.5. [5]Trovacenol (28[˙])

2.5.1. Introduction

It is well known that covalent linkage between donor and acceptor units plays a key role in the electron transfer process, however, in recent years, many researchers have testified that hydrogen-bonded linkage is another important way for ET,[6a] in particular in the biological electron transfer processes, for example, photosynthesis.[63]

The hydrogen bond (2-10 kcal/mol) can act as an efficient channel for the electron transfer from donor to acceptor. The studies of the interaction via hydrogen bonds could offer constructive suggestions to learn about the electron transfer process in biological systems. For example, Branda [64] reported the controlled photo-induced electron transfer within a hydrogen-bonded porphyrin-phenoxynaphthacenequinone photochromic system, in which light energy works as the regulatory stimulus (below).

trans-isomer
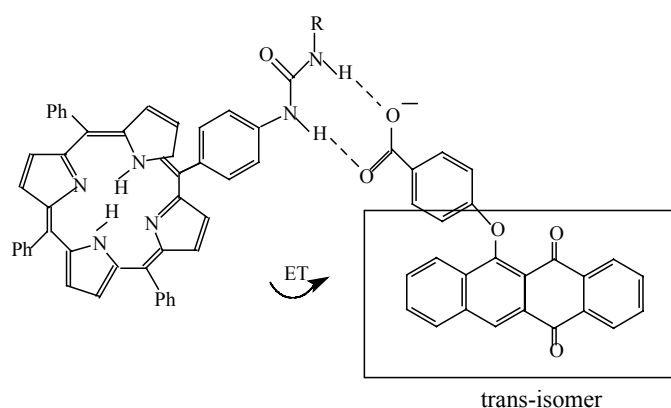
According to Marcus theory [65] for nonadiabatic electron transfer of weakly interacting D-A systems, Gopidas [66] has systematically studied the dependence of the rate constant of electron transfer (k_{et}) on the free energy ($\Delta G°$) in hydrogen bond systems.

$$k_{et} = (\pi / h^2 \lambda k_B T)^{1/2} | H_{el} |^2 \exp [-(\Delta G° + \lambda)^2 / 4 \lambda k_b T]$$

h: Planck´s constant divided by 2π, λ: the reorganization energy,
k_B: Boltzmann constant, T: temperature, H_{el}: the coupling matrix element

46

However, for organometallic species, there are few reports about inter or intramolecular interactions between two redox centers via hydrogen bonds (below).[6a]

31   **32**
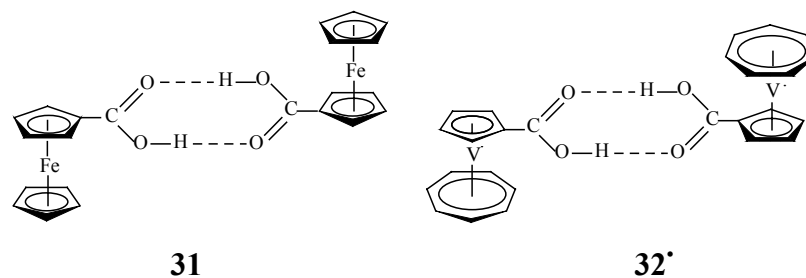
Hydroxymetallocene, in which oxygen atom links directly to the cyclopentadienyl ring, is incompletely studied (below **33**, **34**,[69] **35** and **36** [70]), because of the low stability and tedious multi-step synthesis. In most cases, Cp-ring substituted complexes are obtained by the reaction of lithiometallocene with electrophile, such as alkyl halide. But this approach is not very successful for the synthesis of amino- or hydroxy- metallocene by the reaction of lithiometallocene with oxygen, nitrogen or electrophilic synthons R_2N^+, RO^+.

33   **34**

35   **36**
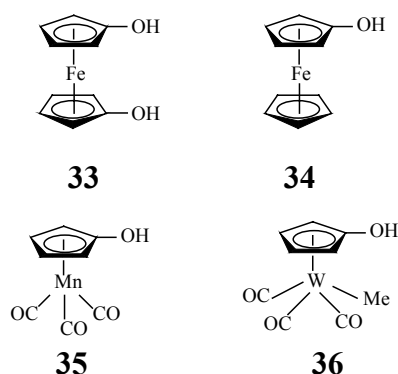
Thus, until now, there are still no convenient methods available. In earlier days, A. N Nesmeyanov et al.[67] had reported the formation of hydroxyferrocene via the reaction of $FcB(OH)_2$ with $Cu(OAc)_2$ and following steps. This method can not be used as a facile way to synthesize other analogues. Fortunately, two other methods have been reported recently. For example, the reaction of cyclopentenones with trialkylsilyltrifluoromethanesulfonic acid esters afforded the corresponding cyclopentadienyl silyl ethers. It was converted easily to the respective ferrocenylsilyl ethers by Plenio et al.[68].
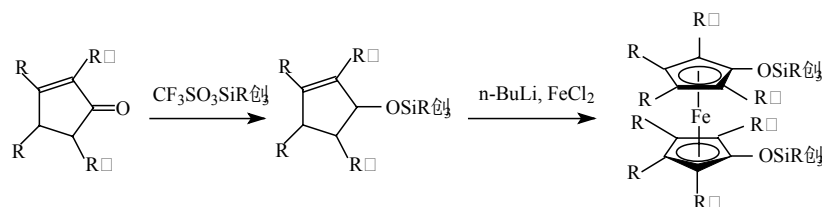
Or, reaction of lithioferrocene with bis(trimethylsilyl)peroxide resulted in hydroxyferrocene.[69] Both ways utilize the silyl protecting group which can be removed easily, but the choice of the silyl protecting group had to be noted, because the stability of silyl ethers crucially depends on the steric demand of the alkyl group ($-SiMe_3 < -SiEt_3 < -SitBuMe_2 < -SiPr_3$).

2.5.2. Synthesis of [5]trovacenol (28˙)

27˙   **28˙**
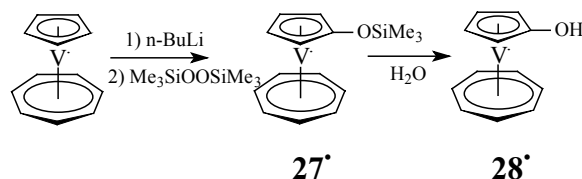
Bis(trimethylsilyl)peroxide was added dropwise to the solution of lithiotrovacene at -78°C over 3h and the mixture was warmed slowly to room temperature with vigorously stirring overnight. Then H_2O was added to the formed red-violet solution, the organic phase was separated, dried by $MgSO_4$, and evaporated. The residue was chromatographied (Al_2O_3, elution with ethanol) to give analytically pure **28˙** as red violet solid in low yield (5%). Recrystallization from benzene/PE at 8°C gave the crystals suitable for X-ray diffraction, together with small amount of uncharacterized pale-yellow powder. It should be mentioned that all the manipulation should be performed at 0°C due to thermal lability.

The formed crucial intermediate, silyl ether **27˙**, had been isolated only once by chromatography (Al_2O_3) as pale violet solid which was characterized by mass spectra and elemental analysis. Unfortunately, repeated effort was not successful. This may be due to its strongly thermal lability: most of them might decompose in the column during the isolation. Therefore, it is not necessary to purify the intermediate silyl ether, the reaction mixture of **27˙** was utilized directly for the followed procedure without purification.

In solid state, **28˙** is to some degree stable at low temperature; but in solution, it is fairly unstable. It would decompose slowly to result in pale yellow powder in spite of low temperature. Additionally, it may be due to the strong polarity of -OH substituted group, strong polar solvent was used to eluted it from the Al_2O_3 column. The limitation of the formation of large amount of **28˙** comes from the unstable property of reactant and product. The $Me_3SiOOSiMe_3$ reagent, must be freshly synthesized. Although n-Bu$_4$NF.3H$_2$O [70] was reported to cleave the silyl ether group, it was found that water can also work well.
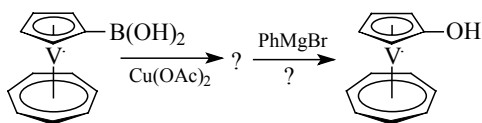
In addition, we have attempted to make use of the method described by A. N Nesmeyanov to synthesize **28˙**. Unfortunately, no satisfactory result could be obtained. Purple TVC-B(OH)$_2$ [71] reacted with $Cu(OAc)_2$ in EtOH/H_2O to result in large amount of brown precipitate which further reacted with PhMgBr. At last, more complex components were obtained above on the result of EI-MS.

2.5.3. Results of Cyclic Voltammetry (28˙)

Figure 2.15 shows the cyclic voltammogram of **28˙**, and the data are summarized in Table 2.16. The oxidation at 153 mV (ΔE_p = 116 mV) is similar to other trovacenyl derivatives with a one-electron oxidation. It is obvious that the OH group is an electron-donating substituent. It

is responsible for the cathodic shift of about 100 mV relative to its parent TVC. The delocalization through intermolecular hydrogen bond should not be neglected. The large separation between oxidation and reduction peak could not be reduced by compensation solution resistance.

Only one reduction peak could be observed at -2.2026 V which showed a more anodic shift relative to trovacene. This may be attributed to the strong electron-donating of OH group or probable decomposition during the process.

The sensitivity to air and temperature and instability in solid / solution of **28·**, especially in solution, may be the determined factor for the electrochemically irreversibility.
Until now, there are still no reported literature available about the electrochemistry studies of related hydroxymetallocenes.

Table 2.16. Cyclic Voltammetry Data for **28·**

$E_{1/2}(0/+)$	ΔE_p	I_{pa}/I_{pc}	$E_{pa}(+/2+)$	$E_{pc}(0/-)$
153 mV	116mV	0.9	890mV	-2.206V

Figure 2.15. Cyclic voltammograms for **28·** in DME/TBAP at -40°C, v = 100mV/s
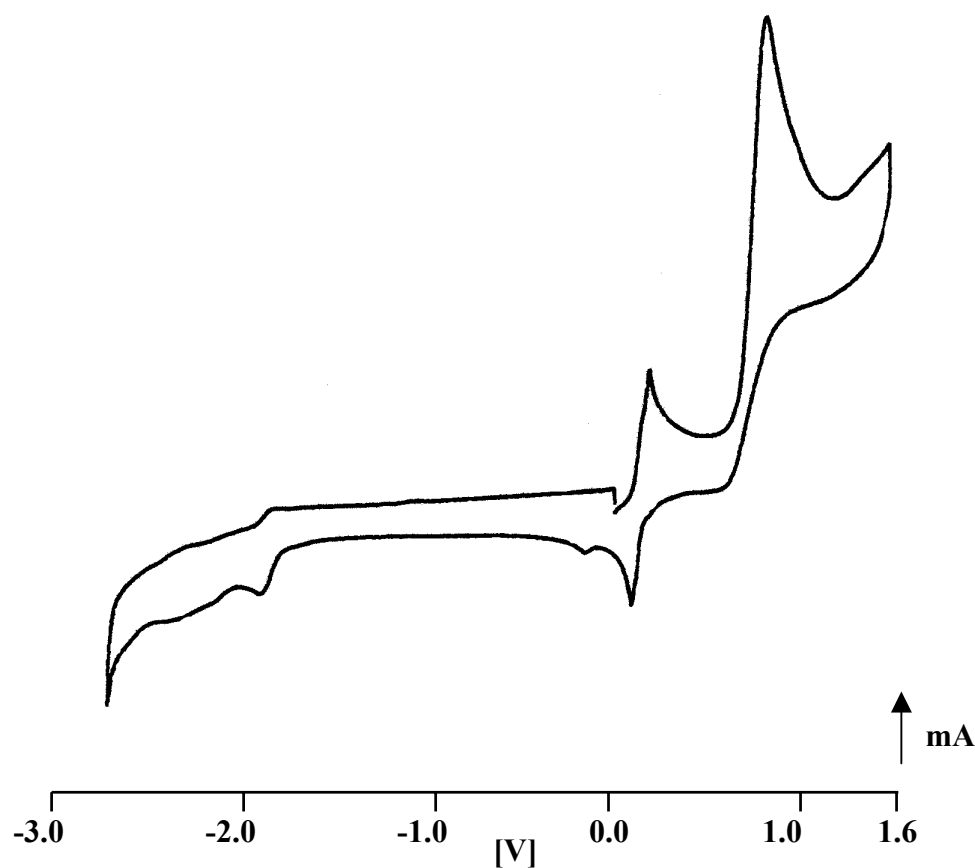
2.5.4. X-ray Crystal Structure Analysis

Compound **28˙** is structurally characterized by X-ray crystallography, and the molecular structure is shown in Figure 2.16. Selected bonds and angles are exhibited in Table 2.17, and 2.18. The orthorhombic disposition is encountered (α=90°, β=90°, γ=90°). The intermolecular hydrogen-bond apparently lead to the linear and layer structure. The neighboring two Cp rings linked by hydrogen bond are almost coplanar with a angle of 0.8(6)°.

The axes of two sandwiches are nearly parallel with a metal-metal distance of 6.59 Å, which is shorter than that of trovacenylcarboxylic acid (10.10 Å) dimmer via hydrogen bond.
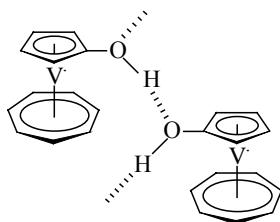
The distances O-H, H¨O and O-H¨O are similar to those of carboxylic acid dimmer. The bond length of C(1) - O(1) and C(1´) - O(1´A) are 1.407(12) and 1.83(4) Å, respectively. The linear zigzag staggered conformation via the hydrogen bond and the typically layer structure are the significant character, the stereoview plot of the X-ray structural analysis reflect these.

Table 2.17. Selected bond lengths [Å] of **28˙**

C(1) - O(1)	1.407(12)	V(1) - C(6)	2.173(8)
C(1´) - O(1´A)	1.83(4)	V(1) - C(7)	2.166(6)
O(1) - H(1)	0.4890	V(1) - C(8)	2.170(9)
V(1) - C(1)	2.281(9)	V(1) - C(9)	2.152(11)
V(1) - C(2)	2.261(7)	V(1) - C(10)	2.208(11)
V(1) - C(3)	2.246(10)	V(1) - C(11)	2.151(14)
V(1) - C(4)	2.249(7)	V(1) - C(12)	2.194(11)
V(1) - C(5)	2.275(7)	**V(1)-C$_7$ Ring (mean)**	2.173(10)
V(1)-C$_5$ Ring (mean)	2.262(8)	C(6) - C(7)	1.411(17)
C(1) - C(2)	1.429(15)	C(6) - C(12)	1.417(15)
C(1) - C(5)	1.391(13)	C(7) - C(8)	1.403(18)
C(2) - C(3)	1.366(15)	C(8) - C(9)	1.420(15)
C(3) - C(4)	1.406(13)	C(9) - C(10)	1.378(17)
C(4) - C(5)	1.379(9)	C(10) - C(11)	1.390(13)
O(1)-H(1)¨O(1´)	2.8895	O(1´)-H(1´)¨O(1)	2.9554
C-C (mean for C$_5$)	1.394(13)	C(11) - C(12)	1.379(16)
V(1) - V(2)	6.5902(13)	**C-C (mean for C$_7$)**	1.400(16)

Figure 2.16. Molecular structure and stereoview of **28**·
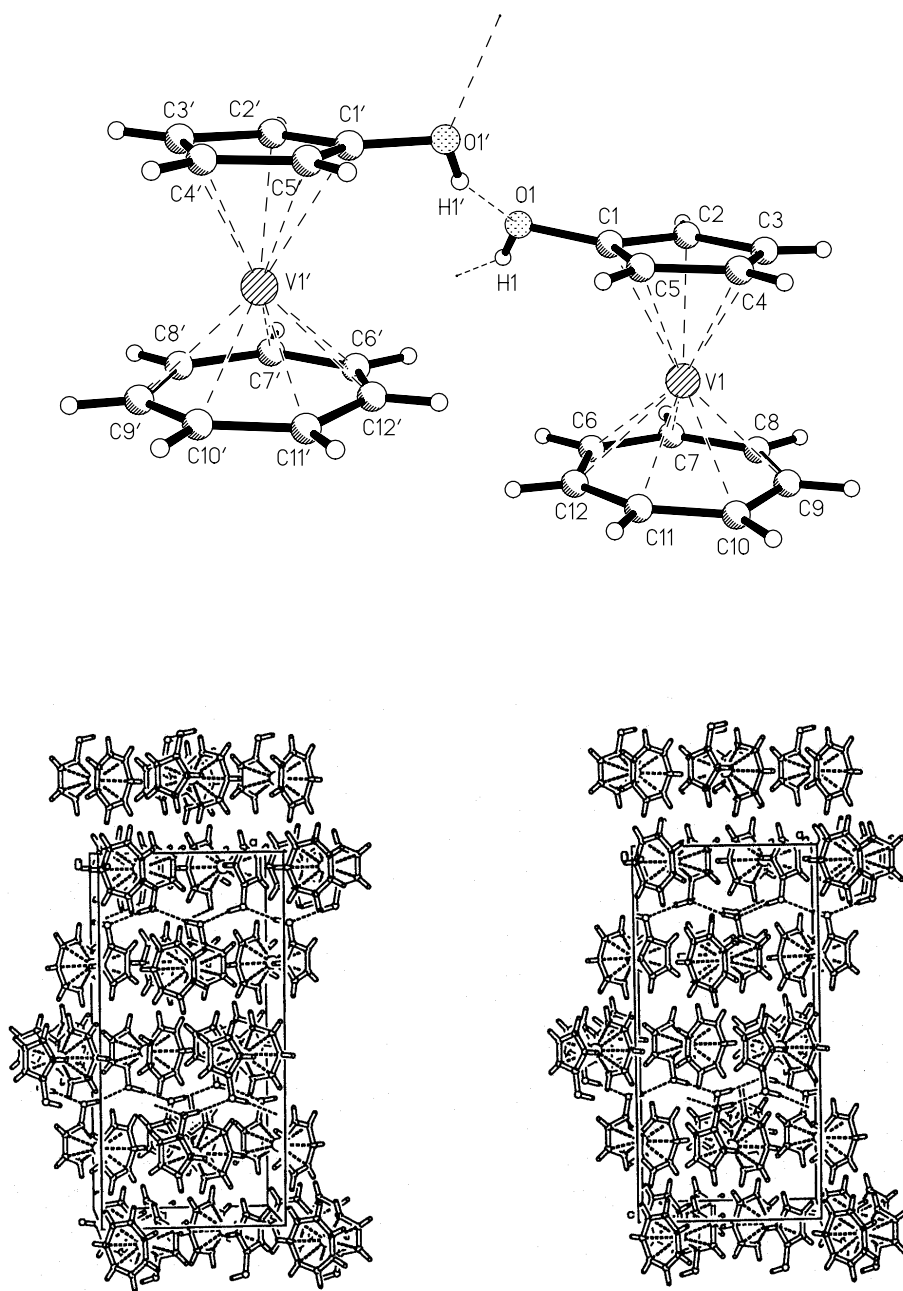
Table 2.18. Selected angles and torsion [°] of **28⋅**

O(1)-C(1)-C(2)	129.2(9)	O(1)-C(1)-C(5)-C(4)	-172.1(8)
C(5)-C(1)-O(1)	122.3(9)	O(1)-C(1)-C(2)-C(3)	172.2(9)
C(5)-C(1)-C(2)	108.1(8)	O(1)-C(1)-C(5)-O(1A)	9.5(11)
C(1)-O(1)-H(1)	109.5	C(2)-C(1)-C(5)-O(1A)	-177.0(4)
C(5)-O(1A)-H(1A)	109.5	C(2′)-C(1′)-C(5′)	108.0(9)
C(11)-C(12)-(6)	128.3(11)	**Torsion C₅ ring (mean)**	**0.1(7)**
O(1′)-C(1′)-C(2′)	130.1(11)	**Torsion C₇ ring (mean)**	**-.02(13)**

2.5.4 EPR Spectra (28⋅)

The EPR spectra of **28⋅** in fluid solution and rigid solution (toluene) are shown in Figure 2.17, and the parameters are summarized in Table 2.19 and 2.20.

An eight-line spectrum was obtained from **28⋅** in fluid solution with g_{iso} = 1.9835 and $A_{iso}(^{51}V)$ = 70.6 G, characteristic of monomers. Compared with the analog trovacenylthiol, the g_{iso} values are almost identical. This may be due to the intermolecular hydrogen-bond and the strong electron-donating group OH relative to SH group. In glassy solution, the parameters g_{xx} = 1.9733, g_{yy} = 1.9755, g_{zz} = 1.9956 and $A(^{51}V)_{xx}$ = 100.05G, $A(^{51}V)_{yy}$ = 100.65G, $A(^{51}V)_{zz}$ = 12.2 G can be obtained by computer simulation.

Figure 2.17. EPR spectra of **28⋅** in fluid solution (toluene) and rigid solution (toluene); A) experimental and B) simulated at 260K, ν = 9.2142GHz; C) experimental and D) simulated at 131K, ν = 9.2153GHz.

A) 260K   Exp.

B) 260K   Sim.
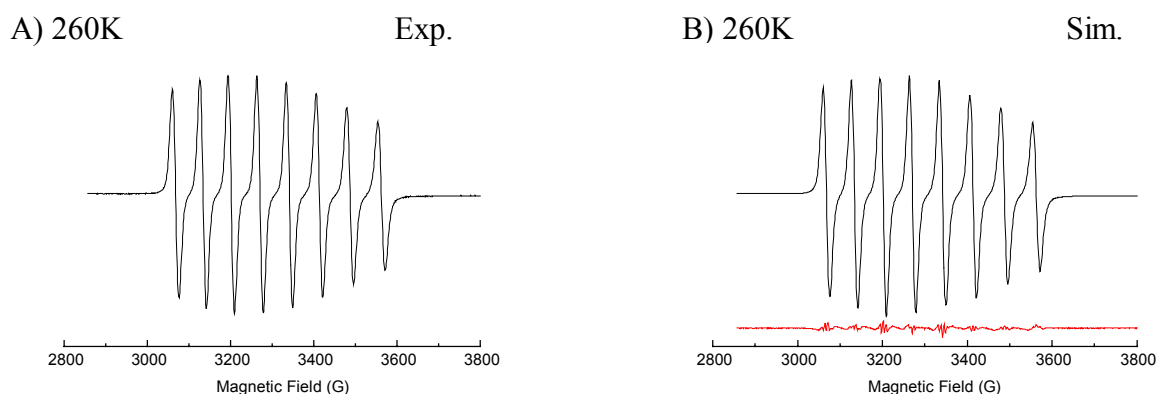
C) 131K Exp.
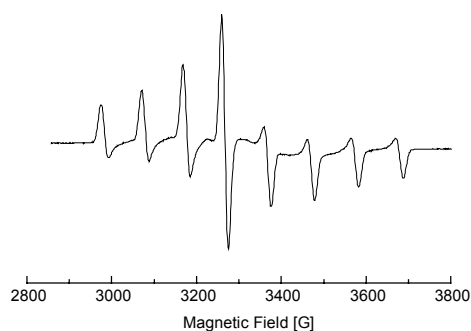
D) 131K Sim.
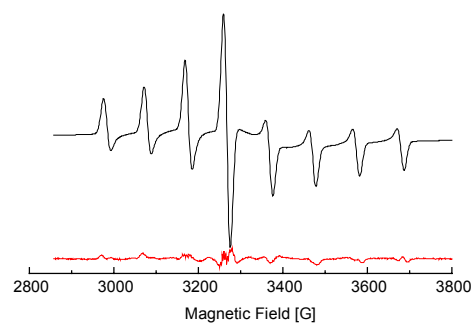
Table 2.19. EPR Data of **28**$^{\bullet}$ (fluid)

A(^{51}V)$_{iso}$	g$_{iso}$	α	β	γ	ΔB*
7.06 mT	1.9835	-0.63	2.25	-2×10^{-4}	9.1 G

*: Lorentzian

Table 2.20. EPR Data of **28**$^{\bullet}$ (rigid)

g$_{xx}$	g$_{yy}$	g$_{zz}$	A(^{51}V)$_{xx}$	A(^{51}V)$_{yy}$	A(^{51}V)$_{zz}$	ΔB*
1.9733	1.9755	1.9956	100.05 G	100.65 G	12.2 G	16.9 G

*: Gaussian

Unlike to TVC-COOH (**32**$^{\bullet}$), in which an equilibrium 2 **32**$^{\bullet}$ $\rightleftharpoons$ (**32**$^{\bullet}$)$_2$ caused by hydrogen bond is set up, due to the life time of the components of the association equilibrium exceeding to the EPR time scale, the EPR spectra of **28**$^{\bullet}$ did not give the superpostion of monomer and dimer. This suggests that the possible equilibrium 2 **28**$^{\bullet}$ $\rightleftharpoons$ (**28**$^{\bullet}$)$_2$ might not exceed the EPR time scale, thus, the predicted superposition could not be observed.

3. Group 15 Derivatives

3.1. Introduction

The metal-metal interaction of binuclear complexes in which `group 15 ` elements are utilized in the bridges to link two redox units, has been studied in recent years. It has been demonstrated that group 15 elements - 'electron rich' atoms, are efficient bridges for metal-metal interactions, for example, FcN=NFc, Fc_2PPh, Fc_3P [72]. Previous results of our group also gave some group 15 derivatives, e.g. diphenyl([5]trovacenyl)phosphorus (**37·**) and bis[(diphenylphosphano-η^5-cyclopentadienyl)(η^7-cycloheptatrienyl) vanadium] tetracarbonyl chromium (**38··**).[73] For **38··**, a fairly weak metal-metal interaction *via* P-Cr-P bridge was observed due to the long distance between the two metals. Recently, in order to study the intermolecular interaction *via* hydrogen bond of N-H···N, amino[5]trovacene (**39·**) and (dimethylamino)[5]trovacene (**40·**) were also synthesized.[74]
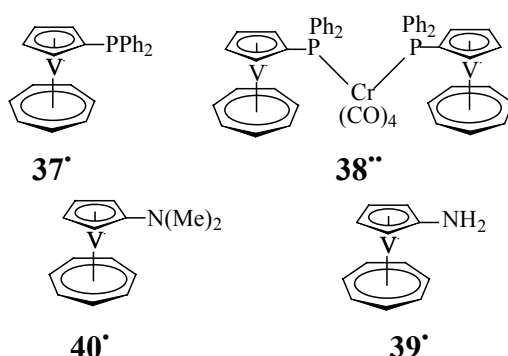
Therefore, in order to fully investigate the role of ´ group 15´ element bridges in the metal-metal interaction, several analogues have been synthesized and studied by CV, EPR. Since P has a strong electron-donating ability, the molecule in which single P element links the two trovacene units shows a relatively strong interaction. Simultaneously, various substituted As bridged binuclear complexes are synthesized and the different effects from various substituents to the metal-metal interaction have been investigated by CV.

3.2. Phosphane derivatives

3.2.1. Synthesis of di([5]trovacenyl)phenylphosphane (41··) and Tri([5]trovacenyl)phosphane (42···)
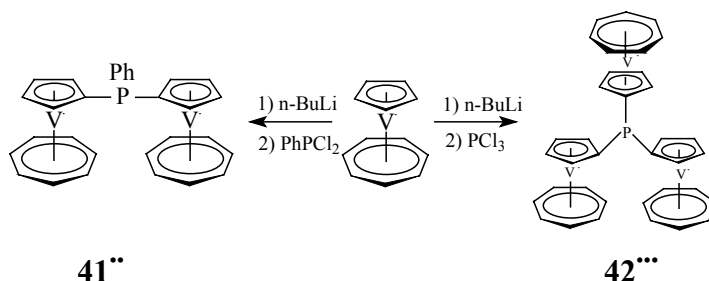
Reaction of lithiotrovacene with $PhPCl_2$ was performed at 0°C for 1h, then the mixture was warmed slowly to r.t. and stirred overnight to form a large amount of pale green precipitate, while the solution was violet in color. Filtration and recrystallization from THF/benzene/PE

gave pale green precipitate, although a molecular ion peak at 520 by EI-MS (70eV) was observed, the result of elemental analysis indicated that the pale green precipitate was not the expected product **41**$^{..}$, the further characterization had not been performed. Thus, the filtrate was brought to dryness *in vacuo*, then the residue was chromatographed (Al$_2$O$_3$, 2×30cm) and eluted with THF to give **41**$^{..}$ as purple solid in 36% yield. **41**$^{..}$ was characterized by mass spectroscopy, elemental analysis (see experimental part) and X-ray diffraction analysis. The crystals suitable for X-ray diffraction were generated from saturated benzene solution at 8°C within 24h. **41**$^{..}$ has a good solubility in common organic solvents.

Reaction of lithiotrovacene with stoichiometric PCl$_3$ at -40°C also afforded a large amount of pale green precipitate, but contrary to the reaction of lithiotrovacene with PhPCl$_2$, it was identified to be the excepted product tri([5]trovacenyl)phosphane **42**$^{...}$ by EI-MS (70eV), while the filtrate was identified to be TVC. Furthermore, despite excess PCl$_3$ was added to the solution of lithiotrovacene in Et$_2$O at -40°C, 0°C or r.t., it stilled formed large amount of pale green precipitate which was characterized not to be (TVC)$_3$P, (TVC)$_2$PCl or (TVC)PCl$_2$ by EI-MS, the further characterization was not performed.

Tri([5]trovacenyl)phosphane has a moderate solubility in CH$_2$Cl$_2$, THF, but it does not dissolve in many other general organic solvents, such as, PE, Et$_2$O, benzene, toluene etc.. This indicates that it is difficult to get analytically pure product by normal purification method. Although recrystallization can be utilized for purification, unsatisfactory elemental analysis always was obtained. **42**$^{...}$ is considerably air sensitive, and after exposure to air for few minutes, it was slightly oxidized to be pale blue in color which was not further identified. Lack of efficient isolation methods to give analytically pure samples limits our further attempts to investigate its properties by CV and EPR.

3.2.2. Results of Cyclic Voltammetry (41$^{..}$)

The electrochemical data of **41**$^{..}$ are summarized in Table 3.1, and Figure 3.1 shows the cyclic voltammogram of **41**$^{..}$. The first oxidation wave at 346mV is assigned to the two-electron oxidation ($E_{1/2}(0/2+)$), which is close to the value of $E_{1/2}(0/+)$ of **37**$^{.}$ (350 mV). The large peak separation (ΔE_p = 148mV) indicates that two successive one-electron oxidation with a small redox splitting ($\Delta E_{1/2}(0/+)(+/2+) \leq 70$mV) were overlapped. Two successive one-electron reduction peaks with a separation of 152 mV ($\Delta E_{1/2}(0/-)(-/2-)$) are observed. The large difference between the redox splitting ($\Delta E_{1/2}(0/+)(+/2+)$ and $\Delta E_{1/2}(0/-)(-/2-)$ can be attributed to the fact, the electron delocalization through the bridge P by a trovacenyl group is more pronounced for the radical anion compared to the radical cation in view of the expanded nature of the vanadium $V(3d_z^2)$ orbital in the former, compared to their contracted nature in the latter.

Compared to that of [5,5]bitrovacene **10**$^{..}$ (224mV), the metal - metal interaction of **41**$^{..}$ is slightly weaker. The redox splitting suggests a weak metal-metal interaction in the phosphorus bridged species. Because the P atom has a lone pair electrons, it can act as an electron-donor to influence the interaction between two metals, the conjugation between two cyclopentadienyl p_π. orbital through P may be the contributing factor.

Additionally, phenyl as an electron-accepting group linked to the P bridge also influence the distribution of electron density of the two redox centers.

Figure 3.1. Cyclic voltammograms for **41··** in DME/TBAP at -40°C, v = 100mV/s
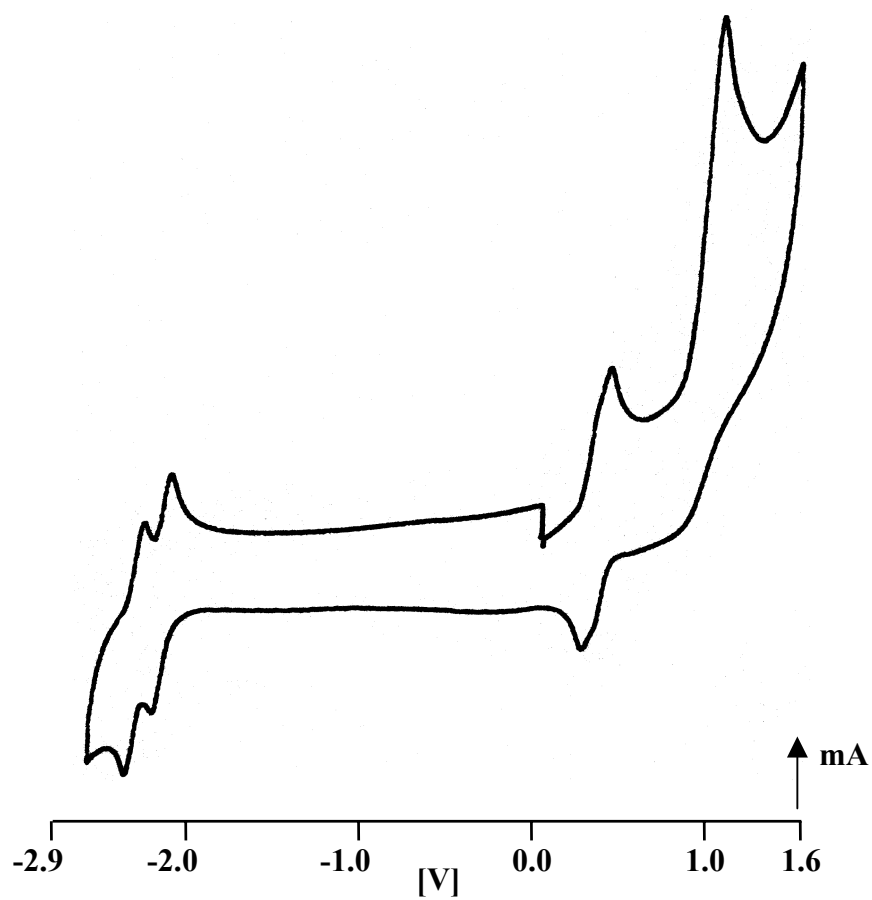
Table 3.1. Cyclic Voltammetry Data for **41··**

	41··
$E_{1/2}(0/2+)$	346 mV
ΔE_p	148 mV
I_{pa}/I_{pc}	1
$\Delta E_{1/2}(0/+)(+/2+)$	≤ 70mV
$E_{pa}(2+/3+)$	1.064 mV
$E_{1/2}(0/-)$	-2.445
ΔE_p	74 mV
I_{pa}/I_{pc}	1
$E_{1/2}(-/2-)$	-2.592 V
ΔE_p	82 mV
I_{pa}/I_{pc}	1
$\Delta E_{1/2}(0/-)(-/2-)$	152 mV

3.2.3. X-ray Crystal Structure Analysis of 41¨

The structure of **41¨** was confirmed by an X-ray diffraction analysis. Its crystal system is monoclinic and crystallize in the space group of $P2_1/n$ (Z=4). The molecular structure of **41¨** is shown in Figure 3.2, the selected bonds, angles and torsion are exhibited in Table 3.2 and 3.3, respectively. **41¨** adopts a distorted pyramidal geometry, in which P is linked to two TVC fragments and one phenyl group. The angles between P and linked carbon atoms, C(13)-P(1)-C(1), C(1)-P(1)-C(25) and C(13)-P(1)-C(25), are 98.69(8)°, 100.08(8)° and 102.21(8)°, respectively. Due to the steric hindrance, the axes of the two TVC moiety are not orthogonal.
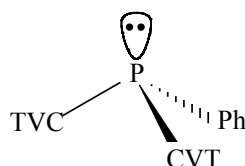
The dihedral angle between two Cp rings is 86.63(11)°, and the dihedrals between Ph and Cp rings are 75.72(10) and 65.98(11)°. The bond lengths of P-C are close to each other; P(1)-C(1) (1.8315(17)Å), P(1)-C(13) (1.8236(18)Å) and P(1)-C(25) (1.8374(17)Å), they are somewhat longer than that of TVC-PPh$_2$ (P-C$_{Cp}$, 1.812 Å, mean).[74] The bond C-C (Cp ring), 1.415(3) Å, is slightly longer than that of C-C (phenyl) (1.385(3)Å). The metal-metal distance is 6.4969(29)Å, which is longer than that of [5,5]bitrovacene (5.5009Å). The P atom is almost coplanar with respectively linked Cp ring, for example, the torsion angles of P(1)-C(13)-C(14)-C(15) and P(1)-C(1)-C(5)-C(4) are 174.36(14)° and 178.47(12)°, respectively.

Table 3.2. Selected bonds [Å] of **41¨**

P(1) - C(1)	1.8315(17)	V(1) - C(6)	2.171(2)
P(1) - C(13)	1.8236(18)	V(1) - C(7)	2.164(2)
P(1) - C(25)	1.8374(17)	V(1) - C(8)	2.160(2)
P(1) - C(mean)	1.8308(17)	V(1) - C(9)	2.179(2)
V(1) - C(1)	2.2734(16)	V(1) - C(10)	2.197(2)
V(1) - C(2)	2.2665(17)	V(1) - C(11)	2.198(2)
V(1) - C(3)	2.2527(19)	V(1) - C(12)	2.191(2)
V(1) - C(4)	2.2516(19)	**V(1)-C$_7$ Ring (mean)**	2.189(2)
V(1) - C(5)	2.2559(18)	**V(1)-C$_7$ (centroid)**	1.641(1)
V(1)-C$_5$ Ring (mean)	2.2600(18)	C(6) - C(7)	1.396(3)
V(1)-C$_5$ (centroid)	1.9129(9)	C(6) - C(12)	1.395(5)
C(1) - C(2)	1.417(3)	C(7) - C(8)	1.411(4)
C(1) - C(5)	1.419(3)	C(8) - C(9)	1.416(4)
C(2) - C(3)	1.413(3)	C(9) - C(10)	1.400(4)
C(3) - C(4)	1.407(3)	C(10) - C(11)	1.392(3)
C(4) - C(5)	1.418(3)	C(11) - C(12)	1.401(3)
C-C (mean for C$_5$)	1.415(3)	**C-C (mean for C$_7$)**	1.401(4)
C(25) - C(26)	1.393(3)	**V(1) - V(2)**	6.4969(29)
C(27) - C(28)	1.378(3)	C(26) - C(27)	1.382(3)
C(28) - C(29)	1.376(3)	C(29) - C(30)	1.386(3)
C(25) - C(30)	1.393(3)	**C-C (mean for C$_6$)**	1.385(3)

Figure 3.2. Molecular structure and stereoview of **41**¨
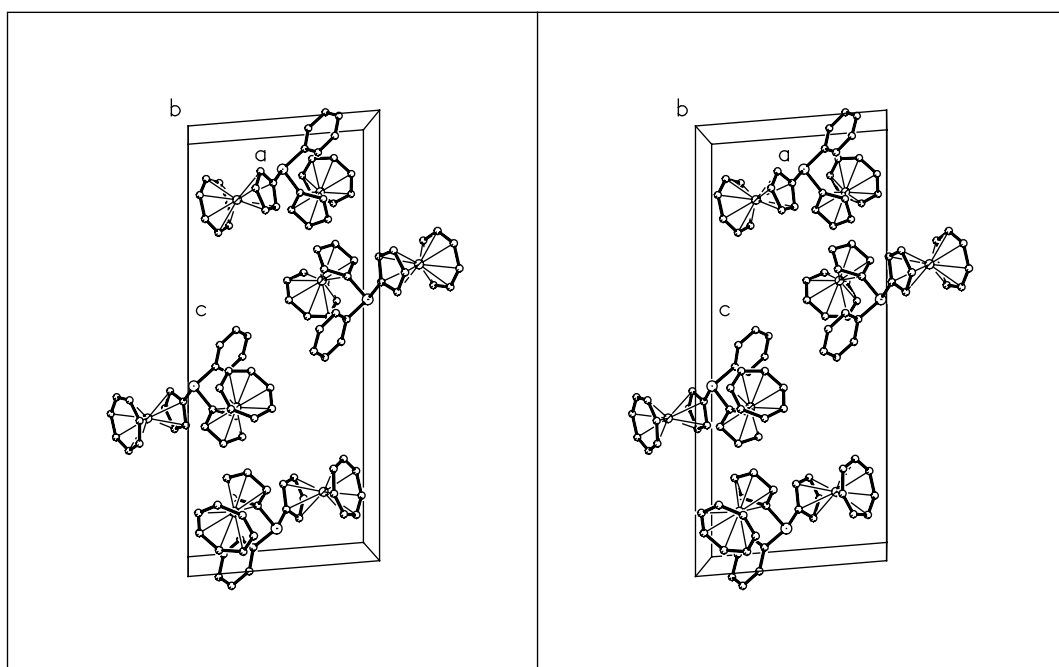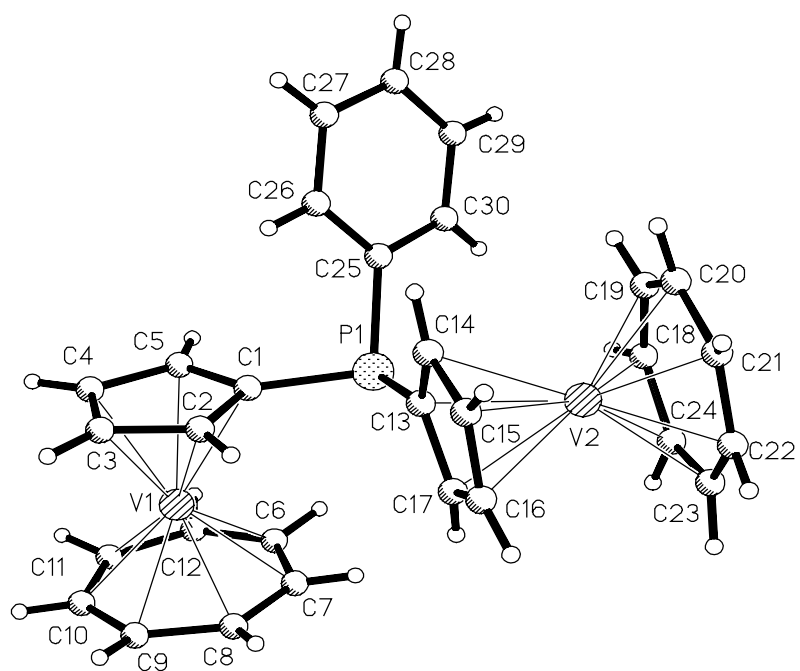
Table 3.3. Selected angles and torsion [°] of **41··**

C(13)-P(1)-C(1)	98.69(8)	C(1)-P(1)-C(25)-C(26)	27.59(17)
C(1)-P(1)-C(25)	100.08(8)	C(1)-P(1)-C(13)-C(14)	-80.95(17)
C(13)-P(1)-C(25)	102.21(8)	C(13)-P(1)-C(1)-C(2)	-9.55(16)
C(5)-C(1)-P(1)	124.68(14)	C(13)-P(1)-C(25)-C(26)	-73.69(16)
C(2)-C(1)-P(1)	128.06(13)	C(25)-P(1)-C(13)-C(14)	21.42(18)
C(14)-C(13)-P(1)	129.38(14)	C(25)-P(1)-C(1)-C(2)	-113.71(16)
C(17)-C(13)-P(1)	123.72(14)	P(1)-C(25)-C(26)-C(27)	-179.83(15)
C(17)-C(13)-C(14)	106.66(17)	P(1)-C(13)-C(14)-C(15)	174.36(14)
C(26)-C(25)-P(1)	123.74(13)	P(1)-C(13)-C(17)-C(16)	-174.61(13)
C(30)-C(25)-P(1)	117.92(14)	P(1)-C(1)-C(5)-C(4)	178.47(12)
C(30)-C(25)-C(26)	118.31	P(1)-C(1)-C(5)-C(2)	-9.55(16)
C(2)-C(1)-C(5)	107.23(15)	C(1)-P(1)-C(13)-C(17)	92.59(16)

3.2.4. EPR Spectra

Fluid solution spectra (toluene) of **41··** at 293K, 250K, and rigid solution spectra (toluene) at 128K are shown in Figure 3.3. The spectral parameters are summarized in Table 3.4.

41·· in fluid solution gives rise to a typical binuclear spectrum - 15-line hyperfine pattern, due to the strong electron-spin coupling of two ^{51}V nucleus. The line splitting is half the value of that of mono-nuclear parent trovacene ($a(^{51}V)$ = 6.98mT) and diphenyl(trovacenyl)phosphorus ($a(^{51}V)$ = 7.23mT).[74]

The exchange coupling constant J provided by computer simulation is ~30,000 G (2.8 cm^{-1}), which indicate that, |J|>>|a|. Compared to that of [5,5]bitrovacene, the P bridge does not remarkably attenuate metal - metal interaction. This behavior can be attributed to the unpaired electrons of P atom and the electron-accepting phenyl group linked to the P bridge. Additionally, the vacant 3d orbital of the P atom provides an opportunity to conjugate with the cyclopentadienyl π electrons, which is available for the exchange coupling between two metals. The $a(^{31}P)$ is near 5G provided by the computer spectral simulation.

The glassy solution spectrum of **41··** apparently shows many lines in the region g ≈ 2, it should be noted that a half-field signal ($\Delta M_s = 2$) could not be detected.

Table 3.4. EPR data of **41··**

$A(^{51}V)_{iso}$	g_{iso}	J	α	β	γ	ΔB	$A(^{31}P)_{iso}$
72.2	1.9838	30,000	-0.114	-0.129	0.023	25.2	5G

Figure 3.3. EPR spectra of **41**·· in fluid solution (toluene), A) experimental and B) simulated spectrum, ν = 9.2447GHz, 293K, C) experimental, ν = 9.2451GHz, 250K, and D) experimental rigid solution (toluene) spectra, ν = 9.2463GHz, 128K.
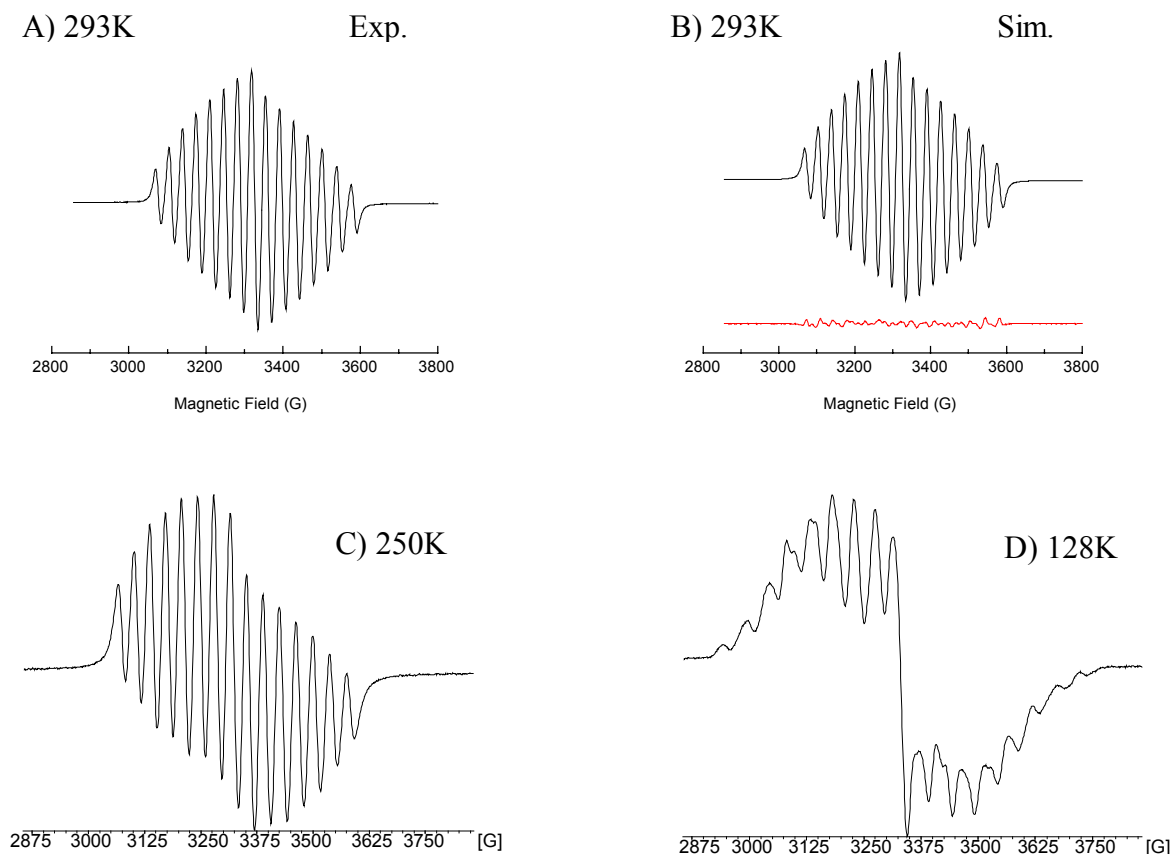
3.3. Arsane Derivatives

3.3.1. Introduction

Currently, arsane bridged binuclear complexes have been poorly studied, and the role of arsane linkage to the intramolecular communication between redox centers is still unclear. Herein, we describe the synthesis of arsane bridged complexes and the various As bridge substituted species and their impact on the electron communication.

Hydrogen bonded linkage[75] and non-bonded linkage[76] have been also reported to be involved in the electron transfer process. For example, Warldeck and co-workers[77] recently provided quantitative evidence that the electronic coupling through non-bonded moieties can compete effectively with covalent linkages, when the mediating moiety lies between the electron donor and acceptor groups.

In addition to the nature of the bridge and the distance between two redox centers, the inductive effect (or Push-Pull effect) and super-exchange mechanism of various substituents linked to the bridging atom would also give some hints to interpret the efficient electron transfer (ET).

Herein, the Cl substituted complex (**43""**) acts as an ideal precursor. It offers a valuable opportunity, because it can be converted easily to other substituted complexes, such as (TVC)$_2$As(OH), (TVC)$_2$As(H), etc.. We choose different substituted groups, H, Cl, n-Bu, OH, to investigate how electron withdrawing or electron donating groups impact on the interaction between metals.
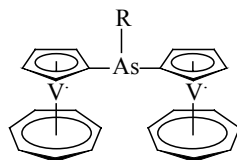
R = Cl, **43""**; n-Bu, **44""**; H, **45""**; OH, **46"**

It is worth noting that di([5]trovacenyl)arsinous acid **46"** is a considerably interesting compound, because probably intermolecular interaction - hydrogen bonding linkage and intramolecular interaction - covalent linkage between two trovacene units may exist together. Unfortunately, currently, **46"** and phenyl-substituted complex have not been investigated by CV, EPR or X-ray diffraction analysis due to the time constraints.

3.3.2. Reaction of lithiotrovacene with AsCl$_3$
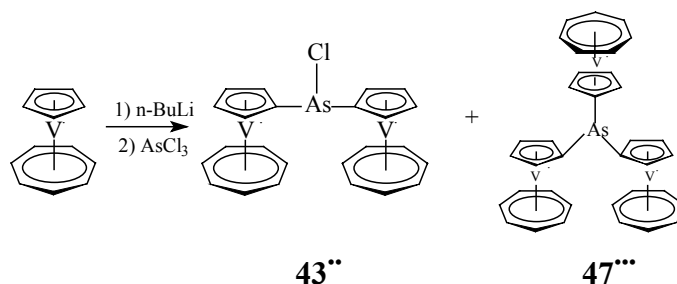
Reaction of lithiotrovacene with stoichiometric AsCl$_3$ at -40°C afforded tri([5]trovacenyl)arsine (**47"""**) as pale violet-red solid. When the reaction mixture was warmed to room temperature, plenty of pale green precipitate - di([5]trovacenyl)chlorarsine (**43"**) was formed. **43"** could be separated from the mixed precipitate by extraction with benzene, filtration and recrystallization. PE was added carefully to the concentrated green benzene solution as the top layer and shaken slightly till the green precipitate formed. **43"** is very sensitive to moisture and air. The suspension of **43"** in PE/benzene could not be stored for long time, e.g. 24h, despite at low temperature. Otherwise, it gave some slightly pale yellow decomposed material which was not further identified. This behavior is different from the reaction of lithiotrovacene with stoichiometric SbCl$_3$. Wherein only (TVC)$_3$Sb (**48"""**) was isolated as dark violet-red powder, no corresponding (TVC)$_2$SbCl was formed (see experimental part).

After extraction by benzene, the residue was washed by PE, Et$_2$O, H$_2$O, and THF, dried *in vacuo* to give **47"""** as pale violet-red powder in 9% yield. According to the purification procedure, we noticed that **47"""** has not a good solubility in common organic solvents, such as PE, Et$_2$O, DME, THF, benzene, toluene etc., and some strong polar solvent, such as, CH$_3$CN, DMSO, only except slightly in CH$_2$Cl$_2$. Therefore, it is basically impossible to purify **47"""** by chromatography. When the CH$_2$Cl$_2$ extraction was filtered through small amounts of Al$_2$O$_3$, it

gave small amounts of **47**''' as violet solution. Both **43**'' and **47**''' have been characterized by mass spectroscopy (EI) and unsatisfactory elemental analysis.

Furthermore, it was found that if large excess of $AsCl_3$ was added to the solution of lithiotrovacene in Et_2O, **43**'' also was obtained as pale green precipitate in good yield at room temperature. However, if the reaction time was stand for long, for example, more than 3h, the pale green precipitate changed into uncharacterized yellow solid.

In addition, we have attempted to synthesize $(TVC)_2As-As(TVC)_2$ by reduction of **43**'' with lithium powder and cobaltocene[78] at ambient temperature according to the literature reported method, but no characterized results could be obtained based on EI-MS (70eV) results.

49''''

3.3.3. Reactivity of 43'', and synthesis of 44'', 45'' and 46''

43'' was converted to stable di([5]trovacenyl)-butyl-arsane **44**'' by reaction with n-BuLi in benzene for 0.5h at room temperature in nearly quantitative yield. After hydrolysis by water, **44**'' was purified by chromatography (Al_2O_3) as red-violet solid and identified by mass spectra, elemental analysis and X-ray structure. It has a good solubility in common organic solvent, such as PE, toluene, the single crystal was generated from saturated benzene solution of **44**'' at 8°C.

43'' reacted with $LiAlH_4$ in benzene and then hydrolysis by H_2O, **45**'' was obtained by chromatography (Al_2O_3) as purple solid in 40% yield. **45**'' has a good solubility in THF. Compared to the n-Bu-derivative, the hydride derivative has a small steric hindrance.

46'' was formed by addition of 10% NaOH solution to the green solution of **43**'' in THF at r.t, the mixture changed into red-violet in color immediately with vigorously stirring. After drying with $MgSO_4$ and followed procedures, **46**'' was isolated by chromatography (1×10cm, Al_2O_3) eluted with ethanol as red-violet solid in good yield. However, it should be stated that chromatography is not the best choice for isolation **46**'', due to its strong polarity. **46**'' was characterized by mass spectra and elemental analysis. It has a good solubility in polar solvent.

3.3.4. Results of Cyclic Voltammetry ($43^{..}$, $44^{..}$ and $45^{..}$)

Cyclic voltammograms of $43^{..}$, $44^{..}$, $45^{..}$ are displayed in Figure 3.5. The data are shown in Table 3.5. All three arsane derivatives exhibit two successive one-electron reduction waves, and one two-electron oxidation wave. A conclusion that the overlap of two one-electron oxidation waves with a small redox splitting ($\Delta E_{1/2}(0/+)(+/2+) \leq 70mV$) could be inferred from the large ΔE_p value of oxidation.

It is found that the separation $\Delta E_{1/2}(0/-)(-/2-)$ (126mV) of $44^{..}$ is slightly smaller than that of $41^{..}$ (152 mV). Compared to the reduction potential of parent trovacene (-2.55V), almost all the reduction potential $E_{1/2}(0/-)$ and $E_{1/2}(-/2-)$ show anodic shifts, excluding $E_{1/2}(-/2-)$ of $44^{..}$ (-2.575 V). The oxidation potentials ($E_{1/2}(0/2+)$) at 309 mV ($45^{..}$), 417 mV ($43^{..}$) and 323 mV ($44^{..}$) exhibit an anodic shift relative to that of trovacene, but close to $E_{1/2}(+/2+)$ of [5,5]bitrovacene (364 mV). This indicates that As bridging does not significantly block the electron communication between metals due to the increasing of the distance between two metals.

Unlike the sharp reduction peaks of $44^{..}$, and distinct reduction peaks of $43^{..}$, $45^{..}$ shows two largely resolved reduction waves at -2.416 V and -2.524 V. The difference of the inductive effect of the various substituents afford the different metal - metal interactions as H < Cl < n-Bu, according to the values of potential separation ($\Delta E_{1/2}(0/-)(-/2-)$), 109 mV ($45^{..}$) < 126 mV ($43^{..}$) < 156 mV ($44^{..}$) (Figure 3.4). Additionally, a proposal that the geometry of the molecules in the solution may be more important than the inductive effect should not be neglected. A continuing study should be done in the future.

Figure 3.4. Redox splitting of $10^{..}$, $43^{..}$, $44^{..}$ and $45^{..}$

$\Delta E_{1/2}(0/-)(-/2-)(mV)$

$(TVC)_2As(R)$ R = H, Cl, n-Bu, 0* : TVC-CV'
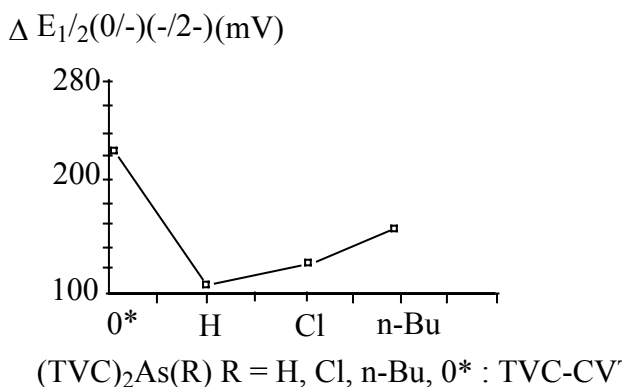
It demonstrates that the electron donating effect of alkyl groups is beneficial to the metal-metal interaction more than that of H, and it is assumed that phenyl substitution would lead to a large potential separation and strong metal - metal interaction.

Figure 3.5. Cyclic voltammograms for **43··**, **44··** and **45··** in DME/TBAP at -40°C, v=100mV/s

43··

44··

45··

mA

-2.9   -2.0   -1.0   [V]   0.0   1.0   1.6
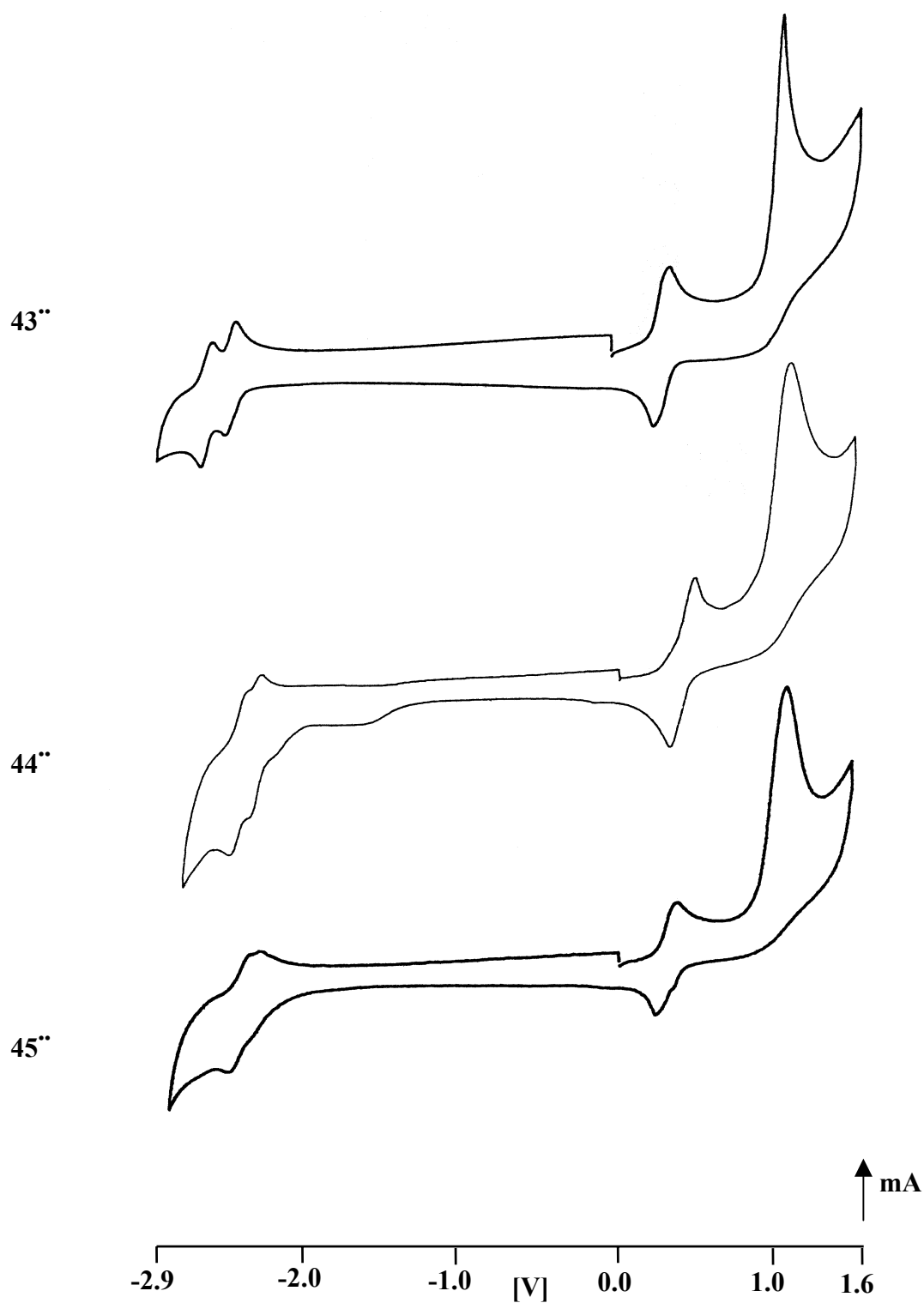
Table 3.5. Cyclic Voltammetry Data for **43**, **44** and **45**

	45	**43**	**44**
$E_{1/2}(0/2+)$	309 mV	417 mV	323 mV
ΔE_p	114 mV	178 mV	86 mV
I_{pa}/I_{pc}	1	1	1
$\Delta E_{1/2}(0/+)(+/2+)$	$\leq$ 70mV	$\leq$ 70mV	$\leq$ 70mV
$E_{pa}(2+/3+)$	1.134 V	1.162 v	1.064 V
$E_{1/2}(0/-)$	-2.416 V	-2.392 V	-2.419 V
ΔE_p	88 mV	84 mV	58 mV
I_{pa}/I_{pc}	1	1	1
$E_{1/2}(-/2-)$	-2.524 V	-2.518 V	-2.575 V
ΔE_p	154 mV	116 mV	66 mV
I_{pa}/I_{pc}	0.95	0.92	1
$\Delta E_{1/2}(0/-)(-/2-)$	109 mV	126 mV	156 mV

3.3.5. X-ray Crystal Structure Analysis of 44

The molecular structure of **44** is illustrated in Figure 3.6, the selected bonds and angles are shown in Table 3.6 and 3.7, respectively.

Similar to the geometry of P, the As atom displays a distorted trigonal pyramidal coordination sphere, in which As lies on the top and links to three fragments, namely to the carbon atom of n-Bu and to the carbon atom of two TVC units. The axis of the two TVC fragments are almost perpendicular to each other in order to minimize steric repulsion. The dihedral angle between two Cp rings is 77.91(16)°.

The distance between As and C (Cp ring) are 1.957(2) and 1.943(2)Å, which are slightly shorter than that of $As-C_{n-Bu}$ (1.976(3)Å), but all of them are shorter than the reported As-C distance in cyclopentadienyl derivatives of arsenic ($\approx$2 Å). The bond angles C(13)-As(1)-C(1), C(1)-As(1)-C(25) and C(13)-As(1)-C(25) are 96.75(9)°, 97.94(10)° and 96.39(10)°, respectively. They indicate that the lone pair at the arsenic atom is predominantly of s-character.

The As atom is nearly coplanar with the two Cp rings (179°). It differs from the previously reported AsX_2 moiety of $Cp*AsX_2$[79] which is perpendicular to the best plane of the cyclopentadienyl ring. The torsional angle of C(25)-As(1)-C(13)-C(14) is -179.88(19)°.

The Cp and Tr rings of each sandwich unit are parallel with the same C-C distances. The distance between metals is 6.4434(28)Å which is close to that of **41** (6.4969(29)Å). The different hindrance from Ph and n-Bu in the molecules would influence the distance between the two metals.

Figure 3.6. Molecular structure and stereoview of **44**[**]
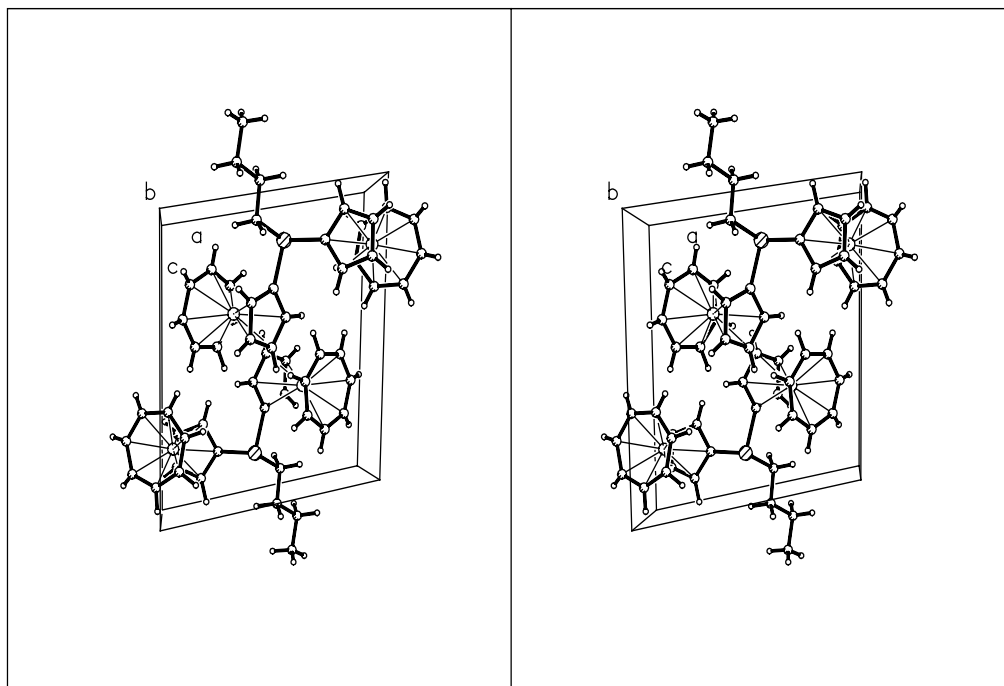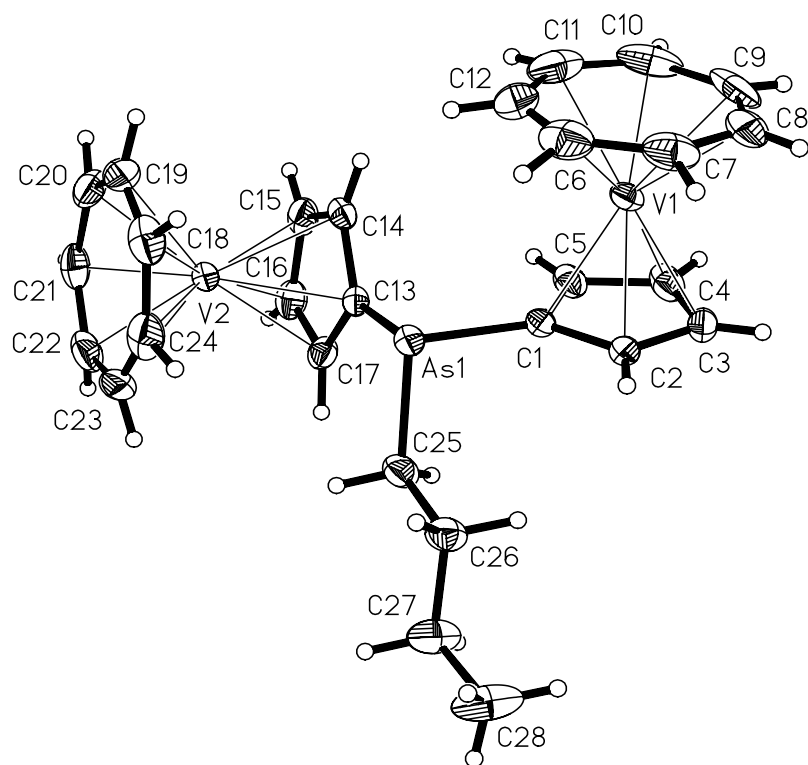
Table 3.6. Selected bonds [Å] of **44··**

As(1) - C(1)	1.957(2)	V(1) - C(6)	2.186(2)
As(1) - C(13)	1.943(2)	V(1) - C(7)	2.192(3)
As(1) - C(25)	1.976(3)	V(1) - C(8)	2.181(3)
As(1) - C(mean)	1.959(2)	V(1) - C(9)	2.165(3)
V(1) - C(1)	2.266(2)	V(1) - C(10)	2.181(3)
V(1) - C(2)	2.248(3)	V(1) - C(11)	2.186(3)
V(1) - C(3)	2.255(2)	V(1) - C(12)	2.189(3)
V(1) - C(4)	2.256(2)	**V(1)-C$_7$ Ring (mean)**	2.183(3)
V(1) - C(5)	2.263(2)	**V(1)-C$_7$ (centroid)**	1.462(1)
V(1)-C$_5$ Ring (mean)	2.258(2)	C(6) - C(7)	1.389(4)
V(1)-C$_5$ (centroid)	1.9107(4)	C(6) - C(12)	1.401(5)
C(1) - C(2)	1.423(3)	C(7) - C(8)	1.406(5)
C(1) - C(5)	1.416(3)	C(8) - C(9)	1.408(5)
C(2) - C(3)	1.409(4)	C(9) - C(10)	1.424(5)
C(3) - C(4)	1.402(4)	C(10) - C(11)	1.403(5)
C(4) - C(5)	1.418(3)	C(11) - C(12)	1.390(5)
C-C (mean for C$_5$)	1.414(3)	**C-C (mean for C$_7$)**	1.403(5)
C(25) - C(26)	1.519(3)	**V(1) - V(2)**	6.4434(28)

Table 3.7. Selected angles and torsion [°] of **44··**

C(13)-As(1)-C(1)	96.75(9)	C(25)-As(1)-C(1)-C(5)	106.7(2)
C(1)-As(1)-C(25)	97.94(10)	C(25)-As(1)-C(1)-C(2)	-74.8(2)
C(13)-As(1)-C(25)	96.39(10)	C(1)-As(1)-C(13)-C(14)	-80.95(17)
C(5)-C(1)-As(1)	127.48(17)	C(13)-As(1)-C(1)-C(2)	-172.3(2)
C(2)-C(1)-As(1)	125.25(18)	C(13)-As(1)-C(1)-C(5)	9.3(2)
C(14)-C(13)-As(1)	125.50(18)	C(1)-As(1)-C(25)-C(26)	27.59(17)
C(17)-C(13)-As(1)	127.97(18)	C(1)-As(1)-C(13)-C(14)	-81.06(19)
C(26)-C(25)-As(1)	112.67(18)	C(1)-As(1)-C(13)-C(17)	101.5(2)
C(5)-C(1)-C(2)	107.3(2)	C(25)-As(1)-C(13)-C(17)	2.7(2)
C(17)-C(13)-C(14)	106.5(2)	C(25)-As(1)-C(13)-C(14)	-179.88(19)
As(1)-C(1)-C(5)-C(4)	179.00(17)	As(1)-C(1)-C(2)-C(3)	-179.36(17)

3.3.6. EPR Spectra (44··)

Fluid solution and rigid solution spectra of **44··** in toluene recorded at X-band frequency are shown in Figure 3.7. The parameters are summarized in Table 3.8.

Similar to the P bridged binuclear complex **41··**, a typical binuclear 15-line spectrum is observed for **44··**. The hyperfine splitting of **44··** is a(^{51}V) = 7.21mT. The slightly larger coupling constant of **44··** relative to **41··** may be due to the facts that n-Bu replace the electron-accepting phenyl group and bridge As instead of P atom. Although phenyl can increase slightly positive partial charge on the central metal atom, the study of which factor should be mainly responsible for the large coupling constant must be done in the further work.

Although As belongs the same group as P in the periodic table, a smaller exchange coupling constant J ~16000 G (-1.496 cm^{-1}), |J|>>|a|, is furnished by spectral simulation relative to that

of **41**$^{..}$, however, it is close to that of [5,5]bitrovacene. This may indicate that the interaction or exchange coupling through As bridge is remarkable weaker than that through the P atom. Thus, it might be necessary to prepare (TVC)$_2$As-Ph to investigate the exchange coupling constant J and to learn how the exchange coupling constant J varies with the changing of the bridge atom. Hence, the non-aromatic alkyl replacing Ph should also be responsible for the large difference of J value. In addition, the hyperfine coupling constant a(^{75}As) (3G) is given by the computer spectral simulation. The half-field signal ($\Delta M_s = 2$) of glassy solution spectrum of **44**$^{..}$ could not be detected.

Table 3.8. EPR Data of **44**$^{..}$

A(^{51}V)$_{iso}$	g$_{iso}$	J	α	β	γ	ΔB	A(^{75}As)$_{iso}$
72.07G	1.9829	-1.496 cm^{-1}	-0.134	-0.086	0.058	30.8G	3G

Figure 3.7. EPR spectra of **44**$^{..}$ in fluid solution and rigid solution (toluene); 294K; ν = 9.2441 GHz; A) Experimental, B) Simulated; 330K, ν = 9.2444 GHz, C) Experimental; D) Simulated; E) 250K, ν = 9.2450 GHz; F) 220K, ν = 9.2447 GHz; G) 130K, ν = 9.2457 GHz.
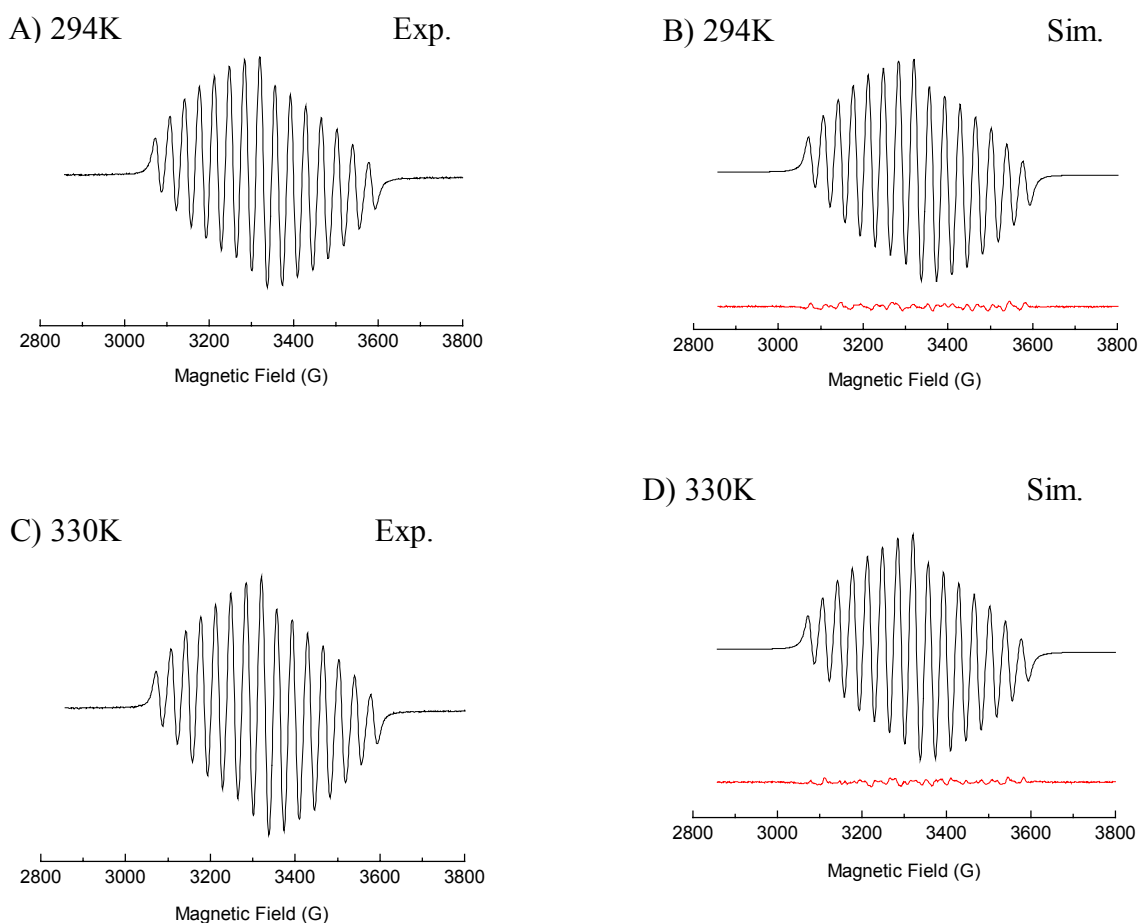
E) 250K
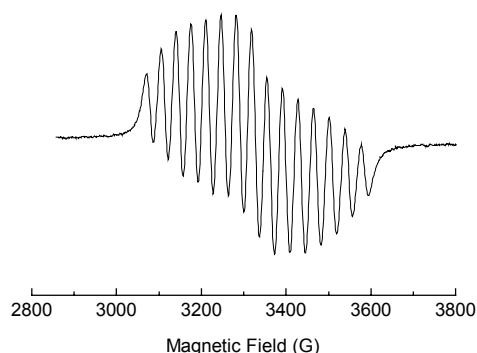
F) 220K
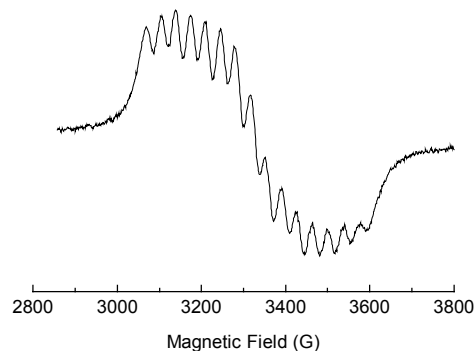
G) 130K
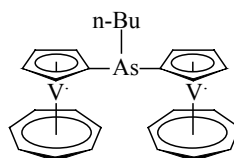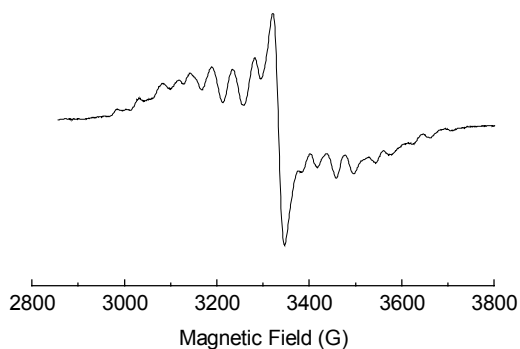
3.3.7. Discussion and Conclusion

The distance between metals and the nature of the bridge play the key role in electron communication. If the bridges are similar to each other, then the *chemical environment* around the metals will be the important factor.

H, Cl, or OH, as the α-position substituents to the bridging atom As, will result in the two trovacene units relatively expanded in the space, due to the decrease of the steric hindrance. In other words, the distance between metals should slightly increase. Meanwhile, if Ph or other large groups, such as biphenyl, were used as the substituent, the two trovacene units should be close to each other. However, based on the V-V distances of **10"** (5.50Å), **18"** (6.99Å) and **44"** (6.44Å), and the angles of C_{C5}-S-C_{C5} (98.96°), C_{C5}-As-C_{C5} (96.75°), we can conclude that there is little effect on the metal-metal distance from the various α-position substituents. On the other hand, the distance between two metals is not the determining factor for the same As bridging complexes.

Evidence for the effectiveness of an aromatic ring for mediating the electronic coupling relative to that of an alkyl unit have been provided.[80]

The $\Delta E_{1/2}$(0/-)(-/2-) values of **45"** (109mV), **43"** (126mV) and **44"** (156mV) are smaller than that of **10"** (224mV). They are close to those of **18"** (134mV) and **41"** (152mV). These results support the conclusion that the α-position substituent groups would be involved in the ET

69

between two nuclei. It is consistent with the tendency of H < Cl < n-Bu < Ph and this relates to their different inductive effect. Additionally, for **45"**, the interaction between metal centers, to some extent, should be slightly more complex due to the intermolecular hydrogen-bonding. We originally thought it were an example of non-bonded interaction. But because they are linked directly to the bridge (As), we would not simply name them `not through-bond ´, but ´ non-bonded ´ interactions.

4. Group 14 Derivatives

4.1. Introduction

The representative examples: Fc_2CH_2,[81] Fc_2SiMe_2,[82] Fc_2SnMe_2,[83] Fc_2PbPh_2,[84] had provided the chance to study the metal-metal interaction of binuclear complexes containing group 14 elements as the bridge. Previous work of our group also gave some examples of bis(benzene)chromium /vanadium derivatives linked by silicon bridges[85,73] (Scheme 1).

Scheme 1.

M = Cr, **50**; V, **51**   M = Cr, **52**; V, **53**

R = -, **54**; CH₂, **55**, Si(Me)₂, **56**   M = **57**··
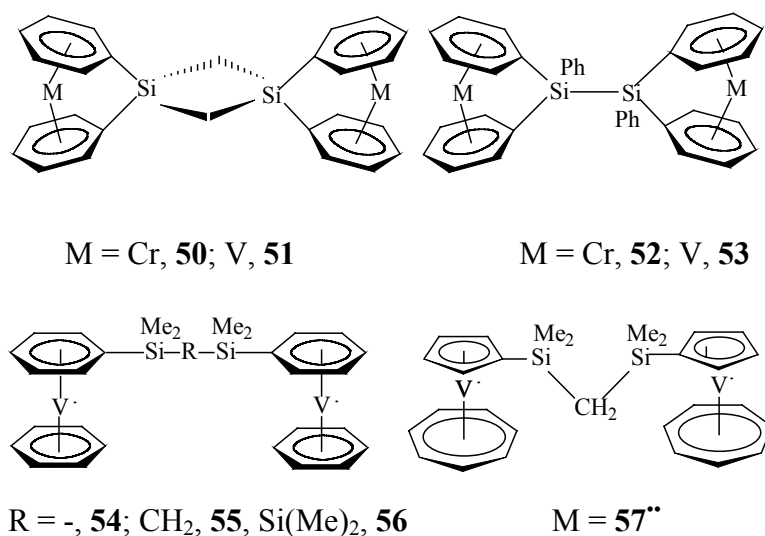
It is well-known that the nature of the bridge always play a crucial role in the interaction between two units. In order to systematically investigate the function of different bridging atoms, as well as the influence of methyl and phenyl groups linked to the bridging atom on the interactions, various cyclopentadienyl-substituted complexes are synthesized and studied by CV, EPR.

Silicon as a highly effective semi-conductor, due to its remarkable electronic property, has attracted much interest in recent years. Polysilanes can be described as one-dimensional potential precursors for molecular electronics. The Si-Si bridge as the simplest sub-unit has been studied for long range electron transfer in binuclear molecule.

4.2. Synthesis of 59··, 60··, 62··, 63··, 64··, 65·· and 67·

Reactions of lithiotrovacene with corresponding dichloro reagents (R_2MCl_2, R = Me, Ph, M = Si, Ge, Sn, Pb; and $ClMe_2SiMe_2SiCl$) (Scheme 2) were performed at ambient temperature. In order to avoid side-reaction, the reaction mixture was stirred at r.t. overnight. The analytically pure products were obtained by chromatography, and characterized by mass spectroscopy, elemental analysis, and/or X-ray diffraction analysis. The physical properties and the yields are shown in the experimental part. It was found that the yield of product may slightly depend on the ratio of reactants due to the half yield of the lithiation of trovacene. These compounds have good solubility in common organic solvent.

Scheme 2.
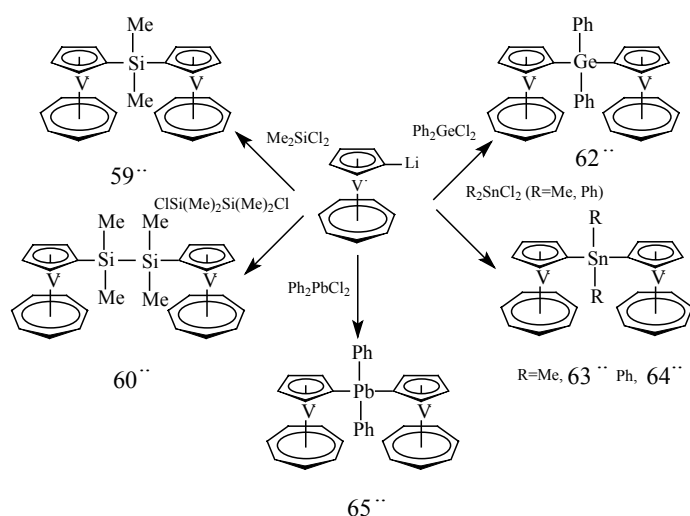
The Si-bridged complexes (**59**, **60**) are somewhat difficult to isolate by chromatography (Al_2O_3), although the strong polar solvent ethanol has been utilized as eluent. It should be noted that the reaction of Ph_2SiCl_2 with lithiotrovacene did not result in the expected binuclear **61** rather than a mononuclear **67** as the main product after isolation by chromatography.

Ph_2PbCl_2 was synthesized according to the literature,[86] and reacted with lithiotrovacene to result in a pale purple solid after isolation by chromatography(Al_2O_3). Although this pale purple solid did not give the molecular ion peak of $(TVC)_2Pb(Ph)_2$ (**65**) but a peak at 767.6 ($[M^+-6]$) from EI-MS (70eV). The pale purple product was characterized by elemental analysis and X-ray diffraction analysis.

67
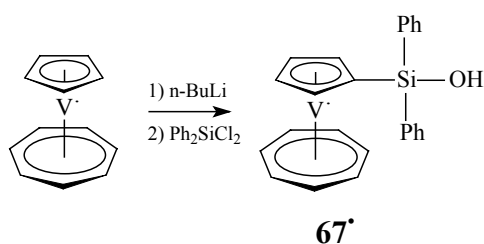
It was very surprising to obtain **67** as the main product in the reaction of lithiotrovacene with Ph_2SiCl_2. After isolation by chromatography (Al_2O_3, 2.5×30cm, elution with $EtOH/Et_2O$) and recrystallization from saturated ethanol solution, the violet crystal was obtained and it was characterized by mass spectroscopy, elemental analysis and X-ray diffraction analysis to be di(phenyl)([5]trovacenyl)silanol (**67**). **67** has a good solubility in polar solvent. Furthermore, the same compound has been obtained from the repeated reactions after isolation by chromatography.

^{1}H-NMR spectroscopy of commercial Ph_2SiCl_2 (85-95°C/0.01 torr, Lit., 305°C/750 mmHg) only displays the typical phenyl proton spectrum at 7-8 ppm (ranging from 1-15 ppm). The same conditions were reported for $2,6\text{-}Mes_2C_6H_3Si(OH)_2H$ and $(Me_3Si)_3CSi(OH)_2H$.[105]

One possible assumption of the formation of **67**[·] is that the unstable mono-substituted intermediate $(TVC)Si(Ph)_2Cl$ may be formed, and it can convert to **67**[·] during the isolation process when ethanol (containing trace H_2O) was utilized as eluent. Because ethanol is not absolutely dried reagent, only dried by refluxing with CaO under inert atmosphere. Additionally, the molecular ion peak of $(TVC)Si(Ph)_2Cl$ was observed from the results of EI-MS of the reaction residue.

But another possibility that the reagent Ph_2SiCl_2 was hydrolysis to afford $Ph_2Si(OH)Cl$ before purification should not be neglected, because no literature has reported the physical property of $Ph_2Si(OH)Cl$, such as boiling point and ^{1}H-NMR spectra. Therefore, the reason is still not completely certain, and the study of $(TVC)_2Si(Ph)_2$ (**61**[··]) should be attempted in the further work.

In addition, contrary to other dichloro regents, CH_2Cl_2 does not react with lithiotrovacene to afford the corresponding carbon-bridge bimetallic complex $(TVC)_2CH_2$ (Scheme 3) under the same reaction condition. No evidence for $(TVC)_2CH_2$ (M = 428) was observed from the result of mass spectroscopy (EI-MS 70eV: 438, 7% ?; 207, 100%, TVC).

Scheme 3.

58[··]
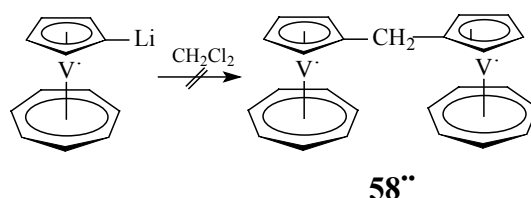
4.3. Results of Cyclic Voltammetry

Inductive effects, electrostatic interactions, solvent effects and electron delocalization should be fully considered for the possible impact on the redox behavior. Since the nature of the bridge, such as, electronic structure, polarity, determines the redox behavior of complexes.

4.3.1. Methyl-substituted silicon and tin bridging complexes (59[··], 60[··] and 63[··])

The cyclic voltammetric traces of $(TVC)_2(SiMe_2)_x$ (X=1, **59**[··]; 2, **60**[··]) are shown in Figure 4.3. The pertinent resulting data are recorded in Table 4.1 (contained the analog, [5,5]bitrovacene (X=0), for comparison).

Since the wave height indicates the number of electron transfer,[87] both **59**[··] and **60**[··] exhibit one distinct two-electron reversible oxidation and two indistinct successive one-electron reductions, on the contrast to the redox behavior of [5,5]bitrovacene (**10**[··]) which showed two distinct successive one-electron oxidations and reductions. But the large ΔE_p values indicate that the small redox splitting $(\Delta E_{1/2}(0/+)(+/2+) \leq 70mV)$ and the overlap of two one-electron oxidation waves and the small redox splitting was observed. The oxidation potential of **59**[··] exists a anodic shift $(E_{1/2}(0/2+) = 316$ mV) relative to that of parent trovacene (226mV). However, the oxidation potential of **60**[··] $(E_{1/2}(0/2+) = 278$ mV) is close to that of trovacene.

The first reduction potentials $(E_{1/2}(0/-))$ of **59**[··] and **60**[··] are close to each other, but significant anodic shift of the second reduction $(E_{1/2}(-/2-))$ for **59**[··] (-2.524 V) and **60**[··] (-2.559 V) are

discovered, relative to that of **10$^{\bullet\bullet}$** (-2.708 mV). The separation ($\Delta E_{1/2}(0/-)(-/2-)$) between the two reductions for X=0, 1, 2 are 224 mV, 75 mV, and 116 mV, respectively. Despite the distance between the two metal centers caused by the great length of the C-Si and Si-Si bond, the redox splitting do not become progressively smaller, rather X = 0 > 2 > 1 (Figure 4.1). This differs from that of the analogous ferrocene derivatives $Fc(SiMe_2)_xFc$ (X = 0 > 1 > 2).[88]

Figure 4.1. Redox splitting of **10$^{\bullet\bullet}$**, **59$^{\bullet\bullet}$** and **60$^{\bullet\bullet}$**

$\Delta E_{1/2}(0/-)(-/2-)(mV)$

Number of Si(Me)$_2$ (n)
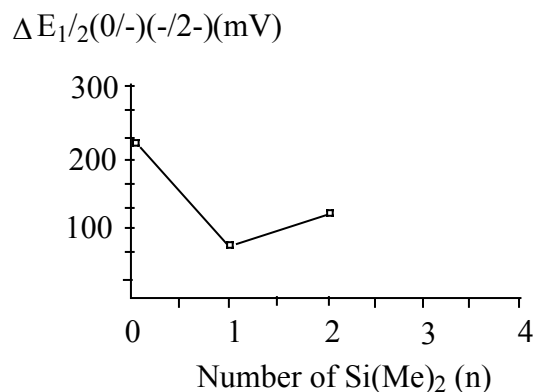
The larger difference between the redox splitting ($\Delta E_{1/2}(0/+)(+/2+)$ and $\Delta E_{1/2}(0/-)(-/2-)$ can be elucidated by the fact. Since oxidation and reduction of trovacene must be regarded as metal-centered and the redox splitting $\Delta E_{1/2}(0/-)(-/2-)$ governs the extension of the $V(3d_z{}^2)$ orbitals in the radical anion, the extent of intramolecular interaction depends on complex charge. The electron delocalization through the bridge Si by a trovacenyl group is more pronounced for the radical anion compared to the radical cation in view of the expanded nature of the vanadium orbitals in the former, compared to their contracted nature in the latter.

One of the differences between Si and Si-Si bridges lies in the low ionization potential (I_p) of the Si-Si bond. It leads to a similar effective electron donating property to the C=C bond.[89] In addition, it has demonstrated that electron delocalization exists between Si-Si σ bonds and π systems.[90] For example, in recent days, Chujo[91] et al. calculated that the electron density of the LUMO on the Si and Si-Si of the molecules (as shown below) corresponded to `no´ and ´larger´, respectively. (donor: thioketene dimer, acceptor: Si-Si moiety.)

$$R\text{-}HC = \left\langle \begin{matrix} S \\ S \end{matrix} \right\rangle = CH\text{-}R$$

R = -Si$_2$Me$_3$, -SiMe$_3$
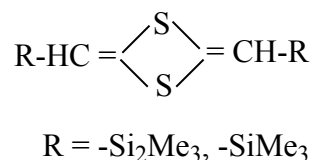
The redox splitting $\Delta E_{1/2}(0/-)(-/2-)$ of (Z, E) TVC-CH=CH-TVC [92] are 130mV and 170mV. The Si-Si bridge of **60$^{\bullet\bullet}$** may support the distortion of two trovacene units which could afford a short distance between the two metals and a slightly greater splitting potential.

On the contrary, due to the repulsion from the two TVC fragments and the tetrahedron structure of bridge Si, **59$^{\bullet\bullet}$** may place a considerable structural strain upon the single atomic bridge, which may increase the distance between two metals.

It has been demonstrated that metal-metal interaction is attenuated with increasing bridge length in the series of silicon-bridged bimetallics. For example, bis(ferrocenyl)oligosilanes $Fc(SiMe_2)_xFc$ (X=1, 2, 3, 6).[81] It was found that the redox splitting and associated interaction between the two iron centers decreased with increasing the number of silicon atoms in the spacer group. The redox splitting were 150 mV, 110 mV, 80 mV and only a single redox wave detected, respectively (Figure 4.2).[93] Furthermore, doubly dimethylsilyl-bridged oliogo(ferrocenylsilanes) were investigated to show three reversible redox waves.[94]

Figure 4.2. Difference of oxidation potential (ΔE_{pa}) of $Fc(SiMe_2)_xFc$ (X=1, 2, 3, 6)

$\Delta Epa\,(mV)$

400
300
200
100

0 1 2 3 4 5 6 7 8
Number of spacer group (n)
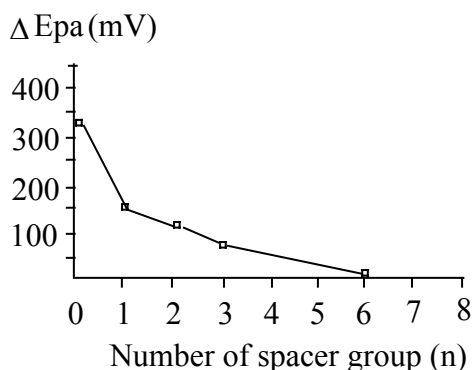
The cyclic voltammogram of **63**$^{\cdot\cdot}$ is shown in Figure 4.5, and the data are summarized in Table 4.1. Similar to **59**$^{\cdot\cdot}$, **63**$^{\cdot\cdot}$ also exhibits a reversible two-electron oxidation peak at 277mV, and two indistinct one-electron reductions with a separation of 95mV, which is slightly greater than that of **59**$^{\cdot\cdot}$ (75 mV). On the contrary, $\Delta E_{1/2}$ of $(Fc)_2Sn(n\text{-}Bu)_2$ bridge (240 mV) was smaller than that of $(Fc)_2Si(n\text{-}Bu)_2$ (290 mV).[95]

Table 4.1. Cyclic Voltammetry Data of **59**$^{\cdot\cdot}$, **60**$^{\cdot\cdot}$ and **63**$^{\cdot\cdot}$

	10$^{\cdot\cdot}$	**59**$^{\cdot\cdot}$	**60**$^{\cdot\cdot}$	**63**$^{\cdot\cdot}$
$E_{1/2}(0/+)^*$	217 mV			
$E_{1/2}(0/2+)$		316 mV	278 mV	277 mV
ΔE_p	62 mV	88 mV	120 mV	70 mV
I_{pa}/I_{pc}	1	1	1	1
$E_{1/2}(+/2+)$	364 mV			
$\Delta E_{1/2}(0/+)(+/2+)$	147 mV	≤ 70 mV	≤ 70 mV	≤ 70 mV
$E_{pa}(2+/3+)$		1.124 V	1.270 V	1.036 V
ΔE_p	64 mV			
I_{pa}/I_{pc}	1			
$E_{1/2}(0/-)$	-2.484 mV	-2.449 V	-2.443 V	-2.431 V
ΔE_p	60 mV	78 mV	62 mV	54 mV
I_{pa}/I_{pc}	1	0.9	1.1	
$E_{1/2}(-/2-)$	-2.708 mV	-2.524 V	-2.559 V	-2.526 V
ΔE_p	60 mV	84 mV	74 mV	84 mV
I_{pa}/I_{pc}	1	0.7	0.7	1
$\Delta E_{1/2}(0/-)(-/2-)$	224 mV	75 mV	116 mV	95 mV

Figure 4.3. Cyclic voltammograms for **59**[··], **60**[··] and **63**[··] in DME/TBAP at -40°C, v=100mV/s

59[··]

60[··]

63[··]

mA

-2.9   -2.0   -1.0   0.0   1.0   1.6

[V]
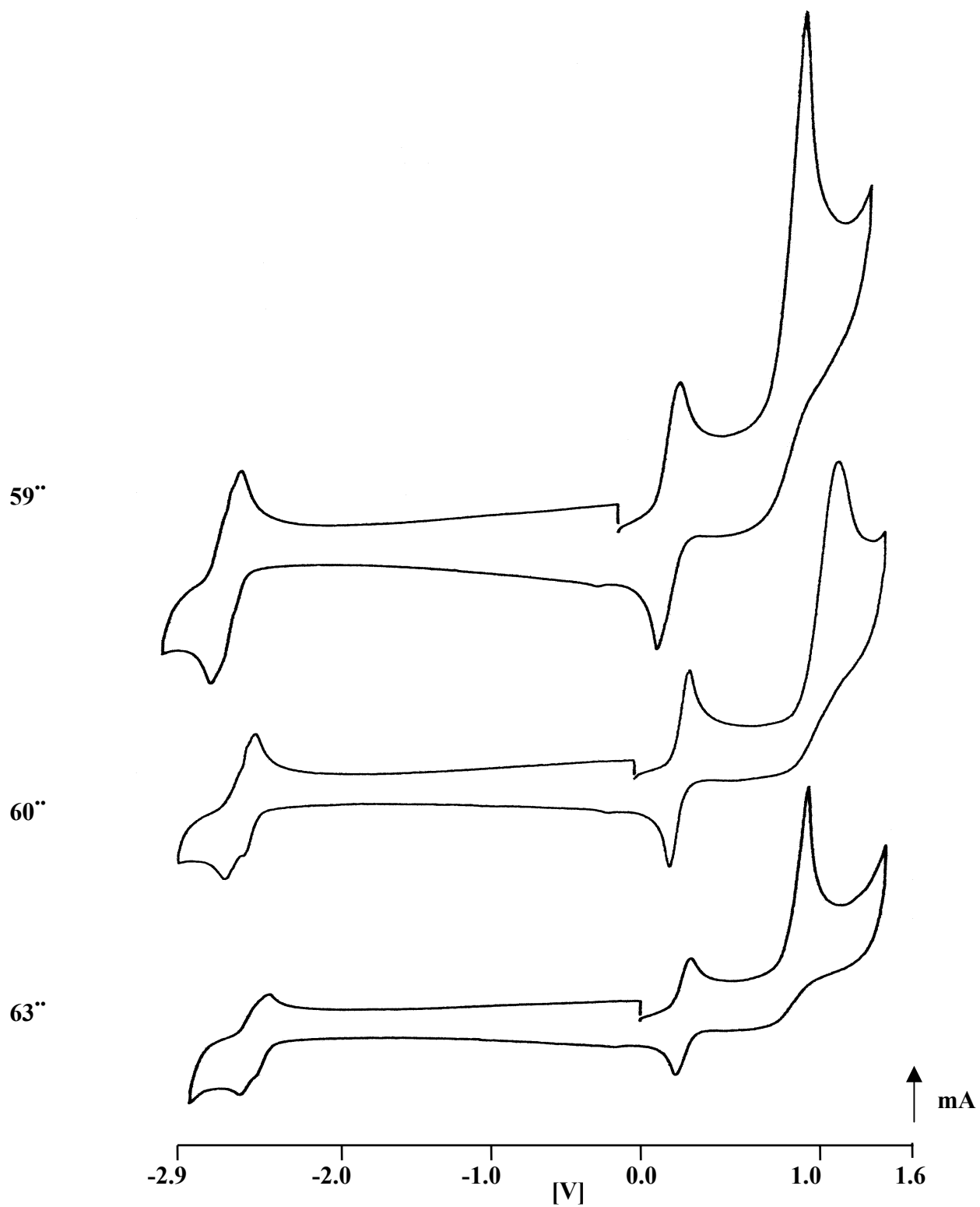
If a *through bond* effect was mainly responsible for the interaction, d-orbitals of Sn and cyclopentadienyl orbital overlap more, it would give a larger $\Delta E_{1/2}$ value. However, due to the longer distance of Sn-C bond than that to Si-C bond, the *through space* effect would be weakened. So, both the *through-space* and *through-bond* mechanism are contributed to the interactions in silicon-bridged species.

4.3.2. Phenyl-substituted complexes (62**, 64**, 65** and 67*)

The cyclic voltammogram of **62**, **64**, **65** are shown in Figure 4.4. The data are summarized in Table 4.2.

The Ge-bridged complex **62** exhibits a two-electron oxidation at 317 mV, and two distinct reversible successive one-electron reductions at -2.436V and -2.609V, respectively. The Sn-bridged **64** complex shows a two-electron oxidation at 319 mV, and two distinct one-electron reductions at -2.522 V and -2.81 V, respectively. **65** gives a reversible two-electron oxidation at 329mV. Similar to the analogue **59** and **63**, the large ΔE_p value of **62**, **64**, and **65** indicate the overlap of successive two one-electron oxidation waves and the small redox splitting ($\Delta E_{1/2}(0/+)(+/2+) \leq 70$mV).

Due to the different substituents linked to the bridging atom - methyl and phenyl, the electrochemical behavior of responding binuclear complexes are not identical. This relates to the electron-accepting effect of phenyl group. It is apparent that the separation $\Delta E_{1/2}(0/-)(-/2-)$ of phenyl-substituted complex **64** is greater than that of methyl-substituted Sn bridged complex **63**.

The electrochemistry of **65** shows three reduction peaks at -2.190, -2.518, and -2.820V. However, for the first reduction peak, it does not give the corresponding reversed oxidation peak. The following two successive reversible reductions give the separation of 313 mV, which is the greatest $\Delta E_{1/2}$ value in the 14 group atoms bridging binuclear complexes. However, the $\Delta E_{1/2}$ value of the analogous Fc_2PbPh_2 was 165mV (in CH_2Cl_2), which was smaller than that of $Fc_2Sn(n\text{-Bu})_2$ (240 mV). Additionally, the first reduction of **65** is more anodic shift than that of other atom-bridging complexes, such as Si, Ge bridging species. It could be ascribed to the large π electron density of phenyl. Meanwhile, the second E_{pc} of **65** is close to -2.458 V observed for **64**. Taking into consideration the X-crystal structure analysis, it seems that *through bond* interaction mainly contributes to the metal-metal interaction of **65**.

The first reduction potentials (**62**, **64** and **65**) are close to that of trovacene, the second reduction potentials show the cathodic shift because of the electron-delocalization effect of the two phenyl substituent. From Table 4.1 and 4.2, it is easy to see that the separation $\Delta E_{1/2}$ increases as Si < Ge < Sn < Pb. **64** and **65** reveal the stronger interactions between metal centers than that of **10** (Figure 4.5).

The cyclic voltammograms of **67** is depicted in Fig.4.6, and the data are summarized at Table 4.3. Since the wave height indicates the number of electron transfer,[87] the first reversible oxidation at 301 mV should be assigned to the two-electron process, with an anodic shift due to two phenyl linkages and Si p_π electrons. The large ΔE_p indicates the overlap of successive two one-electron transfer and the small redox splitting ($\Delta E_{1/2}(0/+)/(+/2+) < 70$mV).

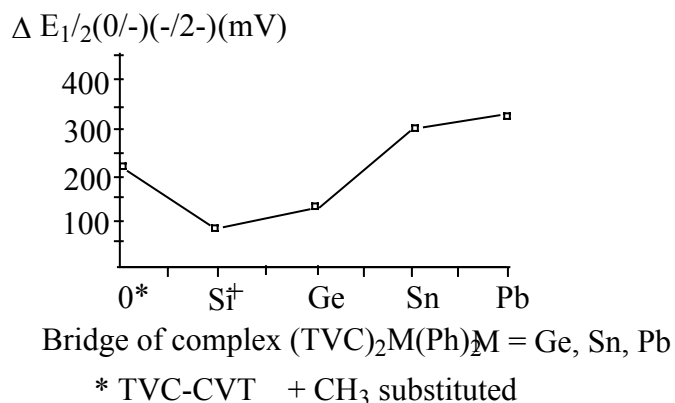**Figure 4.5.** Redox splitting $\Delta E_{1/2}(0/-)(-/2-)$ of $10^{\bullet\bullet}$, $62^{\bullet\bullet}$, $64^{\bullet\bullet}$ and $65^{\bullet\bullet}$

$\Delta E_{1/2}(0/-)(-/2-)(mV)$

```
400
300
200
100
     0*    Si⁺    Ge    Sn    Pb
```

Bridge of complex $(TVC)_2M(Ph)_2$ M = Ge, Sn, Pb

* TVC-CVT   + CH_3 substituted

Table 4.2. Cyclic Voltammetry Data of $62^{\bullet\bullet}$, $64^{\bullet\bullet}$ and $65^{\bullet\bullet}$

	$62^{\bullet\bullet}$	$64^{\bullet\bullet}$	$65^{\bullet\bullet}$
$E_{1/2}(0/2+)$	317 mV	319 mV	329 mV
ΔE_p	86 mV	122 mV	114 mV
I_{pa}/I_{pc}	1	1	1
$\Delta E_{1/2}(0/+)(+/2+)$	≤ 70 mV	≤ 70 mV	≤ 70 mV
$E_{pa}(2+/3+)$	1.126 V	1.056 V	1.140 V
E_{pc}			-2.190 V
$E_{1/2}(0/-)$	-2.436 V	-2.522 V	-2.477 V
ΔE_p	96 mV	80 mV	82 mV
I_{pa}/I_{pc}	1	0.52	1
$E_{1/2}(-/2-)$	-2.609 V	-2.81 V	-2.79 V
ΔE_p	70 mV	80 mV	60 mV
I_{pa}/I_{pc}	1	1	1
$\Delta E_{1/2}(0/-)(-/2-)$	173 mV	288 mV	313 mV

Surprisingly, two reductions at -2.489V and -2.686V are observed. This is different from other monomer trovacene derivatives. A possible mechanism that the dehydrolysis of $67^{\bullet}$ gave the dimer 1,3-di([5]trovacenyl-diphenyl)siloxane ($81^{\bullet\bullet}$) during the electrochemical process is proposed (below). Therefore, in order to prove the proposal, the synthesis and investigation by CV of 1,3-di([5]trovacenyl-diphenyl)siloxane ($81^{\bullet\bullet}$) should be done in the future study.

$67^{\bullet}$ $81^{\bullet\bullet}$
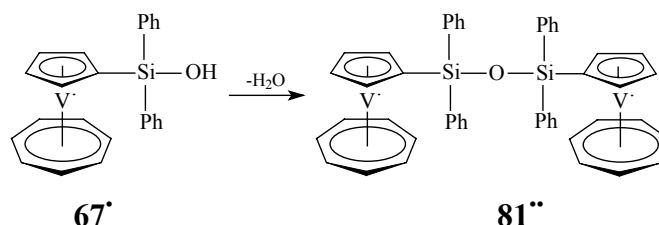
Figure 4.5. Cyclic voltammograms for **62**", **64**" and **65**" in DME/TBAP at -40°C, v=100mV/s

65"

64"

62"

mA

-3.0   -2.0   -1.0   0.0   1.0   1.6

[V]
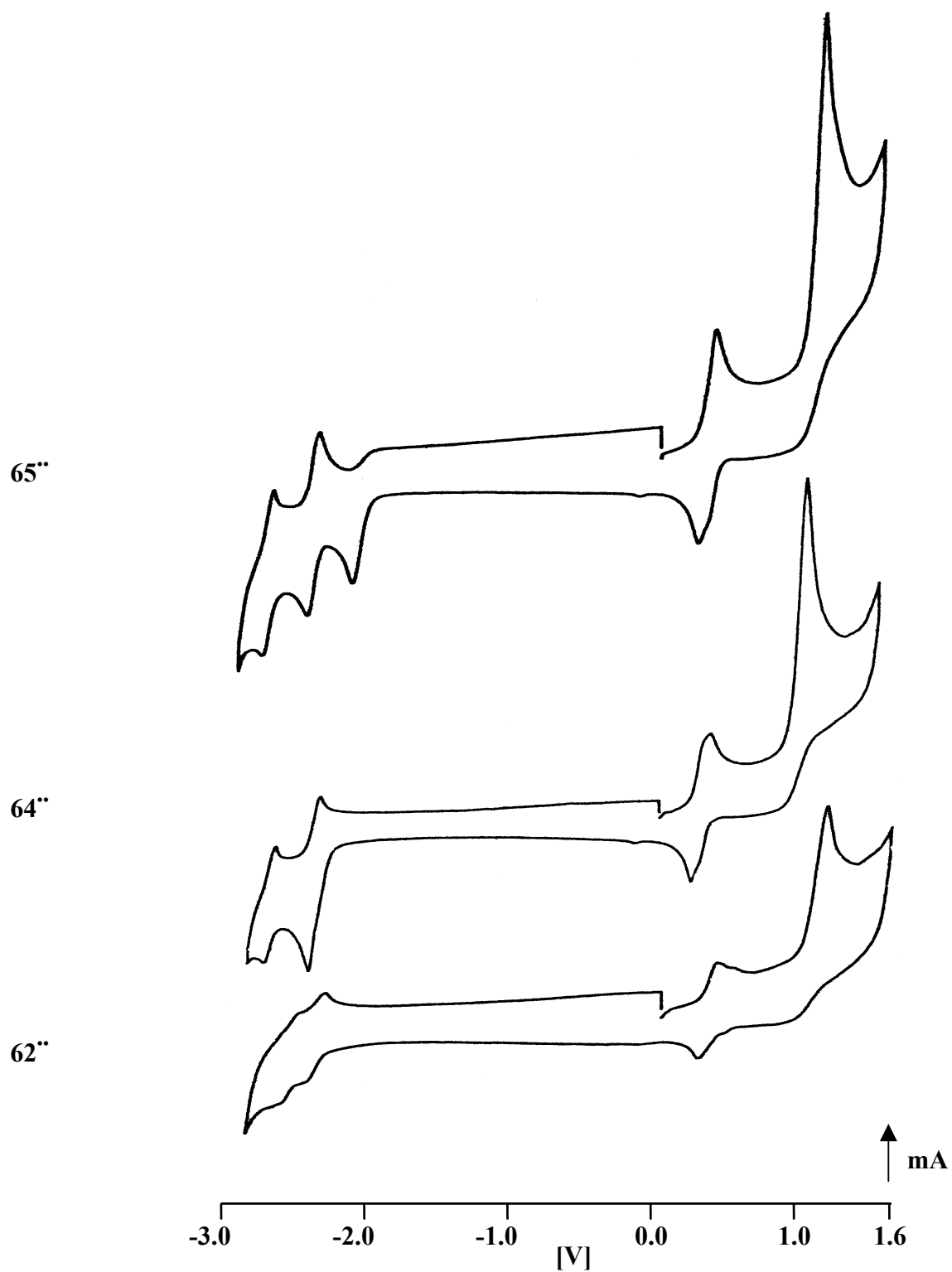
Figure 4.6. Cyclic voltammograms for **67·** in DME/TBAP at -40°C, v = 100mV/s
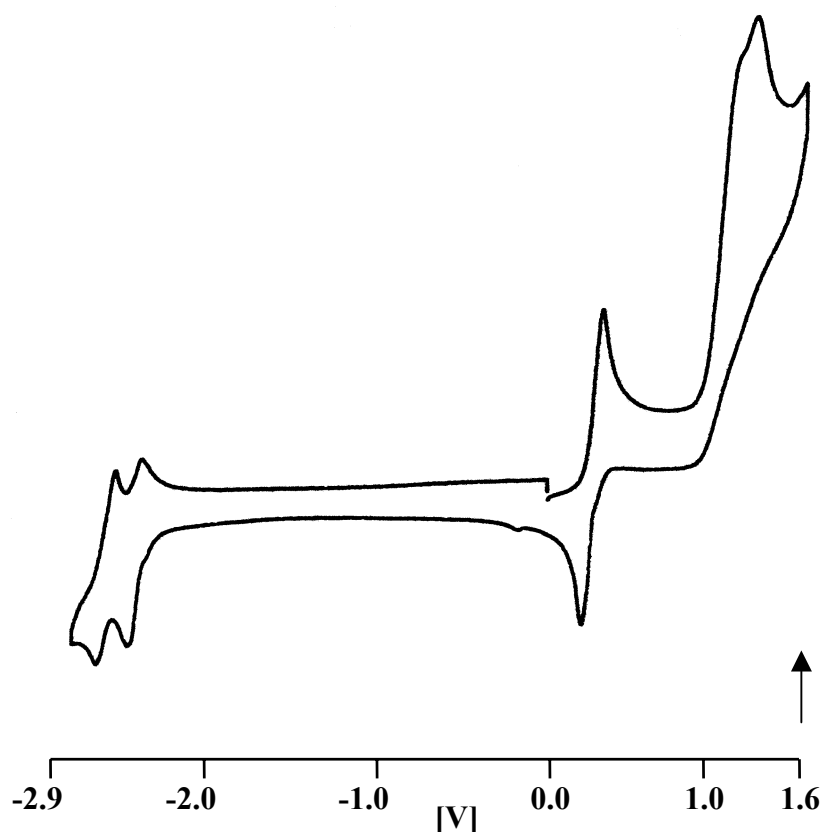
Table 4.3. Cyclic Voltammetry Data (**67·**)

$E_{1/2}(0/+)$	301 mV
ΔE_p	106 mV
I_{pa}/I_{pc}	1
E_{pa}	1.270 V
$E_{1/2}(0/-)$	-2.489 V
ΔE_p	66 mV
I_{pa}/I_{pc}	0.3
$E_{1/2}(-/2-)$	-2.686 V
I_{pa}/I_{pc}	1
ΔE_p	96 mV

4.3.3. Conclusion and Discussion

In conclusion, it has been demonstrated that the separation between redox waves also depends on the nature of the substituent to the bridging atom. Alternative steric and electronic arguments have been proposed.[96] For example, for [poly[Fe(C$_5$H$_4$)$_2$SiMe$_2$], [poly[Fe(C$_5$H$_4$)$_2$SiEt$_2$], [poly[Fe(C$_5$H$_4$)$_2$Si(n-Bu)$_2$], the $\Delta E_{1/2}$ values were given as 210, 270, 290 mV, respectively.[97]

The distance between two nuclei influences the size of $\Delta E_{1/2}$. If the interaction posses mainly by *through space*, the distance between two metals increases, the $\Delta E_{1/2}$ values will decrease.

Based on **65**[..] and **64**[..], although the distances of V...V are longer than that of **10**[..] due to the increasing bonds between two trovacenyl units, the interactions between the two metals are still stronger than that of **10**[..]. This confirms that the nature of metal bridges determines the interactions between two redox centers and affords efficient route for the electron transfer, because of their sufficient out-shell *d* electrons. Furthermore, the larger radius atom bridge would lead to the more overlap between the bridging atom's *d*-orbital and the cyclopentadienyl π orbital.

4.4. X-ray Crystal Structure Analysis

4.4.1. Dimethyldi([5]trovacenyl)tin (**63**[..])

Crystals of **63**[..] were generated from slowly cooling a saturated benzene solution. **63**[..] crystallizes in the monoclinic space group $P2_1/c$. Views of the structure are shown in Figures 4.7, and important bond length and angles are listed in Table 4.4 and 4.5, respectively. The central Sn atom adopts a tetrahedral coordination, in which the angle of C-Sn-C (mean) is 109.41(11)°, and presents almost coplanar with C_5 ring (mean torsion angle176.46(15)°). The dihedral angle (mean) of two cyclopentadienyl is 79.93(13)°. The $C_{C5\ ring}$ atoms are coplanar with a slightly torsion angle of 0.0(2)°.
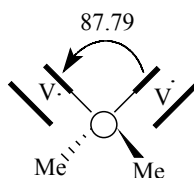
The V-$C_{C5\ ring}$ distances fall in the range of 2.249(2) ~ 2.259(2)Å, with a mean value of 2.252(2) Å. The V-C_{C7ring} distances fall in the range of 2.170(3)~2.180(3)Å (mean 2.175(3)Å).

Table 4.4. Selected bond lengths [Å] of **63**[..]

Sn(1) - C(1)	2.1234(19)	V(1) - C(6)	2.170(3)
Sn(1) - C(13)	2.132(2)	V(1) - C(7)	2.180(3)
Sn(1) - C(26)	2.129(3)	V(1) - C(8)	2.178(3)
Sn(1) - C(25)	2.130(3)	V(1) - C(9)	2.177(3)
Sn(1) - C(mean)	**2.128(3)**	V(1) - C(10)	2.175(3)
V(1) - C(1)	2.2577(19)	V(1) - C(11)	2.173(3)
V(1) - C(2)	2.249(2)	V(1) - C(12)	2.171(3)
V(1) - C(3)	2.259(2)	**V(1)-C_7 Ring (mean)**	**2.175(3)**
V(1) - C(4)	2.262(2)	**V(1)-C_7 (centroid)**	1.466(1)
V(1) - C(5)	2.253(2)	C(6) - C(7)	1.427(6)
V(1)-C_5 Ring (mean)	**2.252(2)**	C(6) - C(12)	1.464(6)
V(1)-C_5 (centroid)	1.912(1)	C(7) - C(8)	1.353(5)
C(1) - C(2)	1.419(3)	C(8) - C(9)	1.348(5)
C(1) - C(5)	1.422(3)	C(9) - C(10)	1.355(5)
C(2) - C(3)	1.415(3)	C(10) - C(11)	1.375(6)
C(3) - C(4)	1.405(4)	C(11) - C(12)	1.436(6)
C(4) - C(5)	1.416(3)	**C-C (mean for C_7)**	**1.396(6)**
C-C (mean for C_5)	**1.415(3)**	**V(1) - V(2)**	**7.695(2)**

Figure 4.7. Molecular structure and stereoview of **63**[¨]
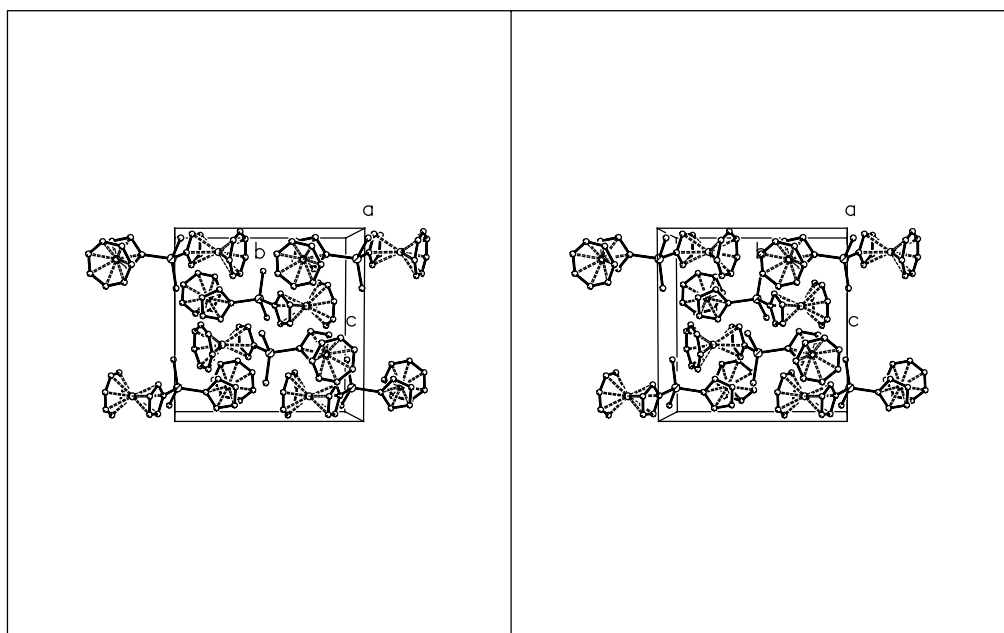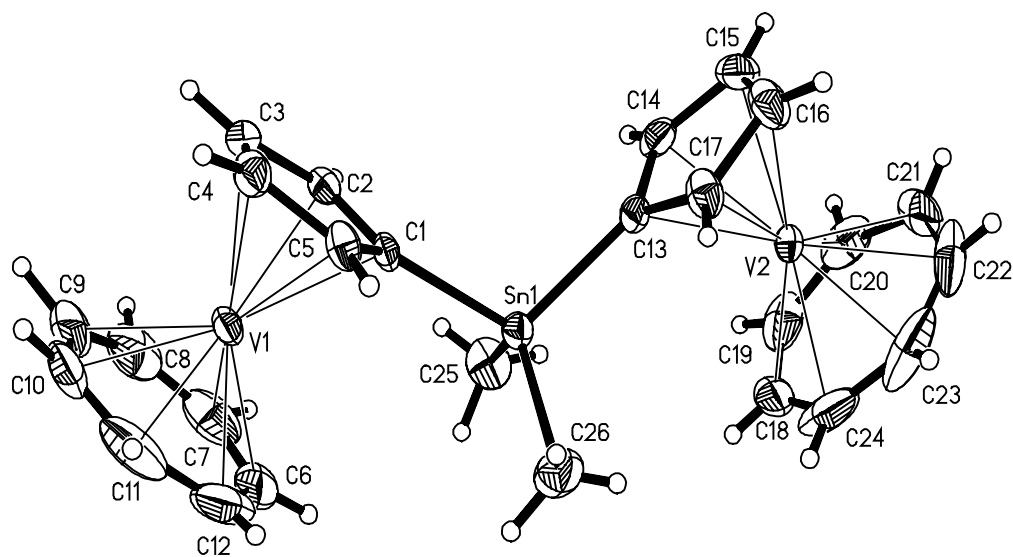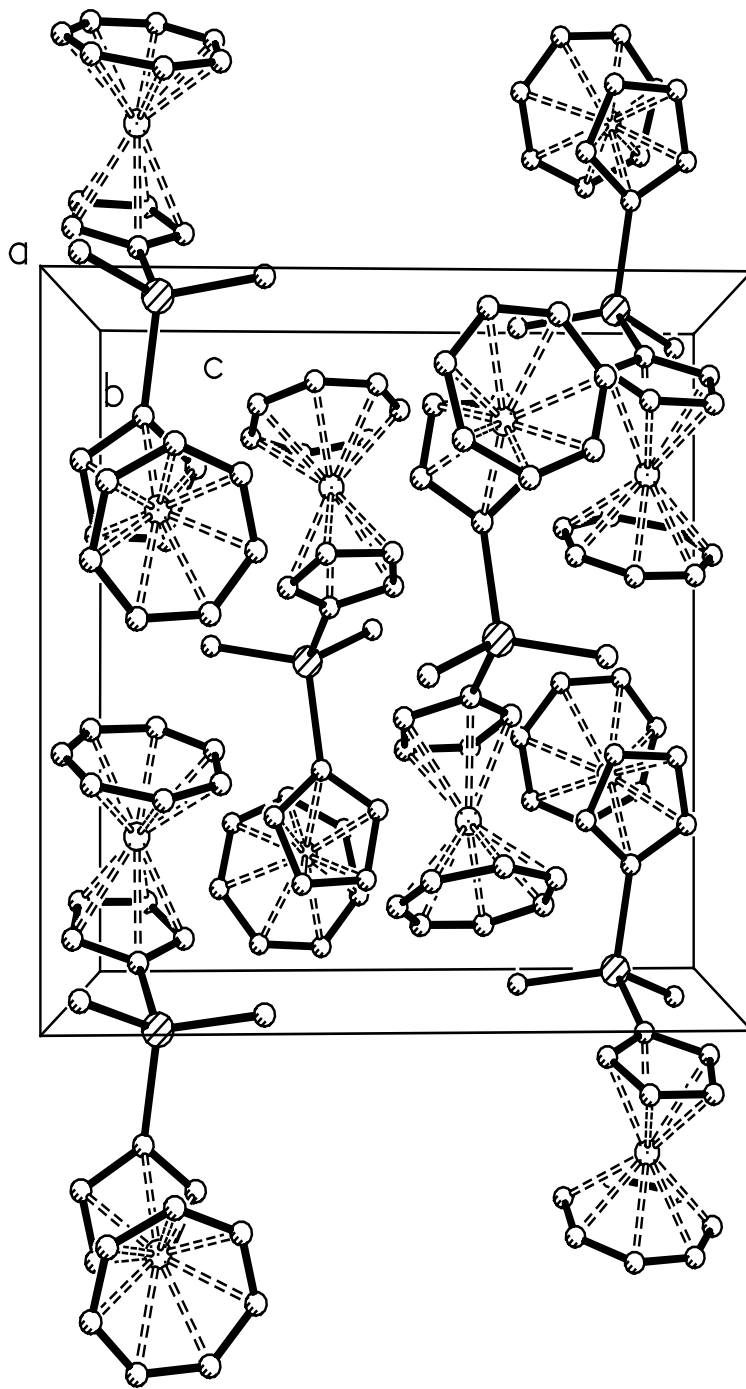
These distance are typical for trovacene and **10**^{˙˙}. It is notable that all the Sn-C distance are close to each other, the mean length is 2.128(3)Å. The Sn-C$_{C5ring}$ bond has not been sterically elongated due to linked to two cyclopentadienyl rings. The metal-metal distance is 7.695(2), which is 40% longer than that of **10**^{˙˙} (5.501Å).

Table 4.5. Selected angles [°] and Torsional angles [°]of **63**^{˙˙}

C(1)-Sn(1)-C(26)	110.24(11)	C(2)-C(1)-C(5)	106.31(18)
C(1)-Sn(1)-C(25)	107.65(11)	C(14)-C(13)-C(17)	105.9(2)
C(1)-Sn(1)-C(13)	105.78(7)	Sn(1)-C(1)-C(2)-C(3)	-176.80(14)
C(25)-Sn(1)-C(13)	109.49(10)	Sn(1)-C(1)-C(5)-C(4)	176.34(15)
C(26)-Sn(1)-C(25)	114.66(14)	Sn(1)-C(13)-C(17)-C(16)	-176.47(15)
C(26)-Sn(1)-C(13)	108.64(12)	Sn(1)-C(13)-C(14)-C(15)	176.21(15)
C(5)-C(1)-Sn(1)	129.41(16)	C(1)-Sn(1)-C(13)-C(14)	-87.93(19)
C(2)-C(1)-Sn(1)	124.17(15)	C(1)-Sn(1)-C(13)-C(17)	87.67(19)
C(14)-C(13)-Sn(1)	128.84(17)	C(13)-Sn(1)-C(1)-C(2)	85.45(17)
C(17)-C(13)-Sn(1)	125.14(17)	C(13)-Sn(1)-C(1)-C(5)	-90.1(2)
Torsion C$_7$ Ring (mean)	**-0.04(6)**	**Torsion C$_5$ Ring (mean)**	**0.0(2)**

4.4.2. Diphenyldi([5]trovacenyl)tin (**64**^{˙˙})

The crystals of **64**^{˙˙} suitable for X-ray diffraction were generated from the diffusion of PE to the solution of benzene at 8°C. **64**^{˙˙} crystallizes in the triclinic space group $P2_1$/c. Views of the structure are shown in Figures 4.8, and important bond length and angles are listed in Table 4.6 and 4.7, respectively.

Table 4.6. Selected bond lengths [Å] of **64**^{˙˙}

Sn(1) - C(1)	2.132(2)	V(1) - C(6)	2.196(2)
Sn(1) - C(13)	2.121(2)	V(1) - C(7)	2.184(3)
Sn(1) - C(25)	2.137(2)	V(1) - C(8)	2.182(3)
Sn(1) - C(31)	2.138(2)	V(1) - C(9)	2.178(3)
Sn(1) - C(mean)	**2.132(2)**	V(1) - C(10)	2.175(3)
V(1) - C(1)	2.272(2)	V(1) - C(11)	2.175(3)
V(1) - C(2)	2.261(2)	V(1) - C(12)	2.180(3)
V(1) - C(3)	2.248(3)	**V(1)-C$_7$ Ring (mean)**	**2.181(3)**
V(1) - C(4)	2.249(2)	**V(1)-C$_7$ (centroid)**	1.467(1)
V(1) - C(5)	2.255(2)	C(6) - C(7)	1.402(4)
V(1)-C$_5$ Ring (mean)	**2.257(2)**	C(6) - C(12)	1.397(4)
V(1)-C$_5$ (centroid)	1.912(1)	C(7) - C(8)	1.407(4)
C(1) - C(2)	1.414(3)	C(8) - C(9)	1.394(5)
C(1) - C(5)	1.423(3)	C(9) - C(10)	1.401(5)
C(2) - C(3)	1.411(4)	C(10) - C(11)	1.406(5)
C(3) - C(4)	1.402(4)	C(11) - C(12)	1.418(4)
C(4) - C(5)	1.411(4)	**C-C (mean for C$_7$)**	**1.403(4)**
C-C (mean for C$_5$)	**1.412(4)**	C(31)-C(32)	1.381(4)
C(25)-C(26)	1.393(4)	**C-C (mean for C$_6$)**	**1.384(4)**
C-C (mean for C$_6$)	**1.383(4)**	**V(1) - V(2)**	**6.961(2)**

Figure 4.8. Molecular structure and stereoview of **64**[¨]
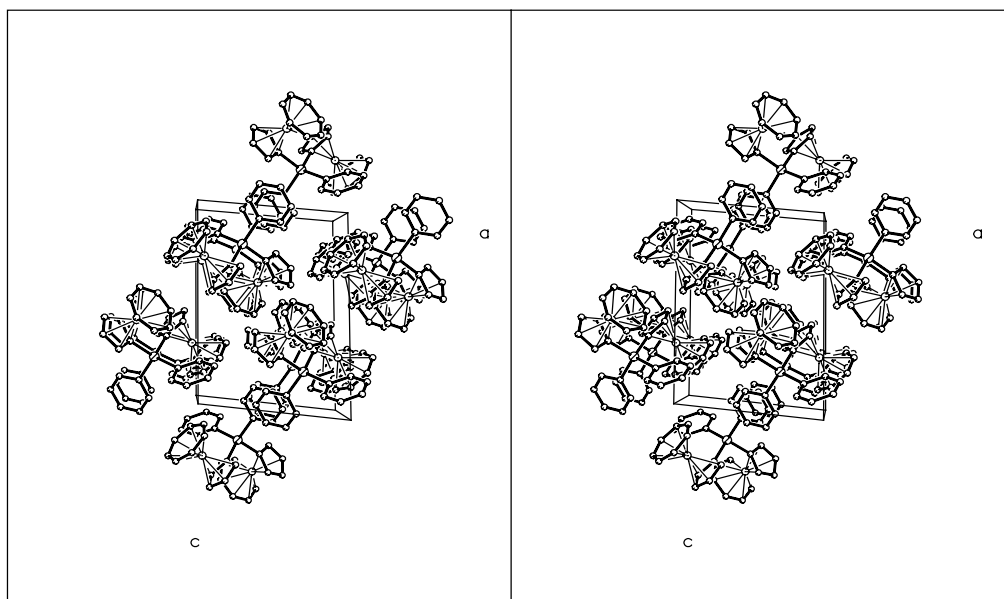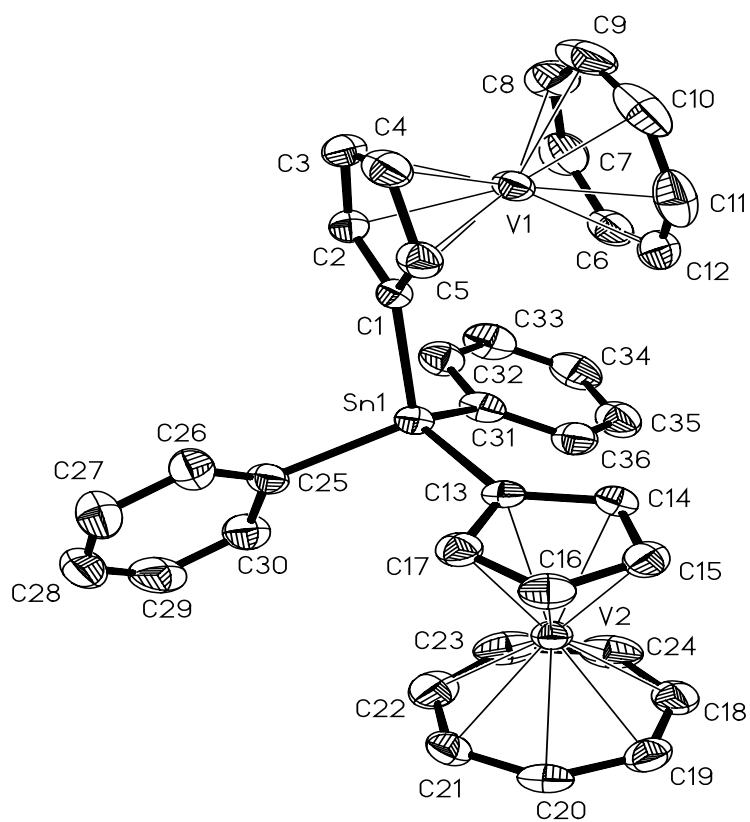
Table 4.7. Selected angles [°] and Torsional angles [°] of **64**^{··}

C(13)-Sn(1)-C(1)	107.60(8)	Sn(1)-C(1)-C(2)-C(3)	176.89(16)
C(13)-Sn(1)-C(25)	106.09(9)	Sn(1)-C(13)-C(14)-C(15)	176.99(15)
C(1)-Sn(1)-C(25)	108.20(8)	Sn(1)-C(25)-C(30)-C(29)	172.7(2)
C(13)-Sn(1)-C(31)	114.30(9)	Sn(1)-C(31)-C(32)-C(33)	169.05(19)
C(1)-Sn(1)-C(31)	107.13(8)	C(25)-Sn(1)-C(1)-C(2)	-71.3(2)
C(25)-Sn(1)-C(31)	113.26(9)	C(31)-Sn(1)-C(1)-C(2)	51.2(2)
C(5)-C(1)-Sn(1)	126.91(17)	C(1)-Sn(1)-C(13)-C(17)	91.04(18)
C(2)-C(1)-Sn(1)	126.07(17)	C(13)-Sn(1)-C(1)-C(2)	174.49(18)
C(14)-C(13)-Sn(1)	129.95(17)	C(13)-Sn(1)-C(31)-C(32)	-172.76(18)
C(17)-C(13)-Sn(1)	124.24(17)	C(1)-Sn(1)-C(31)-C(32)	-53.7(2)
C(14)-C(13)-C(17)	105.7(2)	C(25)-Sn(1)-C(31)-C(32)	65.6(2)
C(2)-C(1)-C(5)	106.9(2)	C(25)-Sn(1)-C(13)-C(14)	158.89(19)
C(1)-Sn(1)-C(31)-C(36)	116.37(19)	C(31)-Sn(1)-C(13)-C(14)	33.3(2)
C(25)-Sn(1)-C(31)-C(36)	-124.40(19)	C(13)-Sn(1)-C(31)-C(36)	-2.7(2)
Torsion C₅ Ring (mean)	**0.0(3)**	C(36)-C(31)-C(32)-C(33)	-1.2(4)
Torsion C₇ Ring (mean)	**-0.1(5)**		

Similar to **63**^{··}, the central Sn atom of **64**^{··} also adopts a tetrahedral structure, in which the angle of C-Sn-C (mean) is 109.41(11)°, and almost is coplanar with C_5 ring (mean torsion angle 176.46(15)°). The dihedral angles of two Cp rings and two Ph rings are 88.08(14) and 80.78(14)°, respectively. The dihedral angles of Cp(1) with two Ph rings are 88.36(14) and 63.28(14)°.

The length of Sn-C (mean 2.132(2)Å) is close to that of **63**^{··}. All the carbon atoms of the two phenyl groups almost lie in the corresponding plane. The metal-metal distance, 6.961(2)Å, is slightly longer than that that of **63**^{··}, due to the steric hindrance from the two phenyl group. The distance of C-C is consist with the tendency of $C_6 < C_7 < C_5$, 1.383Å, 1.403Å and 1.412Å, respectively.

4.4.3. Diphenyldi([5]trovacenyl)lead (**65**^{··})

The crystals of **65**^{··} suitable for X-ray diffraction analysis were generated from saturated benzene solution at 8°C in two days. Molecular structure and selected bond and angles are shown in Figure 4.9 and Table 4.8, 4.9, respectively. Obviously, the four C atoms linked Pb atom do not lie in the same plane, rather than adopt a tetrahedral form similar to that of CH_4. The mean value of Pb-C $_{Cp ring}$ distance is 2.193(2) Å and the Pb-C$_{Ph}$ bond is 2.207(3) Å. The dihedral angle between two Cp rings is 88.57(18)°. The dihedral angles between Cp(1) and two Ph rings are 87.78(18) and 64.44(18)°, for Cp(2) are 74.47(16) and 24.84(16)°.
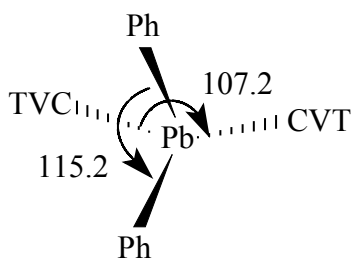
Figure 4.9. Molecular structure and stereoview of **65¨**
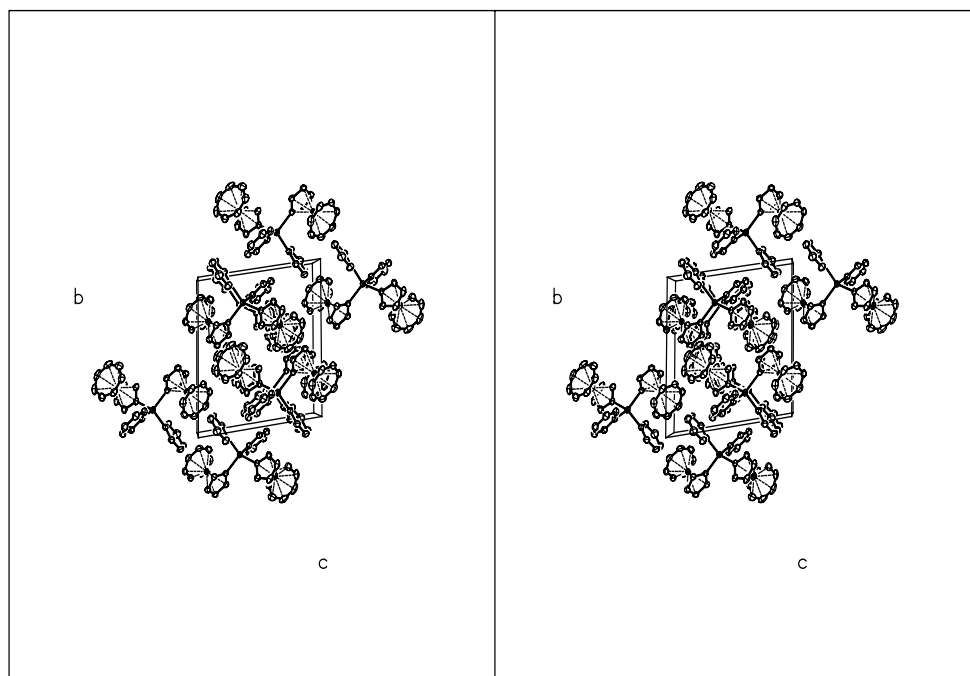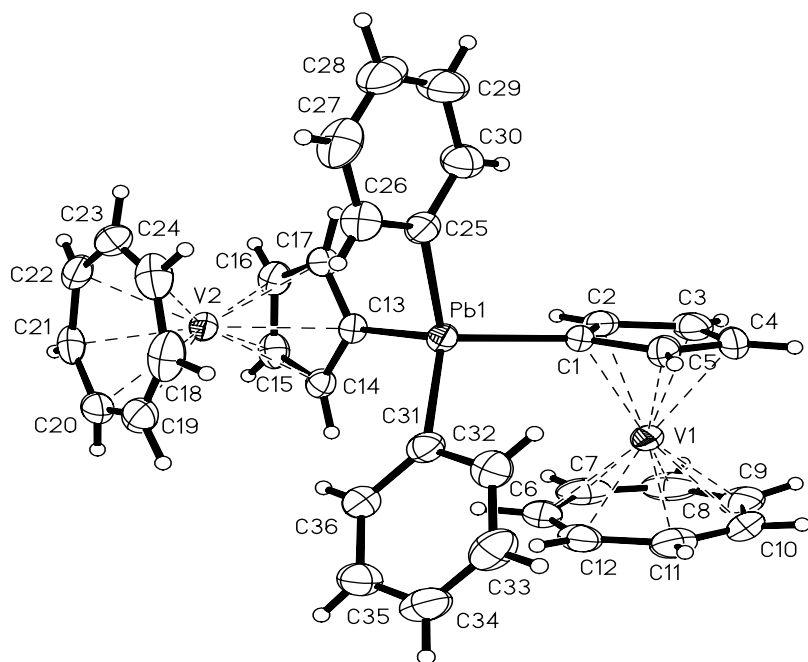
Table 4.8. Selected bond lengths [Å] of **65**

Pb(1) - C(1)	2.195(3)	V(1) - C(6)	2.185(3)
Pb(1) - C(13)	2.192(2)	V(1) - C(7)	2.178(3)
Pb(1) - C(25)	2.217(3)	V(1) - C(8)	2.173(4)
Pb(1) - C(31)	2.197(3)	V(1) - C(9)	2.184(3)
Pb(1) - C(mean)	**2.200(3)**	V(1) - C(10)	2.184(3)
V(1) - C(1)	2.279(3)	V(1) - C(11)	2.180(3)
V(1) - C(2)	2.257(3)	V(1) - C(12)	2.201(3)
V(1) - C(3)	2.247(3)	**V(1)-C$_7$ Ring (mean)**	**2.284(3)**
V(1) - C(4)	2.255(3)	**V(1)-C$_7$ (centroid)**	1.466(1)
V(1) - C(5)	2.266(3)	C(6) - C(7)	1.414(6)
V(1)-C$_5$ Ring (mean)	**2.261(3)**	C(6) - C(12)	1.403(5)
V(1)-C$_5$ (centroid)	1.912(1)	C(7) - C(8)	1.409(6)
C(1) - C(2)	1.412(4)	C(8) - C(9)	1.398(6)
C(1) - C(5)	1.421(4)	C(9) - C(10)	1.397(6)
C(2) - C(3)	1.427(4)	C(10) - C(11)	1.395(5)
C(3) - C(4)	1.413(5)	C(11) - C(12)	1.411(5)
C(4) - C(5)	1.408(6)	**C-C (mean for C$_7$)**	**1.395(6)**
C-C (mean for C$_5$)	**1.416(5)**	C(31)-C(32)	1.389(4)
C(25)-C(26)	1.380(4)		
C-C (mean for C$_6$)	**1.383(5)**	**V(1) - V(2)**	**9.1370(1)**

The angles of C(13)-Pb(1)-C(1) and C(25)-Pb(1)-C(31) close to 109.28°, are 107.21(10)° and 115.28(11)°, respectively. The C atoms of phenyl are almost coplanar. The V(1)-V(2) distance is 9.1370(1)Å, which is nearly double that of **10**(5.501(1)Å) and greater than that of **64** (6.906Å). In comparison with their relative redox splitting, it can be concluded that the metal-metal distances do not determine the interaction between metals, but the nature of the bridges or *through bond* interaction play the crucial role.

Table 4.9. Selected angles [°] and Torsional angles [°] of **65**

C(13)-Pb(1)-C(1)	107.21(10)	C(2)-C(1)-C(5)	107.1(2)
C(1)-Pb(1)-C(31)	106.48(10)	C(14)-C(13)-C(17)	106.9(2)
C(1)-Pb(1)-C(25)	108.19(10)	C(26)-C(25)-C(30)	119.1(3)
C(13)-Pb(1)-C(31)	113.93(10)	C(32)-C(31)-C(36)	119.3(3)
C(13)-Pb(1)-C(25)	105.38(9)	C(25)-Pb(1)-C(1)-C(5)	73.2(2)
C(31)-Pb(1)-C(25)	115.28(11)	C(31)-Pb(1)-C(1)-C(5)	-51.3(3)
C(5)-C(1)-Pb(1)	125.9(2)	Pb(1)-C(1)-C(2)-C(3)	177.2(3)
C(2)-C(1)-Pb(1)	126.97(19)	Pb(1)-C(1)-C(5)-C(4)	-177.0(2)
C(14)-C(13)-Pb(1)	129.2(19)	Pb(1)-C(13)-C(17)-C(16)	178.17(19)
C(17)-C(13)-Pb(1)	123.9(2)	Pb(1)-C(13)-C(14)-C(15)	-177.98(19)
C(26)-C(25)-Pb(1)	121.8(2)	C(1)-Pb(1)-C(13)-C(14)	85.7(2)
C(30)-C(25)-Pb(1)	118.8(2)	C(1)-Pb(1)-C(13)-C(17)	-91.8(2)
C(36)-C(31)-Pb(1)	120.4(2)	C(13)-Pb(1)-C(1)-C(2)	9.8(3)
C(32)-C(31)-Pb(1)	119.6(2)	C(13)-Pb(1)-C(1)-C(5)	-173.6(2)
Torsion C$_7$ Ring (mean)	**0.0(0)**	**Torsion C$_5$ Ring (mean)**	**0.0(0)**

4.4.4. X-ray Crystal Structure Analysis of 67[.]

The crystal suitable for X-ray diffraction was generated from saturated ethanol solution at r.t. The molecule structure is depicted in Figure 4.10, and the selected bond, angles and torsion are summarized in Table 4.10 and 4.11, respectively.

Two hydrogen bonds are formed between two neighboring **67[.]** and one molecule **67[.]** with C_2H_5OH. The distances of O(1)-H(1)...O(1') and O(1')-H(1')...O(100) are 2.742(3) and 2.740(4)Å, respectively, in which the bond length of O(1)-H(1) is 0.78(5)Å. The bond length of Si-C_{Cp}, 1.861(3)Å, is close to that of Si-C_{phenyl} (1.869(4)Å, 1.877(3)Å), and fall in the range of Si-C (1.86-1.92 Å). However, the Si-O bond distance (1.626(2)Å) is slightly shorter than the typical Si-O (1.63-1.65 Å).[106] The angle of Si(1)-O(1)-H(1) is 120(3)°.

In order to reduce the steric hindrance, the geometry of the molecule adopts a slightly distorted tetrahedral structure around the Si atom. This can be inferred from the angles of O(1)-Si(1)-C(1) (109.85(15)°), O(1)-Si(1)-C(13) (109.21(15)°), C(1)-Si(1)-C(13) (109.31(15)°) and C(13)-Si(1)-C(19) (107.29(15)°).

The Si atom lies in the planes of the linked respective Cp ring or phenyl groups. For example, Si(1)-C(1)-C(2)-C(3), -177.4(3)° and Si(1)-C(13)-C(14)-C(15) 179.7(3)°. All carbon atoms of phenyl rings almost lie in the same plane. The torsional angles of O(1)-Si(1)-C(1)-C(2) and O(1)-Si(1)-C(13)-C(14) are -137.5(3)° and -172.7(3)°, respectively. The dihedral angles between Cp and two Ph rings are 88.3(2) and 45.1(2)°.
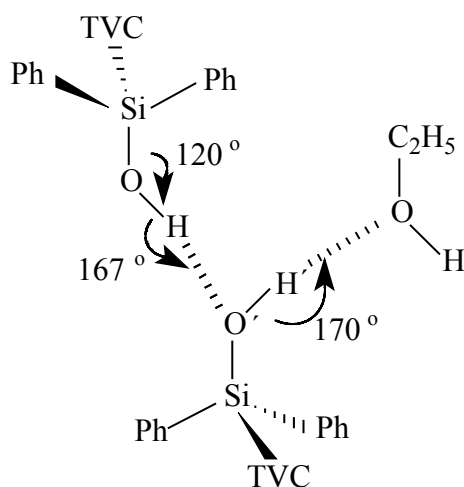
Figure 4.10. Molecular structure and stereoview plot of **67**
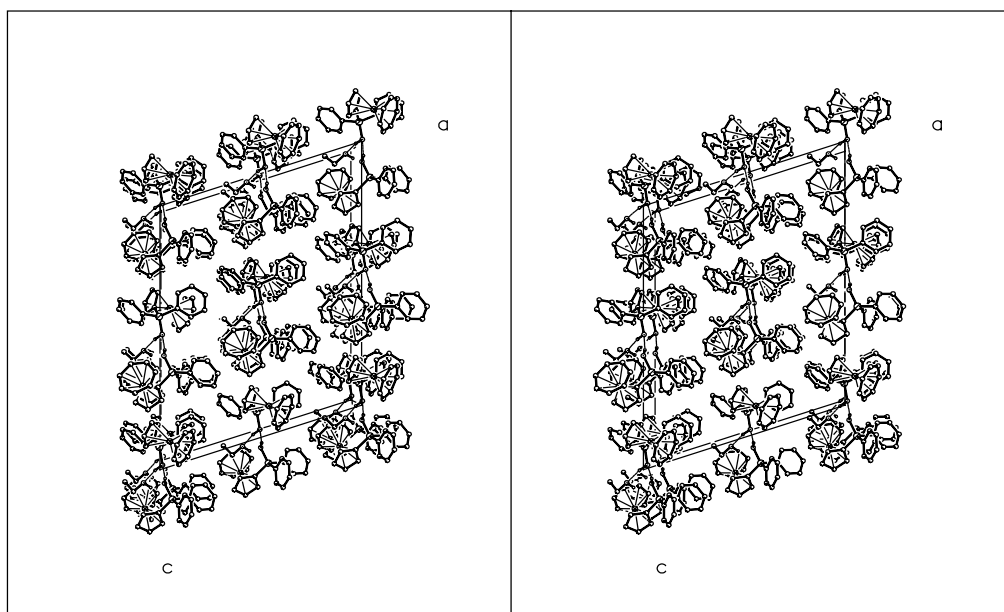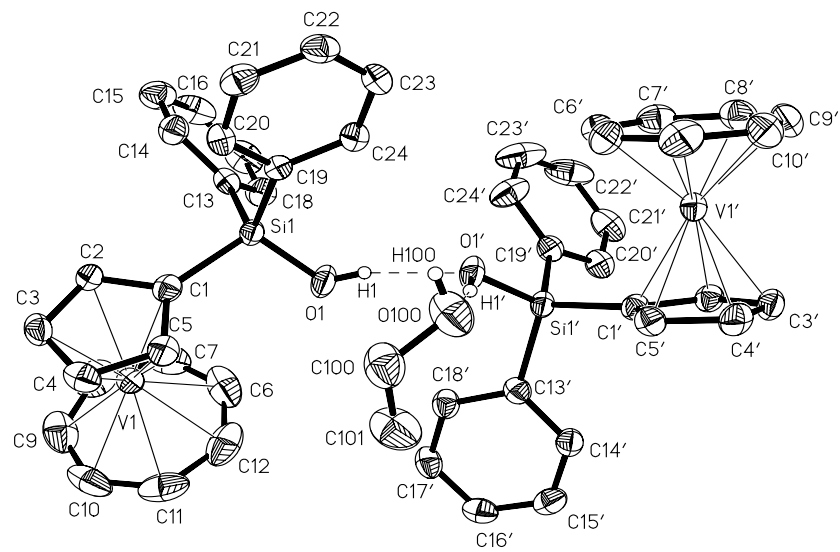
Table 4.10. Selected bond lengths [Å] of **67**$^\bullet$

Si(1) - C(1)	1.861(3)	V(1) - C(6)	2.171(4)
Si(1) - C(13)	1.869(4)	V(1) - C(7)	2.172(4)
Si(1) - C(19)	1.877(3)	V(1) - C(8)	2.180(5)
Si(1) - C(mean)	1.869(3)	V(1) - C(9)	2.188(5)
V(1) - C(1)	2.275(3)	V(1) - C(10)	2.185(5)
V(1) - C(2)	2.260(3)	V(1) - C(11)	2.178(4)
V(1) - C(3)	2.268(3)	V(1) - C(12)	2.172(4)
V(1) - C(4)	2.255(4)	**V(1)-C$_7$ Ring (mean)**	2.178(4)
V(1) - C(5)	2.247(4)	**V(1)-C$_7$ (centroid)**	**1.468(1)**
V(1)-C$_5$ Ring (mean)	2.261(3)	C(6) - C(7)	1.382(7)
V(1)-C$_5$ (centroid)	1.913(2)	C(6) - C(12)	1.414(8)
Si(1)-O(1)	1.626(2)	C(7) - C(8)	1.410(7)
O(1)-H(1)	0.78(5)	C(8) - C(9)	1.394(7)
C(1) - C(2)	1.433(5)	C(9) - C(10)	1.372(8)
C(1) - C(5)	1.426(5)	C(10) - C(11)	1.394(8)
C(2) - C(3)	1.401(5)	C(11) - C(12)	1.406(7)
C(3) - C(4)	1.406(6)	**C-C (mean for C$_7$)**	1.396(8)
C(4) - C(5)	1.422(5)	O(1)-H(1)...O(1')	2.742(3)
C-C (mean for C$_5$)	1.417(5)	O(1')-H(1')...O(100)	2.740(4)

Table 4.11. Selected angles [°] and Torsional angles [°] of **67**$^\bullet$

O(1)-Si(1)-C(1)	109.85(15)	C(20)-C(19)-Si(1)	122.3(3)
O(1)-Si(1)-C(13)	109.21(15)	O(1)-Si(1)-C(1)-C(5)	45.8(3)
C(1)-Si(1)-C(13)	109.31(15)	C(13)-Si(1)-C(1)-C(5)	165.6(3)
O(1)-Si(1)-C(19)	110.50(14)	C(19)-Si(1)-C(1)-C(5)	-76.5(3)
C(1)-Si(1)-C(19)	110.63(15)	O(1)-Si(1)-C(1)-C(2)	-137.5(3)
C(13)-Si(1)-C(19)	107.29(15)	Si(1)-C(1)-C(2)-C(3)	-177.4(3)
Si(1)-O(1)-H(1)	120(3)	C(5)-C(1)-C(2)-C(3)	0.0(4)
C(5)-C(1)-Si(1)	128.6(3)	O(1)-Si(1)-C(13)-C(14)	-172.7(3)
C(2)-C(1)-Si(1)	126.3(3)	C(1)-Si(1)-C(13)-C(14)	67.1(3)
C(14)-C(13)-Si(1)	121.5(3)	C(19)-Si(1)-C(13)-C(14)	-52.9(3)
C(5)-C(1)-C(2)	105.0(3)	Si(1)-C(13)-C(14)-C(15)	179.7(3)
C(14)-C(13)-C(18)	116.6(3)	C(13)-C(14)-C(15)-C(16)	-1.5(6)
C(20)-C(19)-C(24)	116.8(3)	O(1)-Si(1)-C(19)-C(20)	-149.3(3)
O(1)-H(1)...O(1')	2.742(3)	C(1)-Si(1)-C(19)-C(20)	-27.4(3)
O(1')-H(1')...O(100)	2.740(4)	**Torsion C$_7$ Ring (mean)**	**0.0(0)**
		Torsion C$_5$ Ring (mean)	**0.0(0)**

4.5. EPR Spectra (60$^{\bullet\bullet}$, 62$^{\bullet\bullet}$, 63$^{\bullet\bullet}$, 64$^{\bullet\bullet}$ and 67$^{\bullet}$)

The EPR spectra in fluid solution and rigid solution (toluene) of $(TVC)_2(SiMe_2)_2$ (**60**$^{\bullet\bullet}$), $(TVC)_2GePh_2$ (**62**$^{\bullet\bullet}$), $(TVC)_2SnMe_2$ (**63**$^{\bullet\bullet}$), $(TVC)_2SnPh_2$ (**64**$^{\bullet\bullet}$) are shown in Figure 4.11, 4.12, 4.13, 4.14, respectively. The respective parameters are summarized in Table 4.12.

The EPR spectra of the four binuclear complexes exhibit the typical 15-line type, which indicates that the unpaired electrons couples with the two vanadium nuclei. The line splitting of these binuclear complexes are half the value of the mononuclear complexes. The coupling

constants shown in Table 4.8 are significantly larger than those of trovacene ($A_{iso}(^{51}V)$ = 6.98mT). The coupling between cyclopentadienyl π orbital and the corresponding vacant p_π or d_π orbital of the bridging atom, and the spin-transfer from metal to ligand, contribute to the large value. The hyperfine splitting of ($^{Sn}A_{aniso}$) (**63$^{..}$**) is 10.2G.

Although the numerical value of exchange interaction J provided by the computer simulation can not be confided completely, an information that the mono-atom bridging binuclear complex has a relative rather stronger coupling between two V centers than that of di-atoms bridging binuclear complex, can still be inferred. For example, Sn (**63$^{..}$**) (J ~12,000G) > Si-Si (**60$^{..}$**) (J ~5,000G).

Compared to the exchange coupling constant of di([5]trovacene)disulfide (**18$^{..}$**), it can be concluded that with the radius of saturated bridging di-atoms decreased, the exchange coupling increased. There are some other factors to determine the magnitude of the exchange coupling constant, such as, the polarizability of the bridging atom, inductive effect from the substituent. Simultaneously, it may be predicted that in the same column, with the radius of the bridging atom increasing, the exchange coupling increase. However, the detailed analysis must await the results of the computer spectral simulations and investigation of all the relative binuclear complexes by EPR due to the reason of time constraint.

Table 4.12. EPR data of **60$^{..}$**, **62$^{..}$**, **63$^{..}$** and **64$^{..}$**

	$A(^{51}V)_{iso}$	g_{iso}	J	α	β	γ	ΔB
60$^{..}$	7.24mT	1.9847	0.467 cm^{-1}	-0.21	-0.07	0.80	28 G
62$^{..}$	7.34mT	1.9895					
63$^{..}$	7.23mT	1.9815	1.122 cm^{-1}	-0.075	-0.14	-0.135	37.8G
64$^{..}$	7.22mT	1.9869					

Figure 4.11. EPR spectra of **60$^{..}$** in fluid solution (toluene) and rigid solution (toluene); 300K, ν = 9.2080 GHz, A) experimental, B) simulated; C) 340K, ν = 9.2083 GHz ; D) 260K, ν = 9.2099 GHz; E) 220K, ν = 9.2084 GHz; F) 131K, ν = 9.2158 GHz.
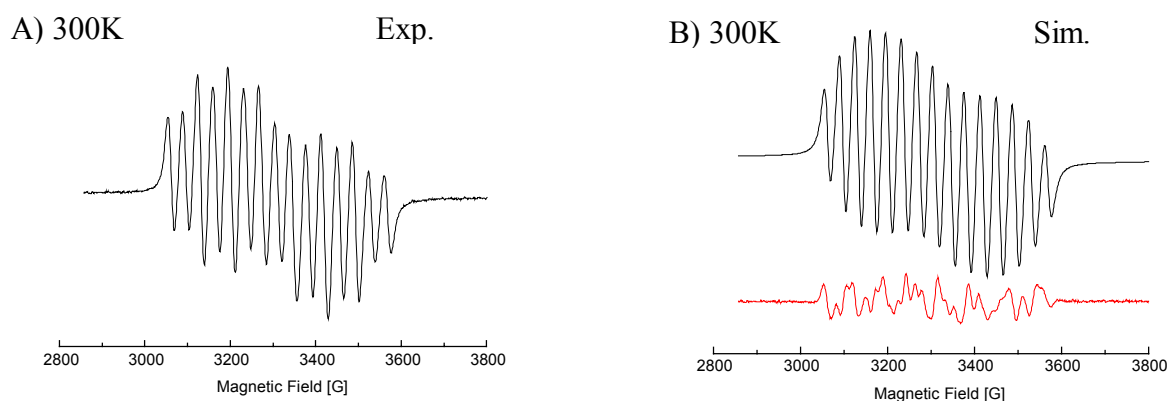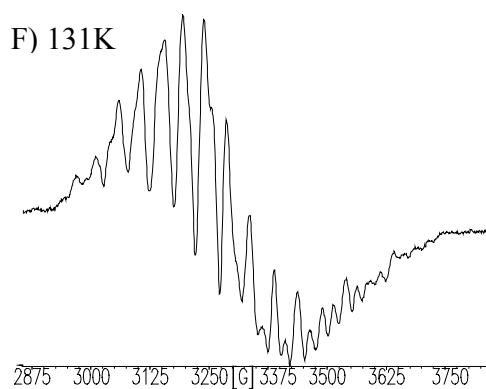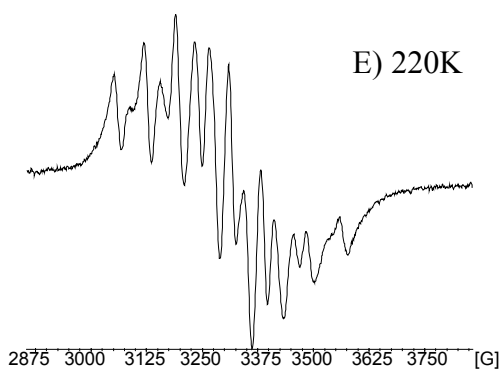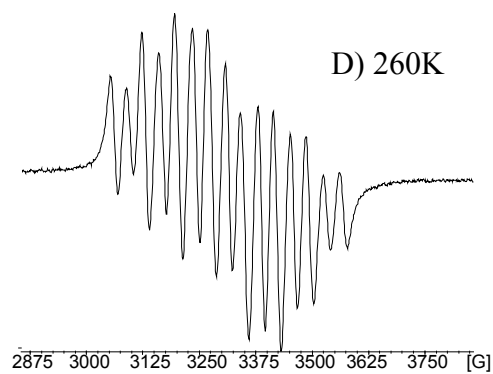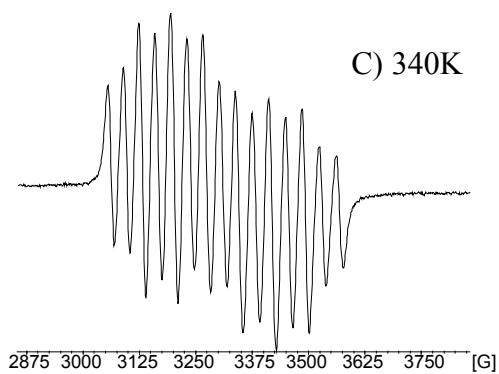
Figure 4.12. Experimental EPR spectra of **62**·· in fluid solution (toluene) and rigid solution (toluene); A) 295K, ν = 9.2149GHz; B) 260K, ν = 9.2158GHz; C) 136K, ν = 9.2149GHz.

C) 136K
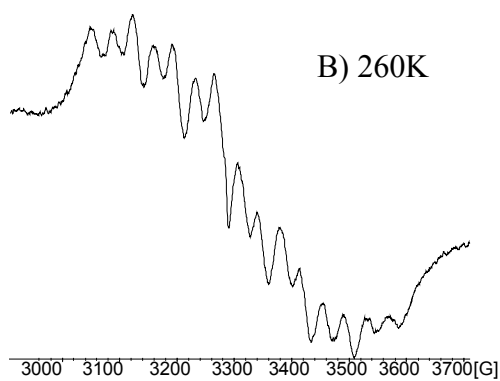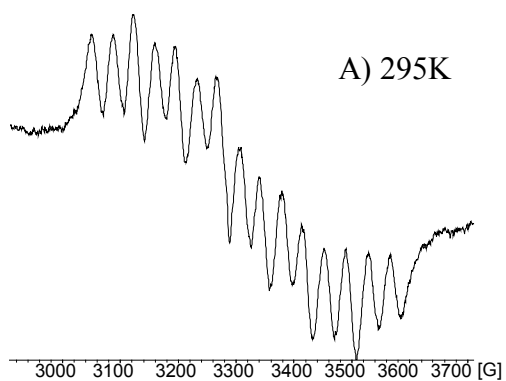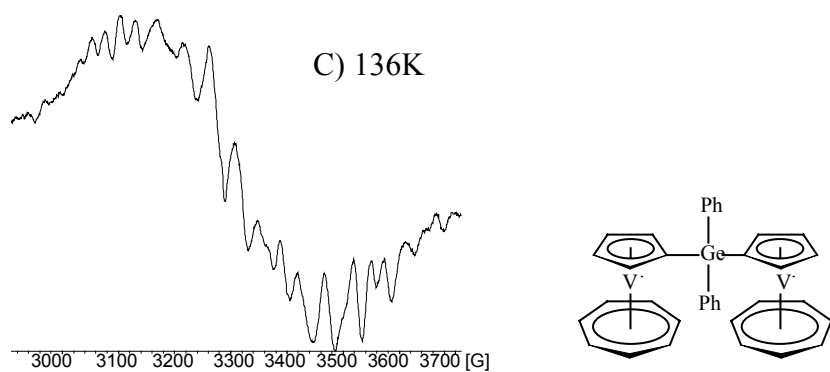
Figure 4.13. EPR spectra of **63** in fluid solution (toluene) and rigid solution (toluene); experimental A) and B) simulated at 294K, ν = 9.2472 GHz; C) 250K, ν = 9.2474 GHz; D) 210K, ν = 9.2477 GHz; E) 127K, ν = 9.2471 GHz; F) 330K, ν = 9.2469 GHz.

A) 294K   Exp.

B) 294K   Sim.

C) 250K

D) 210K
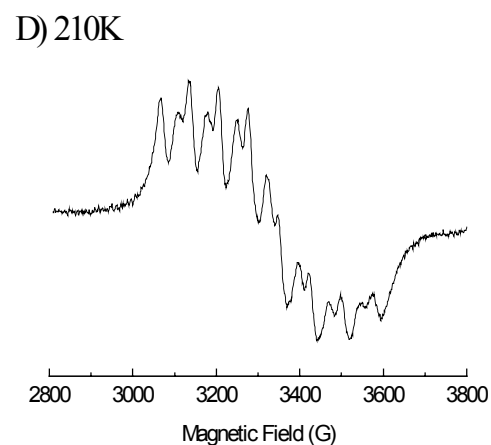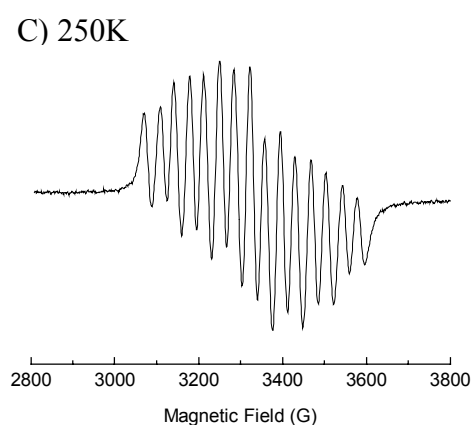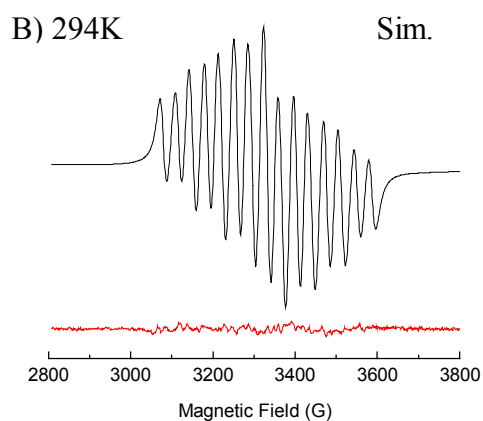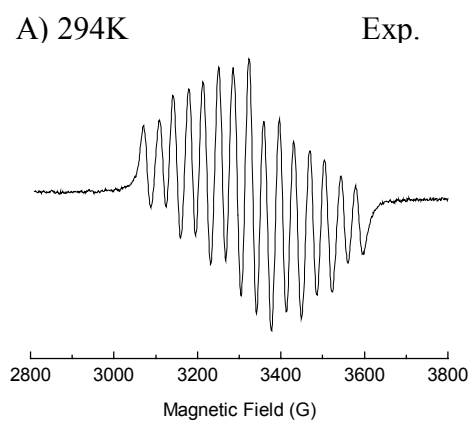
E) 127K
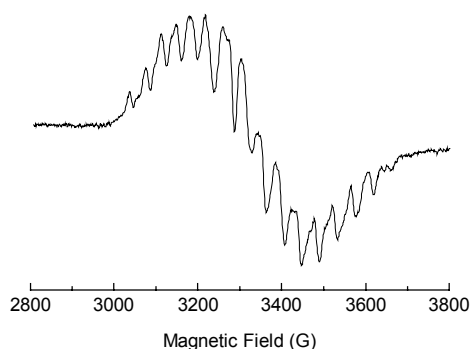
F) 330K
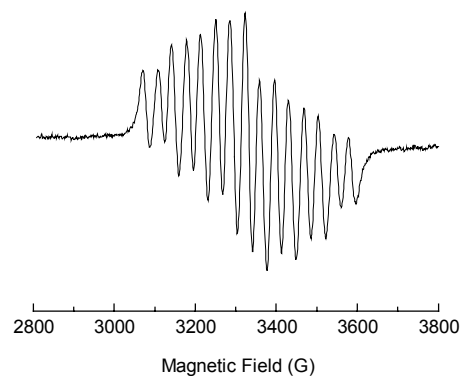
Figure 4.14. Experimental EPR spectra of **64**·· in fluid solution (toluene) and rigid solution (toluene); A), 300K, ν = 9.2166GHz; B); 131K, ν = 9.2174GHz.
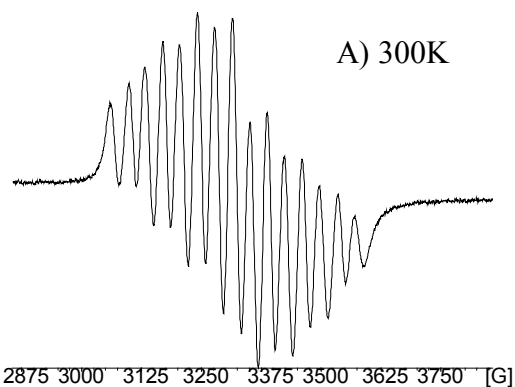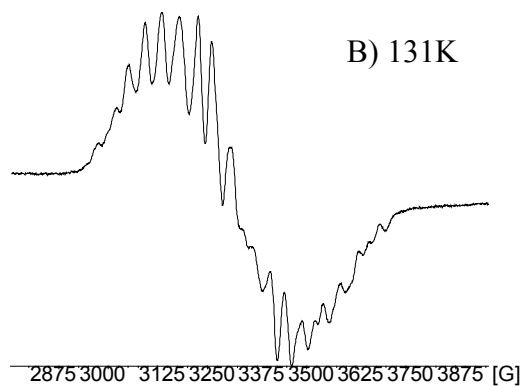
A) 300K

B) 131K

Figure 4.15. EPR spectra of **67**· in fluid solution (toluene) and rigid solution (toluene); A) experimental and B) simulated at 300K, ν = 9.2058 GHz; C) experimental and D) simulated , at 131K, ν = 9.2147 GHz; E) 260K, ν = 9.2094 GHz.

A) 300K   Exp.

B) 300K   Sim.

C) 131K   Exp.

2800 3000 3200 3400 3600 3800
Magnetic Field [G]

D) 131K   Sim.

2800 3000 3200 3400 3600 3800
Magnetic Field [G]

E) 260K

2875 3000 3125 3250 [G] 3375 3500 3625 3750
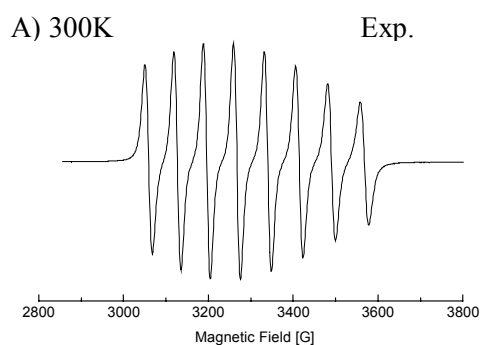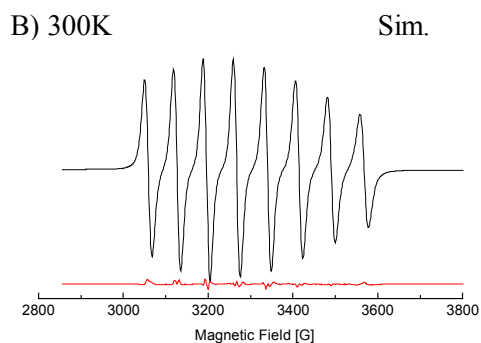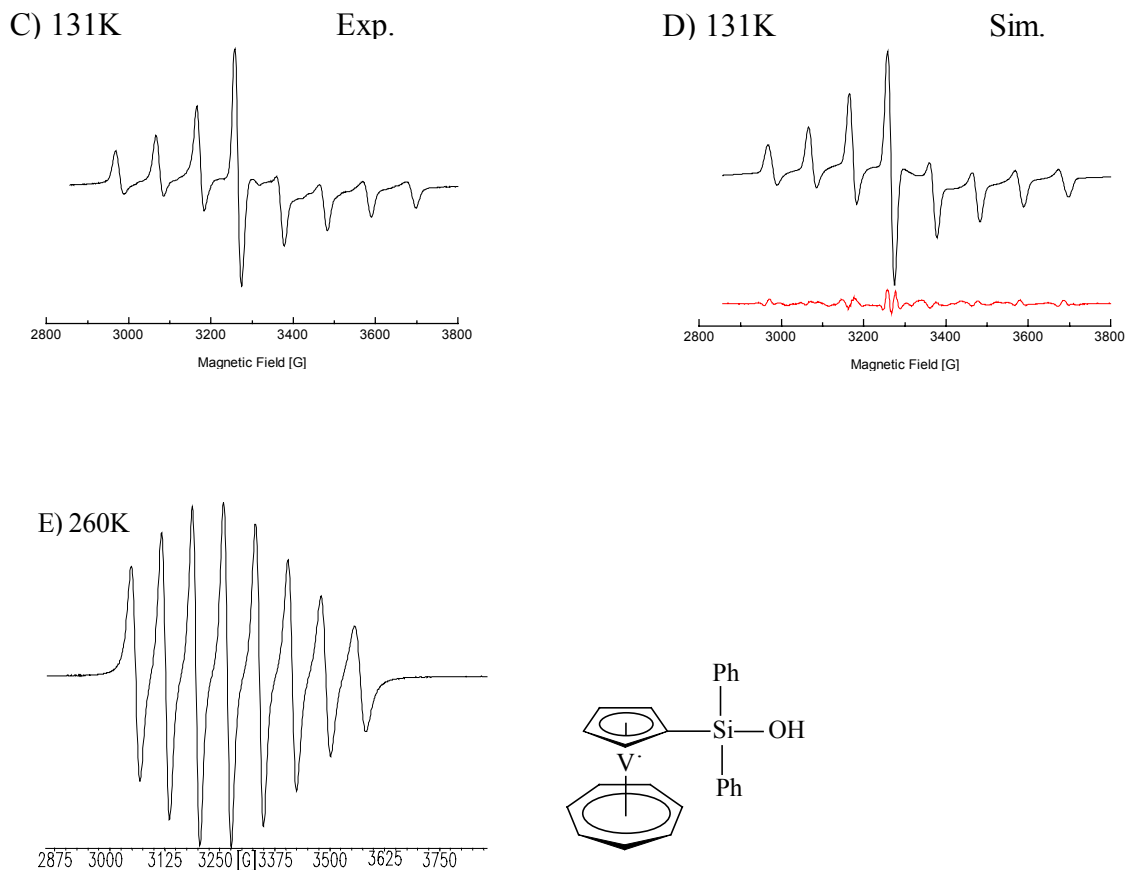
EPR spectra of **67˙** in fluid and rigid solution (toluene) are shown in Figure 4.15, and the spectral parameters are summarized in Table 4.13.

A typical monomer 8-line spectrum is observed. The coupling constant ($A_{iso}(^{51}V)$ = 72.6 G) is slightly larger than that of parent trovacene. The two electron-accepting phenyl linkage to Si atom and the electron donating (Cp→Si) lead to metal-ligand spin delocalization which contribute to the large value of coupling constant. From the rigid spectrum at 131K, the parameters, g_{xx} =1.9740, g_{yy} = 1.9733, g_{zz} = 1.9955, $A(^{51}V)_{xx}$ = 100.25G, $A(^{51}V)_{yy}$ = 104.8G, $A(^{51}V)_{zz}$ = 2.9G, could be derived by computer simulation.

Table 4.13. EPR data of **67˙**

300K	$A_{iso}(^{51}V)$	g_{iso}	α	β	γ	ΔB	
	72.6 G	1.9834	-0.89	3.86	-0.03	12.6 G	
131K	$A(^{51}V)_{xx}$	$A(^{51}V)_{yy}$	$A(^{51}V)_{zz}$	g_{xx}	g_{yy}	g_{zz}	ΔB
	100.25 G	104.8 G	12.9 G	1.9740	1.9733	1.9955	18.1 G

4.6. Reaction of lithiotrovacene with SnCl₂

4.6.1. Trinuclear Compound[20a,98]

If the molecular species contains trinuclear centers, it will display a complex interaction between adjacent centers. The simple isosceles triangle model can be described the interactions among them.
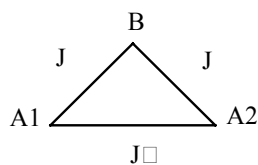
$J_{A1B} = J_{A2B} = J$ describe the interactions of B center with A1 and A2, J′ represents the interaction between A1 and A2 centers. The spin Hamiltonian in zero field can be written as :

$$\mathbf{H} = - J(\mathbf{S}_{A1} \cdot \mathbf{S}_B + \mathbf{S}_{A2} \cdot \mathbf{S}_B) - J'\mathbf{S}_{A1} \cdot \mathbf{S}_{A2}$$

or

$$\mathbf{H} = - J(\mathbf{S}_{A1} \cdot \mathbf{S}_B + \mathbf{S}_{A2} \cdot \mathbf{S}_B + \rho\, \mathbf{S}_{A1} \cdot \mathbf{S}_{A2})$$
$$\rho = J'/J$$

The relative energies in zero field can be expressed as:

$$E(S,S') = -J\, S\,(S+1)/2 - S'\,(S'+1)(J'-J) / 2$$

in which, $S = \mathbf{S}_{A1} + \mathbf{S}_{A2}$, $S` = S + \mathbf{S}_B$

The three local spin $\mathbf{S}_{A1} = \mathbf{S}_{A2} = \mathbf{S}_B = 1/2$, and J, J′ are negative in value. The ratio ρ decides the ground state. If $\rho < 1$, the ground state can be expressed as below I, in which the local spin S_{A1} and S_{A2} are aligned parallel, and the large interactions between B and A1, A2 are antiferromagnetic. If $\rho > 1$, the ground state is II, and a large antiferromagnetic interaction between A1 and A2 is presented. Both of the above noted cases can be named competing interaction. If $\rho = 1$, the degenerated states can be described (below, III), and this behavior can be expressed as frustration.
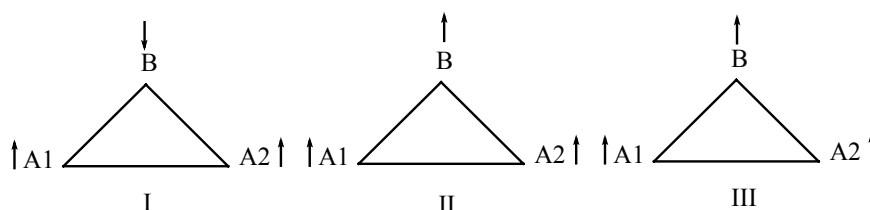
4.6.2. Generation of dichloro[tri([5]trovacenyl)]tin cation 66$^{\cdots}$

Lithiotrovacene in Et_2O was added dropwise to the suspension of slightly excess $SnCl_2$ in toluene with vigorously stirred at 0°C. Large amounts of pale yellow precipitate was formed soon. After stirring at r.t. overnight, the solution was decanted carefully. The solid was washed by Et_2O till colorless, then extracted by toluene/THF (3:1) to result in a yellow-red

solution. After stored at 8°C for two months, violet-red crystals suitable for X-ray diffraction were formed. The crystal was characterized to be a stannate which contains three trovacene units linked by Sn atom and two chloro atoms in the molecule. Because of the lack of sufficient crystals and the solvent molecule involved in the generation of crystals, **66**··· has not been characterized by elemental analysis, but mass spectroscopy (EI) and X-ray diffraction.

The original purpose of this reaction was to synthesize mono-substituted trovacenyl intermediate (TVC-SnCl) which may be converted to TVC-Sn≡Sn-TVC (Scheme 4), similar to its analogue Sn(Cl)Ar.[99] Although C≡C bonding two metallocene fragments have been described. For example, Fc-C≡C-Fc, TVC-C≡C-TVC.[100] Until now, there are still no studies about stable heavier group 14 metallocene derivatives, such as Fc-Sn≡Sn-Fc, etc., similar to $Na_2[ArGa≡GaAr]$[101] or $[ArSn≡SnAr]^-$.[99]

Scheme 4.
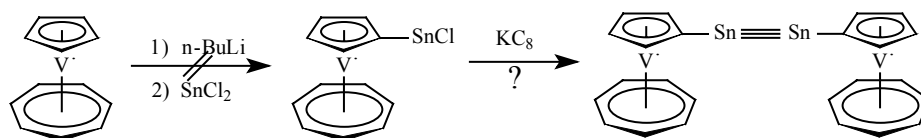
The steric hindrance of ortho-substituent of Ar makes the formation of $[ArSn≡SnAr]^-$ to be possible. But for trovacene, there is no efficient ortho-substituent in cyclopentadienyl ring to prevent from forming polymetal intermediate. This may be the main reason for the unsuccessful synthesis of TVC-SnCl as expected.

In addition, it was surprising that the reaction of $SnCl_2$ with lithiotrovacene did not afford $(TVC)_2Sn$. Although many researchers[102] reported that organolithium reacted with $SnCl_2$ lead to $(R)_2Sn$, for example, $\{CH(SiMe_3)_2\}_2Sn$, $\{C_6H_2(CF_3)_3-2,4,6\}_2Sn$, $\{C_6H_2Pri_3-2,4,6\}_2Sn$. Power[103] reported the reaction of $LiC_6H_3-2,6-Mes_2$ with $GeCl_2$, $SnCl_2$, $PbCl_2$ (ration 2:1) to result in $M\{C_6H_3-2,6-Mes_2\}_2$, if the ration was 1:1, $[M(Cl)\{C_6H_3-2,6-Mes_2\}_2]_2$ (Scheme 5) were isolated. The stability of $SnMes*_2$ and $Sn\{C_6H_2-2,4,6(CF_3)_3\}_2$ are higher.

Scheme 5.
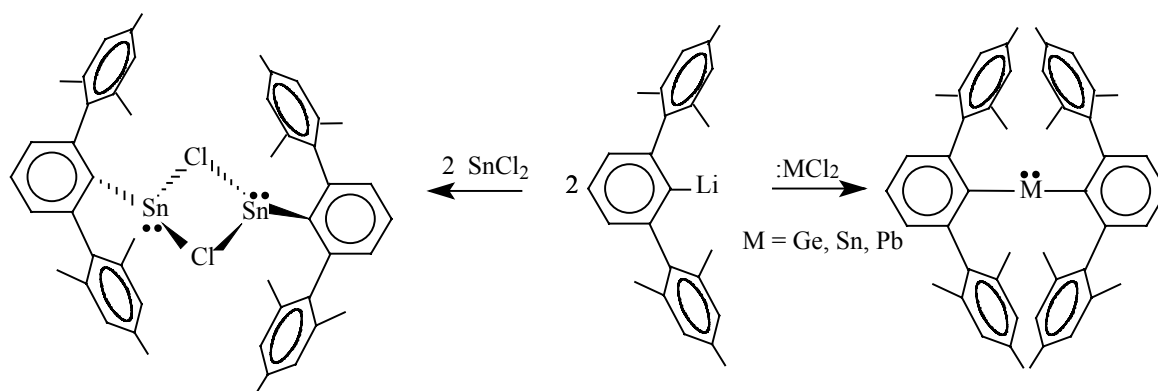
Mak et al. recently reported that the reactions of $[LiR^N(tmda)]_2$ with $SnCl_2$ in various stoichiometric ratios afforded $[Sn(Cl)R^N]_2$ and zwitterionic lithium trialkylstannate complexes;

$[\{SnR^N{}_3)Li\{(\mu^3\text{-}Cl)Li(tmda)_2\}(\mu^2\text{-}Cl)]$ and $[\{SnR^N{}_3)Li\}(\mu^3\text{-}Cl)Li(tmda)]_2$. A zwitterionic distannene as well as a tin cluster compound also were reported by Weidenbruch.[104]

$$SnCl_2 + RNa \cdot 2THF \xrightarrow{\text{toluene}} R_2SnSnR_2 + (RSn)_4 + R\text{-}R$$

$$R = tBu_3Si$$
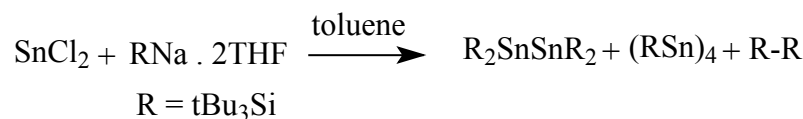
In a word, these examples indicate that the reaction of $SnCl_2$ with various organolithium would lead to different complexes. A comparison of the reaction of $SnCl_4$ with lithiotrovacene should be investigated in the further study.

4.6.3. X-ray Crystal Structure Analysis of 66[***]

The molecular structure of **66[***]** is shown in Figure 4.16. Important bonds and selected angles are summarized in Table 4.14 and 4.15, respectively. **66[***]** exhibits a five-coordinate Sn atom. It is comprised of one Sn(IV) center, three carbon atoms and two halogen atoms. Three trovacene units bridged by Sn(IV) atom via C-Sn bond look like a pinwheel, in which the axis of trovacene units are almost perpendicular to the axis of Cl(1)-Sn-Cl(2) due to the steric hindrance. Sn atom and the three linked carbon atom are nearly coplanar. The three C-Sn-C angles are close to 120° (C(1)-Sn(1)-C(25)=118.10(9)°, C(1)-Sn(1)-C(13)=122.68(10)°, C(13)-Sn(1)-C(25)=118.89(10)°).

A distorted pentagonal bipyramidal geometry is adopted with the chlorine atoms *trans* to each other. The Cl(1)-Sn-Cl(2) axis performs almost linear (Cl(1)-Sn(1)-Cl(1)=91.69(7)°). One of the Cl atoms links Li atom which is coordinated by three THF molecules. The steric hindrance prevents the axes of trovacene units from parallel to that of Cl(1)-Sn-Cl(2).
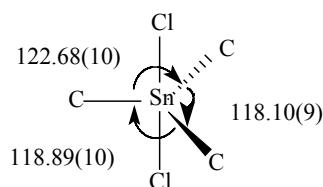
The three Sn-C bond lengths are close to each other with a mean value of 2.130(2) Å which is slightly shorter than that of [ArSnSNAr]-.(2.236(5)Å.[99] There is a significant difference (0.19 Å) in bond lengths between the two Sn-Cl bonds.

The Sn-Cl(2) bond (2.6935(7) Å) is longer than the Sn-Cl bond (1) (2.5092(7) Å). The distance between Li and Cl(2) is 2.316(5) Å. The distance between metals are 6.8630(08)Å (V(1)-V(2)), 6.7364(42)Å (V(1)-V(3)) and 6.7612(578)Å (V(2)-V(3)), which are shorter than that of **63[**]** (7.695(2)Å) and **64[**]** (6.961(2)Å).

Figure 2.16. Molecular structure and stereoview of **66**···
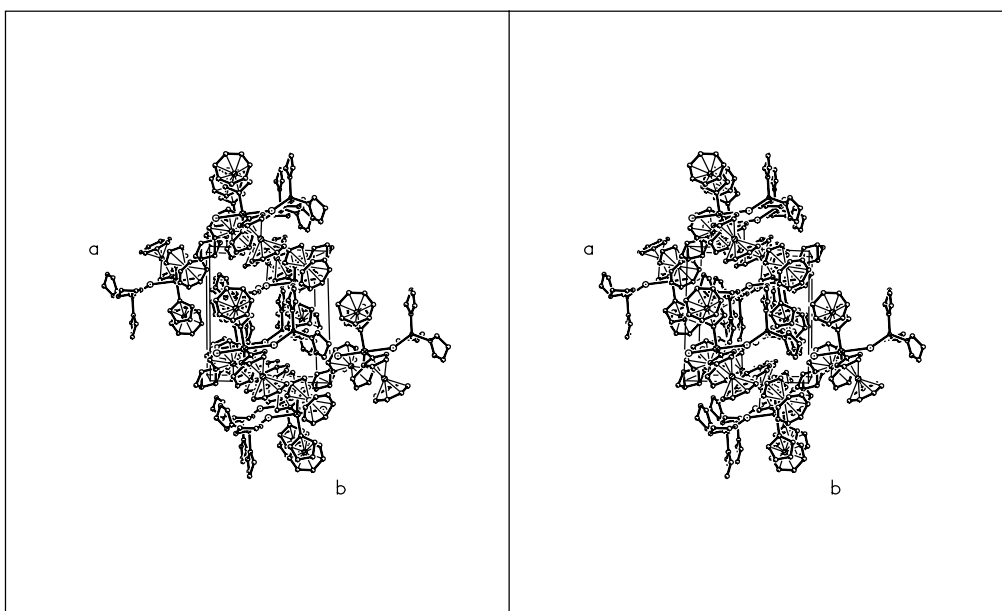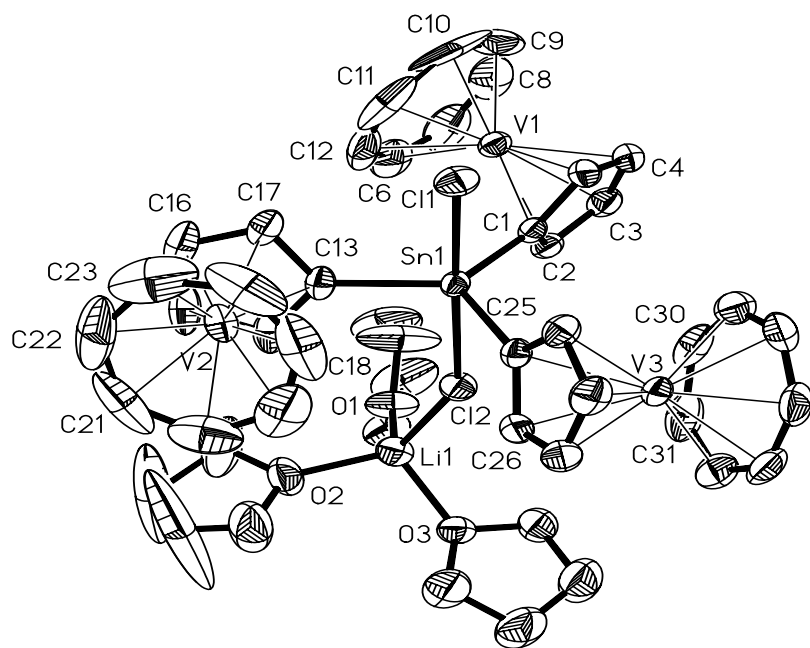
Table 4.14. Selected bond lengths [Å] of **66'''**

Sn(1) - C(1)	2.128(2)	V(1) - C(6)	2.180(4)
Sn(1) - C(13)	2.130(3)	V(1) - C(7)	2.180(4)
Sn(1) - C(25)	2.130(2)	V(1) - C(8)	2.164(4)
Sn(1) - C(mean)	2.130(2)	V(1) - C(9)	2.144(4)
Sn(1)-Cl(1)	2.5092(7)	V(1) - C(10)	2.141(4)
Sn(1)-Cl(2)	2.6935(7)	V(1) - C(11)	2.152(4)
V(1) - C(1)	2.260(3)	V(1) - C(12)	2.171(4)
V(1) - C(2)	2.243(3)	**V(1)-C₇ Ring (mean)**	2.162(4)
V(1) - C(3)	2.255(3)	C(6) - C(7)	1.364(6)
V(1) - C(4)	2.261(3)	C(6) - C(12)	1.366(6)
V(1) - C(5)	2.256(3)	C(7) - C(8)	1.341(7)
V(1)-C₅ Ring (mean)	**2.255(3)**	C(8) - C(9)	1.339(8)
C(1) - C(2)	1.420(4)	C(9) - C(10)	1.479(10)
C(1) - C(5)	1.429(4)	C(10) - C(11)	1.472(10)
C(2) - C(3)	1.411(4)	C(11) - C(12)	1.342(8)
C(3) - C(4)	1.401(4)	**C-C (mean for C₇)**	1.358(8)
C(4) - C(5)	1.411(4)	Li(1)-Cl(2)	2.316(5)
C-C (mean for C₅)	**1.414(4)**	**V(1) - V(2)**	6.8630(08)
O(1)-Li(1)	1.929(5)	**V(1) - V(3)**	6.7364(42)
Li(1)-O(2)	1.915(5)	**V(2) - V(3)**	6.7612(578)
Li(1)-O(3)	1.938(6)		

The torsional angles of Sn atom with three Cp rings are Sn(1)-C(1)-C(5)-C(4), 174.87(19)°; Sn(1)-C(13)-C(14)-C(15), 176.4(2)° and Sn(1)-C(25)-C(26)-C(27), -174.92(19)°. This indicates that the three planes of Cp rings are nearly perpendicular to the plane of C(1), C(13) and C(25). The angle of Sn-Cl(2)-Li is 150.89(13)°. The dihedral angles among three Cp rings are 63.69(19)° (Cp(1)-Cp(2)), 58.2(2)° (Cp(2)-Cp(3)) and 59.97(18)° (Cp(1)-Cp(3)).

Table 4.15. Selected angles [°] and Torsional angles [°]of **66'''**

C(1)-Sn(1)-Cl(1)	91.49(7)	C(2)-C(1)-C(5)	106.2(2)
C(1)-Sn(1)-C(25)	118.10(9)	C(9)-C(8)-C(7)	130.8(5)
C(1)-Sn(1)-C(13)	122.68(10)	Li(1)-Cl(2)-Sn(1)	150.89(13)
C(13)-Sn(1)-C(25)	118.89(10)	Sn(1)-C(1)-C(5)-C(4)	174.87(19)
C(13)-Sn(1)-Cl(1)	92.55(8)	Sn(1)-C(13)-C(14)-C(15)	-176.4(2)
C(1)-Sn(1)-Cl(2)	92.55(8)	Sn(1)-C(25)-C(26)-C(27)	-174.92(19)
C(13)-Sn(1)-Cl(2)	88.91(8)	C(13)-Sn(1)-C(1)-C(2)	-72.2(3)
C(25)-Sn(1)-Cl(2)	87.33(7)	Cl(1)-Sn(1)-Cl(2)-Li(1)	177(68)
C(1)-Sn(1)-Cl(1)	91.69(7)	C(25)-Sn(1)-C(1)-C(2)	101.1(2)
Cl(1)-Sn(1)-Cl(2)	178.51(2)	Cl(1)-Sn(1)-C(1)-C(2)	-166.2(2)
C(2)-C(1)-Sn(1)	128.53(19)	Cl(2)-Sn(1)-C(1)-C(2)	15.2(2)
C(14)-C(13)-Sn(1)	127.8(2)	C(25)-Sn(1)-Cl(2)-Li(1)	128.0(3)
C(26)-C(25)-Sn(1)	128.31(19)	C(13)-Sn(1)-C(1)-C(5)	113.9(2)
Torsion C₇ Ring (mean)	**-0.3(9)**	**Torsion C₅ Ring (mean)**	**0.1(22)**

4.6.4. Result of Cyclic voltammetry

The electrochemical property of **66$^{•••}$** is investigated in DME with a poor solubility at -40°C. The cyclic voltammetric traces for **66$^{•••}$** are show in Figure 4.17, the pertinent data are given in Table 4.16.

Table 4.16. Cyclic Voltammetry Data **66$^{•••}$**

$E_{1/2}(0/+)$	89 mV
ΔE_p	78 mV
I_{pa}/I_{pc}	1
$E_{pa}(+/2+)$	236 mV
E_{pc}	64 mV
I_{pa}/I_{pc}	1
$\Delta E_{1/2}(0/+)(+/2+)$	147 mV
$E_{pa}(2+/3+)$	335 mV
ΔE_p	82 mV
I_{pa}/I_{pc}	1
$\Delta E_{1/2}(+/2+)(2+/3+)$	99 mV
$E_{pa}(3+/4+)$	1.142 V
E_{pc}	-2.488 V

Differing from the electrochemical behavior of $(TVC)_2Sn(R)_2$ (R = Me, Ph), **66$^{•••}$** exhibits three successive reversible one-electron oxidations at 89 mV, 236 mV and 335 mV. As for the $[(TVC)_3SnCl_2]^-$ anion, the first oxidation shows a large cathodic shift. The redox splitting are 147 mV and 99 mV, corresponding to $\Delta E_{1/2}(0/+)(+/2+)$ and $\Delta E_{1/2}(+/2+)(2+/3+)$, which indicate the weak interactions among the three redox centers. However, only one reduction peak is observed at -2.488 V, with an anodic shift relative to trovacene. An undistinguished E_{pa} near -2.340V may be shown in the reverse scan term, unlike that of trovacene with a discernible reversible reduction potential at -2.55V.

Figure 4.17. Cyclic voltammograms for **66**··· in DME/TBAP at -40°C, v = 100mV/s
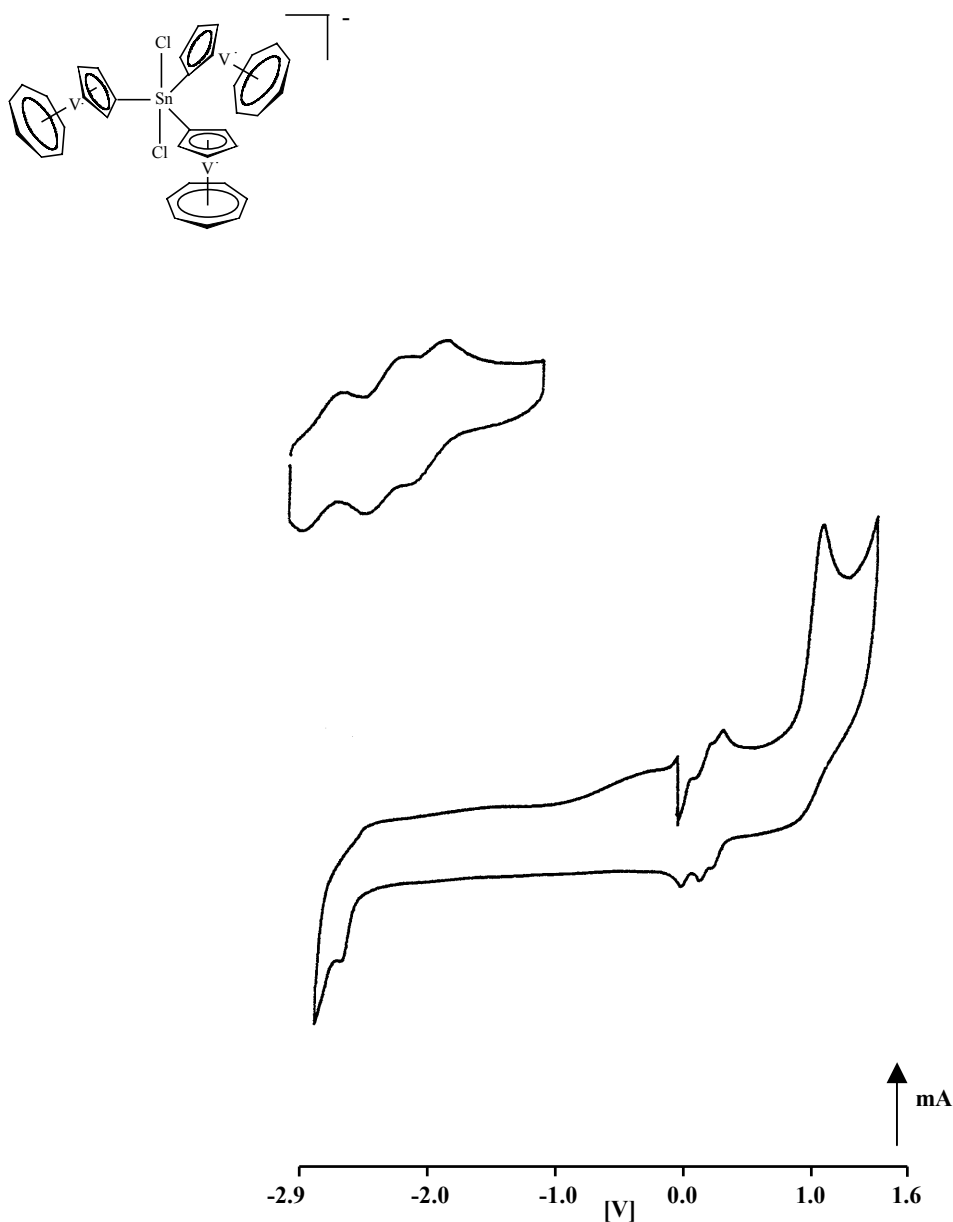
4.6.5. ERP Spectra (66···)

Since **66**··· has a poor solubility in toluene, the fluid and rigid solution EPR spectra of **66**··· in THF were recorded at X-band frequency at 340K, 300K, and 133K, respectively (Figure 4.18).

A 22-line spectrum is displayed which is consist with the rule of 2nI+1. It indicates that the unpaired electrons interacts with three vanadium nuclei. The splitting is only one-third of its parent trovacene. Based on the characteristic patter of the spectra, the degree of exchange interaction conforms with the relation J>a. However, a definitive analysis must await the results of the fitted magnetic susceptibility measurements.

Figure 4.18. Experimental fluid solution spectra (THF) of **66***; A) 340K, ν = 9.2060GHz, B) 300K, ν = 9.2101GHz, and C) experimental rigid solution spectra (THF) at 133K, ν = 9.2169GHz.

A) 340K
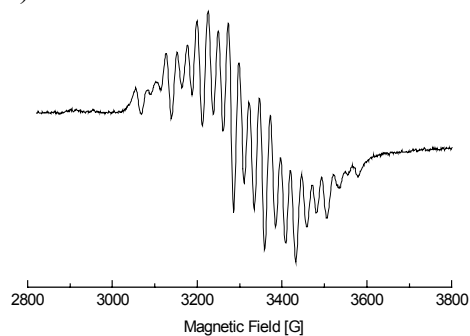
B) 300K
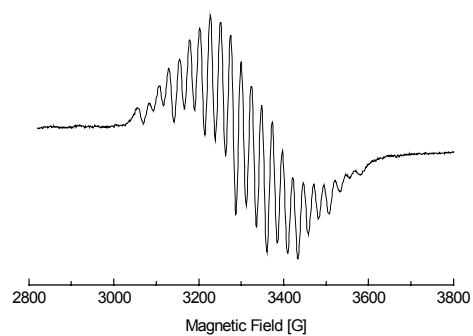
C) 133K
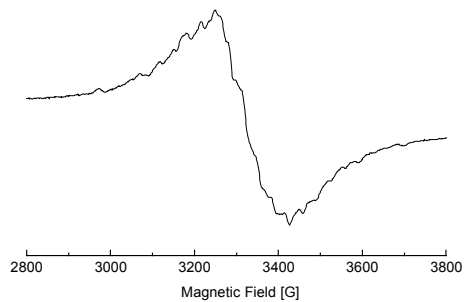
5. Termetallocenes

5.1. Introduction

Much interest in developing molecule components for use in the construction of nanoscale electronic devices has evolved in recent years.[107] Conjugated polyynes as a potentially important class of molecular wire materials have been treated by many studies.[108] One of the most popular methods for testing the electronic communication through a potential molecular wire is to examine the interaction between redox centers which are located at the termini of the chain.

Metallocene, a potential molecular wire model probe, has been utilized to investigate the interaction (Scheme 1). In particular, ferrocene is a satisfactory parent compound.[109] There are many reports about the interaction between two metal centers of homo- or hetero-bimetallocene complexes - the simplest sub-units of extended metallocene polymers.[110]

Scheme 1.
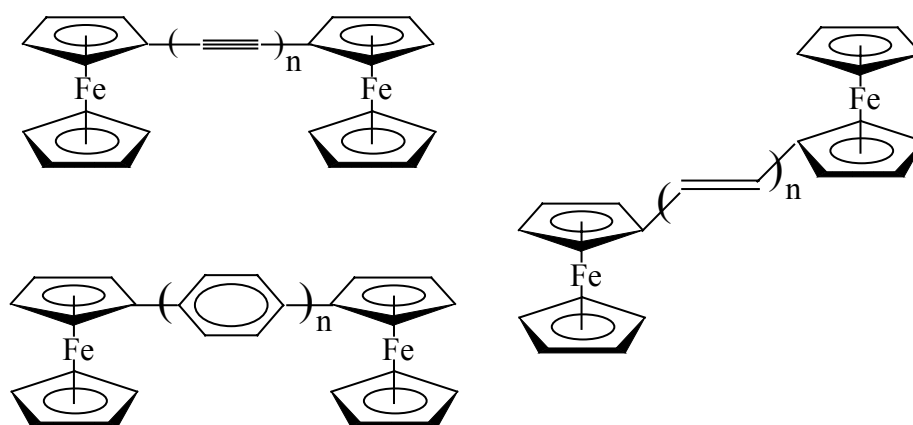
It is well-known that the multiple bond could transfer the electron along the molecular line from one center (or donor) to another center (or acceptor), e.g. C≡C, C=C, C=N. The fixed neighboring pendent p_π orbital as an efficient extended conductor involves in the ET, in other words, π bond unit is a better conductor than σ bond unit.

Cyclopentadienyl ring (C_5H_5, or Cp) is another crucial π-electron system and may be used as a potential molecular wire unit too. Yet until now, there are no reports about Cp as the basic bridge linked two metallocene at the two termini. However, it is worth noting that some complexes comprising pyridyl,[111] furan, thiophene,[112] have been obtained recently (Scheme 2).

McCleverty and co-worker have demonstrated[113] that a dinuclear molybdenum complex linked by pyridyl exhibits an exceptionally strong electronic interaction, because of a particularly favorable interaction between the metal $d\pi$ and the bridge $\pi*$ orbital. Additionally, oligothiophenes have attracted much interest recently. Since it has been found that the electronic interaction across this kind of bridge is significantly stronger than that of the comparable length with polyene bridges.[114]

Scheme 2.

n = 1, 2, 3, 4
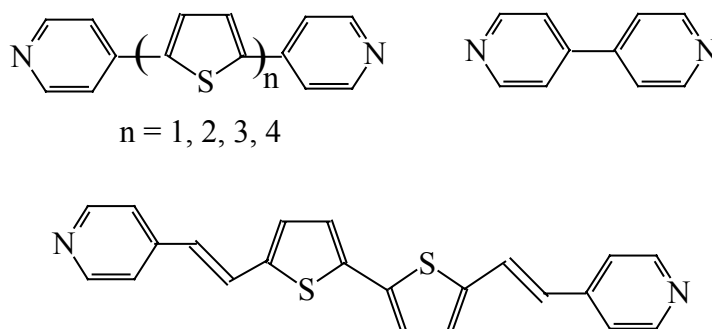
The possibility of extended metallocene polymers to act as molecular wires should not be neglected too. Metallocene as a unit of the molecular wire, or as a modification group to control the communication (Scheme 3) provides a useful basis for investigating the electron communication between redox centers. From that, it is possible to conceive that the selective addition or proper arrangement of metal centers along the molecule wire could modify or control the electron communication through the wire.

Scheme 3.
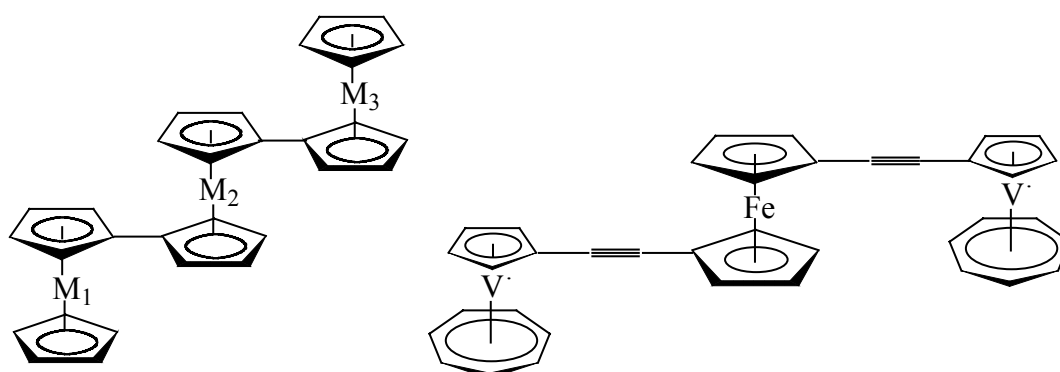
Trovacene as an ideal parent compound suggests the possibility of magnetic interactions between the metal centers. Herein, trovacene was chosen as the terminal unit and ferrocene as the bridge to form a termetallocene. With the help of CV and EPR, the electron communication between the metal centers was investigated. This simple model offers an opportunity to learn the possibility of polyfulvalene or metallocene as efficient molecular wire to transmit the electron through them.

5.2. Synthetic Methods

Synthesis, characterizations and properties of metallofulvalenes have been extensively studied for many years since the first synthesis of ferrocene,[115] particularly of homobimetallic bisfulvalene complexes.[116]

The development of synthetic routes toward metallofulvalene complexes has been progressed following the initial reports on preparation of bisferrocene.[117] 1) Fulvalene dianion as one of the basic precursors reacts with transition metal halides to form metallocyclopentadienyl.[118] 2)

Sodium cyclopentadienyl anion reacts with metallocene to give metallocyclopentadienyl.[119] 3) Cyclopentenones as a starting material reacts with lithiometalllocenes to yield cyclopentenols. After water elimination, the cyclopentenols is converted to the corresponding metallocenylcyclopentadienides. The major disadvantages are competitive 1,4 additions and low yields.[120]

In recent years, a novel strategy has been developed: norborn-2-en-7-one was used as the key starting material to afford cyclopentadienyl anionic intermediate by retro Diels-Alder reaction.[121] The multi-step synthesis and purification of the crude material are the disadvantage.

Higher fulvalene-based metallocene oligomers as the favorable models for the studies of interactions between redox-active linked moieties have attracted much attention. For example, Schottenberger, Schwarzhans and co-workers have described alternative synthesis of home- and hetero-termetallocenes by utilizing norborn-2-en-7-one, i. e., Fe-Co-Fe, Ni-Fe-Ni; or using lithiometallocene and metallocenium hexafluorophosphates, i. e., Co-Fe-Co, Co-Fe-Rh (Scheme 4), Co-Ru-Co, Co-Os-Co, and Rh-Fe-Rh.[122]

Plenio has obtained the substituted termetallocene from the reaction of lithioferrocene with 3,4-dimethylcyclopent-2-enone.[123]

Scheme 4.

| 68 | 69 |
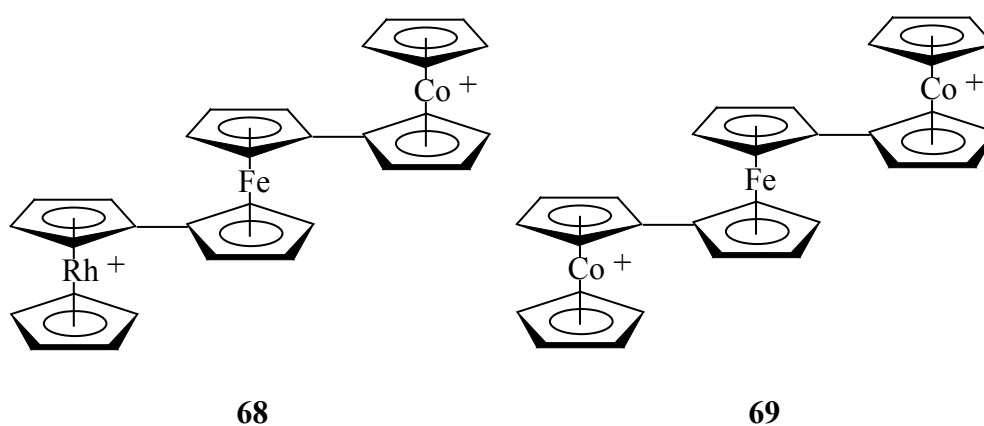
In order to obtain bistrovacenylmetallocene, we have chosen norbornenone as the starting material. Unsatisfactory results have been obtained due to the limitation of the crude material norbornenone. Thus, we attempted to use 2,3,4,5-tetramethylcyclopenten-1-one as the staring material, in which the methyl substitutents make the ketone less susceptible to enolization.[124] We have successfully identified the probability of synthesizing this kind of termetallocene.

5.3. Generation of Di([5]trovacenyl-tetramethyl-η^5-cyclopentadienyl)iron (71$^{\cdot\cdot}$)

70$^{\cdot}$ **71$^{\cdot\cdot}$**
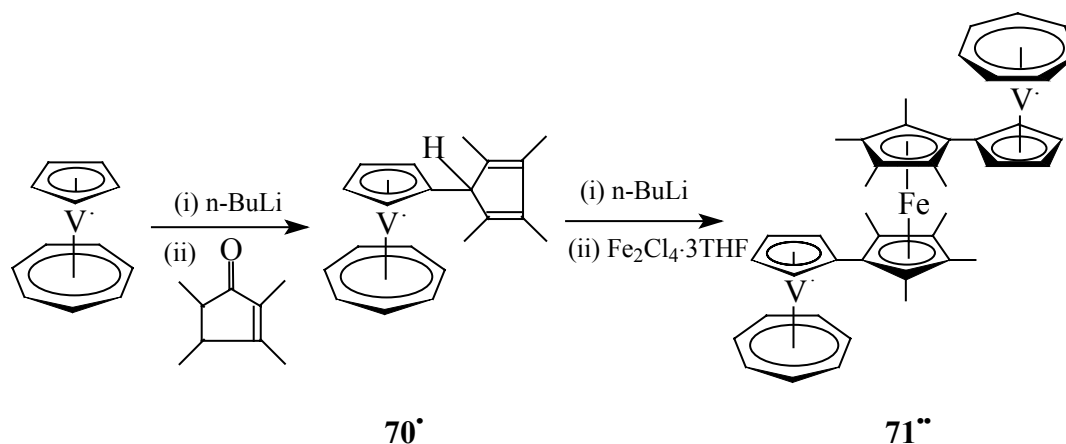
In order to reduce the probability of side-reactions, lithiotrovacene was reacted with 2,3,4,5-tetramethylcyclopenten-1-one at -78°C for 1h and at r.t. overnight, then followed by hydrolysis (15%HCl). Normally, the hydrolysis should give an alcohol intermediate. Presumably due to its thermal instability, the alcohol intermediate could not be isolated by chromatography or other ways. It was converted directly to [5]trovacenyl-tetramethylcyclopentadiene (**70$^{\cdot}$**). Meanwhile, no evidence from EI-MS (70eV) spectroscopy was observed to testify the formation of the alcohol intermediate. It gave the molecular ion peak of **70$^{\cdot}$**. **70$^{\cdot}$** has a good solubility in common organic solvent, such as PE. This character makes it very difficult to be isolated directly from the mixture by chromatography (Al$_2$O$_3$).

Probably due to its thermal instability, most of **71$^{\cdot\cdot}$** was decomposed during the chromatography (Al$_2$O$_3$) at room temperature. Thus, the reaction of lithiated (2,3,4,5-tetramethylcyclopentadienyl)trovacene with Fe$_2$Cl$_4$.3THF should be performed at low temperature. Proceeded in a similar fashion, the thermal instability might be the main reason for the failure of generation of 1,1′-bistrocenylferrocene **74$^{\cdot\cdot}$** using norbornenone by retro Diels-Alder sequences.[121,125] Since the reaction of lithiated cyclopentadienyltrovacene with Fe$_2$Cl$_4$.3THF was performed at 50°C with stirring overnight.

Both of the green precursor **70$^{\cdot}$** and the light yellow-brown **71$^{\cdot\cdot}$** have been characterized by mass spectroscopy (EI) and elemental analysis (see experimental part), and investigated by cyclic voltammetry, and/or EPR. **71$^{\cdot\cdot}$** also has a good solubility in polar organic solvent, except a medium solubility in non-polar solvent, i.e. PE. Additionally, whether in solid state or in solvent, **71$^{\cdot\cdot}$** is thermally unstable. Specially in solution, **71$^{\cdot\cdot}$** decomposes slowly at r.t. or low temperature to give slightly yellow-brown powder. This limits its generation of single crystal.

5.4. Results of Cyclic Voltammetry

Cyclic voltammetry of **70$^{\cdot}$** and **71$^{\cdot\cdot}$** at -40°C are shown in Figure 5.1. The data are summarized in Table 5.1.

For compound **70$^{\cdot}$**, the reversible oxidation potential (E$_{1/2}$(0/+) = 271 mV) shows a slight anodic shift relative to that of parent trovacene (**6$^{\cdot}$**) (E$_{1/2}$(0/+) = 260 mV),[126] but cathodic shift

relative to that of analogue [5]trovacenylbenzene ($E_{1/2}(0/+) = 297$ mV).[12] This is related to the electron-accepting properties of the phenyl substituent and the electron-donating nature of the trovacene unit. However, the reduction potentials are close to each other since -2.440 V (**70·**), -2.55V(**1·**), and -2.458 V ([5]trovacenylbenzene).

The cyclic voltammetry of **71··** shows three largely resolved oxidation peaks at approximately 170 mV, 360 mV and 450 mV at a scan rate of 100 mV/s. It should be contributed to the successive three one-electron transfer processes.

Comparing the potentials with those of trovacene and substituted-ferrocene,[126b] the waves at 170 mV can be assigned to the one-electron oxidation of substituted-ferrocene moiety. And the other waves at 360 mV and 450 mV can be interpreted to the two separated one-electron oxidations of trovacene units, depicted as follow:

$$(V^0/Fe^{2+}/V^0) \underset{\longleftarrow}{\overset{170mV}{\longrightarrow}} (V^0/Fe^{3+}/V^0) \underset{\longleftarrow}{\overset{360mV}{\longrightarrow}} (V^+/Fe^{3+}/V^0) \underset{\longleftarrow}{\overset{450mV}{\longrightarrow}} (V^+/Fe^{3+}/V^+)$$
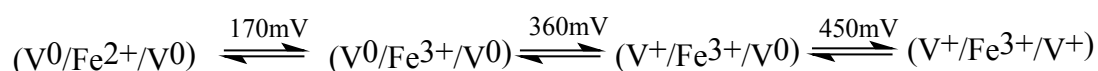
Relative to $[(Me_4Fv)_2FeTHCl_2]^{126b}$ and $[(Me_4Fv)_2Fe_2]$ which underwent oxidation at -0.15V and -0.5 V in CH_2Cl_2, the first oxidation, iron center (**71··**), shows an anodic shift because of the two linked trovacene moieties. Due to the positive charge, the second oxidation exhibits a remarkable anodic shift relative to that of the parent trovacene (260mV). Another vanadium center has also to be given a significant more anodic shift since the two positive charges make it more difficult to be oxidized again. The redox splitting correspond to 195 mV and 87 mV, indicating a weak interaction between the vanadium centers.

Reduction of **71··** leads to two potentials at -2.450 V and -2.560 V corresponding to the two successive one-electron reductions of trovacene units, with a potential separation ($\Delta E_{1/2}(0/-)(-/2-)$) of 107 mV. All these indicate the extent of the communication of the linked metal centers.

$$(V^0/Fe^{2+}/V^0) \underset{\longleftarrow}{\overset{-2.450\ V}{\longrightarrow}} (V^-/Fe^{2+}/V^0) \underset{\longleftarrow}{\overset{-2.560\ V}{\longrightarrow}} (V^-/Fe^{2+}/V^-)$$
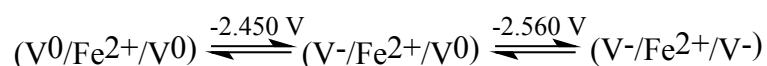
Furthermore, it should be noted that all the peaks are not sharp in shape including the oxidation of iron center, contrary to the waves of substituted-ferrocene. In addition, with a scan rate of 400 mV/s, only one wave was observed at -40°C.

In conclusion, due to the hindrance of methyl substituent, two trovacene units could not rotate freely along the axes of Cp*-Cp in the solution, and an orthogonal conformation between Cp* (tetramethyl-cyclopentadienyl ring) and Cp (cyclopentadienyl ring) was preferred which would attenuate the π conjugation between them. Only the σ interaction contributed to the weak metal-metal interaction which was shown as a small redox splitting. Thus, a comparison with the analogous di([5]trovacenyl-η^5-cyclopentadienyl)iron (**74··**) should be done in the future study.

Figure 5.1. Cyclic voltammograms for **70·** and **71··** in DME/TBAP at -40°C, v = 100mV/s
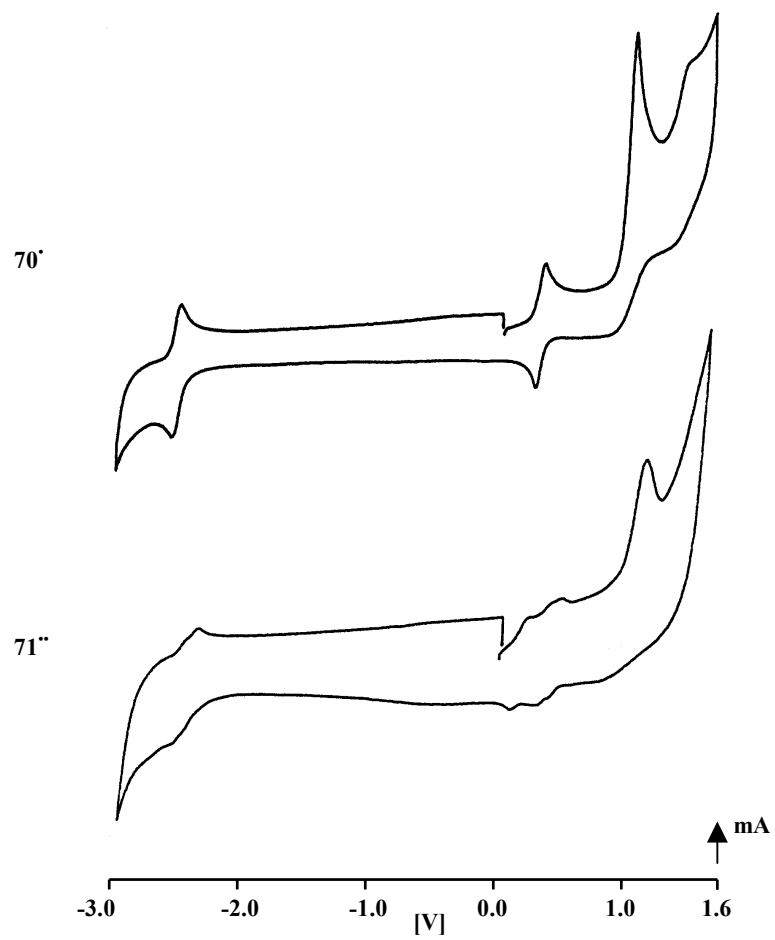
Table 5.1. Cyclic Voltammetry Data for **70**· and **71**··

	70·	**71**··
$E_{1/2}(0/+)$	271 mV	169 mV
ΔE_p	72 mV	122 mV
I_{pa}/I_{pc}	1	1
$E_{1/2}(+/2+)$	986 mV	364 mV
ΔE_p		72 mV
I_{pa}/I_{pc}		1
$\Delta E_{1/2}(0/+)(+/2+)$		195 mV
$E_{pa}(2+/3+)$		451 mV
ΔE_p		46 mV
I_{pa}/I_{pc}		1
$\Delta E_{1/2}(+/2+)(2+/3+)$		87 mV
$E_{pa}(3+/4+)$		1.118 V
$E_{1/2}(0/-)$	-2.440 V	-2.453 V
ΔE_p	56 mV	98 mV
I_{pa}/I_{pc}	1	1
$E_{1/2}(-/2-)$		-2.560 V
ΔE_p		92 mV
I_{pa}/I_{pc}		1
$\Delta E_{1/2}(0/-)(-/2-)$		107 mV

5.5. EPR Spectra (71··)

The EPR spectra of **71**·· at 300K, 260K, and 133K are given in Figure 5.2, respectively. EPR spectral parameters are summarized in Table 5.2. Surprisingly, the spectra did not give the expected 22-line. It was observed a 8-line pattern caused by the hyperfine coupling of the one unpaired electron with one V nucleus. This indicates that the unpaired electron of the two trovacene units are localized on the corresponding metal center in the EPR time scale.

This behavior may be elucidated by the fact: together with the results of CV (a small redox splitting) and the hindrance from the methyl substitution, the lack of the π conjugation between Cp* and Cp ring would attenuate the metal-metal interaction. So, only the σ interaction in 6-bonds, a long distance between two vanadium nuclei, contributed to the weak metal-metal interaction.

The hyperfine coupling value ($a(^{51}V)$ = -7.11mT) of **71**·· is close to that of [5,5]bitrovacene. It is slightly larger than that of trovacene. Because the 18e ferrocene unit links directly to the Cp ring of trovacene units, it could increase the positive charge some extent on the center metal similar to that of [5,5]bitrovacene and influence the metal to ligand interaction.

Figure 5.2. X-band EPR spectra of **71**[¨] in fluid solution (toluene): A) 300K, ν =9.21192GHz, B) 260K, ν = 9.21367GHz; and rigid solution (toluene) C) 133K, ν = 9.21822GHz.

A) 300K

2875 3000 3125 3250 3375 3500 3625 3750 [G]

B) 260K

2875 3000 3125 3250 3375 3500 3625 3750 [G]

C) 133K

2750 2875 3000 3125 3250 3375 3500 3625 3750 3875 [G]
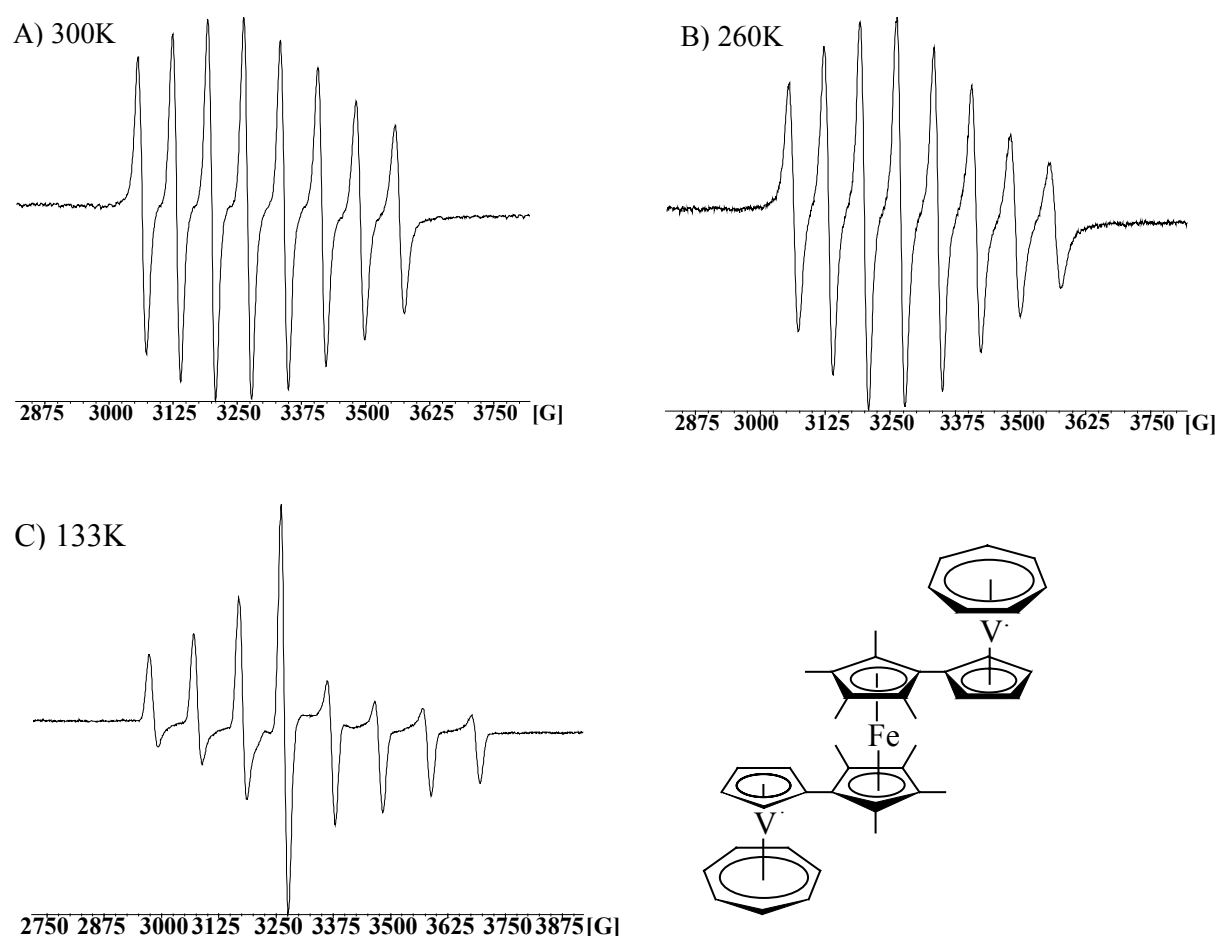
Table 5.2. EPR Data of **71**[˙]

$\langle g\rangle$	$a(^{51}V)$	$A_\perp(^{51}V)$	$A_\parallel(^{51}V)$	$g_\perp$	$g_\parallel$
1.9843	-7.11mT	-9.97mT	-1.38mT	1.9743	2.0043

5.6. Attempts to synthesize Di([5]-trovacenyl-η⁵-cyclopentadienyl)iron (74[¨])

5.6.1. Method

Bicyclo[2.2.1]hept-2-en-7-one (norbornenone) as the precursor of cyclopentadienyl has been reported.[121c] Lithiotrovacene reacted with norbornenone and then hydrolysis to give anti-or syn- 1-[7-hydroxybicyclo[2,2,1]hept-2-en-7yl]trovacene, which were further reacted with diethylchlorophosphate to form the chloro-derivatives. The result of mass spectra of chloro-derivatives has testified the rationality of the highly stabilizing effect from trovacene exerted to the positive α-carbon atom,[127] and the good leaving group ability of the phosphate ester,[120a] despite chloro-derivatives had not been purified by chromatography.

Cleavage of chloride by lithium powder and elimination of gaseous ethene by retro Diels-Alder reaction gave the corresponding [5]trovacenyl(cyclopentadienyl) ions. It had not be

further characterized by neutralization rather than directly used to react with $Fe_2Cl_4.3THF$ at refluxing condition. Unfortunately, no observation of 1,1′-Ditrovacenyl-ferrocene **74··** was possible from the result of mass spectra (EI) or purification by chromatography (Scheme 5).

Scheme 5.

74··
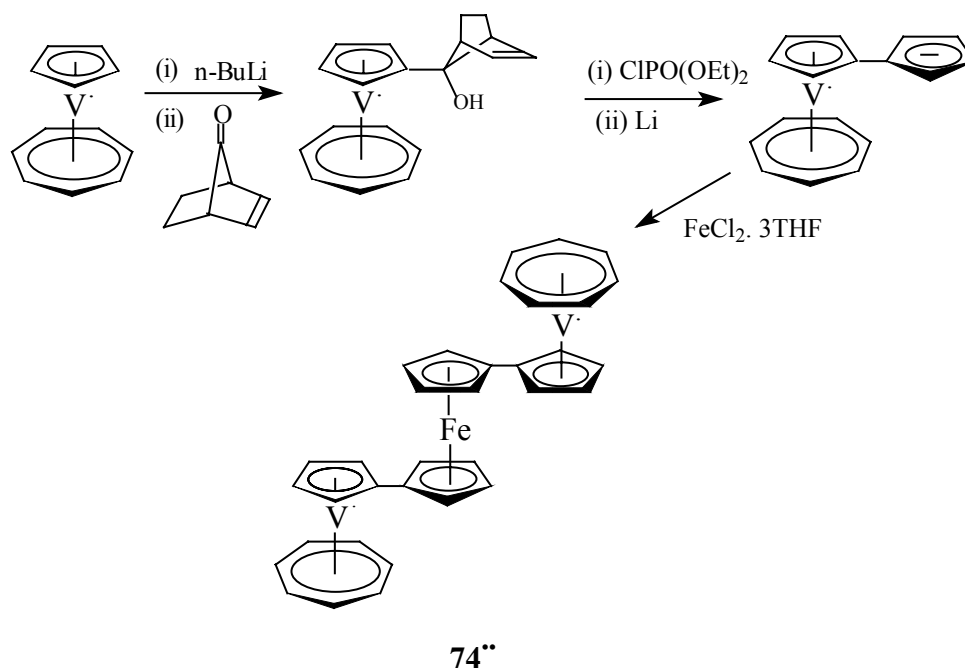
At last, due to the limitation of the crude material norbornenone and uncertain reaction condition, **74··** had not been obtained successfully, although the same reaction condition as literature said have been performed. The main reason may be the reaction temperature. The importance of the reaction temperature has been identified by the synthesis of the analogue, Di([5]trovacenyl-tetramethyl-η^5-cyclopentadienyl)iron (**71··**) . Therefore, if the reaction of trovacenyl(cyclopentadienyl) ions with $Fe_2Cl_4.3THF$ was performed at low temperature, for example, 0°C or below, **74··** may be obtained.

In addition, it should be noted that we have successfully synthesized bicyclo[2.2.1]hepten-7-one according to the literature.[128] It has been characterized by ^{1}H-NMR, ^{13}C-NMR spectroscopy and the reaction with lithiotrovacene to afford the alcohol **72·**. But due to its strongly volatile property and the closed boiling points between bicyclo[2.2.1]hepten-7-one (b.p. 96-100°, 115mm) and its precursor 7,7′-dimethoxybicyclo[2.2.1]heptene (b.p. 58-68°, 17mm), if without convenient precise reduced-pressure distilled apparatus, it would be very difficult to successfully isolate pure bicyclo[2.2.1]hepten-7-one from the mixture.

5.6.2. Synthesis and X-ray crystal structure analysis of [5]trovacenyl-1(anti,syn)-7-hydroxybicyclo[2,2,1]hept-2-en-7-yl (72·)

Lithiotrovacene reacted with norbornenone at ambient temperature,[121a,c] then following with the conventional aqueous work-up to give isomeric alcohol. If the reaction was performed with the ratio of 1:1:1 (trovacene: n-BuLi: norbornenone) in step, a moderate yield was obtained. Isolation by chromatography (Al_2O_3) afforded the mixture of isomeric alcohol

[5]trovacenyl-1-(anti, syn)-7-hydroxybicyclo[2,2,1]hept-2-en-7-yl (**72**•) as violet solid, which could not be separated further by chromatography. **72**• was characterized by mass spectroscopy, elemental analysis, and X-ray structural analysis. It has a good solubility in general organic solvent.

The crystal of alcohol **72**• was generated from the solution of benzene/PE at 8°C. A view of the molecular structure of alcohol is shown in Figure 5.3. Important lengths and angles are listed in Table 5.3 and 5.4, respectively.

Intermolecular hydrogen bond O-H-O′ bridge the neighboring molecules. It is similar to other trovacene derivatives containing OH group in the molecule, such as TVC-OH. The lengths of C(1)-O(1) and O(1)-H(1) are 1.420(4)Å and 0.68(3)Å, respectively. The C-C bonds of bicyclo[2.2.1] rang from 1.556(7) to 1.330(5)Å, C(1)-C(8) (1.496(4)Å), which indicate the distortion/torsion lengthen or shorten the general C-C bond. Furthermore, according to the C-C bond distantce, C(4)-C(3) can be determined to be double bond with the distance of 1.330(5)Å. It is significantly beyond the range of C(6)-C(1) single carbon-carbon bond, 1.493(8)Å. Meanwhile, the average C-C distance of C_5 ring is 1.424(5)Å, C_7 ring 1.385(8)Å.

The angle of C(1)-O(1)-H(1) is 113(3)°. The angles of O(1)-C(1)-C(8), O(1)-C(1)-C(5) and O(1)-C(1)-C(2) are 110.0(3)°, 108.7(3)° and 114.2(3)°, respectively. The torsion angles of C(8)-C(1)-C(2)-C(7), O(1)-C(1)-C(8)-C(12) and O(1)-C(1)-C(2)-C(7) are 175.5(3), 44.3(4) - 54.4(4)°, respectively.

Figure 5.3. Molecular structure and stereoview of **72**•
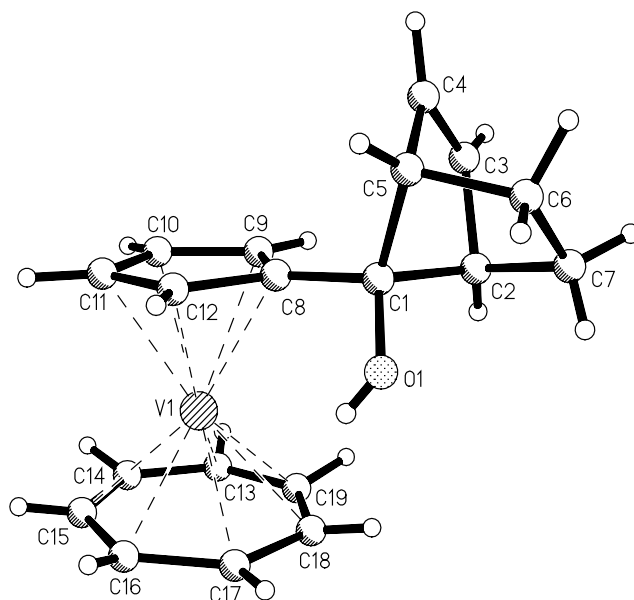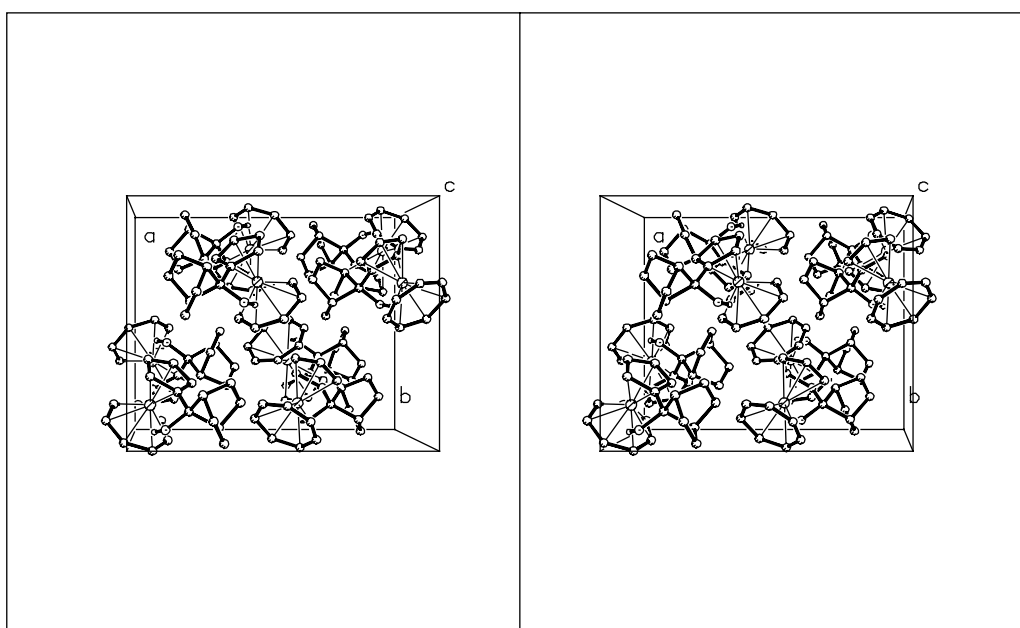
Table 5.3. Selected bond lengths[Å] of **72**˙

C(1)-O(1)	1.420(4)	V(1) - C(16)	2.170(4)
C(1) - C(8)	1.496(4)	V(1) - C(17)	2.179(4)
O(1) - H(1)	0.68(3)	V(1) - C(18)	2.168(4)
C(1) - C(2)	1.544((5)	V(1) - C(19)	2.167(4)
C(2) - C(3)	1.496(7)	**V(1)-C$_7$ Ring (mean)**	2.167(4)
C(3) - C(4)	1.330(5)	C(8) - C(9)	1.419(4)
C(4) - C(5)	1.492(5)	C(9) - C(10)	1.402(5)
C(5) - C(6)	1.538(5)	C(10) - C(11)	1.385(6)
C(6) - C(7)	1.493(8)	C(11) - C(12)	1.396(5)
C(2) - C(7)	1.556(7)	C(18) - C(12)	1.424(4)
V(1) - C(8)	2.287(3)	**C-C (mean for C$_5$)**	1.424(5)
V(1) - C(9)	2.251(3)	C(13) - C(14)	1.322(8)
V(1) - C(10)	2.237(4)	C(14) - C(15)	1.333(8)
V(1) - C(11)	2.254(3)	C(15) - C(16)	1.433(8)
V(1) - C(12)	2.269(3)	C(16) - C(17)	1.464(8)
V(1)-C$_5$ Ring (mean)	2.260(3)	C(17) - C(18)	1.429(7)
V(1)-C$_5$ (Centroid)	1.9172(4)	**V(1)-C$_7$ (Centroid)**	1.467(1)
V(1) - C(13)	2.174(5)	C(18) - C(19)	1.374(7)
V(1) - C(14)	2.158(5)	C(13) - C(19)	1.337(7)
V(1) - C(15)	2.155(4)	**C-C (mean for C$_7$)**	1.385(8)

Table 5.4. Selected angles and torsion [°] of **72**$^\bullet$

O(1)-C(1)-C(8)	110.0(3)	O(1)-C(1)-C(2)-C(3)	-161.8(3)
O(1)-C(1)-C(5)	108.7(3)	O(1)-C(1)-C(2)-C(7)	-54.4(4)
O(1)-C(1)-C(2)	114.2(3)	O(1)-C(1)-C(8)-C(9)	-140.9(3)
C(1)-O(1)-H(1)	113(3)	O(1)-C(1)-C(5)-C(4)	167.8(3)
C(8)-C(1)-C(2)	116.6(3)	O(1)-C(1)-C(8)-C(12)	44.3(4)
C(8)-C(1)-C(5)	114.1(3)	C(5)-C(1)-C(2)-C(3)	-50.3(3)
C(1)-C(2)-C(7)	100.1(4)	C(5)-C(1)-C(2)-C(7)	57.1(3)
C(6)-C(7)-C(2)	103.8(3)	C(8)-C(1)-C(2)-C(7)	175.5(3)
C(7)-C(6)-C(5)	103.4(4)	C(8)-C(1)-C(2)-C(3)	68.0(4)
C(4)-C(5)-C(6)	105.9(4)	C(1)-C(2)-C(3)-C(4)	33.4(4)
C(6)-C(5)-C(1)	101.3(3)	C(2)-C(3)-C(4)-C(5)	1.1(4)
C(3)-C(4)-C(5)	106.8(3)	C(3)-C(4)-C(5)-C(1)	-35.3(4)
C(4)-C(3)-C(2)	107.9(4)	C(8)-C(1)-C(5)-C(4)	-69.0(3)
C(3)-C(2)-C(1)	100.5(3)	C(2)-C(1)-C(5)-C(6)	-57.5(4)
C(3)-C(2)-C(7)	105.0(4)	C(1)-C(5)-C(6)-C(7)	36.4(5)
C(12)-C(8)-C(1)	124.8(3)	C(3)-C(2)-C(7)-C(6)	66.3(6)
C(9)-C(8)-C(1)	129.8(3)	C(5)-C(1)-C(8)-C(9)	96.6(4)
C(10)-C(9)-C(8)	109.0(4)	C(5)-C(6)-C(7)-C(2)	0.7(6)
C(14)-C(13)-C(19)	130.7(5)	C(2)-C(1)-C(8)-C(12)	176.3(3)
Torsion C$_5$ ring (mean)	0.0(4)	**Torsion C$_7$ ring (mean)**	0.0(8)

5.6.3. Results of Cyclic Voltammetry (72$^\bullet$)

Cyclic voltammetry of **72**$^\bullet$ at -50°C is depicted in Figure 5.4. The data are shown in Table 5.5. The oxidation potential ($E_{1/2}(0/+)$ = 221 mV) is a cathodic shift relative to that of parent trovacene ($E_{1/2}(0/+)$ = 260 mV). It indicates that **72**$^\bullet$ is even more readily oxidized that trovacene. Presumably the α position OH group can contribute to the shift.

The reduction potential is -2.336 V with a significant anodic shift relative to that of trovacene. The rigid unsaturated bridging structure (C_7H_8) of substituent to cyclopentadienyl and the electron-accepting character would presumably lead to the shift.

Table 5.5. Cyclic Voltammetry Data for **72**$^\bullet$

$E_{1/2}(0/+)$	ΔE_p	I_{pa}/I_{pc}	$E_{1/2}(+/2+)$	$E_{1/2}(0/-)$	ΔE_p	I_{pa}/I_{pc}
221 mV	174 mV	0.69	1.016 V	-2.336 V	160 mV	0.67

Figure 5.4. Cyclic voltammograms for **72$^{\bullet}$** in DME/TBAP at -50°C, v = 100mV/s
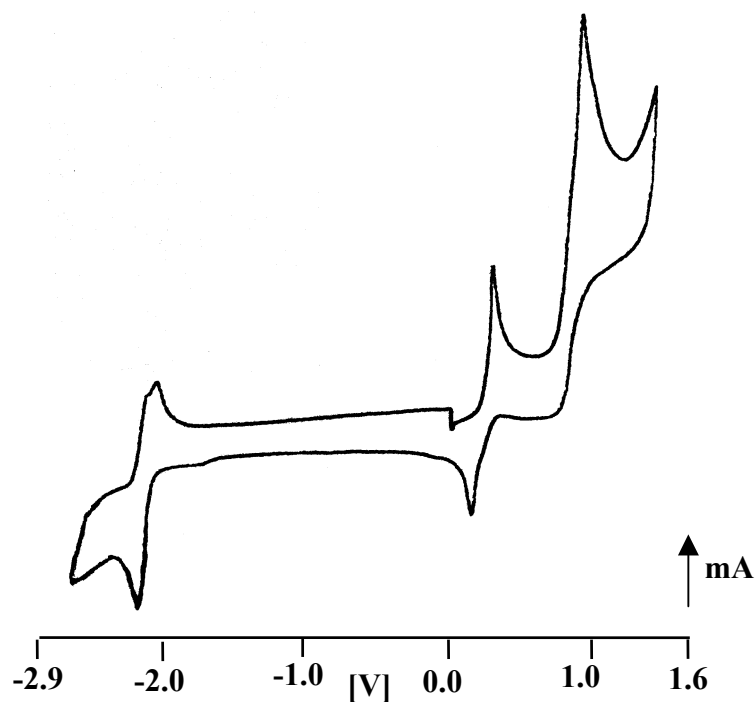
5.6.4. Attempts to synthesize Di([5]trovacenyl-η^{5}-cyclopentadienyl)iron (74$^{\bullet\bullet}$)

[5]trovacenyl-1-(anti, syn)-7-chloro-bicyclo[2,2,1]hept-2-en-7-yl (**73$^{\bullet}$**) were obtained from the reaction of lithium alcoholate with ClPO(OEt)$_2$ at 50°C. In order to avoid hydrolysis, **73$^{\bullet}$** had not been further purified by chromatography, but characterized by mass spectroscopy (EI). After cleaving the chloride by utilizing lithium powder at r.t., Fe$_2$Cl$_4$.3THF was added and the mixture was stirred at 50°C overnight. According to the result of mass spectra, the molecular ion peak of di([5]trovacenyl-η^{5}-cyclopentadienyl)iron (**74$^{\bullet\bullet}$**) was not observed. Considering the stability of di([5]trovacenyl-tetramethyl-η^{5}-cyclopentadienyl)iron (**72$^{\bullet\bullet}$**), the reason for failure may be the poor thermal stability of the expected product **74$^{\bullet\bullet}$**.

Scheme 6.
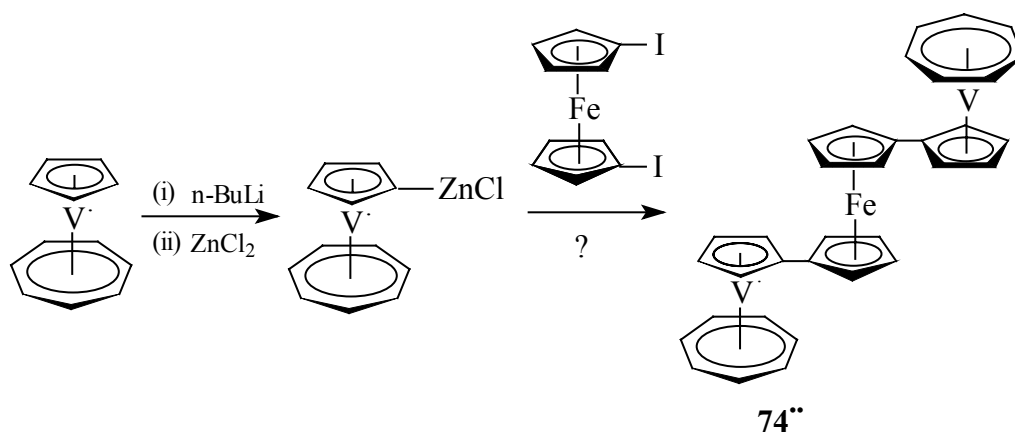
In order to find a formation and isolation method for **74**[..], another route was attempted (Scheme 6).[129] At 0°C, 1,1'-diiodo-ferrocene and catalyst $Pd(dppf)_2Cl_2$ were added slowly to the solution of TVC-ZnCl,[80] then the mixture was refluxed for 1h. After removal all the volatiles, the brown residue was dissolved into THF and then refluxed for 1h. But there was still no observation of the molecular ion peak of **74**[..] in EI-MS (70eV).

6. Experimental Section

6.1. General Operations

All manipulation were performed under inert atmosphere (nitrogen, argon) using standard Schlenk techniques. Nitrogen was deoxygenated by BTS-catalyst which was reactivated with the help of hydrogen at 130°C for two days beforehand, and dried by two columns which were filled with Silica gel and Potassium hydroxide, Magnesium perchlorate and Phosphorus pentoxide, respectively. Solvents were freshly distilled under nitrogen over various standard drying agents as the following table describes. Deoxidized H_2O was obtained by refluxing the distilled water and cooling down under the nitrogen atmosphere three times.

Solvents	Drying agents
Acetonitrile	CaH_2
Benzene	K
Diethylether (Et$_2$O)	K / Na
dichloromethane	P_2O_5
Ethanol	CaO
1,2-Dimethoxyethan (DME)	K / Na
Hexane	K / Na
Petroether (PE, 40-60°C)	K / Na
Toluene	K / Na
Tetrahydrofuran (THF)	1. CaH_2; 2. K

Chromatography were carried out on Aluminiumoxide (neutral-grade II) and silica gel. Aluminiumoxide was deoxygenated and preheated at 120°C under high vacuum for 2 days and stored under nitrogen.

6.2. General Methods

Analysis

Electron ionization mass spectra (EI-MS) were run on a Varian CH7a spectrometer at 70eV, the sample was filled in small can (*Tiegel*) which was put inside a special glass apparatus under nitrogen.

Infrared spectra (IR) were measured on Bruker IFS 88 spectrometer (KBr). ^{1}H-NMR were recorded at Bruker ARX 200 instrument (CDCl$_3$).

Elemental analysis were performed with Heraeus CHN-Rapid-Elemental Analyzer, the sample was filled in small soft tin can (*Zinntiegelchen*) under nitrogen.

X-ray crystal structure determinations were performed with Siemens P4 diffractometer, the data were collected by means of a STOE IPDS system employing MoKα radiation (71.073 pm) (Dr. K. Harms).

Cyclic Voltammetry (CV)

Cyclic voltammetry (CV) was performed with electrochemical equipment from AMEL (Milano) consisting of a Model 552 potentiostat, Model 568 function generator, Model 563 multipurpose unit, Nicolet Model 3091 storage oscilloscope, and Kipp & Zonen Model BD 90 x/y recorder. Glassy carbon, platinum wire and saturated calomel (SCE) served as the working, counter and reference electrode, respectively. The manipulations were carried out under argon atmosphere at -30°C ~ -50°C by cooling bath (ethanol/liquid nitrogen). The CV traces were recorded in the medium dimethoxyethane (DME)/n-Bu$_4$NClO$_4$, DME was purified by refluxing and distillation from CaH$_2$ and K/Na.

Electron Paramagnetic Resonance Spectra (EPR)

EPR were carried out on an X-Band Spectrometer ESR 300 (Bruker). The simulation of EPR spectra were performed with the least squares fit program CWSIM on a Power Mac 7100/80 AV. The solution of sample (10^{-5}~10^{-4} M) in toluene or THF were filled in a quartz or glass tube ($\varnothing$ 4mm) and sealed under high vacuum.

Magnetic Susceptibility Measurement

Magnetic susceptibility was studied with a SQUID susceptometer (Quantum Design) in the temperature range from 1.4 to 300K. The external magnetic field was 55KG (0.1% correction) with the help of a supra-conduct reel. The sample, about 20mg, was filled in a small teflon can (*Tiegel*) with a lid under nitrogen (Prof. Dr. J. Pebler).

6.3. Reagents

The following compounds were commercially available and some of them were purified prior to use (distillation[1], sublimation[2], dehydrate[3], or recrystallization[4]):

n-BuLi (1.68M/hexane, or 1.6M/hexane), lithium powder, sulfur powder[2], selenium powder, tellurium powder, cobalt chloride, lead chloride, zinc chloride[3], tin (II) chloride$_2$[3], cupric acetate, chlorosulphuric acid, dimethyldisulfide[1], 1,2-dichlorotetramethyldisilane, chlorobenzene[1], perchlorocyclopentadiene, cyclopentadiene[1], cycloheptatriene, chromium hexacarbonyl, molybdenum hexacarbonyl, tetramethylcyclopentenone, n-Bu$_4$NF·3H$_2$O, CS$_2$[1], SCl$_2$[1], S$_2$Cl$_2$[1], CHI$_3$, ClP(O)(OEt)$_2$, MoCl$_4$(CH$_3$CN)$_2$, Me$_2$SiCl$_2$[1], Ph$_2$SiCl$_2$[1], Ph$_2$GeCl$_2$, Me$_2$SnCl$_2$[4], Ph$_2$SnCl$_2$[4], PhPCl$_2$[1], PCl$_3$[1], AsCl$_3$[1], SbCl$_3$[2], BiCl$_3$[2], LiAlH$_4$, B(OC$_4$H$_9$)$_3$[4] (Aldrich Chemical Co.).

The following compounds were synthesized according to literature:

Me$_3$SiOOSiMe$_3$,[133] Ph$_2$PbCl$_2$,[86] Fe$_2$Cl$_4$·3THF,[134] (Me$_3$Si)$_2$NH,[135] Bi[N(SiMe$_3$)$_2$]$_3$,[136] norbornenone,[128] 1, 1´-diiodoferrocene,[137] (nbd)Mo(CO)$_4$,[138] TVC-B(OH)$_2$,[71] trovacene (TVC)[130, 131] (Scheme 1).

Scheme 1.

$$VCl_3 \xrightarrow{\text{THF}} VCl_3 \cdot 3THF \xrightarrow{\text{Zn}} [(V_2Cl_3)(THF)_6]_2[Zn_2Cl_6]$$

$$CpVTr \xleftarrow{C_7H_8} CpV(CO)_4 \xleftarrow{CO/Na} Cp_2V \xleftarrow{\text{CpNa}}$$
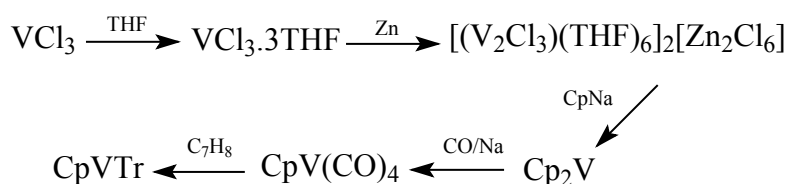
VCl$_3$[132] was obtained by the reaction of V$_2$O$_5$ with S$_2$Cl$_2$ at refluxing, and the formed S was removed by extraction with CS$_2$. Violet VCl$_3$ was refluxed in THF for 12h to form VCl$_3$·3THF as red solid. After reduction by zinc powder overnight, the formed green suspension was added the solution of Cp$^-$Na$^+$ in THF and resulted in Cp$_2$V (vanadocene). The strongly air-sensitive purple Cp$_2$V was obtained by sublimation or extraction with PE after removal of all the solvents, and it was found the sublimation method is an efficient way. Cp$_2$V reacted with CO in step, and sodium sand for 2 days to generate orange CpV(CO)$_4$. After removal of the solvent, the residue was extracted by toluene and filtered through Al$_2$O$_3$ to give CpV(CO)$_4$ which could be purified by sublimation. After refluxing overnight in cycloheptatriene (C$_7$H$_8$), CpV(CO)$_4$ was converted to violet trovacene which could be purified by extraction with toluene and recrystallization.

6.4. Preparations

Synthesis of Di([5]trovacenyl)sulfide (16⁻⁻)
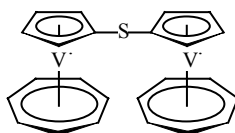
To a solution of TVC (784mg, 3.79mmol) in Et$_2$O (150ml), n-BuLi (2.4ml, 3.84mmol, 1.6M/Hexane) was added and the mixture was stirred overnight at r.t. to give a red-brown solution. The freshly distilled SCl$_2$ (0.12ml) in 10ml Et$_2$O was added dropwise in 1h at 0°C. A large amount of green precipitate was formed. After filtration, the green solid was dissolved in benzene and filtered through Celite to give a dark green solution. The analytically pure **16⁻⁻** was isolated by chromatography (2.5×25cm, Al$_2$O$_3$, PE/Toluene) and recrystallized from benzene/PE as violet crystals (115mg, yield 14%).

IR (KBr): 3043 (w), 2958 (w),1730 (m), 1423 (w), 1025 (s), 957 (s), 890 (s), 851 (s), 778 (vs), 433 (m), 420 (m)
EI-MS (70eV): 444 (M$^{+\cdot}$, 100), 238 (TVC-S$^+$, 17)
C$_{24}$H$_{22}$SV$_2$ (444.18):   Calcd.:   C, 64.89,   H, 4.95
                    Found: C, 63.78,   H, 4.90

Synthesis of Di([5]trovacenyl)disulfide (18$\cdot\cdot$)
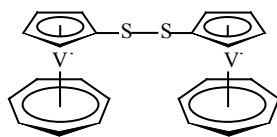
To a solution of TVC (450mg, 2.2mmol) in 150ml Et$_2$O, n-BuLi (1.3ml, 2.2mmol, 1.68M/Hexane) was added and the mixture was stirred overnight at r.t. to give a red-brown solution. The solution was concentrated to ~50ml, then sublimed powdered sulfur S$_8$ (36mg, 1.1mmol) was added and stirred at -20°C for 1h, at 0°C for another 1 h, and at r.t. for further 1h. Then another half equiv. S$_8$ (36mg, 1.1mmol) was added and stirred at r.t for 3h to afford a large amount of pale green precipitate (18$\cdot\cdot$). The suspension was filtered and washed by Et$_2$O (2×20ml). The analytically pure 18$\cdot\cdot$ was obtained by recrystallization from benzene and PE as green powder (250mg, yield 50%, based on TVC). Violet crystals suitable for X-ray diffraction were generated by diffusion of PE to the solution of 18$\cdot\cdot$ in benzene at 8°C.

IR (KBr): 3037 (w), 2960 (w), 1770 (m), 1643 (m), 1482 (m), 1420 (m), 1399 (w), 261 (s), 1167 (s), 1095 (s), 1020 (vs), 957 (s), 852 (s), 779 (vs), 643 (m), 477 (m), 454 (m), 430 (s).
EI-MS (70eV): 476 (M$^+$, 7), 238 (TVC-S$^+$, 100).
C$_{24}$H$_{22}$S$_2$V$_2$ (476.24):   Calcd,   C, 60.52,   H, 4.62
                           Found: C, 60.69,   H, 5.09

Synthesis of lithium trovacenylthiolate (19$\cdot$)
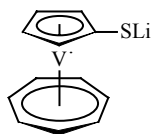
To a solution of TVC (420mg, 2mmol) in Et$_2$O (100ml), n-BuLi (1.3ml, 2.1mmol, 1.68M/hexane) was added and stirred at r.t. overnight to give a red-brown solution. The red-brown solution was reduced in volume to *ca* 30ml. Half equiv. S$_8$ (32mg, 1mmol) was added and the mixture was stirred at -20°C for 1h, then at 0°C for 1 h, and at r.t. for 1h. All the solvents were evaporated under reduced pressure. The residue was suspended in PE (30ml), filtered and washed by PE till colorless, then dried in vacuo to give lithium-trovacenylthiolate as pale violet powder which had not been further purified and was used directly for further reaction. Yield, 240mg, 50 % based on TVC. The formation of 19$\cdot$ was identified by acidification (HCl 15%) to afford 17$\cdot$.

Synthesis of Di([5]trovacenylthio)methane (20⁰⁰)
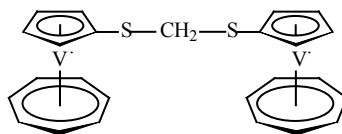
To a solution of TVC-SLi (256mg, 1.04mmol) in DME (20ml), CH_2Cl_2 (0.05ml, 0.84mmol) in DME (2ml) was added slowly at 0°C. The reaction mixture was stirred for 1h and was warmed slowly to r.t. with stirring overnight. All the volatiles were removed in vacuo and the residue was purified by chromatography (2×20cm, Al_2O_3, elution with PE and toluene, respectively). The first band was TVC, and followed with green band which had been characterized by MS to be di([5]trovacenyl)disulfide. The third band was collected and the solvent was evaporated in vacuo to give **20⁰⁰** as violet solid (40mg, yield 20%).

IR (KBr): 3096 (w), 3046 (w), 2954 (w), 2900 (w), 1764 (w), 1641 (m), 1424 (w), 1243 (w), 1191 (s), 1170 (m), 1034 (s), 1019 (s), 958 (s), 891 (m), 849 (s), 813 (m), 7904 (vs), 776 (vs), 473 (m), 455 (m), 429 (vs)

EI-MS (70eV): 490 ($M^{+\cdot}$, 47), 252 ($TVC-S-CH_2^+$, 20), 238 ($TVC-S^+$, 21), 173 ($CpV-SCH_2^+$, 100), 116 (CpV^+, 5), 91 ($C_7H_7^+$, 29)

$C_{25}H_{24}S_2V_2$ (490.25):   Calcd.:   C, 61.24;   H, 4.90
                             Found: C, 60.93;   H, 6.62

Synthesis of [5]Trovacenylthiol (21˙)
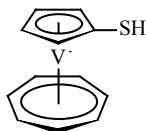
Method **A**:

To a solution of di(trovacenyl)disulfide (120mg, 0.25mmol) in 50ml DME, the suspension of $LiAlH_4$ (60mg, 1.6mmol) in 20ml DME was added dropwise over 1h with vigorously stirring at r.t.. After refluxing for 2h, HCl (10ml, 15%) was added dropwise to give a purple solution. The suspension was filtered through Celite. The filtrate was dried over $MgSO_4$. After filtration, all the volatiles were removed under reduced pressure, the residue was characterized by chromatography (Al_2O_3, 1×13cm) to give **17˙** as purple solid (40mg, yield 90%, based on disulfide).

IR (KBr): 2963 (s), 2537 (w), 1428 (w), 1262 (vs), 1097 (s), 1023(s), 957 (m), 915 (w), 853 (w), 800 (vs), 704 (w), 477 (w), 432 (w).

EI-MS (70eV): 239 ($M^{+\cdot}$, 36%), 207(TVC^+, 100%)

$C_{12}H_{12}SV$ (239.12):   Cald.:   C, 60.27,   H, 5.02
                         Found: C, 60.75,   H, 5.77

Method **B**:

To a solution of TVC (230mg, 1.11mmol) in Et$_2$O (50ml), n-BuLi (1.68mmol, 1ml, 1.68M/hexane) was added and stirred at r.t. overnight to give a red-brown solution. The solution was concentrated to *ca* 20ml, then S$_8$ (18mg, 0.56mmol) was added and stirred at -20°C for 1h, at 0°C for 1h, then at r.t. for further 1h. The solvent was removed, the residue was suspended in 50ml PE , filtered and washed by PE till colorless to give TVC-SLi (130mg) as pale purple powder. The formed TVC-SLi was dissolved in 30ml DME, and HCl (2ml, 15%) was added dropwise to result in a purple solution. After filtration through Celite, the filtrate was dried over MgSO$_4$ and evaporated in vacuum. The product **17**˙ was isolated by chromatography (Al$_2$O$_3$, 1×10cm). Yield: 120mg, 45%, based on TVC.

EI-MS (70eV): 239 (M$^{+\cdot}$, 16%), 207 (TVC,100%).

Synthesis of Benzyl([5]trovacenyl)thioether (22˙)
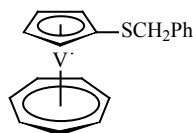
PhCH$_2$Cl (0.14ml, 1.17mmol) in DME (10ml) was added slowly to the solution of TVC-SLi (255mg, 1.04 mmol) in DME (10 ml) at 0°C. The mixture was stirred for 1h and was allowed to warm to r.t. and stirred for 4h. The solvent was removed under reduced pressure and the residue was chromatographed on silica gel (eluted by PE, PE/toluene (v/v, 1:1), respectively) to give **22**˙ (130mg) as violet solid, yield 40%.

IR (KBr): 3091 (w), 3029 (w), 2918 (w), 1762 (m), 1492 (s), 1448 (s),1425 (m), 1024 (s), 956 (s), 849 (s), 808 (s), 781 (vs), 708 (vs), 6 42(m), 562 (m), 490 (m), 455 (m), 442 (m), 430(s)
EI-MS (70eV): 329 (M$^{+\cdot}$, 15), 238 (TVC-S$^+$), 207 (TVC$^+$, 100), 116 (CpV$^+$, 36), 91 (C$_7$H$_7^+$, 81), 51(V, 47)
C$_{19}$H$_{18}$SV (329.19):   Calcd.:   C, 69.32;   H, 5.47
                   Found: C, 68.92;   H, 5.81

Synthesis of Methyl([5]trovacenyl)thioether (23˙)
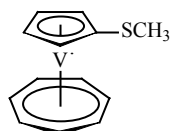
n-BuLi (3ml, 5.1mmol, 1.68 M/hexane) was added to a solution of TVC (1.058g, 5.1mmol) in diethyl ether (150ml), the mixture was stirred at r.t. overnight to form a red-brown solution. At -40°C, CH$_3$SSCH$_3$ (0.46ml, 5.1mmol) was added to the solution, and the mixture was stirred for 1h and then was allowed to warm slowly to 0°C and stirred for further 1h, then to

r.t. overnight. All of the volatiles were removed in vacuo and the residue was chromatographyed on a silica gel column using toluene/PE (v/v, 1:1) as eluent to yield **23**$^{\cdot}$ (450mg, 1.78mmol) as violet solid. Yield; 36%.

IR (KBr): 3093 (w), 3043 (w), 2959 (w), 2820(w), 2361(w), 1843 (w), 1492 (s), 1448 (s), 1425 (m), 1261 (s), 956 (s), 849 (s), 808 (s), 781 (vs), 6 42(m), 562 (m), 490 (m), 455 (m), 442 (m), 430(s)

EI-MS (70eV): 253 (M$^{+\cdot}$, 60), 207 (TVC^{+}, 100), 147 (CpVS^{+}, 20), 116 (CpV^{+}, 74), 91 (C$_7$H$_7^{+}$, 27), 51 (V^{+}, 88)

C$_{13}$H$_{14}$SV (253.13): Calcd,   C, 61.68;   H, 5.53
  Found,   C, 60.51;   H, 5.72

Synthesis of Di([5]trovacenylthio)dimethyltin (24$^{\cdot\cdot}$)
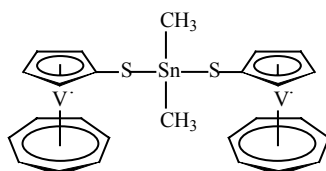
TVC-SLi (870mg, 3.55mmol) was dissolved in benzene (50ml), and Me$_2$SnCl$_2$ (390mg, 1.77mmol) was added to the solution and stirred at r.t. overnight. The reaction mixture was filtered through Celite, the filtrate was evaporated and the residue was isolated by chromatography (2×30cm, Al$_2$O$_3$, Et$_2$O/toluene) to give **24**$^{\cdot\cdot}$ (80mg) as dark violet solid, yield 7%.

EI-MS (70eV): 626 (M$^{+\cdot}$+1, 43), 625 (M^{+}, 14), 401 (M-TVC-Me^{+}, 100), 358 (TVC-S-Sn^{+}, 50), 238 (TVC-S^{+}, 70), 207 (TVC^{+}, 8)

C$_{26}$H$_{28}$S$_2$SnV$_2$ (624.95):   Calcd.:   C, 49.97;   H, 4.48
  Found: C, 53.69;   H, 4.77

Synthesis of Di([5]trovacenyl)diselenium (25$^{\cdot\cdot}$)
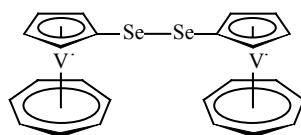
n-BuLi (2.4ml, 3.84mmol, 1.6M/Hexane) was added to a solution of TVC (715mg, 3.45mmol) in Et$_2$O (200ml), the mixture was stirred at r.t. overnight. Then the red-brown solution was concentrated to ~ 50ml. At -20°C, selenium powder (137mg, 1.73mmol) was added and stirred for 1h, then warmed slowly to 0°C for further 1 h, and to r.t. for 1h. Another equiv. Se (153mg, 1.73mmol) was added, and stirred at r.t. overnight to form much pale green precipitate. The solvent was removed in vacuo and the residue was extracted by hot toluene, then filtered through Celite and washed by toluene. The analytically pure product **25**$^{\cdot\cdot}$ was

obtained by chromatography (Al$_2$O$_3$, 2×30cm, toluene/THF) as green powder (330mg, yield 34%).

IR (KBr): 3451 (w), 2963 (s), 1729 (w), 1639 (w), 1414 (w), 1261 (s), 1096 (s), 1021 (s), 875 (w), 802 (vs), 703 (w), 428 (w).

EI-MS (70eV): 572 (M$^+$·+2, 5), 570 (M$^+$·, 5), 286 (TVC-Se$^+$, 100)

C$_{24}$H$_{22}$Se$_2$V$_2$ (570.15): Calcd, C, 50.56, H, 3.86
                                        Found: C, 49.73, H, 3.95

Synthesis of Di([5]trovacenyl)ditellurium (26··)
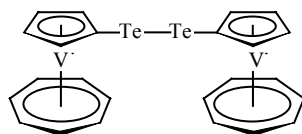
n-BuLi (3.2ml, 5.12mmol, 1.6M/Hexane) was added to a solution of TVC (950mg, 4.59mmol) in Et$_2$O (200ml), the mixture was stirred overnight at r.t. To the concentrated solution of lithiotrovacene (50ml), at -20°C, tellurium powder (296mg, 2.3mmol) was added and stirred for 1h, then at 0°C for 1 h, and at r.t. for further 1h. Another half equiv. molecule tellurium powder (294mg, 2.3mmol) was added and stirred overnight. No large amount of precipitate was formed exclude small amount of unreacted black Te powder, then half equiv. molecule S$_8$ (74mg, 2.3mmol) was added to the suspension and stirred at r.t. overnight again, and much pale green precipitate was generated. The solvent was removed in vacuo and the residue was extracted by hot toluene, filtered through Al$_2$O$_3$ column (3.5×9cm) and first eluted by toluene/PE (1:1) to give the violet TVC, followed by hot THF/benzene (1:1) to afford **26··** as yellow-green solution. The analytically pure product **26··** was obtained by recrystallization from benzene and PE as yellow-green powder (760mg, yield 44%, based on TVC).

IR (KBr): 2961 (m), 2921 (s), 2852 (m), 1731 (m), 1618 (m), 1384 (w), 1353 (w), 1261 (vs), 1092 (m), 1019 (m), 862 (m), 799 (vs), 618 (w), 417 (w)

EI-MS (70eV): 572 (M$^+$·+2, 5), 570 (M$^+$·, 5), 286 (TVC-Te$^+$, 100)

C$_{24}$H$_{22}$Te$_2$V$_2$ (476.24): Calcd, C, 43.19, H, 3.30
                                         Found: C, 44.81, H, 3.67

Synthesis of Trimethylsiloxy[5]trovacene (27·)
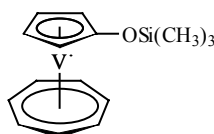
At -78°C, to the solution of lithiotrovacene (from TVC 242mg, 1.17mmol; and n-BuLi 0.9ml/1.6M, 1.44mmol), freshly synthesized Me$_3$SiOOSiMe$_3$ (0.3ml) was added dropwise over 2h and then the mixture was stirred at r.t. overnight to give a pale red-violet suspension.

Then H_2O (5ml) was added. The ether layer was dried over $MgSO_4$ and filtered through Celite. Isolation by chromatography (1×10ml, Al_2O_3) gave **27** as pale violet solid (16mg; yield, 5% based on TVC). Owing to its thermal instability, most of the **27** was decomposed during the isolation at r.t. which has been proved by repeated experiments. Therefore, the crude product was used directly without isolation for the following procedure to form [5]trovacenol **28**.

EI-MS (70eV): 295 ($M^{+\cdot}$, 100), 281 (M^+-CH_3, 27), 223 (TVC-O^+, 2), 207 (TVC^+, 89), 129 ($C_6H_6^+$, 37), 116 (CpV^+, 29)
$C_{15}H_{20}OSiV$ (295.17):   Calcd.;   C; 61.03;   H, 6.78
                          Found: C, 58.83;   H, 6.53

Isolation of [5]trovacenol (28·)
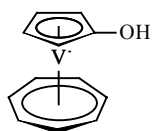
28· was obtained as by-product from hydrolysis (H_2O, 2ml) of trimethylsiloxy[5]trovacene **(27·)**, which was prepared by the reaction of lithiotrovacene (from TVC, 390mg, 1.88mmol and n-BuLi, 1.2ml/1.6M, 1.92mmol) and $Me_3SiOOSiMe_3$ (0.5ml). Isolation by chromatography (2×30cm, Al_2O_3, eluted with ethanol) gave [5]trovacenol (20mg, yield, 4%) as red-violet solid. Meanwhile, all the silyl ethers were decomposed during the isolation course and/or converted to **28·**. **28·** was not stable in solution and decomposed slowly to give some pale yellow solid which had not been further characterized. **28·** was recrystallized from benzene/PE at 8°C to form violet crystal which was suitable for the X-ray diffraction.

EI-MS (70eV): 223 ($M^{+\cdot}$, 100), 142 (VTr^+, 8), 132 ($C_5H_4OH^+$, 11), 129 ($C_6H_6^+$, 10), 116 (CpV^+, 4)
$C_{12}H_{12}OV$ (223.06):   Calcd.:   C, 64.61;   H, 5.38
                      Found: C, 64.11;   H, 5.98

Synthesis of Di([5]trovacenyl)-phenyl-phosphane (41··)
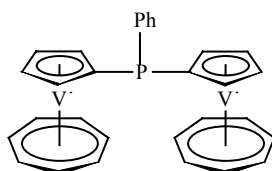
n-BuLi (3.2ml, 5.12mmol) was added to a solution of TVC (960mg, 4.64mmol) in Et_2O (150ml), and stirred at r.t. overnight to give a red brown solution. Then freshly distilled $PhPCl_2$ (0.16ml, 1.18mmol) was added dropwise at 0°C over 1h, the mixture changed into violet in color. After warmed to r.t., another equiv. molecule $PhPCl_2$ (0.16ml, 1.18mmol) was added dropwise in 0.5h and resulted in a large amount of pale yellowish green precipitate. Filtered and washed by PE, the yellow-green solid was characterized to be by-product by EI-

MS. The dark violet filtrate was evaporated in vacuo. The residue was chromatographed (2×30cm, Al$_2$O$_3$, eluted with Et$_2$O/toluene 1:1) to give **41**$^{..}$ (435mg, yield, 36%) as purple solid.

IR (KBr): 3041 (w), 2956 (w), 1431 (s), 1390 (m), 1198 (m), 1161 (s),1029 (m), 1029 (vs), 957 (s), 850 (s), 809 (w), 782 (vs), 744 (s), 696 (s), 648 (m), 542 (s), 429 (s), 413 (m).
EI-MS (70eV): 520 (M$^{+.}$, 100), 315 (M$^+$-TVC, 15), 207 (TVC$^+$, 5)
C$_{30}$H$_{27}$PV$_2$ (520.15):   Calcd.:   C, 69.27;   H, 5.19
                               Found: C, 68.95;   H, 5.31

Synthesis of Di([5]trovacenyl)chloroarsane (43$^{..}$)
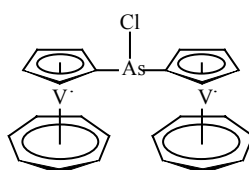
To a solution of lithiotrovacene (from TVC 370mg, 1.79mmol and n-BuLi 1.1ml, 1.6M/hexane, 1.76mmol) in 150ml Et$_2$O, AsCl$_3$ (0.4ml, 4.7mmol) in Et$_2$O (2ml) was added dropwise at r.t. and stirred for 2h to yield a large amount of pale green precipitate. Filtered and washed by Et$_2$O (2×10ml), extracted by toluene, then recrystallized from benzene /PE gave **43**$^{..}$ as green powder (150mg, yield: 32%). Due to its strong polarity, **43**$^{..}$ can not be purified by chromatography (Al$_2$O$_3$ or silica).

EI-MS (70eV): 522.7 (M$^{+.}$, 9), 431 (M$^+$-C$_7$H$_8$), 281 (TVC-As$^+$, 2), 207 (TVC$^+$, 9)
C$_{24}$H$_{22}$AsClV$_2$ (522.49): Calcd.: C, 55.17;   H, 4.21
                               Found: C, 53.31;   H, 5.02

Synthesis of Di([5]trovacenyl)-butyl-arsane (44$^{..}$)
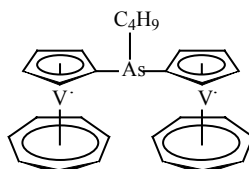
To a green solution of (TVC)$_2$AsCl (60mg, 0.12mmol) in benzene (30ml), n-BuLi (0.2ml/1.6M, 0.32mmol) was added dropwise and the mixture was stirred at r.t. for 0.5h. Then H$_2$O (1ml) was added dropwise, the mixture was dried over MgSO$_4$ and filtered. The solvent was removed in vacuo, the residue was chromatographed (1×10cm, Al$_2$O$_3$, toluene/PE) to give **44**$^{..}$ (60mg, yield: ~100%) as red-violet powder. The single crystal suitable for X-ray was generated from saturated benzene solution at 8°C.

IR (KBr): 3033 (w), 2938 (w), 2919 (w), 2859 (w), 1732 (m), 1460 (w), 1387 (w), 1263 (w), 1146 (m), 1081 (w) , 1026 (s), 955 (s), 877 (w), 850 (s), 774 (vs), 715 (m), 636 (m), 435 (s).

EI-MS (70eV): 544 ($M^{+\cdot}$, 3), 488 ($M-C_4H_9^+$, 4), 394 ($TVC-As-CpV^+$, 3), 282 ($TVC-As^+$, 5), 207 (TVC^+, 8)

C$_{28}$H$_{31}$AsV$_2$ (544.08): Cald.: C, 61.81; H, 5.70

Found: C, 60.26; H, 5.83

Synthesis of Di([5]trovacenyl)arsane (45$^{\cdot\cdot}$)
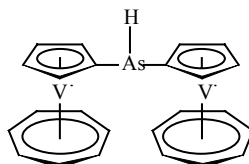
To a green solution of (TVC)$_2$AsCl (438mg, 0.84mmol) in THF (50ml), LiAlH$_4$ (110mg, 2.9mmol) was added stepwise and stirred vigorously at r.t. The mixture changed into pale violet in color immediately. After stirring for 0.5h, H$_2$O (5ml) was added dropwise carefully, then the mixture was dried over MgSO$_4$, filtered through Celite, and removed of all the solvents. The analytically pure **45$^{\cdot\cdot}$** was isolated by chromatography (1×10cm, Al$_2$O$_3$) as red-violet solid (160mg; yield, 40%).

EI-MS(70eV): 488 ($M^{+\cdot}$, 3), 281 ($TVC-As^+$, 11), 207 (TVC^+, 100), 129 ($C_6H_6V^+$, 26), 116 (CpV^+, 17), 51 (V^+, 27)

C$_{24}$H$_{23}$AsV$_2$ (488.04): Cald.: C, 59.06; H, 4.71

Found: C, 58.45; H, 4.84

Synthesis of Di([5]trovacenyl)arsinouse acid (46$^{\cdot\cdot}$)
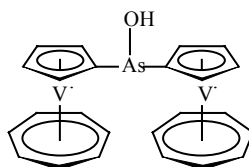
(TVC)$_2$AsCl (85mg, 0.16mmol) was dissolved into THF (10ml) to form a green solution, and then 10% NaOH solution (2ml) was added dropwise with vigorously stirring at r.t. The mixture changed into red-violet in color soon, then dried over MgSO$_4$ and filtered through Celite. After removal of the solvent, the residue was chromatographed (1×10cm, Al$_2$O$_3$, ethanol as the eluent) to give **46$^{\cdot\cdot}$** as red-violet solid (80mg, yield, 90%).

EI-MS(70eV): 504 ($M^{+\cdot}$, 100), 413 ($M^+-C_7H_7$, 7), 281 ($TVC-As^+$, 14), 207 (TVC^+, 51), 129 ($C_6H_6^+$, 10), 116 (CpV^+, 8)

C$_{24}$H$_{23}$OAsV$_2$ (504.04): Cald.: C, 57.19; H, 4.56

Found: C, 59.74; H, 5.35

Synthesis of Dimethyldi([5]trovacenyl)silane (59")
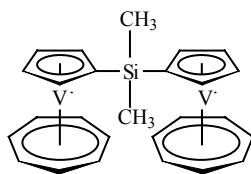
To a red-brown solution of lithiotrovacene (from TVC 695mg, 3.36mmol and n-BuLi 2.4ml, 3.84mmol, 1.6M/hexane) in Et$_2$O (150ml), Me$_2$SiCl$_2$ (0.1ml, 0.84mmol) was added dropwise at 0°C in 1h to afford a violet solution, then the mixture was warmed to r.t. and Me$_2$SiCl$_2$ (0.13ml, 1.09mmol) was added stepwise again. After stirring for 1h, the mixture was filtered through Celite and freed of all the volatiles. The analytically pure **59"** was obtained by chromatography (Al$_2$O$_3$, 2×30cm, toluene/PE and THF as the eluent) as violet solid (193mg, yield, 24%).

EI-MS (70eV): 470 (M$^{+\cdot}$, 34), 207 (TVC$^+$, 100)
C$_{26}$H$_{28}$SiV (470.23):   Calcd.:   C, 66.41;   H, 5.95
                        Found: C, 66.36;   H, 5.61

Synthesis of Tetramethyldi([5]trovacenyl)disilane (60")
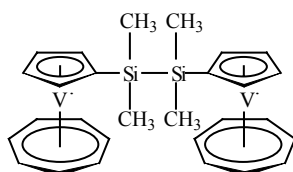
To a red-brown solution of lithiotrovacene (from TVC 1.013g, 4.89mmol and n-BuLi 3.1ml, 4.96mmol, 1.6M/hexane) in Et$_2$O (150ml), tetramethyldichlorsilane (0.23ml, 1.22mmol) was added stepwise at 0°C over 1h to afford violet solution. After addition of another equiv. molecule tetramethyldichlorsilane (0.23ml, 1.22mmol) at r.t., a large amount of white precipitate was formed, and the suspension was stirred for further 2h. Filtration and removal of all the volatiles gave dark violet residue. Isolation by chromatography (3×30cm, Al$_2$O$_3$, THF) gave **60"** (562mg, yield, 44%) as pale purple solid.

IR (KBr): 3043 (m), 2953 (s), 2894 (w), 1481 (m),1404 (s), 1243 (s), 1164 (s), 1036 (s), 957
        (s), 851 (s), 801 (m), 774 (vs), 450 (s)
EI-MS (70eV): 528 (M$^{+\cdot}$, 19), 437 (M$^+$-Tr, 2), 321 (M$^+$-TVC, 2), 264 (TVC-Si(Me)$_2$$^+$; 26),
          207 (TVC$^+$, 100), 129 (C$_6$H$_6$V$^+$, 41), 116 (CpV$^+$, 29)
C$_{28}$H$_{34}$Si$_2$V$_2$ (528.34):   Calcd.:   C, 63.65;   H, 6.44
                      Found: C, 63.48;   H, 6.32

Synthesis of Diphenyl([5]trovacenyl)silanol (67[•])
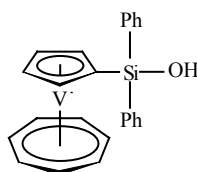
To a solution of TVC (860mg, 4.15mmol) in Et_2O (150ml), n-BuLi (2.6ml, 4.16mmol, 1.6M/hexane) was added and stirred at r.t. overnight to give a red-brown solution. Then Ph_2SiCl_2 (0.22ml, 1.0mmol) was added dropwise at 0°C in 1h, then the mixture was warmed to r.t. and another equiv. amount Ph_2SiCl_2 (0.22ml, 1.0mmol) was added dropwise again. After stirring overnight, the mixture was filtered through Celite and freed of all the volatiles. Isolation by chromatography (Al_2O_3, 2×30cm, eluted by $EtOH/Et_2O$) gave **67[•]** (third band) as purple solid (220mg, yield, 18%). The single crystal suitable for X-ray diffraction was generated from saturated ethanol solution.

IR (KBr): 3524 (m), 3043 (w), 2972 (w), 1425 (m), 1394 (s), 1263 (s), 1172 (s), 1113 (vs), 1029 (s), 957 (s), 899 (s), 854 (vs), 812 (s), 782 (s), 743 (s), 704 (vs), 644 (m), 531 (s), 503 (s), 435 (m), 420 (m).
EI-MS (70eV): 405 ($M^{+\cdot}$, 48)
$C_{24}H_{22}OSiV$ (594.33):   Calcd.:   C, 71.12;   H, 5.43
                       Found: C, 69.13   H, 5.78

Synthesis of Diphenyldi([5]trovacenyl)germanium (62[••])
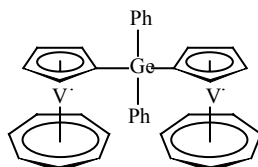
To a solution of TVC (680mg, 3.29mmol) in Et_2O (100ml), n-BuLi (2.2ml/1.6M, 3.52mmol) was added and stirred at r.t overnight to form a red-brown solution. Then Ph_2GeCl_2 (0.18ml, 0.86mmol) was added stepwise at 0°C. The mixture was stirred for 1h, then warmed to r.t. and stirred for 1h. Another equiv. molecule Ph_2GeCl_2 (0.17ml, 0.85mmol) was added and stirred overnight to give a violet suspension. After filtration through Celite, all the volatiles were removed in vacuo. The residue was chromatographed (3×30cm, Al_2O_3, benzene) to give **62[••]** (120mg, yield 20%) as pale purple solid.

IR (KBr): 3039 (m), 2959 (w), 1728 (m), 1428 (s), 1263 (w), 1155 (s), 1089 (s), 1033 (s), 957 (m), 851 (m), 781 (vs), 735 (s), 699 (s), 677 (s), 632 (m), 435 (s), 408 (m).
EI-MS (70eV): 640 ($M^{+\cdot}+1$, 100), 639 ($M^{+\cdot}$, 72)
$C_{36}H_{32}GeV_2$ (638.83):   Calcd.:   C, 67.68;   H, 5.01
                       Found: C; 66.13;   H, 4.66

Synthesis of Dimethyldi([5]trovacenyl)tin (63··)
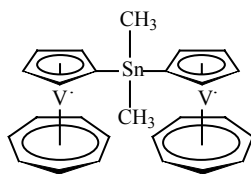
The solution of TVC (470mg, 2.27mmol) in Et$_2$O (100ml) was added n-BuLi (1.6ml/1.6M, 2.56mmol) and stirred at r.t. overnight to result in a red-brown solution. Me$_2$SnCl$_2$ (140mg, 0.64mmol) was added and the mixture was stirred at r.t. overnight to give a red-violet suspension. After filtration, the solvent was removed in vacuo. The residue was chromatographed (3×30cm, Al$_2$O$_3$), Et$_2$O/toluene) to give **63··** as dark violet powder (80mg, yield, 13%).

IR (KBr): 2963 (s), 1732 (w), 1417 (w), 1261 (vs), 1096 (s), 1022 (s), 956 (m), 849 (w), 802 (vs), 704 (w), 432 (m).

EI-MS (70eV): 563 (M$^{+\cdot}$+2, 14), 561 (M$^{+\cdot}$, 5), 207 (TVC$^+$, 100)

C$_{26}$H$_{28}$SnV$_2$ (560.83):   Calcd.:   C, 55.68;   H, 4.99
                             Found: C, 56.01;   H, 5.16

Synthesis of Diphenyldi([5]trovacenyl)tin (64··)
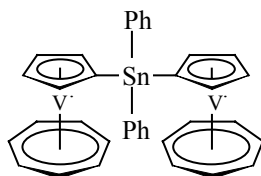
n-BuLi (2.3ml/1.6M, 3.68mmol) was added to a solution of TVC (742mg, 3.58mmol) in Et$_2$O (100ml) and the mixture was stirred at r.t. overnight to result in a red-brown solution. Ph$_2$SnCl$_2$ (615mg, 1.79mmol) was added in 2h, and then the mixture was stirred at r.t. overnight to give a purple suspension, filtered and the solvent was removed. The product **64··** was isolated by chromatography (2×20cm, Al$_2$O$_3$, toluene/Et$_2$O) as purple solid (260mg, yield, 21%).

IR (KBr): 3039 (w), 3004 (w), 1644 (m), 1426 (s), 1387 (m), 1190 (s), 1142 (m), 1025 (s), 957 (s), 849 (m), 805 (m), 781 (vs), 726 (s), 699 (s), 447 (s), 431 (s).

EI-MS (70eV): 687 (M$^{+\cdot}$+2, 9), 685(M$^{+\cdot}$, 6), 207 (TVC$^+$, 67), 129 (C$_6$H$_6$V$^+$, 41), 116 (CpV$^+$, 29), 91 (C$_7$H$_7^+$, 100)

C$_{36}$H$_{32}$SnV$_2$ (684.93):   Calcd.:   C, 63.12;   H, 4.67
                             Found: C, 61.88;   H, 4.88

Synthesis of Diphenyldi([5]trovacenyl)lead (65··)
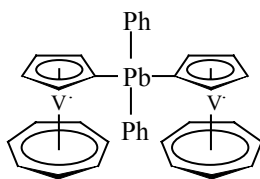
To a solution of TVC (775mg, 3.74mmol) in Et_2O (100ml), n-BuLi (2.4ml/1.6M, 3.84mmol) was added and stirred at r.t. overnight. Ph_2PbCl_2 (410mg, 0.95mmol) was added stepwise at 0°C with vigorously stirring. After stirring at r.t. overnight, the red-violet suspension was filtered and evaporated in vacuo. The residue was chromatographed (3×30cm, Al_2O_3, toluene/Et_2O) to give **65··** as pale purple solid (286mg, yield, 20%).

IR (KBr): 3039 (w), 2963 (s), 1568 (w), 1473 (w), 1426 (m), 1384 (w), 1261 (vs), 1097 (m), 1020 (s), 956 (s), 848 (m), 799 (vs), 722 (s), 694 (s)614 (w), 442 (w), 429 (s).

EI-MS (70eV): 767 ($M^{+·}$-6, 80), 491 (TVC-Pb-Ph$^+$, 4), 412 (TVC-Pb$^+$, 44), 283 (PhPb$^+$, 36), 207 (TVC$^+$, 37)

$C_{26}H_{28}PbV_2$ (773.43):   Calcd.:   C, 55.90;   H, 4.14
                              Found: C, 55.34;   H, 4.07

Synthesis of the salt $[Li(THF)_3]^+[(TVC)_3SnCl_2]^-$ (66···)
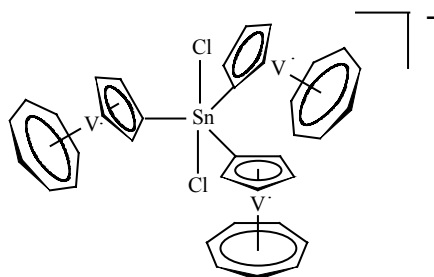
To a white suspension of $SnCl_2$ (260mg, 1.39mmol) in toluene (10ml), a solution of lithiotrovacene in Et_2O (from TVC 270mg, 1.3mmol and n-BuLi 0.9ml, 1.44mmol, 1.6M/hexane) was added dropwise with vigorously stirring at r.t. During the course, much slightly yellow precipitate was formed. After stirring overnight, the solution was decanted carefully, and the yellow precipitate was washed with Et_2O till colorless, then dried in vacuo. The solid was extracted by THF/Toluene (3:1) and the extract was filtered through Celite to give a slightly yellow solution. The extract was stored in a refrigerator (8°C) for two months to afford some red-violet needle-like crystals which were suitable for X-ray diffraction analysis. According to the structural analysis, the molecule unit is comprised of $(THF)_3Li^+(TVC)_3SnCl_2^-$ and ½ toluene (**66···**).

EI-MS (70eV): 772 ($[(TVC)_3SnCl]^+$, 22), 770 ($[(TVC)_3SnCl]^+$-2, 100), 326 (TVC-Sn$^+$, 5), 207 (TVC$^+$, 23)

Synthesis of [5]Trovacenyl-tetramethylcyclopentandiene (70˙)
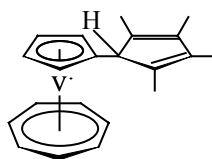
At 0°C, 2,3,4,5-tetramethylcyclopenten-1-one (0.49ml, 3.3mmol) was added dropwise to the stirred solution of lithiotrovacene (from TVC, 684mg, 3.3mmol; n-BuLi, 2.2ml, 3.52mmol) in ether (150ml) over 0.5h. The mixture was stirred at r.t. overnight, then H_2O (30ml) was carefully added to the red-violet solution. The violet-green ether solution was dried over $MgSO_4$, filtered and evaporated. The violet residue was washed by small amount PE (2×10ml) to give a dark green-violet suspension with much violet solid which had been identified to be unreacted TVC. Filtration and evaporation gave green solid. After sublimed at 50°C in high vacuum to get rid of a small amount of TVC, the analytically pure **70˙** was obtained by chromatography (2.5×25cm, Al_2O_3, PE) as green powder (430mg, yield 40%).

IR (KBr): 3094-2865 (w), 1759 (w), 1642 (w), 1438 (m), 1366 (w), 1261 (vs), 1095 (s), 1041 (w), 1020 (w), 957 (m), 874 (m), 851 (m), 790 (vs)702 (m),447 (m), 434 (s).
EI-MS (70eV): 327 ($M^{+ \cdot}$, 12), 207 (TVC^+, 10)
$C_{21}H_{24}V$ (327.15):   Calcd.:   C, 77.09;   H, 7.34
                              Found: C, 76.22;   H, 7.44

Synthesis of Di([5]trovacenyl-tetramethyl-η^5-cyclopentandienyl)iron (71˙˙)
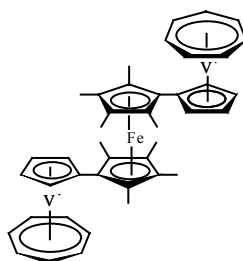
[5]Trovacenyl-tetramethylcyclopentandiene **(70˙)** (700mg, 2.14mmol) was dissolved in 30ml ether, and n-BuLi (1.4ml/1.6M, 2.24mmol) was added to dropwise. After stirring overnight at r.t., the precipitation of light green solid began to occur. At 0°C, the suspension of $Fe_2Cl_4(THF)_3$ (560mg, 1.22mmol) in Et_2O (20ml) was added dropwise with vigorously stirring. The mixture changed into yellow-green in color immediately, then was stirred at ambient temperature overnight. At 0°C, the mixture was filtered through Celite. The analytically pure **71˙** was obtained by chromatography (2×25ml, Al_2O_3, THF) at 0°C as light yellow-brown solid (80mg, yield, 10%). It was sensitive to temperature and decomposed slowly at r.t.

EI-MS (70eV): 708 ($M^{+ \cdot}$, 5), 325 ($TVC-Cp^{*+}$, 100)
$C_{42}H_{46}FeV_2$ (708.15):   Calcd.:   C, 71.23;   H, 6.50
                              Found: C, 70.98;   H, 6.36

Synthesis of [5]trovacenyl-1-(anti, syn)-7-hydroxybicyclo[2.2.1]hept-2-ene-7yl (72$^\cdot$)
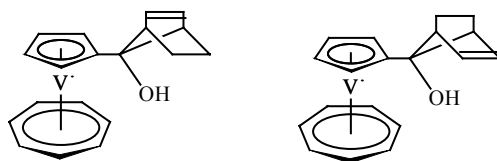
n-BuLi (2ml, 3mmol, 1.55M/Hexane) was added dropwise to the solution of TVC (620mg, 3mmol) in Et_2O (100ml) and the mixture was stirred at r.t. overnight to give a red-brown solution. After evaporation all the volatiles in vacuo, the red-brown residue was dissolved into 100ml DME. Norbornenone (0.33ml, 3mmol) was added dropwise at -78°C and stirred for 1h, then the mixture was warmed to 0°C and stirred overnight. Diluted by Et_2O (50ml) and H_2O (30ml), the separated organic layer was further washed by H_2O (3×30ml), dried over $MgSO_4$. After removal of all the solvents, the residues was chromatographed (5×40cm, Al_2O_3) to give the isomeric alcohol **72$^\cdot$** as violet solid (250mg, yield:, 27%). The anti- or syn- isomeric alcohol could not be isolated by chromatography on silica or Al_2O_3.

IR (KBr): 3451(m), 3045 (w), 2961 (w), 1429 (m), 1266 (s), 1108 (s), 1015 (m), 1004 (w), 802 (m), 784 (vs), 472 (s).

EI-MS (70eV): 315 (M$^{+\cdot}$, 74), 234 (M$^+$-C_6H_9, 28), 207 (TVC$^+$, 30)
$C_{19}H_{20}OV$ (315.13):   Calcd.;   C; 72.41;   H, 6.35
                              Found: C, 70.36;   H, 6.03

Synthesis of [5]trovacenyl-1-(anti, syn)-7-chloro-bicyclo[2.2.1]hept-2-ene-7yl (73$^\cdot$)
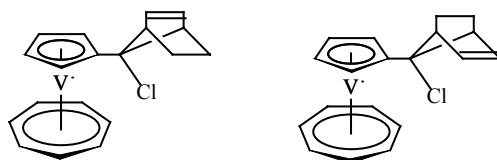
ClP(O)(OEt)$_2$ (0.66ml, 1.6mmol) was added to the solution of **72$^\cdot$** in DME (80ml) at r.t., and the mixture was heated at 50°C with stirring overnight. After removal of all the volatiles in vacuo, the residue was extracted by PE (50ml) and Et_2O (20ml), and filtered through Celite. In order to avoid the possibility of hydrolysis, the extract was evaporated to afford a violet slurry which was not further purified and used directly for further step. The result of mass spectra demonstrated the formation of **73$^\cdot$**. Crude product: 250 mg.

EI-MS (70eV): m/z 333 (M$^{+\cdot}$, 72), 207 (TVC$^+$, 100)

Synthesis of Tri([5]trovacenyl)phosphane (42···)
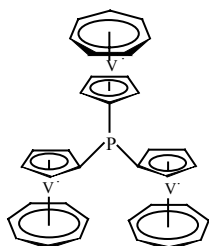
At -40°C, to a solution of lithiotrovacene (from TVC, 807mg, 3.9mmol; n-BuLi, 2.7ml/1.6M, 4.32mmol) in 150ml ether, PCl$_3$ (0.07ml, 0.7mmol) was added dropwise over 0.5h with vigorously stirring. Then the mixture was warmed slowly to r.t. and stirred for further 2h. A large amount of pale green precipitate was formed, filtered and washed by PE, Et$_2$O and H$_2$O, respectively; then dried in vacuo. Recrystallization (THF/PE) gave **42···** (464mg) as pale green powder, yield, 47%.This compound has a very poor solubility in benzene and toluene, therefore it can not be purified by chromatography.

EI-MS (70eV): 649 (M$^{+\cdot}$, 21), 444 (M$^+$-TVC, 100), 237 (TVC-P$^+$, 91), 207 (TVC$^+$, 17)

C$_{36}$H$_{33}$PV$_3$ (649.15):   Calcd.:   C, 66.60;   H, 5.08

                            Found: C, 57.12;   H, 5.07

Synthesis of Tri([5]trovacenyl)arsane (47···)
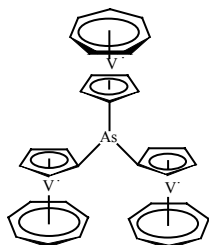
n-BuLi (2.4ml /1.6M, 3.84mmol) was added to the solution of TVC (728mg, 3.52mmol) in Et$_2$O (150ml) and stirred at r.t. overnight. At -40°C, AsCl$_3$ (0.05ml, 0.6mmol) in 0.2 ml Et$_2$O was added dropwise over 0.5h. Some pale red-violet precipitate was formed, then the suspension were allowed warm to r.t. and stirred for 2h to form plenty of pale green precipitate. Filtered, washed by PE, benzene, H$_2$O, respectively; and dried in vacuo to result in **47···** as dark red-violet powder (70mg). Yield: 9%. Due to its poor solubility in common organic solvent, such as THF, toluene, CH$_3$CN, DMSO and DME etc., the results of elemental analysis were not satisfactory. Furthermore, the pale green precipitate was identified to be (TVC)$_2$AsCl.

EI-MS (70eV): 693 (M$^{+\cdot}$, 100), 487(M$^+$-VC 34), 207(TVC$^+$ 37)

C$_{36}$H$_{33}$AsV$_3$ (693.10):   Calcd.:   C, 62.38;   H, 4.76

                              Found: C, 53.86;   H, 4.74

Synthesis of Tri([5]trovacenyl)stibane (48···)
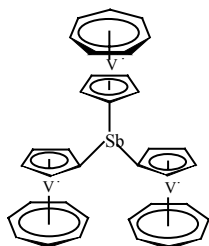
To the solution of TVC (807mg, 3.9mmol) in Et₂O (150ml), n-BuLi (2.7ml, 4.32mmol, 1.6M/hexane) was added and the mixture was stirred at r.t. overnight to give a red brown solution. At -40°C, SbCl₃ (140mg, 0.6mmol) was added to the solution stepwise and the mixture was stirred for 0.5h, then warmed slowly to r.t. and stirred for further 3h to yield a dark violet-red precipitate. The suspension was concentrated and PE was added. After filtration, the solid was washed by PE, Et₂O, benzene, H₂O, THF and DME, respectively, and dried in vacuo to give **48···** as dark violet-red powder (80mg). Yield: 8%. **48···** has a very poor solubility in common organic solvents and it is very difficult to obtain analytically pure sample.

EI-MS (70eV): 740 (M$^{+\cdot}$, 11), 739 (M$^+$-1, 8), 441 (M$^+$-C₅H₅V, 4), 207 (TVC$^+$ 20)
C₃₆H₃₃SbV₃ (739.93): Calcd: C, 58.43; H, 4.46
                                       Found: C, 51.05, H, 4.17

Synthesis of Tri([5]trovacenylthio)antimony (29···)
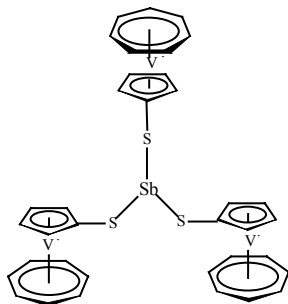
To a solution of TVC-SLi (810mg, 3.27mmol) in DME (40ml) at -40°C, SbCl₃ (224mg, 0.98mmol) was added stepwise. The mixture was stirred for 1h, then warmed slowly to r.t. and stirred overnight. The solvent was evaporated under reduced pressure, the residue was extracted by benzene and filtered through a short Al₂O₃ (3×5cm) column, the second green band was collected and the solvent was removed in vacuo to afford **29···** as green powder (120mg) Yield: 18%.

IR (KBr): 3095(w), 3037(w), 2953(w), 1759(m), 1644(m), 1422(s), 1165(s), 1096(m),
        1056(m), 1027(s), 957(s), 886(s), 852(s), 779(vs), 678(m), 477(m), 453(w), 431(s)
EI-MS (70eV): 239 (TVC-S$^+$, 100), 207(TVC$^+$, 4),
C₃₆H₃₃S₃SbV₃ (836.11) Cald: C, 51.71, H, 3.95
                                       Found: C, 51.72, H, 4.29

Synthesis of Tri([5]trovacenylthio)bismuth (30''')
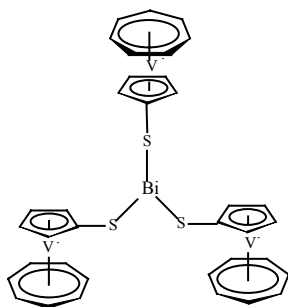
At -40°C, BiCl$_3$ (315mg, 0.94mmol) was added stepwise to a solution of TVC-SLi (840mg, 3.42mmol) in DME (50ml). After stirring for 1h, the mixture was warmed slowly to r.t. and stirred overnight. The mixture changed from red-violet into dark red-brown in color with formation of a large amount of pale red-brown precipitate. Filtration, washed by Et$_2$O and dried in vacuo gave a red-brown powder (600mg) which has a partial solubility in hot toluene, DME and THF. The filtrate was concentrated to ~10 ml and stored at -30°C to form a dark red-brown solid which was purified by extraction with hot toluene and identified by mass spectroscopy to be the same component as the above described precipitate. The moderately pure **30'''** was obtained by recrystallization from hot toluene/PE for several times.

EI-MS (70eV): 505 (?, 18), 329 (?, 14), 239 (TVC-S$^+$, 100), 207 (TVC$^+$, 4),

C$_{36}$H$_{33}$S$_3$BiV$_3$ (923.34)   Cald: C, 46.83,   H, 3.57

                                    Found: C, 42.81,   H, 3.35

Synthesis of [5]Trovacenylselenol (76$^•$)
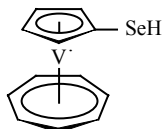
To a solution of Di([5]trovacenyl)diselenium (300mg, 0.53mmol) in DME (30ml), LiAlH$_4$ (200mg, 5.3mmol) was added and the suspension was refluxed for 1h, then the mixture was stirred at r.t. overnight. The suspension turned from green to pale red in color. HCl (1ml, 15%) was added dropwise to the suspension. After addition H$_2$O (2ml), Et$_2$O (30ml) was added to extract the product, the extraction was dried over MgSO$_4$, filtered through Celite. After removal all the solvents, the violet product **76$^•$** was isolated by chromatography (Al$_2$O$_3$, 1×10cm) as dark violet oil. Yield: 30mg, 10%.

EI-MS (70eV): 287(M$^{+•}$+1, 33), 286 (M$^{+•}$, 8), 207 (TVC$^+$, 100)

C$_{12}$H$_{12}$SeV (239.12):   Cald.:   C, 50.39,   H, 4.20

                                    Found: C, 53.44,   H, 5.88

6.5. Attempts

Synthesis of Trimethylsilyl([5]trovacenyl)thioether (75·)
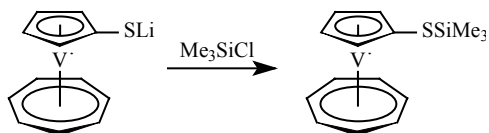
To a solution of TVC-SLi (170mg, 0.7mmol) in DME (20ml), Me₃SiCl (0.15ml, 1.2mmol) was added stepwise by syringe at -50°C, then the mixture was warmed slowly to r.t. with vigorously stirring overnight. All the volatiles were removed under reduced pressure, the residue was extracted by toluene and filtered through Celite, then the solvent was evaporated in vacuo. The red-violet residue **75·** was characterized by mass spectroscopy (EI, 70eV).

EI-MS (70eV): 311 ($M^{+\cdot}$, 9), 239 (TVC-S$^+$, 30), 207 (TVC$^+$;100), 161 ($C_6H_6VS^+$, 12), 129 ($C_6H_6V^+$, 79), 116 ($C_5H_5V^+$, 42), 91 ($C_7H_7^+$, 22), 51 (V^+, 45)

Synthesis of Di([5]trovacenylthio)tin (77··)
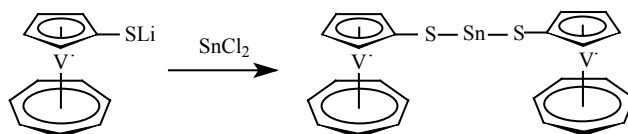
At -40°C, SnCl₂ (152mg, 0.8mmol) was added to the solution of TVC-SLi (417mg, 1.7mmol) in 40ml DME with vigorously stirring. After stirring at r.t. overnight, the solvent was evaporated in vacuo. The reside was washed by Et₂O, toluene/DME and filtered through Celite. Removal of the solvent, the violet solid **77··** was characterized by mass spectroscopy (EI, 70eV).

EI-MS (70eV): 595 ($M^{+\cdot}$, 1), 444 (?, 10), 357 (TVC-SSn$^+$, 13), 303 (?, 13), 239 (TVC-S$^+$, 100), 207 (TVC$^+$, 28), 161 ($C_6H_6VS^+$, 30), 129 ($C_6H_6V^+$, 4), 116 ($C_5H_5V^+$, 25), 91 ($C_7H_7^+$, 37), 51 (V^+, 10)

Reaction of lithium trovacenylthiolate with lead chloride
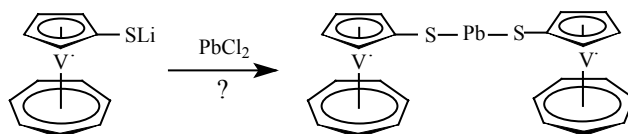
At -40°C, PbCl₂ (250mg, 0.9mmol) was added to a solution of TVC-SLi (447mg, 1.82mmol) in 30ml DME. After stirring for half hour, the suspension was warmed slowly to r.t., and

stirred overnight to afford plenty of red-brown precipitate. The suspension was decanted carefully, the red-brown solid was washed by PE, toluene, DME and benzene till colorless, and dried in vacuo (273 mg). The red-brown solid can not dissolve in common organic solvents, such as, Et_2O, benzene, toluene, CH_3CN etc., with the exception of a very poor solubility in THF. It was characterized by EI-MS and elemental analysis, but the results can not identify the formation of the expected product.

EI-MS (70eV): 445 (TVC-S-Pb$^+$, 3), 238 (TVC-S$^+$, 36), 207 (TVC$^+$, 76), 161 ($C_6H_6VS^+$, 9), 147 (?, 21), 129 ($C_6H_6V^+$, 19), 116 ($C_5H_5V^+$, 52), 91 ($C_7H_7^+$, 32), 51 (V$^+$, 32)

$C_{24}H_{22}S_2PbV_2$ (683.43) Cald: C, 42.18, H, 3.22
                              Found: C, 23.30, H, 2.56

Reaction of lithium trovacenylthiolate with zinc chloride
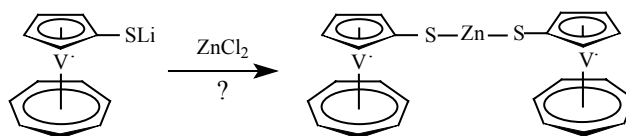
$ZnCl_2$ (110mg, 0.8mmol) was added to a solution of TVC-SLi (470mg, 1.92mmol) in 30ml DME at -40°C. After stirring at r.t. overnight, the solvent was removed under reduced pressure. The residue was washed by PE till colorless to give some brown solid. It was characterized by EI-MS and elemental analysis. The result can not prove the formation of the desired product.

EI-MS (70eV): 295 (?, 8), 238 (TVC-S$^+$, 10), 207 (TVC$^+$, 8), 161 ($C_6H_6VS^+$, 2), 147 (?, 2), 129 ($C_6H_6V^+$, 1), 116 ($C_5H_5V^+$, 6), 91 ($C_7H_7^+$, 7), 51 (V$^+$, 3), 28(100)

$C_{24}H_{22}S_2ZnV_2$ (541.62) Cald: C, 53.20, H, 4.06
                              Found: C, 19.39, H, 3.34

Reaction of lithium trovacenylthiolate with cobalt chloride
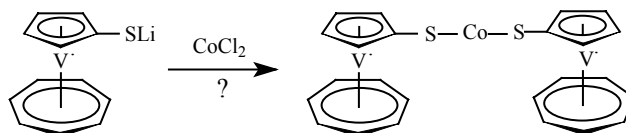
$CoCl_2$ (130mg, 1.0mmol) was added to a solution of TVC-SLi (470mg, 1.92mmol) in DME at -40°C. The mixture changed into yellow-brown at once. After stirring at r.t. overnight, the solvent was removed under reduced pressure. The residue was washed by PE till colorless to result in pale black solid. It was characterized by EI-MS.

EI-MS (70eV): 916 (6), 841 (5), 768 (11), 694 (21), 619 (13), 445 (90), 412 (20), 282 (51), 265 (87), 207 (100), 116 (42)

Reaction of Di([5]trovacenyl)chloroarsane with lithium
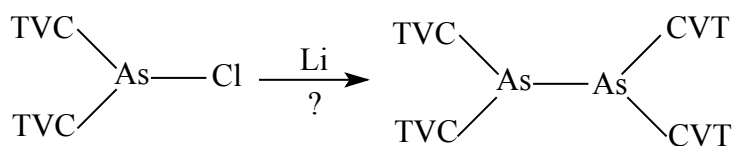
At 0°C, a suspension of Li powder (30mg, 4.3mmol) in Et$_2$O (30 ml) was added to a solution of (TVC)$_2$AsCl (252mg, 0.48mmol) in 50ml Et$_2$O/THF(3:2). After stirring at r.t. overnight, the dark black suspension was filtered through Celite. All the solvents were removed in vacuo, and the residue was washed by Et$_2$O (2×10ml), then extracted by benzene. Isolation by chromatography (1×10cm, Al$_2$O$_3$) gave violet solid (40mg).

EI-MS (70eV): 618 (?, 87), 544 (?, 29), 453 (?,15), 207 (TVC$^+$, 100), 129 (C$_6$H$_6$V$^+$, 32), 116 (C$_5$H$_5$V$^+$, 19), 91 (C$_7$H$_7$V$^+$, 1), 51 (V$^+$, 32)

Reaction of Lithiotrovacene with dichloromethane
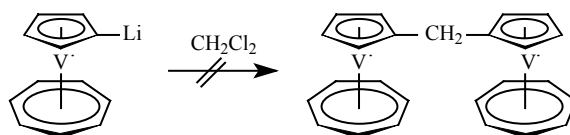
At -78°C, CH$_2$Cl$_2$ (0.07ml, 1.09mmol) was added dropwise to a solution of lithiotrovacene (from TVC 418mg, 2.02 mmol and n-BuLi 1.3ml, 1.6M/hexane, 2.08mmol) and stirred for 2h. A further 1h at 0°C followed, then the solution was warmed to r.t. and stirred overnight. Much pale white precipitate was formed. After filtration through Celite, all the volatiles were evaporated in vacuo to give a red-violet solid which was characterized by mass spectroscopy (EI, 70eV). After isolation by chromatography (Al$_2$O$_3$), only TVC was obtained.

EI-MS (70eV): 438 (?, 7), 207 (TVC$^+$, 100), 129 (C$_6$H$_6$V$^+$, 38), 116 (C$_5$H$_5$V$^+$, H$_5$V$^+$, 59), 90 (C$_7$H$_7$V$^+$, 12), 51 (V$^+$, 84)

Reaction of [5]trovacenylthiol with Bismuthtri[di(trimethylsilyl)ammid)]
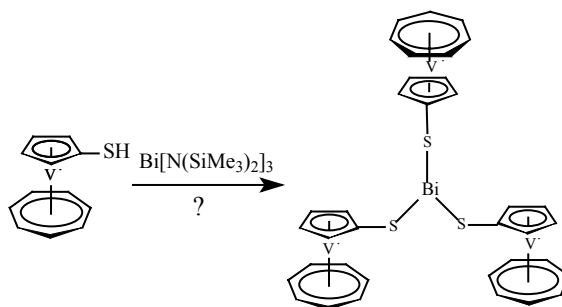
At -78°C, the white solution of Bi[N(SiMe$_3$)$_2$]$_3$ (350mg, 0.51mmol) in Et$_2$O (20ml) was added dropwise to a solution of [5]trovacenylthiol (695mg, 2.84mmol) in Et$_2$O. The mixture

changed into yellow-brown in color. After stirring for 2h, all the volatiles were removed in vacuo. The residue was washed by PE till colorless to result in red-brown solid (500mg) which was characterized by mass spectroscopy (EI, 70eV) and gave the similar results as in the reaction of TVC-SLi with $BiCl_3$.

EI-MS (70eV): 238 (TVC-S$^+$, 43), 207 (TVC$^+$,100)

Reaction of Diiodoferrocene with [5]trovacenylzincchloride
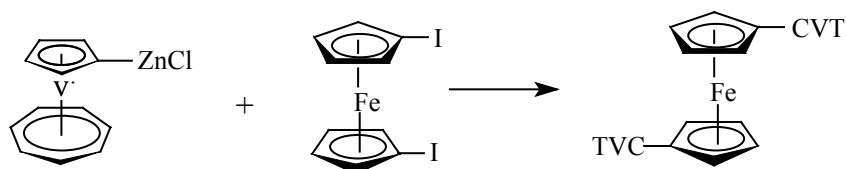
To a solution of TVC (214mg, 1mmol) in Et_2O (50ml), n-BuLi (1.8ml, 3mmol, 1.68M/hexane) was added and stirred overnight at r.t. to give a red-brown solution. The solution of $ZnCl_2$ (141mg, 1mmol) in THF (10ml) was added stepwise with formation of a precipitate which was disappeared later. Diiodoferrocene (81mg, 0.2mmol) and Pd(dppf)$_2Cl_2$ (8mg, 1%) were dissolved in THF (10ml), and added to the TVC-ZnCl mixture over 0.5h at 0°C. After refluxing for 1h, the solvent was evaporated in vacuo, and the reside was dissolved in 30ml THF and refluxed for 1h. All the volatiles were removed, the residue was characterized by EI-MS (70eV). The molecular ion peak of the product was not observed.

EI-MS (70eV): 438 ((C$_5$H$_4$I)$_2$Fe$^+$, 9), 207 (TVC$^+$, 100)

Attempt to synthesize [5]trovacenol via [5]Trovacenylboronic acid
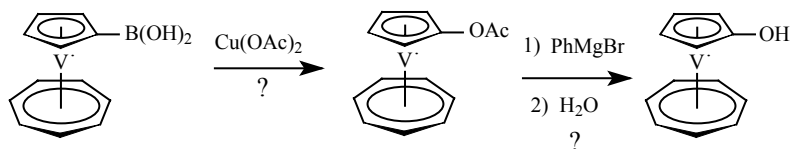
To a hot solution of TVC-B(OH)$_2$ (1g, 3.98mmol) in $EtOH/H_2O$ (80ml, 50%), the solution of Cu(OAc)$_2$ (1.7g, 0.9mmol) in $EtOH/H_2O$ (20ml, 50%) was added dropwise. The mixture was changed from red-violet to brown in color immediately. After heating with stirring for 10 min, the mixture was cooled down to r.t and stirred overnight to form a suspension. Filtered and washed by Et_2O, PE and water gave some yellow-brown solid. The filtrate were removed all the ethanol, and extracted by Et_2O to afford red-brown solution which were dried by $MgSO_4$, removed all the solvent and recrystallized by Et_2O/PE to result in small mount of yellow-brown solid. The combined yellow-brown solid (200mg) which had not been further characterized were dissolved in Et_2O (10ml), then PhMgBr (bromobenzene 0.16ml, Mg 39mg, 1.6mmol) was added and stirred for 2h. After hydrolysis (H_2O), extracted (Et_2O) and dried ($MgSO_4$), all the solvent were removed under reduced pressure to a give small amount of a red-brown solid which was characterized by mass spectroscopy (EI).

EI-MS (70eV): 265 (3%), 245 (12%), 233 (6%), 223 (4%), 207 (TVC$^+$, 69%)

7. References

1]   H. Taube, *Angew. Chem.*, 1984, 96, 315.

[2]   R. A. Marcus; *Angew. Chem.*, 1993, 105, 1161.

[3]   (a) H. Taube; H. Myers; R. L. Rich, *J. Am. Chem. Soc.*; 1953, 75, 4118.
        (b) H. Taube; H. Myers; *J. Am. Chem. Soc.*, 1954, 76, 2103.

[4]   (a) H. Taube; *Electron-Transfer Reactions of Complex Ions in Solution*. Academic Press, New York, 1970.
        (b) T. J. Meyer; H. Taube; *Comprehensive Coordination Chemistry*, G. Willkinson; R. Guillard; J. A. Mcafferty; eds., Pergamon Press, Oxford, 1987, vol. 1, chapt. 7.2.

[5]   (a) R. A. Marcus, *Annu. Rev. Phys. Chem.* 1964, 15, 155.
        (b) R. A. Marcus, *J. Chem. Phys.* 1956, 24, 966 and 979.
        (c) R. A. Marcus, *J. Chem. Phys.* 1957, 26, 867 and 872, 1965, 43, 679.
        (d) R. A. Marcus, *Trans. N. Y. Acad. Sci.* 1957, 19, 423.

[6]   (a) C. Elschenbroich; O. Schiemann; O. Burghaus; K. Harms; *J. Am. Chem. Soc.*; 1997, 119, 7452.
        (b) A. M. Napper, I. Read, D. H. Waldeck, *J. Am. Chem. Soc.*, 2000, 122, 5220.
        (c) A. J. Myles; N. R. Branda, *J. Am. Chem. Soc.* 2001, 123, 177.

[7]   (a) N. Sutin, *Acc. Chem. Res.* 1982, 15, 275.
        (b) N. Sutin, *Inorganic Biochemistry* G. L. Eichhorn, ed., Vol 2, Elsevier, New York, 1973, 611.
        (c) A. Haim; N. Sutin, *J. Am. Chem. Soc.*, 1966, 88, 434 and 5343, 1965, 4210.
        (d) A. Haim, *Acc. Chem. Res.,* 1975, 8, 264, *J. Am. Chem. Soc.*, 1966, 88, 2324; 1963, 85, 1016, *Inorg. Chem.*, 1970, 9, 426; 1968, 7, 1475; 1966, 5, 2081.

[8]   C. Creutz; H. Tabue, *J. Am. Chem. Soc.*, 1969, 91, 3988.

[9]   M. B. Robin; P. Day, *Adv. Inorg. Chem. Radiochem.* 1967, 10, 247.

[10]   (a) C. Creutz; H. Taube, *J. Am. Chem. Soc.* 1973, 95, 1086.
        (b) C. Creutz, In *Prog. Inorg. Chem.*, S. J. Lippard, ed. Wiley, New York, 1983, 30, 1.
        (c) P. C. Ford; D. F. P. Rudd; R. Gaunder; H. Taube, J. *Am. Chem. Soc.*, 1968, 90, 1187.
        (d) P. C. Ford, *Coord. Chem. Rev.*, 1970, 5, 75.
        (e) H. E Toma; J. M. Malin, *Inorg. Chem.* 1973, 12, 2080.
        (f) *Mixed-valency Systems: Application in Chemistry, Physics and Biology*. K. Prassides, ed. Kluwer, Dordrecht, 1991.

[11]   J.-P. Launay, In *The Time Domain in Surface and Structural Dynamics*. G. J. Long, F. Grandjean, eds., Kluwer, Amsterdam, 1988, Chapter 13.

[12]   C. Elschenbroich; O. Schiemann; O. Burghaus; K. Harms; J. Pebler, *Organometallics*, 1999, 18, 3273.

[13]   T. T. Chin; S. R. Lovelace; W. E. Geiger; C. M. Davis; R. N. Grimes, *J. Am. Chem. Soc.*, 1994, 116, 9359.

[14]   (a) J. E. Wertz; J. B. Bolton, *Electron Spin Resonance, Elementary Theory and Practical Applications*, New York, McGraw Hill, 1986.
        (b) F. E. Mabbs, D. Collison, *Electron Paramagnetic Resonance of d-Transition Metal Compounds*, Amsterdam, Elsevier, 1992.

[15]   F. G. Cloke; A. N. Dix; J. C. Green; E. A. Seddon. *Organometallics* 1983, 2, 1150.

[16]   F. E. Mabbs, *Chem. Soc. Rev.* 1993, 22, 312.

[17]   (a) D. Kivelson, *J. Chem. Phys.*, 1960, 33, 1094.
        (b) R. Wilson; D. Kivelson, *J. Chem. Phys.*, 1966, 44, 154, and reference therein.

[18]   (a) G. R. Luckhurst, *Mol. Phys.,* 1966, 10, 543.
        (b) S. H. Glharum; J. H. Marshall, *J. Chem. Phys.*, 1967, 47, 1374.

(c) A. Hudson; G. R. Luckhurst, *Chem. Rev.,* 1969, 69, 191.

(d) I. Bertini; G. Martini; C. Luchinat, *Handbook of Electron Spin Resonance*, Eds., Jr. C. P. Poole; H. A. Farach, AIP Press, New York, 1995.

[19] (a) R. Hoffman, *Acc. Chem. Res.*, 1971, 4, 1.

(b) H. Weihe; H. U. Güdel, *J. Am. Chem. Soc.* 1997, 119, 6539.

[20] (a) O. Kahn, *Molecular Magnetism*, Weinheim, VCH-Verlag, 1993.

(b) R. L. Carlin, *Magnetochemistry*, Berlin, Springer-Verlag, 1986.

[21] (a) M. P. Andrews; S: M. Mattar; G. A. Ozin, *J. Phys. Chem.* 1986, 90, 1037.

(b) M. Rettig; D. Stout; A. Klug; P. Farnham, *J. Am. Chem. Soc.*, 1970, 92, 5100.

[22] A. J. Bard; R. F. Faulkner, *Electrochemical Methods*. Wiley, New York, 1980.

[23] G. A. Mabbott, *J. Chem. Edu.*, 1983, 697.

[24] P. T. Kissinger; W. R. Heineman, *J. Chem. Edu.*, 1983, 702.

[25] (a) J. Heinze, *Angew. Chem.*, 1984, 96, 823; *Angew. Chem. Int. Ed. Engl.* 1984, 23, 831.

(b) J. F. Coetzee, *Recommended Methods for Purification of Solvents*. Pergamon; Oxford, 1982.

[26] (a) W. E. Geiger; In *Porg. Inorg. Chem.*, S. J. Lippard, ed., Wiley, New York, 1985, 33, 275.

(b) S. W. Feldberg, *Electroanalytical Chemistry* A. J. Bard ed., Dekker, New York, 1969, Vol3, pp199-296.

(c) *Electochemistry,* J. S. Mattson; H. B. Mark, Mac Donald, H. C. Dekker, New York, 1972.

[27] J. M. Manriquez; et. al. *J. Am. Chem. Soc.* 1995, 117, 6182.

[28] T. T. Chin; S. R. Lovelace; W. E. Geiger; C. M. Davis; R. N. Grimes *J. Am. Chem. Soc.* 1994, 116, 9359.

[29] W. H. Morrison; D. N. Hendrickson, *Inorg. Chem.* 1975, 14, 2331.

[30] J. A. Kramer; D. N. Hendrickson, *Inorg. Chem.* 1980, 19, 3330.

[31] T. Y. Dong; D. N. Hendrickson; C. G. Pierpoint; M. F. Moore, *J. Am. Chem. Soc.* 1986, 108, 963.

[32] (a) M-H. Delville; S. Rittinger; D. Astruc. *Chem. Commun.* 1992, 519.

(b) C. Elschenbroich, J. Heck, *Angew. Chem.,*1981, 93, 278, *Angew. Chem., Int. Ed. Engl.* 1981, 20, 267.

(c) C. Elschenbroich, J. Heck, *J. Am. Chem. Soc.* 1979, 101, 6773.

(d) C. Elschenbroich, J. Heck, *Angew. Chem.,*1977, 89, 497, *Angew. Chem., Int. Ed. Engl.* 1977, 16, 479.

[33] (a) J. M. Lehn, In *Supramolecular Chemistry*: *Concepts and Perspectives*; VCH: Weinheim, Germany, 1995.

(b) M. D. Ward, *Chem. Soc. Rev.* 1995, 121.

[34] S. Campagna; G. Denti; S. Serroni; A. Juris; M. Venturi; V. Riceunto; V. Balzani, *Chem. Eur. J.* 1995, 1, 211.

[35] (a) A. A. Dembeck; R. R. Burch; A. E. Feiring, *J. Am. Chem. Soc.* 1993, 115, 2087.

(b) M. Altmann; U. H. F. Bunz; *Angew. Chem., Int. Ed. Engl.* 1995, 34, 569.

[36] (a) V. Balzani; A. Juris; M. Venturi; S. Campagna and S. Serroni, *Chem. Rev.* 1996, 96, 759 and reference therein.

(b) F. Barigelletti; L. Flamigni, *Chem. Soc. Rev.* 2000, 29, 1.

(c) M. R. Wasielewski, *Chem. Rev.* 1992, 92, 365.

(d) P. F. H. Schwab; M. D. Levin; J. Michl, *Chem. Rev.* 1999, 99, 1863.

[37] (a) M. Herberhold; P. Leitner. *J. Organomet. Chem.* 1987, 336, 153, 1991.

(b) M. Herberhold; P. Leitner; *J. Organomet. Chem.* 1991, 411, 233.

(c) P. Zanello; G. Opromolla; M. Herberhold; H. D. Brendel; *J. Organomet. Chem.*

1994, 484, 67.

(d) A. G. Osborne; R. E. Hollands; A. Nagy; *J. Organomet. Chem.* 1989, 373, 229.

(e) P. Shu; K. Bechgaard; D. O. Cowan; *J. Org. Chem.* 41, 1976, 1849.

(f) D. C. O´Connor Salazar; D. O. Cowan; *J. Organomet. Chem.* 1991, 410, 227.

[38]   (a) M. A. S. Aquino; F. L. Lee; E. J. Gabe; C. Bensimon, J. E. Greeden, and R. J. Crutchley, *J. Am. Chem. Soc.* 1992, 114, 5130.

(b) M. L. Naklicki and R. J. Crutchly, *Inorg. Chim., Acta*, 1994, 225, 123.

(c) M. L. Naklicki and R. J. Crutchly, *J. Am. Chem. Soc.* 1994, 116, 6045.

[39]   N. S. Hush, *Coord. Chem. Rev.* 1985, 64, 135.

[40]   C. A. Stein; N. A. Lewis, G. Seitz and A. D. Baker, *Inorg. Chem.* 1983, 22, 1124.

[41]   C. A. Stein; N. A. Lewis and G. Seitz; *J. Am Chem. Soc.* 1982, 104, 2596.

[42]   *Organic Chemistry*; D. S. Kemp; F. Vellaccio; Worth Publishers, Inc.; USA; 1980; pp1239-1245.

[43]   J. J. Bishop; A. Davison; M. L. Katcher; *J. Organometal. Chem.* 27, (1971), 241.

[44]   G. R. Knox, P. L. Pauson; *J. Chem. Soc.* 1958, 692.

[45]   (a) Sato, Masaru; Sensui, Masaaki; *Chem. Lett.*, (11), 991, 1996.

(b) M. Herberhold; O. Nuyken; T. Pöhlmann; *J. Organometal. Chem.* 501 (1995), 13.

(c) M. Herberhold; O. Nuyken; T. Pöhlmann; *J. Organometal. Chem.* 405 (1991), 217.

[46]   O. N. Kataeva et al. *Eur. J. Inorg. Chem.* 2000, 225.

[47]   (a) Y. Nishibayashi; J. D. Singh; S. Uemura and S. Fukuzawa, *Tetrahedron Lett.* 1994, 35, 3115.

(b) Y. Nishibayashi; J. D. Singh; S. Uemura and S. Fukuzawa, *J. Org. Chem.* 1995, 60, 4114.

[48]   G. Mugesh; A. Panda; H. B. Singh; N. S. Punekar and R. J. Butcher, *Chem. Commmun.* 1998, 2227.

[49]   A. N. Nesmeyanov; E. G. Perevalova; O. A. Nesmeyanova; *Dokl. Akad. Nauk SSSR* 1958, 119, 288.

[50]   (a) M. D. Rausch, *J. Org. Chem.* 1961, 26, 3579.

(b) N. S. Nametkin; V. C. Tyurin; S. A. Sleptsova; A. M. Krapivin; A. Y. Sideridu; *Izv. Akad. Nauk SSSR Ser. Khim.* 1982, 4, 955.

[51]   (a) C. J. Groenenboom; H. J. Liejer; F. Jellink, *Recl. Trav. Chim. Pays. Bas* 1974, 93, 6.

(b) C. J. Groenenboom, H. J. Liejer; F. Jellink, *J. Organomet. Chem.* 1974, 69, 235.

[52]   A. J. Bard; A. H. Cowley; *J. Chem. Soc., Dalton Trans.* 1985, 1303.

[53]   J. B. Flanagan; S. Margel; A. J. Bard; F. C. Anson, *J. Am. Chem. Soc.* 1978, 100, 4248.

[54]   V. V. Demen´tev; F. Cervantes-Lee; L. Parkanyi; H. Sharma; K. H. Pannell; M. T. Nguyen; A. Diaz, *Organometallics* 1993, 12, 1983.

[55]   T. Vondrak; M. Sato, *J. Organomet. Chem.* 364, 207, 1989.

[56]   V. Weinmayr, *J. Am. Chem. Soc.* 1955, 3009.

[57]   A. Atwood; A.H. Cowley; et. al, *Inorg. Chem.* 1993, 32, 2972.

[58]   M. Bochmann; X-J. Song; M. B. Hursthouse and A. Karaulov, *J. Chem. Soc., Dalton Trans.* 1995, 1649.

[59]   C. Elschenbroich, et al. *Z. Naturforsch. B. Chemie.* 47(8), 1157, 1992.

[60]   (a) N. J. Long; J. Martin; A. J. P. White and D. J. Williams, *J. Chem. Soc., Dalton Trans.* 1997, 3083.

(b) R. Fierro, et al. *J. Organomet. Chem.* 472 (1994), 87.

[61]   M. Sato; H. Anano, *J. Organomet. Chem.* 1998, 555, 167.

[62]   A. G. Osborne; R. E. Hollands and A. G. Nagy, *J. Organomet. Chem.* 373, 1989, 229.

[63] (a) C. C. Moser; et al. *Nature* 1992, 355, 796.
(b) H. Pelletier; J. Kraut, *Science* 1992, 258, 1748.
(c) P. N. Beratan; et al. *Science* 1992, 258, 1740.
(d) H. Kurreck, *Angew. Chem. Int. Ed. Engl*. 1995, 34, 849.
(e) C. A. Hunter; R. K. Hyde, *Angew. Chem. Int. Ed. Engl* 1996, 35, 1936.

[64] A. J. Myles and N. R. Branda. *J. Am .Chem. Soc.* 2001, 123, 177.

[65] R. A. Marcus; M. Sutin, *Biochim. Biophys. Acta* 1985, 811, 266.

[66] E. Prasad and K. R. Gopidas, *J. Am. Chem. Soc*. 2000, 122, 3191.

[67] (a) A. N. Nesmeyanov; V. A. Sazonova; V. N. Drozd, *Tetrahedron Lett*. 17, 1959, 13.
(b) A. N. Nesmeyanov; V. A. Sazonova; V. N. Drozd, *Chem. Ber*. 93, 1960, 2717.
(c) A. N. Nesmeyanov; V. A. Sazonova; V. N. Drozd, *Dokl. Akad. Nauk. SSSR* 129 (1959) 1060.
(d) A. N. Nesmeyanov; V. A: Sazonova; V. N. Drozd, *Dokl. Chem. Proc. Acad. Sci. USSR* 129 (1959) 1113.
(e) A. N. Nesmeyanov; V. A: Sazonova; V. N. Drozd, L. A. Nikonova, *Dokl. Akad. Nauk. SSSR*, 133 (1960) 126.
(f) A. N. Nesmeyanov; V. A: Sazonova; V. N. Drozd, L. A. Nikonova, *Dokl. Chem. Proc. Acad. Sci. USSR* 133 (1960) 751.

[68] H. Plenio; C. Aberle, *Chem. Commun*. 1996, 2123.

[69] M. Herberhold; H-D. Brendel; A. Hofmann; B. Hofmann; W. Milius, *J. Organomet. Chem*. 556 (1998) 173.

[70] H. Plenio; A. Warnecke, *Organometallics* 1996, 15, 5066.

[71] M. Wolf, Dissertation, University of Marburg, 1998.

[72] (a) Masaru Kurosawa et al.; *Inorg. Chem.* 1999, 38, 5113.
(b) D. A. Durfey; R. U. Kirss; C. Frommen; W. Feighery; *Inorg. Chem.* 2000, 39, 3506.
(c) M. C. Gimeno; P. G. Jones; A. Laguna; C. Sarroca; *J. Organomet. Chem.* 579, 1999, 206.

[73] A. Behrendt, Dissertation, University of Marburg, 1995.

[74] B. Ibrahim, Diploma, University of Marburg, 1999.

[75] (a) A. Berman; E. S. Lzraeli; H. Levanon; B. Wang; J. L. Sessler, *J. Am. Chem. Soc.* 1995, 117, 8252.
(b) J. L. Sessler; B. Wang; E. Harriman, *J. Am. Chem. Soc*. 1993, 115, 10418.
(c) J. A. Roberts; J. P. Kirby; D. G. Nocera, *J. Am. Chem. Soc*. 1995, 117, 8051.
(d) S. M. LeCours; C. M. Philips; J. C. Depaula; M. J. Therien, *J. Am. Chem. Soc*.; 1997, 119, 12578.
(e) P. J. F. Rege; S. A. Williams; M. J. Therien, *Science* 1995, 269, 1409.
(f) C. Turro; C. K. Chang; G. E. Lerio; R. I. Cukier; D. G. Nocera, *J. Am. Chem. Soc*. 1992, 114, 4013.
(g) T. Arimura; C. T. Brown; S. L. Springs; J. L. Sessler, *Chem. Commun*. 1996, 2293.
(h) J. M. Nocek; J. S. Zhou; S. De Forest; S. Priyadarshy; D. N. Bertatan; J. N. Onuchic; B. M. Hoffman, *Chem. Rev*. 1996, 96, 2459.

[76] (a) K. Kumar; Z. Lin; D. H. Waldeck; M. B. Zimmt, *J. Am. Chem. Soc*. 1996, 118, 243.
(b) I. Read; A. Napper; R. Kaplan; M. B. Zimmt; D. H. Waldeck, *J. Am. Chem. Soc*.; 1999, 121, 10976l.
(c) M. R. Roest; J. W. Verhoeven; W. Schuddeboom; J. M. Warman; J. M. Lawson; M. N. Paddon-Row, *J. Am. Chem. Soc*. 1996, 118, 1762.
(d) K. A. Jolliffe; T. D. E. Bell; K. P. Ghiggino; S. J. Langford; M. N. Paddon-Row,

Angew. Chem., Int. Ed. 1998, 37, 916.

[77]   A. M. Napper; I. Read; D. H. Waldeck; N. J. Head; A. M. Oliver; M. N. Paddon-Row; *J. Am. Chem. Soc.* 2000, 122, 5220.

[78]   X. W. Li; J. Lorberth; K. Harms, *J. Organomet. Chem.* 483 (1994), 229.

[79]   E. V. Avtomonov; K. Megges; S. Wocadlo; J, Lorberth, *J. Organomet. Chem.* 524 (1996), 253.

[80]   (a)this Dissertation.
(b) O. Schiemann, Ph.D Dissertation, University of Marburg, 1998.

[81]   W. H. Morrision; S. Krogsrud; D. N. Hendrickson. *Inorg. Chem.* 1973, 12, 1998.

[82]   D. L. Zechel; D. A. Foucher; J. K. Pudelski; G. P. A. Yap; A. L. Rheingold; I. Manners, *J. Chem. Soc. Dalton Trans* 1995, 1893.

[83]   (a) A. G. Osborne; R. H. Whiteley; R. E. Meads, *J. Organomet. Chem.* 1980, 193, 345.
(b) D. Seyferth; H. P. Withers; *Organometallics* 1982, 1, 1275.
(c) A. Clearfield; C. J. Simmons; H. P. Withers; D. Seyferth, *Inorg. Chim. Acta* 1983, 75, 139.

[84]   G. Utri; K. E. Schwarzhans; G. M. Allmaier, *Z. Naturforsch.* 1990, B45, 755.

[85]   J. Hurley, Dissertation, University of Marburg, 1989; Annette, Bretschneider-Hurley, Dissertation, University of Marburg, 1992.

[86]   *Inorg. Syn.* 1966, 8, 57.

[87]   J. B. Flanagan; S. Margel; A. J. Bard; F. C. Anson, *J. Am. Chem. Soc.* 1978, 100, 4248.

[88]   V. V. Demen´tev; F. Cervantes-Lee; L. Parkanyi; H. Sharma; K. H. Pannell; M. T. Nguyen; A. Diaz, *Organometallics* 1993, 12, 1983.

[89]   (a) T. Fuchigami, *The Chemistry of Organosilicon Compounds* ; John Wiley & Sons , 1998; Vol. 2, Chapter 20.
(b) E. M. Genies; F. E. Omar, *Electrochim. Acta* 1983, 28, 541.

[90]   (a) M. Ishikawa, *Pure Appl. Chem.* 1978, 50, 11.
(b) M. Ishikawa; M. Kumada, *Adv. Organomet. Chem.* 1981, 19, 51.
(c) H. Sakurai, *J. Organomet. Chem.* 1980, 200, 261.
(d) T. Iwahara; S. Hayase; R. West, *Macromolecules* 1990,,23, 1298.

[91]   K. NaKa; T. Uemura; Y. Chujo, *J. Am. Chem. Soc.* 2001, 123, 6209.

[92]   J. Plackmayer, Diploma, Univ. of Marburg, 1997.

[93]   A. B. Bocarsly; E. G. Walton; M. G. Bradeley; M. S. Wrighton, *J. Electroanal. Chem. Interfacial Electrochem.* 1979, 100, 283.

[94]   H. Atzkern; J. Hiermeier; F. H. Köhler; A. Steck, *J. Organomet. Chem.* 1991, 408, 281.

[95]   T. Y. Dong; M.-Y. Hwang; Y.-S. Wenig; W.-S. Hwang, *J. Organomet. Chem.* 1990, 391, 377.

[96]   D. A. Foucher; C. H. Honeyman; J. M. Neslon; B. Z. Tang; I. Manners, *Angew. Chem., Int. Ed. Engl.* 1993, 32, 1709.

[97]   (a) D. Foucher; R. Ziembinski; R. Petersen, J. Pudelski; M. Edwards; Y. Z. Ni; J. Massey; C. R. Jaeger; G. J. Vansco; I. Manners, *Macromolecules* 1994, 27, 3992.
(b) M. T. Nguyen; A. F. Diaz; V. V. Dementév; K. H. Pannell, *Chem. Mater.* 1993, 5, 1389.

[98]   (a) E. Bill; C. Krebs; M. Winter; M. Gerdan; A. X. Trautwein; U. Flörke; H-J Haupt; P. Chaudhuri, *Chem. Eur. J.* 1997, 3, 193.
(b) J. Fujita; M. Tanaka; H. Suemune; N. Koga; K. Matsuda; H. Iwamura, *J. Am. Chem. Soc.* 1996, 118, 9347.
(c) F. Kanno; K. Inoue; N. Koga; H. Iwamura, *J. Phys. Chem.* 1993, 97, 13267.

[99]   M. M. Olmstead; R. S. Simons and P. P. Power. *J. Am. Chem. Soc.* 1997, 119, 11705.

[100]   J. Plackmayer, unpublished results.

[101]   Hu, Li; R. C Crittendon; G. H Robinson, *J. Am. Chem. Soc.* 1997, 119, 5471

[102]   (a) W-P, Leung; L-H, Wenig; W-H, Kwok; Z-Y, Zhou; Z-Y, Zhang; T. C. W. Mak; *Organometallics* 1999, 18, 1482.
(b) P. J. Davidson; M. F. Lappert, *J. Chem. Soc., Chem. Commun.* 1974, 895.
(c) U. Lay; H. Pritzkow; H. Grützmacher, *J. Chem. Soc. Chem. Commun.* 1992, 260.
(d) S. Masamune; L. R. Sita, *J. Am. Chem. Soc.* 1985, 107, 6390.
(e) A. Schäfer, M. Weidenbruch; W. Saak; S. Pohl; H. Marsmann, *Angew. Chem., Int. Ed. Engl.* 1991, 30, 834.
(f) J. R. Babcock; A. L. Rheingold; L. R. Sita; *Organometallics* 1999, 18, 4437.
(g) A. Garoufits et al. *Polyhedron* 1999, 18, 3005.

[103]   R. S. Simons; L-P, Pu; M. M. Olmstead; P. P. Power; *Organometallics* 1997, 16, 1920.

[104]   M. Weidenbruch; A. Stilter; H. Marsmann; K. Peters; H. G. von Schnering; *Eur. J. Inorg. Chem.* 1998, 1333.

[105]   P. D. Lickiss; R. Lucas, *J. Organomet. Chem.* 1995, 521, 229.

[106]   (a) R. S. Simons; K. J. Galat; B. J. Rapp; C. A: Tessier; W. J. Youngs, *Organometallics* 2000, 19, 5799.
(b) S. S. Al-J; C. Eaborn; P. B. Hitchcock; P. D. Lickiss, *J. Organomet. Chem.* 1989, 362, 17.

[107]   (a) *Molecule Electronics: Science and Technology*; A. Aviram, Ed; Conference Proceeding No. 262; Amercian Institute of Physics. New York, 1992.
(b) C. P. Collier, et al. *Science* 1999, 285, 27.
(c) D. Feldheim; C. D. Keating, *Chem. Soc. Rev.* 1998, 27, 1.
(d) S. P. Andreas, et al. *Science* 1996, 273, 1690.

[108]   (a) F. Paul; C. Lapinte, *Coord. Chem. Rev.* 1998, 178, 431.
(b) M. D. Ward, *Chem. Soc. Rev.* 1995, 121.
(c) U. H. F. Bunz, *Angew. Chem., Int. Ed. Engl.* 1996, 35, 969.
(d) T. B. Peters; J. C Bohling; A. M. Arif; J. A. Gladysz, *Organometallics* 1999, 18, 3261.

[109]   (a) H. Fink; N. J. Long; A. J. Martin; G. Opromolla; A. J. P. White; D. J. Williams; P. Zanello, *Organometallics* 1997, 16, 2646. (b) T-Y. Dong; T-J. Ke; S-M. Peng; S-K. Yeh, *Inorg. Chem.* 1989, 28, 2103. (c) Levanda; K. Bechgaard; D. O. Cowan, *J. Org. Chem.* 1976, 41, 2700. (d) A-C. Ribou; J-P. Launay; M. L. Sachtleben; Hu Li; C. W. Spangler; *Inorg. Chem.* 1996, 35, 3735. (e) C. Patoux; C. Coudret; J-P Launay; C. Joachim; A. Gourdon; *Inorg. Chem.* 1997, 36, 5037. (f) K-W. Poon; W. Liu; P-K, Chan; Q-C. Yang; T-W. Dominic Chan; T. C. W. Mak; D. K. P. Ng, *J. Org. Chem.* 2001, 66, 1553. (g) N. L. Narvor; C. Lapinte, *Organometallics* 1995, 14, 634. (h) J. W. Seyler, W-q. Wenig, Y-L. Zhou; J. A. Gladysz, *Organometallics* 1993, 12, 3802. (i) A. D. Hunter; A. B. Sizgety; *Organometallics* 1989, 8, 2670.

[110]   T-Y Dong; D. N. Hendrickson; K. Iwai; M. J. Cohn; S. J. Geib; A. L. Rheingold; H. Sano; I. Motoyama; S. Nakashima, *J. Am. Soc. Chem.* 1985, 107, 7996.

[111]   J. McCleverty and M. D. Ward, *Acc. Chem. Res.* 1998, 31, 842, and references therein.

[112]   (a) M. D. Ward, *J. Chem. Edu.* 2001, 321.
(b) R. Chukwu; A. D. Hunter; B. D. Santarsiero, *Organomtallics*, 1992, 11, 589.

[113]   J. Hock; A. M. W. C. Thompson; J. A. McCleverty; M. D. Ward; *J. Chem. Soc., Dalton Trans* 1996, 4257.

[114]   (a) J. M. Tour; *Acc. Chem. Res.* 2000, 33, 791.

(b) U. Mitschke; P. Baüerle; *J. Chem. Soc., Perkin Trans* 2001, 740.

(c) V. M. Domingo; C. Aleman; E. Brillas; L. Julia; *J. Org. Chem.* 2001, 66, 4058.

[115] T. J. Kealy; P. L. Pauson, *Nature* 1951, 168, 1039-1040.

[116] V. S. B. Mtewa; et al. *J. Chem. Soc. Dalton Trans.* 2, 1994, 207.

[117] M. D. Rausch; R. F. Kovar; C. S. Kraihanzel. *J. Am. Chem. Soc.* 95, 1969, 125.

[118] J. C. Smart; B. L. Pinsky. *J. Am. Chem. Soc.* 99, 1977, 956.

[119] (a) E. O. Fischer; W. Fellman; G. E. Herberich. *Chem. Ber.* 95, 1962, 2254.

(b) Y. H. Lai; W. Tom; K. P. C. Vollhardt. *J. Organomt. Chem.* 216, 1981, 97.

[120] (a) C. Rieker; G. Ingram; P. Jaitner; H. Schottenberger and K. E. Schwarzhans, *J. Organomet. Chem.,* 381 (1990) 127.

(b) W. W. Ellis; T. K. Hollis; et al. *Organometallics* 12 (1993) 4391.

(c) W. A. Herrmann; R. Anwander; H. Riepl, et al. *Organometallics* 12 (1993) 4342.

[121] (a) H. Schottenberger; G. Ingram, D. Obendorf and R. Tessadri, *Synlett* (1991) 905.

(b) P. Jaitner; H. Schottenberger; et al. *J. Organomet. Chem.* 475 (1994) 113.

(c) H. Schottenberger; M. Buchmeiser; C. Rieker; P. Jaitnre; K. Wurst, *J. Organomet. Chem.*, 541 (1997) 249.

[122] (a) M. Andre; H. Schottenberger; R. Tessandri, G. Ingram, P. Jaitner; K. E. Schwarzhans; *Chromatographia* 1990, 30 534.

(b) G. Ingram; P. Jaitner; K. E. Schwarzhans *Z .Naturforsch.* 1990, 45B, 781,

[123] H. Plenio, *Organometallics* 1992, 11, 1856.

[124] B. J. Wakefield, *Organolithium Methods* Academic Press, New York, 1988; Chapter 2.

[125] E. S. Bowman; G. B. Hughes and J. B. Grutzner, *J. A. Chem. Soc.* 1976, 98, 8273.

[126] (a) C. Elschenbroich; E. Bilger and B. Metz, *Organometallic* 1991, 10, 2823.

(b) P. Scott and P. B. Hitchcock, *J. Organomet. Chem.* 497 (1995) C1.

[127] J. Lukasser; H. Angleitner; H. Schottenberger, et al. *Organometallics* 1995, 14, 5566.

[128] *Organic Synthesis* Vol.48, 68.

[129] (a) L. Ingham; M. S. Khan, et al. *J. Organomet. Chem.* 470, 1994, 153.

(b) M. E. Huttenloch; J. Diebold; U. H. Brinteinger; A. M. Gilbert; T. J. Kart; *Organometallics* 1992, 11, 3600.

[130] (a) C. Floriani, *J. Chem. Soc.,* Dalton Trans. 1976, 1046.

(b) R. B. King and F. G. A. Stone, *J. Am. Chem. Soc.* 81, 1959, 5263.

[131] O. Schiemann, *Diplomarbeit*, University of Marburg, 1995.

[132] G. Brauer, *Handbuch der präparativen anorganischen Chemie*, 3 Band, 3. Auflage, Enke 1981, 1099.

[133] P. G. Cookson; A. G. Davies and N. Fazal, *J. Organomet. Chem.* 1975, C31; *Synthesis* 1985, 634.

[134] (a) C. Levanda; K. Bechgaard; D. O. Cowan; U. T. Mueller-Westerhoff; P. Eilbracht, G. A. Candela; R. L. Collins, *J. Am. Chem. Soc.*, 1976, 98, 3181.

(b) S. Herzoger; K. Gustav; E. Krueger; H. Oberender; R. Schuster; *Z. Chem.*, 3, 428, 1963.

[135] R. O. Sauer, *J. A. Chem. Soc.*, 1944, 1707.

[136] M. Bochmann; X. J. Song; M. B. Hursthouse and A. Karaulov, *J. Chem. Soc.*, *Dalton Tans.* 1995, 1649.

[137] R. F. Kovar; M. D. Rausch and H. Rosenberg, *Organometallics in Chem. Synth.* 1, 1970/1971, 173.

[138] J. Eisch; R. B. King, *Organometallic Syntheses*; Academic Press, New York, 1965, Vol.1, p124.

8. Summary

In order to further study the interaction between redox centers in organometallic compounds, trovacene is highly suitable. Group 14, 15 , 16 derivatives and termetallocene derivatives have been synthesized. Many factors influence the electron transfer between redox centers, such as, the nature of the bridges, the distances between the redox centers, the substituent groups of bridges, and so on. They have been systematically studied by CV, EPR, X-ray diffraction or magnetic susceptibility measurement in the present work.

(1) Group 16 derivatives
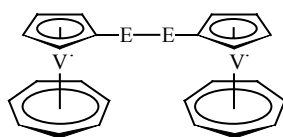
E = S, **18**˙˙; Se, **25**˙˙; Te, **26**˙˙

Di([5]trovacenyl)disulfide (**18**˙˙), di([5]trovacenyl)diselenide (**25**˙˙), di([5]trovacenyl)ditelluride (**26**˙˙) were synthesized by reaction of lithiotrovacene with S, Se, or Te, respectively, at ambient temperature. These binuclear complexes exhibit weak metal-metal interactions due to the large distances between the metals and the saturated atoms bridging the two trovacenyl units. Based on the X-ray structural analysis of **18**˙˙, a *cis* conformation is adopted and a distance of 8.08Å between metals was obtained. The results of CV showed one two-electron oxidation and one reduction couple. With increasing atomic radius, both of the oxidation potential and reduction potential shift as $E_{1/2}(0/2+)_{TeTe} < E_{1/2}(0/2+)_{SeSe} < E_{1/2}(0/2+)_{SS}$ or $E_{1/2}(0/2-)_{TeTe} < E_{1/2}(0/2-)_{SeSe} < E_{1/2}(0/2-)_{SS}$. This indicates that the metal-metal interactions decrease as **18**˙˙ > **25**˙˙ > **26**˙˙.

16˙˙   **20**˙˙
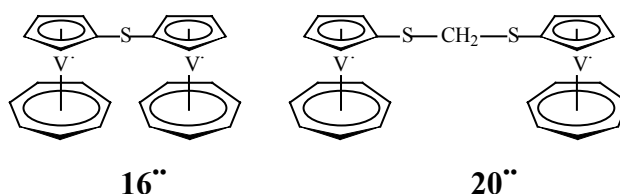
In order to compare with **18**˙˙, di([5]trovacenyl)sulfide (**16**˙˙) and di([5]trovacenylthio)methane (**20**˙˙) were synthesized by reaction of lithiotrovacene with SCl₂ and TVC-SLi with CH₂Cl₂, respectively. The X-ray structural analysis of **16**˙˙, **18**˙˙, **20**˙˙ demonstrate that the distances between two metals increase as $d_s < d_{scs} < d_{ss}$ in solid state. Cyclic voltammetry of **16**˙˙ exhibited two successive reversible one-electron oxidation and reduction waves with a redox splitting of 87mV and 134 mV, respectively. However, as for **20**˙˙, a two-electron oxidation and two successive quasi-reversible one-electron reduction were observed. The computer simulation of the EPR spectra of **16**˙˙, **18**˙˙ and **20**˙˙ supports the metal - metal interactions decreasing as **16**˙˙ > **18**˙˙ > **20**˙˙, their exchange coupling constant J are 2.8 cm⁻¹, 0.65 cm⁻¹ and 0.11 cm⁻¹, respectively. It is apparent that the introduction of CH₂ group between two TVC-S units would attenuate the metal-metal interaction.
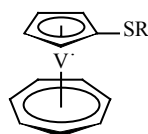
R = CH$_2$Ph, **22$^•$**; Me, **23$^•$**

Furthermore, the reactivity of TVC-SLi has been studied in reactions with various halogen compounds, such as, PhCH$_2$Cl, Me$_2$SnCl$_2$, Me$_2$SiCl$_2$, Me$_3$SiCl, SbCl$_3$, BiCl$_3$, to afford the corresponding benzyl([5]trovacenyl)thioether (**22$^•$**), di([5]trovacenylthio)dimethyltin (**24$^{••}$**), di([5]trovacenylthio)dimethylsilane (**79$^{••}$**), trimethylsilyl([5]trovacenyl)thioether (**75$^•$**), tri([5]trovacenylthio)antimony (**29$^{•••}$**) and tri([5]trovacenylthio)bismuth (**30$^{•••}$**). Methyl([5]trovacenyl)thioether (**23$^•$**) was synthesized by reaction of lithiotrovacene with CH$_3$SSCH$_3$. **22$^•$** and **23$^•$** have been studied by CV.
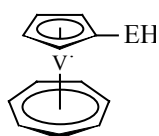
E = S, **21$^•$**; O, **28$^•$**

[5]Trovacenylthiol could be prepared by reduction of **18$^•$** with LiAlH$_4$, or acidification of TVC-SLi with 15% HCl. The analogue hydroxytrovacene **28$^•$** is relatively difficult to be synthesized, due to its thermal instability, by reaction of lithiotrovacene with Me$_3$SiOOSiMe$_3$ and following hydrolysis in poor yield. The hydrogen bonds among the molecules of **28$^•$** offer another possibility for electron exchange coupling, the X-ray structural analysis gives the length of O(1)-H(1)··O(1´) (2.8895 Å). **21$^•$** and **28$^•$** have been investigated by CV and EPR.

(2) Group 15 derivatives.
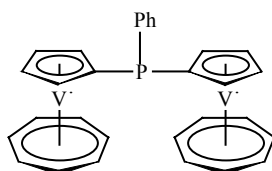
41$^{••}$

P, As bridged binuclear complexes as the representative examples have shown a considerably strong metal - metal interaction. Di([5]trovacenyl)phenylphosphane (**41$^{••}$**) was prepared by means of lithiotrovacene reacted with PhPCl$_2$. The X-ray crystal structure of **41$^{••}$** displays a slightly longer distance V-V than that in [5,5]bitrovacene. Electrochemistry exhibits that the redox splitting $\Delta E_{1/2}$(0/-)(-/2-) is 152mV. The electron spin exchange coupling constant J =-2.8 cm^{-1} is given by the computer simulation of EPR spectroscopy.
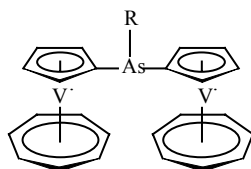
R = Cl, **43··**; n-Bu, **44··**; H, **45··**; OH, **46··**

Additionally, the influence of the inductive effect by the substituent of the bridging As atom to the metal-metal interactions has been systematically investigated. Di([5]trovacenyl)chloroarsane (**41··**) as a versatile precursor could be prepared by the reaction of lithiotrovacene with $AsCl_3$ and could be converted to H, n-Bu, OH-substituted binuclear complexes by reaction with $LiAlH_4$, n-BuLi, or NaOH. The distance of V··V in **44··** is 6.4434(28) Å as shown by X-ray diffraction analysis. **43··**, **44··** and **45··** have been studied by CV and the potential separation ($\Delta E_{1/2}(0/-)(-/2-)$) are 109mV (**45··**), 126mV (**43··**) and 156mV (**44··**), respectively. The exchange coupling constant J of **44··** is -1.5 cm^{-1} which indicate that the metal-metal interaction of **44··** is weaker than that of **41··**. Therefore, it can be concluded that electron donating or electron withdrawing groups linked to the bridging atom would have the contrary impact on the metal-metal interaction.

(3) Group 14derivatives

Si, Ge, Sn, Pb bridged binuclear derivatives were prepared by reaction of lithiotrovacene with corresponding chloro-reagents Ph_2MCl_2 (M = Ge, Sn, Pb) and Me_2MCl_2 (M = Si; Sn).
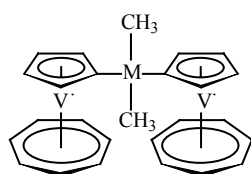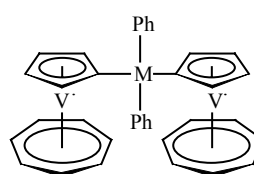
M = Si, **59··**; Sn, **63··**   M = Ge, **62··**; Sn, **64··**; Pb, **65··**

The redox splitting ($\Delta E_{1/2}(0/-)(-/2-)$) increases as Si (**59··**) < Ge (**62··**) < Sn (**64··**) < Pb (**65··**). This indicates that with the radius of bridging atoms increasing in the same group, the metal-metal interactions increase. The X-ray structures of **64··** and **65··** have shown that the distances of V··V are longer than that of [5,5]bitrovacene. Therefore, the nature of bridges plays a crucial role in the electron transfer process and determines the interactions between redox centers.

Meanwhile, the influence of the substitution at the bridging atoms on the metal-metal interaction have also been considered. In comparison with **64··**, the redox splitting ($\Delta E_{1/2}(0/-)(-/2-)$) of **63··** (95mV) was significant smaller than that of **64··** (288mV). The V··V distance of **63··** exhibited by X-ray diffraction is slightly longer than that of **64··**.Thus, it can be concluded that methyl-substituted bridge dinuclear complexes show a slightly weaker metal-metal interaction than that of phenyl-substituted bridge complexes. The large redox splitting can be rationalized in terms of the orbital overlap between the sp^3 and the respective conjugated p$_\pi$ from phenyl and cyclopentadienyl ring.

Additionally, the influence of the bridge length also has been investigated, TVC-(SiMe$_2$)$_n$-TVC (n = 0, **10$^{..}$**; 1, **59$^{..}$**; 2, **60$^{..}$**) binuclear complexes have been chosen as the models. In general, with the length of bridge increasing, the interaction between redox centers will decrease. For example, Fc(SiMe$_2$)$_n$Fc (n = 0, 1, 2, 3, 6), the corresponding redox splitting decreased according to the tendency of 0 > 1 > 2 > 3 > 6.
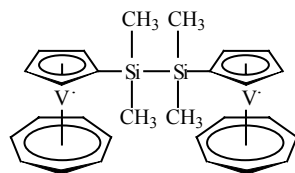
60$^{..}$

However, the redox splitting ($\Delta E_{1/2}(0/-)(-/2-)$) of **60$^{..}$** (116 mV) was remarkably larger than that of **59$^{..}$** (75 mV). It may contribute to the distortion of the molecular geometry which may reduce spatially the direct distance between the two metals, due to the rotating of two trovacene units at the ends of Si-Si bond. Therefore, the *through space* effect can increase the interaction in addition to the *through bond* effect. Excluding the difference of the nature of the bridge, the length of the bridges would experience a remarkable impact on the interaction.

In contrast to the synthesis of (TVC)$_2$Si(Me)$_2$, the reaction of lithiotrovacene with Ph$_2$SiCl$_2$ did not result in the expected (TVC)$_2$SiPh$_2$, rather it yielded TVC-Si(OH)Ph$_2$ (**67$^{..}$**). The X-ray structure shows the hydrogen bonds between the two molecules and one ethanol molecule.
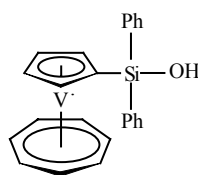
67$^{..}$

Furthermore, the reaction of lithiotrovacene with SnCl$_2$ afforded the stannate [Li(THF)$_3$]$^+$[(TVC)$_3$SnCl$_2$]$^-$ (**66$^{...}$**) which contains three trovacene units. Results of CV of **66$^{...}$** exhibit three successive one-electron oxidation. The EPR spectroscopy give the typical 22-line pattern, demonstrating that three unpaired electrons couple to three vanadium nuclei.
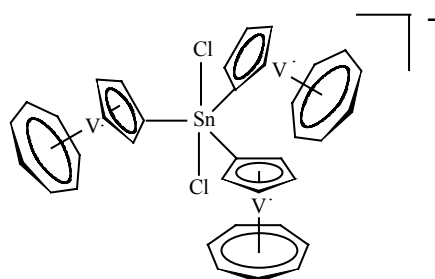
66$^{...}$

(4) Termetallocene

70[•]   **71^{••}**
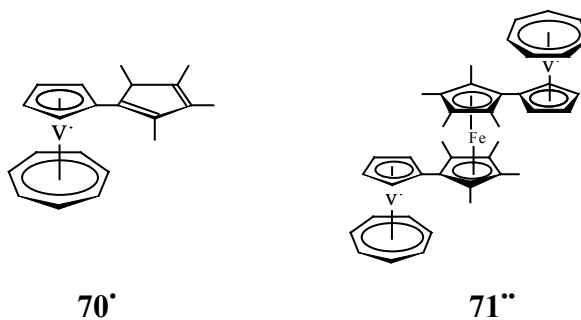
The termetallocene, di([5]trovacenyl-tetramethyl-η^5-cyclopentadienyl)iron (**71^{••}**) was generated from [5]trovacenyl-tetramethylcyclopentadiene (**70[•]**) and $Fe_2Cl_4(THF)_3$, in which **70[•]** was prepared from the reaction of 2,3,4,5-tetramethylcyclopenten-1-one with lithiotrovacene and follow-up procedures. A weak interaction between the two trovacene units through the substituted ferrocene has been detected by CV and EPR.

Zusammenfassung

Um weitere Wechselwirkung zwischen Redox-Zentren zu untersuchen, wird Trovacen als ein geeiganeter Komplex ausgewählt. Die Derivate der 14. 15. und 16. Gruppe und des Termetallocences wurden dargestellt. Viele Faktoren, z. B., die Eigenschaften der Brücke zwischen den Redox-Zentren, der Abstand zwischen den Redox-Zentren und die Substitutionen an der Brücke, beeinflussen den Elektronen-Transfer zwischen den Redox-Zentren. Sie wurden durch Röntgen-Diffraktion, CV, EPR und magnetische Messung in der vorliegenden Arbeit systematisch untersucht.

(1) Gruppe 16 Derivate
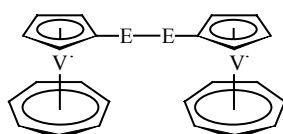
E = S, **18**^{··}; Se, **25**^{··}; Te, **26**^{··}

Di([5]trovacenyl)disulfid (**18**^{··}), Di([5]trovacenyl)diselenid (**25**^{··}) und Di([5]trovacenyl)ditellurid (**26**^{··}) wurden bei entsprechen der Temperatur durch die Reaktion von Lithiotrovacen mit S, Se und Te synthetisiert. Diese zweikernigen Komplexe zeigen eine schwache Metall - Metall - Wechselwirkung wegen des langen Abstandes zwischen den Metallen und der gesättigten - Atom - Verbrückung der beiden Trovacenyl einbeiten. Nach der Röntgen-Untersuchung wurde bewiesen, dass das Disulfid **18**^{··} eine cis-Konformation einnimmt und einen (Metall-Metall) Abstand von (8.071(45) Å) besitzt. Die CV weist eine Zwei-Elektronen-Oxidation und eine reduktive Kopplung nach, aber das oxidative Potential ändert sich in der Reihe mit der Zunahme des Atom-Radiuses. $E_{1/2}(0/2+)_{TeTe} < E_{1/2}(0/2+)_{SeSe} < E_{1/2}(0/2+)_{SS}$ oder $E_{1/2}(0/2-)_{TeTe} < E_{1/2}(0/2-)_{SeSe} < E_{1/2}(0/2-)_{SS}$. Dies zeigt, daß die Metall-Metall-Wechselwirkung von **18**^{··} > **25**^{··} > **26**^{··} abnimmt.

16^{··}   **20**^{··}
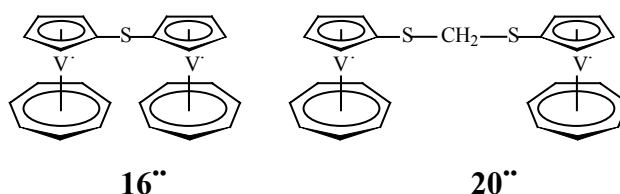
Zum Vergleich mit **18**^{··} wurde Di([5]trovacenyl)sulfid (**16**^{··}) und Di([5]trovacenylthio)methan (**20**^{··}) durch die Reaktion von Lithiotrovacen mit SCl_2 oder TVC-SLi mit CH_2Cl_2 synthetisiert. Die strukturellen Daten von **16**^{··} , **18**^{··} und **20**^{··} zeigen den zunehmenden Trend $d_s < d_{scs} < d_{ss}$. für den (Metall-Metall) Abstand in festem Zustand. Die CV bei **16**^{··} weist zwei reversible Eine-Elektron-Oxidationen und reduktive Kopplung. mit dem Splitting von 87 mV und 134 mV auf. Wie auch für **20**^{··}, wurde eine Zwein-Electronen-Oxidation und zwei aufeinander folgende quasi-reversible Ein-Electron-Reduktion erhalten. Die Computersimulation der EPR-Spektren von **16**^{··} , **18**^{··} und **20**^{··} unterstützen die Abnahme des Metall-Metall-Wechselwirkung von **16**^{··} > **18**^{··} > **20**^{··}, die Austauschwechselwirkungen J sind 2.8 cm⁻¹, 0.65 cm⁻¹ und 0.11 cm⁻¹. Es scheint, daß die Einführung eine CH_2-gruppe zwischen zwei TVC-S-Einleiten die Metall-Metall-Wechselwirkung abschwächen.
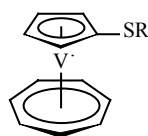
R = CH$_2$Ph, **22˙**; Me, **23˙**

Weiterhin Wurde die Reaktivitäten von TVC-SLi mit verschiedenen Halogen, z. B. PhCH$_2$Cl, Me$_2$SnCl$_2$, Me$_2$SiCl$_2$, Me$_3$SiCl, SbCl$_3$ und BiCl$_3$ untersucht um die Übereinstimmung mit Benzyl([5]trovacenyl)thioether (**22˙**), Di([5]trovacenylthio)dimethylzinn (**24˙˙**), Di([5]trovacenylthio)dimethylsilane (**79˙˙**), Trimethylsilyl([5]trovacenyl)thioether (**75˙**), Tri([5]trovacenylthio)antimon (**29˙˙˙**) und Tri([5]trovacenylthio)bismut (**30˙˙˙**) zu gewährbeisten. Mit der Reaktion von Lithiotrovacen und CH$_3$SSCH$_3$ kann Methyl(trovacenyl)thioether (**23˙**) gewonnen werden. **22˙** und **23˙** wurde mit Hilfe des CV untersuche.
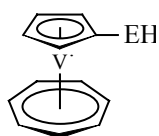
E = S, **21˙**; O, **28˙**

Die Reaktion von **18˙˙** mit LiAlH$_4$ oder das Ansäuren von TVC-SLi mit 15% HCl liefert [5]Trovacenylthiol (**21˙**), aber **28˙** ist relativ schwierig darzustellen, weil es nicht thermodynamisch stabil ist. Die Umsetzung von Lithiotrovacen mit Me$_3$SiOOSiMe$_3$ und die nachfolgende Hydrolyse ergeben eine niedrige Ausbeute. Die Wasserstoffbindung zwischen den Molekülen von **28˙** bieten eine andere Möglichkeit des Elektron-Transfers an. Der Bindungsabstand O(1)-H(1)....O(1') beträgt 2.8895 Å. **21˙** und **28** wurde mit CV und EPR untersucht.

(2) Gruppe 15 Derivate
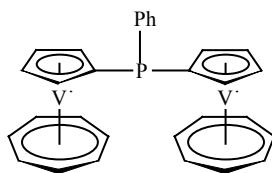
41˙˙

P und As - verbrückte Zweikerner, als representative Beispiele, zeigen eine starke Metall-Metall-Wechselwirkung. Di([5]trovacenyl)phenylphosphin wurde durch die Reaktion von Lithiotrovacen mit PhPCl$_2$ synthetisiert. Die Struktur von **41˙˙** deutet auf einen leicht längeren (V-V) Abstand im Vergleich zu dem von [5,5]Bitrovacen hin. Die Austauschwechselwirkung J = 2.8 cm^{-1} ergab die Computersimulation der EPR-Spektroskopy.
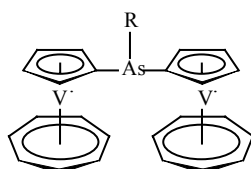
R = Cl, **43··**; n-Bu, **44··**; H, **45··**; OH, **46·**

Weiterhin wurde der Einfluß des induktiven Effekt bei des Substitution der As-Brücke auf die Metall-Metall-Wechselwirkung systematisch untersucht. Di([5]trovacenyl)chloroarsan (**43··**) als Precusor wurde durch die Reaktion von Lithiotrovacene mit AsCl$_3$ dargestellt und wurde in zweikernige Komplexe H, n-Bu, OH-Substituenten mittels der entsprechenden LiAlH$_4$, n-BuLi und NaOH umgewandelt. Der (V-V) Abstand von **44··** mit 6.4434(28) Å wurde durch Röntgen-Diffraktion bestimmt. **43··**, **44··** und **45··** wurde mittels CV untersucht, die Potentialseperationen ($\Delta E_{1/2}(0/-)(-/2-)$) betrugen 109 mV (**45··**), 126mV (**43··**) und 156mV (**44··**). Die Austauschwechselwirkung J von **44··** beträgt 1.5 cm^{-1}, was zeigt, das die Metall-Metall-Wechselwirkung von **44··** schwäche ist als von **41··**.

(3) Gruppe 14 Derivates

Einige verbückte zweikernige Derivate von Si, Ge, Sn und Pb wurden durch die Reaktion von Lithiotrovacen mit Chloro-Reagenzien Ph$_2$MCl$_2$ (M = Ge, Sn und Pb) und Me$_2$MCl$_2$ (M = Si, Sn) erhalten.
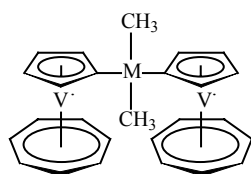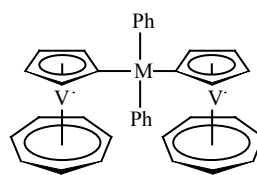
M = Si, **59··**; Sn, **63··**   M = Ge, **62··**; Sn, **64··**; Pb, **65··**

Das Redox-Splitting ($\Delta E_{1/2}(0/-)(-/2-)$) nimmt mit der Tendenz Si (**59··**) < Ge (**62··**) < Sn (**64··**) < Pb (**65··**) zu. Das zeigt, daß mit der Zunahme des Radiuses des Brückenatome der selben gruppe, die Metall-Metall-Wechselwirkung steigt. Die Eigenschaft des Atoms an der Brücke spielt eine kritische Rolle während des Elektron-Transfers und entscheidet die Wechselwirkung zwischen den Redox-Zentren.

Auf der anderen Seite hat die Substitution von den verbrückten Atomen Einfluß auf die Wechselwirkung. Im Vergleich zu **64··** (288mV) ist das Redox-Splitting ($\Delta E_{1/2}(0/-)(-/2-)$) von **63··** (95mV) wesentlich kleiner, während der (V-V) Abstand in **63··** etwas länger als der Abstand in **64··** ist. Auf Grund der großen Elektronen-Dichte des Phenyl-Restes ist die Wechselwirkung zwischen den Metallen von den Methyl-Derivaten verbrückten Komplexe etwas schwächer als sie von den Phenylderivaten verbrückten Komplexen. Das größere Redox-Splitting wird rationalisiert durch die Orbital-Überlappung zwischen der sp^3-Hybridisierung des verbrückten Atoms und dem konjugierten p$_\pi$ -Orbital des Phenyl- oder Cyclopentadienyl-Ringes.

Außerdem wurde der Einfluß der Brücken-Länge auch untersucht. Zweikernige Komplexe TVC-(SiMe$_2$)$_n$-TVC (n=0, **10··**; 1, **59··**; und 2, **60··**) wurden als Modell-Verbindungen

ausgewählt. Mit den zunehmenden Brücken-Längen nimmt die Wechselwirkung ab, z. B. das Redox-Splitting von Fc(SiMe$_2$)$_n$Fc (n=0, 1, 2, 3 und 6) reduziert mit der Tendenz; 0 > 1 > 2 > 3 > 6.

60$^{¨}$
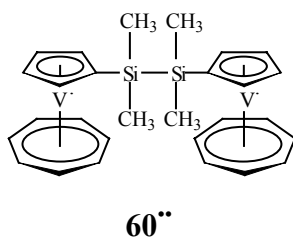
Aber das Redox-Splitting ($\Delta E_{1/2}$(0/-)(-/2-)) von **60$^{¨}$** (116 mV) ist deutlich größer als das von **59$^{¨}$** (75mV). Wegen der Rotation der beiden Trovacen-Einheiten am Ende der (Si-Si)-Bindung wird der Abstand zwischen beiden Metallen durch die Distortion in der molekularen Geometrie verkürzt. Außer des *through bond* Effekts kann der zusätzliche *through space* Effekt die Wechselwirkungen verstärken. Außer dem Unterschied der Eigenschaft der Brücke hat die Brücken-Länge wesentlichen Einfluß auf die Wechselwirkung.

Im Unterschied zu der Synthese, die analog zu (TVC)$_2$Si(Me)$_2$ (**59$^{¨}$**) durchgefühit wurde, lieferte die Reaktion von Lithiotrovacen mit Ph$_2$SiCl$_2$ durch chromatographische Isolierung nicht die gewünschte Verbindung (TVC)$_2$SiPh$_2$ sondern TVC-Si(OH)Ph$_2$ (**67$^{¨}$**). Die Wasserstoff-Bindung zwischen zwei Molekülen und einem Ethanol-Molekül wurde durch Röntgenanalyse bestimmt.

67$^{¨}$
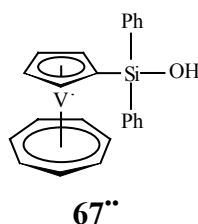
Weiterhin ergibt die Umsetzung von Lithiotrovacene und SnCl$_2$ ein Stannat [Li(THF)$_3$]$^+$[(TVC)$_3$SnCl$_2$]$^-$ (**66$^{¨¨}$**), welches drei. Trovacen-Einheiten. Das Ergebnis der CV **66$^{¨¨}$** zeigt drei reversible Ein- Elektronen - Oxidationen. Das EPR - Spektrum ergibt ein typisches 22-linien Spektrum, welches die drei ungepaarten Electronenpaart der Vanadiumkerne zeigt.

66$^{¨¨}$

(4) Termetallocen

70˙   **71˙˙**
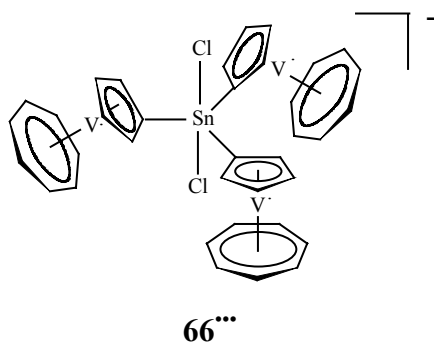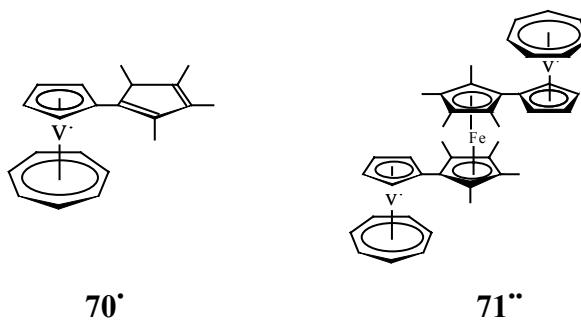
Die Termetallocen, di([5]trovacenyl-tetramethyl-η^5-cyclopentendienyl)eisen (**71˙˙**), wurde durch die Umsetzung von [5]trovacenyl-tetramethylcyclopentendien (**70˙**) mit $Fe_2Cl_4(THF)_3$ erhalten, während **70˙** durch die Reaktion von 2,3,4,5-Tetramethyl-cyclopenten-1-on mit Lithiotrovacen dargestellt wurde. Eine schwache Wechselwirkung zwischen den beiden Trovacen-Einheiten wurde mit dem substituierten Ferrocen durch CV und EPR erklärt.

9. Data for the X-ray Crystallography Analysis

9.1. Crystal data and structure refinement for Di([5]trovacenyl)sulfide (16¨)

Crystal data

Habitus, colour	Plate, dark red
Crystal size	0.57 x 0.12 x 0.03 mm^3
Crystal system	Triclinic
Space group	P$\bar{1}$ Z = 4
Unit cell dimensions	a = 11.7800(10) Å α = 82.508(7)°.
	b = 12.1423(11) Å β = 81.848(7)°.
	c = 13.8083(12) Å ɣ = 84.640(7)°.
Volume	1932.8(3) Å^3
Empirical formula	C24 H22 S V2
Formula weight	444.36
Density (calculated)	1.527 Mg/m^3
Absorption coefficient	1.081 mm^{-1}
F(000)	912

Data collection:

Diffractometer type	Stoe IPDS-II
Wavelength	0.71073 Å
Temperature	193(2) K
Theta range for data collection	1.70 to 25.88°.
Index ranges	-14<=h<=14, -14<=k<=14, -16<=l<=16
Data collection software	Stoe Win-Expose
Cell refinement software	Stoe Win-Cell
Data reduction software	Stoe Win-Integrate

Solution and refinement:

Reflections collected	20948
Independent reflections	7459 [R(int) = 0.0404]
Completeness to theta = 25.88°	99.5 %
Observed reflections	5835[I>2sigma(I)]
Reflections used for refinement	7459
Absorption correction	Empirical from equivalent reflections
Max. and min. transmission	0.4856 and 0.4426
Largest diff. peak and hole	0.319 and -0.323 e.Å^{-3}
Solution	direct methods
Refinement	Full-matrix least-squares on F^2
Treatment of hydrogen atoms	located, isotropic refinement
Programs used	SHELXS-97 (Sheldrick, 1990)
	SHELXL-97 (Sheldrick, 1997)
	SHELXTL, STOE IPDS software
Data / restraints / parameters	7459 / 0 / 663

Goodness-of-fit on F^2	0.953
R index (all data)	wR2 = 0.0740
R index conventional [I>2sigma(I)]	R1 = 0.0300

9.2. Crystal data and structure refinement for Di([5]trovacenyl)disulfide .C_6H_6 (18$^{..}$)

Crystal data

Habitus, colour	Plate, violet-red	
Crystal size	0.55 x 0.15 x 0.05 mm^3	
Crystal system	Monoclinic	
Space group	P2$_1$	Z = 2
Unit cell dimensions	a = 6.5432(7) Å	α = 90°.
	b = 24.063(2) Å	β = 93.134(13)°.
	c = 7.9876(9) Å	γ = 90°.
Volume	1255.8(2) Å^3	
Cell determination	3904 reflections	
Empirical formula	C30 H28 S2 V2	
Formula weight	554.52	
Density (calculated)	1.467 Mg/m^3	
Absorption coefficient	0.928 mm^{-1}	
F(000)	572	

Data collection:

Diffractometer type	Stoe IPDS
Wavelength	0.71073 Å
Temperature	193(2) K
Theta range for data collection	3.12 to 25.92°.
Index ranges	-7<=h<=7, -28<=k<=29, -9<=l<=9
Phi-range, increment	0-205.5, 1.5°.
Expose time	5 min.
Data collection software	Stoe Expose
Cell refinement software	Stoe Cell
Data reduction software	Stoe Integrate

Solution and refinement:

Reflections collected	7136
Independent reflections	3488 [R(int) = 0.0764]
Completeness to theta = 25.92°	75.7 %
Observed reflections	2246[I>2sigma(I)]
Reflections used for refinement	3488
Absorption correction	None
Max. and min. transmission	0.9551 and 0.6293
Flack parameter (absolute struct.)	-0.01(4)
Largest diff. peak and hole	0.314 and -0.380 e.Å^{-3}
Solution	direct/ difmap

Refinement	Full-matrix least-squares on F^2
Treatment of hydrogen atoms	geom, noref
Programs used	SHELXS-97 (Sheldrick, 1990)
	SHELXL-97 (Sheldrick, 1997)
	SHELXTL, STOE IPDS software
Data / restraints / parameters	3488 / 1 / 307
Goodness-of-fit on F^2	0.824
R index (all data)	wR2 = 0.0858
R index conventional [I>2sigma(I)]	R1 = 0.0427

9.3. Crystal data and structure refinement for Di([5]trovacenylthio)methane (20$^{¨}$)

Crystal data

Habitus, colour	Plate, violet
Crystal size	0.36 x 0.15 x 0.03 mm^3
Crystal system	Monoclinic
Space group	C2/c	Z = 4
Unit cell dimensions	a = 12.3240(10) Å	α = 90°.
	b = 22.814(2) Å	β = 103.437(9)°.
	c = 7.7507(6) Å	γ = 90°.
Volume	2119.5(3) Å^3
Cell determination	4838 reflections
Empirical formula	C25 H24 S2 V2
Formula weight	490.44
Density (calculated)	1.537 Mg/m^3
Absorption coefficient	1.088 mm^{-1}
F(000)	1008

Data collection:

Diffractometer type	Stoe IPDS
Wavelength	0.71073 Å
Temperature	193(2) K
Theta range for data collection	2.98 to 25.95°.
Index ranges	-14<=h<=15, -27<=k<=27, -9<=l<=9
Phi-range, increment	0-200, 1.3°.
Expose time	5 min.
Data collection software	Stoe Expose
Cell refinement software	Stoe Cell
Data reduction software	Stoe Integrate
Solution and refinement:	

Reflections collected	6272
Independent reflections	1726 [R(int) = 0.0559]
Completeness to theta = 25.95°	82.9 %
Observed reflections	1162[I>2sigma(I)]
Reflections used for refinement	1726

Absorption correction	None
Largest diff. peak and hole	0.255 and -0.240 e.Å^{-3}
Solution	direct/ difmap
Refinement	Full-matrix least-squares on F^2
Treatment of hydrogen atoms	Located, isotropic refinemnet
Programs used	SHELXS-97 (Sheldrick, 1990)
	SHELXL-97 (Sheldrick, 1997)
	SHELXTL, STOE IPDS software
Data / restraints / parameters	1726 / 0 / 180
Goodness-of-fit on F^2	0.908
R index (all data)	wR2 = 0.0565
R index conventional [I>2sigma(I)]	R1 = 0.0299

9.4. Crystal data and structure refinement for [5]Trovacenol (28˙)

Crystal data

Habitus, colour	Plate, dark	
Crystal size	0.30 x 0.25 x 0.01 mm^3	
Crystal system	Orthorhombic	
Space group	Pna2$_1$	Z = 8
Unit cell dimensions	a = 10.8237(16) Å	α = 90°.
	b = 7.9203(12) Å	β = 90°.
	c = 22.452(3) Å	γ = 90°.
Volume	1924.7(5) Å^3	
Empirical formula	C12 H12 O V	
Formula weight	223.16	
Density (calculated)	1.540 Mg/m^3	
Absorption coefficient	0.988 mm^{-1}	
F(000)	920	

Data collection:

Diffractometer type	Stoe IPDS-II
Wavelength	0.71073 Å
Temperature	193(2) K
Theta range for data collection	1.81 to 24.99°.
Index ranges	-12<=h<=12, -9<=k<=6, -26<=l<=23
Data collection software	Stoe Win-Expose
Cell refinement software	Stoe Win-Cell
Data reduction software	Stoe Win-Integrate

Solution and refinement:

Reflections collected	7208
Independent reflections	3075 [R(int) = 0.1060]
Completeness to theta = 24.99°	99.2 %

163

Observed reflections	1844[I>2sigma(I)]
Reflections used for refinement	3075
Absorption correction	Empirical from equivalent reflections
Max. and min. transmission	0.9902 and 0.7558
Flack parameter (absolute struct.)	0.46(8)
Largest diff. peak and hole	0.340 and -0.449 e.Å^{-3}
Solution	direct methods
Refinement	Full-matrix least-squares on F^2
Treatment of hydrogen atoms	Calculated, fixed isotr. U's
Programs used	SHELXS-97 (Sheldrick, 1990)
	SHELXL-97 (Sheldrick, 1997)
	SHELXTL, STOE IPDS software
Data / restraints / parameters	3075 / 3 / 260
Goodness-of-fit on F^2	0.868
R index (all data)	wR2 = 0.1272
R index conventional [I>2sigma(I)]	R1 = 0.0513

9.5. Crystal data and structure refinement for Di([5]trovacenyl)-phenyl-phosphane (41¨)

Crystal data

Habitus, colour	Prism, violet	
Crystal size	0.40 x 0.25 x 0.10 mm^3	
Crystal system	Monoclinic	
Space group	P2$_1$/n	Z = 4
Unit cell dimensions	a = 10.2860(7) Å	α = 90°.
	b = 9.6088(8) Å	β = 94.738(6)°.
	c = 24.1422(17) Å	γ = 90°.
Volume	2378.0(3) Å^3	
Cell determination	19564 reflections	
Empirical formula	C30 H27 P V2	
Formula weight	520.37	
Density (calculated)	1.453 Mg/m^3	
Absorption coefficient	0.870 mm^{-1}	
F(000)	1072	

Data collection:

Diffractometer type	Stoe IPDS-II
Wavelength	0.71073 Å
Temperature	193(2) K
Theta range for data collection	1.69 to 24.94°.
Data collection software	Stoe Win-Expose
Cell refinement software	Stoe Win-Cell
Data reduction software	Stoe Win-Integrate

Solution and refinement:

Reflections collected	18047
Independent reflections	4137 [R(int) = 0.0422]
Completeness to theta = 24.94°	99.4 %
Observed reflections	3398[I>2sigma(I)]
Reflections used for refinement	4137
Absorption correction	Empirical from equivalent reflections
Max. and min. transmission	0.9180 and 0.7223
Largest diff. peak and hole	0.188 and -0.213 e.Å^{-3}
Solution	direct methods
Refinement	Full-matrix least-squares on F^2
Treatment of hydrogen atoms	located, isotropic ref.
Programs used	SHELXS-97 (Sheldrick, 1990)
	SHELXL-97 (Sheldrick, 1997)
	SHELXTL, STOE IPDS-II software
Data / restraints / parameters	4137 / 0 / 406
Goodness-of-fit on F^2	0.999
R index (all data)	wR2 = 0.0608
R index conventional [I>2sigma(I)]	R1 = 0.0247

9.6. Crystal data and structure refinement for Di([5]trovacenyl)-butyl-arsane (44¨)

Crystal data

Habitus, colour	Prism, dark red	
Crystal size	0.52 x 0.25 x 0.25 mm^3	
Crystal system	Triclinic	
Space group	P$\bar{1}$	Z = 2
Unit cell dimensions	a = 10.3920(7) Å	α = 106.565(7)°.
	b = 10.5841(7) Å	β = 92.161(8)°.
	c = 12.3628(8) Å	ɣ = 113.806(7)°.
Volume	1174.22(13) Å^3	
Cell determination	8000 reflections	
Empirical formula	C28 H31 As V2	
Formula weight	544.33	
Density (calculated)	1.540 Mg/m^3	
Absorption coefficient	2.208 mm^{-1}	
F(000)	556	

Data collection:

Diffractometer type	Stoe IPDS
Wavelength	0.71073 Å
Temperature	193(2) K
Theta range for data collection	2.18 to 25.96°.
Index ranges	-12<=h<=12, -13<=k<=13, -15<=l<=15
Phi-range, increment	0-250, 1°

Expose time	1 min.
Data collection software	Stoe Expose
Cell refinement software	Stoe Cell
Data reduction software	Stoe Integrate
Solution and refinement:	
Reflections collected	11627
Independent reflections	4267 [R(int) = 0.0287]
Completeness to theta = 25.96°	92.8 %
Observed reflections	3626[I>2sigma(I)]
Reflections used for refinement	4267
Absorption correction	Empirical from equivalent reflections (XPREP)
Max. and min. transmission	0.6083 and 0.3931
Largest diff. peak and hole	0.397 and -0.417 e.Å^{-3}
Solution	direct methods
Refinement	Full-matrix least-squares on F^2
Treatment of hydrogen atoms	located positions, isotropic ref.
Programs used	SHELXS-97 (Sheldrick, 1990)
	SHELXL-97 (Sheldrick, 1997)
	SHELXTL, STOE IPDS software
Data / restraints / parameters	4267 / 0 / 404
Goodness-of-fit on F^2	0.994
R index (all data)	wR2 = 0.0692
R index conventional [I>2sigma(I)]	R1 = 0.0269

9.7. Crystal data and structure refinement for Dimethyldi([5]trovacenyl)tin (63¨)

Crystal data

Habitus, colour	Plate, red	
Crystal size	0.45 x 0.18 x 0.10 mm^3	
Crystal system	Monoclinic	
Space group	P2$_1$/c	Z = 4
Unit cell dimensions	a = 13.5170(10) Å	α = 90°.
	b = 12.7765(6) Å	β = 93.837(8)°.
	c = 13.0653(9) Å	ɣ = 90°.
Volume	2251.3(3) Å^3	
Cell determination	8000 reflections	
Empirical formula	C26 H28 Sn V2	
Formula weight	561.05	
Density (calculated)	1.655 Mg/m^3	
Absorption coefficient	1.924 mm^{-1}	
F(000)	1120	

Data collection:

Diffractometer type	Stoe IPDS

Wavelength	0.71073 Å
Temperature	193(2) K
Theta range for data collection	2.20 to 25.93°.
Index ranges	-16<=h<=16, -15<=k<=15, -16<=l<=16
Data collection software	Stoe Expose
Cell refinement software	Stoe Cell
Data reduction software	Stoe Integrate

Solution and refinement:

Reflections collected	17281
Independent reflections	4355 [R(int) = 0.0244]
Completeness to theta = 25.93°	99.0 %
Observed reflections	3906[I>2sigma(I)]
Reflections used for refinement	4355
Absorption correction	Empirical
Max. and min. transmission	0.8309 and 0.4781
Largest diff. peak and hole	0.470 and -0.307 e.Å^{-3}
Solution	direct methods
Refinement	Full-matrix least-squares on F^2
Treatment of hydrogen atoms	located, isotr. Ref.
Programs used	SHELXS-97 (Sheldrick, 1990)
	SHELXL-97 (Sheldrick, 1997)
	SHELXTL, STOE IPDS software
Data / restraints / parameters	4355 / 0 / 374
Goodness-of-fit on F^2	1.054
R index (all data)	wR2 = 0.0564
R index conventional [I>2sigma(I)]	R1 = 0.0212

9.8. Crystal data and structure refinement for Diphenyldi([5]trovacenyl)tin (64¨)

Crystal data

Habitus, colour	Plate, light violet	
Crystal size	0.48 x 0.21 x 0.05 mm^3	
Crystal system	Triclinic	
Space group	P $\bar{1}$	Z = 2
Unit cell dimensions	a = 9.3888(11) Å	α = 80.247(10)°.
	b = 11.7664(15) Å	β = 82.341(10)°.
	c = 13.4341(16) Å	ɣ = 78.299(10)°.
Volume	1424.7(3) Å^3	
Empirical formula	C36 H32 Sn V2	
Formula weight	685.19	
Density (calculated)	1.597 Mg/m^3	
Absorption coefficient	1.536 mm^{-1}	
F(000)	688	

Data collection:

Diffractometer type	Stoe IPDS-II
Wavelength	0.71073 Å
Temperature	193(2) K
Theta range for data collection	1.55 to 24.95°.
Index ranges	-11<=h<=11, -13<=k<=13, -15<=l<=15
Data collection software	Stoe Win-Expose
Cell refinement software	Stoe Win-Cell
Data reduction software	Stoe Win-Integrate

Solution and refinement:

Reflections collected	12471
Independent reflections	4942 [R(int) = 0.0401]
Completeness to theta = 24.95°	99.4 %
Observed reflections	4324[I>2sigma(I)]
Reflections used for refinement	4942
Absorption correction	Gaussian
Max. and min. transmission	0.9271 and 0.5259
Largest diff. peak and hole	0.757 and -0.375 e.Å^{-3}
Solution	direct methos
Refinement	Full-matrix least-squares on F^2
Treatment of hydrogen atoms	located, isotropic refinement
Programs used	SHELXS-97 (Sheldrick, 1990)
	SHELXL-97 (Sheldrick, 1997)
	SHELXTL, STOE IPDS-II software
Data / restraints / parameters	4942 / 0 / 480
Goodness-of-fit on F^2	0.972
R index (all data)	wR2 = 0.0527
R index conventional [I>2sigma(I)]	R1 = 0.0213

9.9. Crystal data and structure refinement for Diphenyldi([5]trovacenyl)lead (65¨)

Crystal data

Habitus, colour	Prism, dark red	
Crystal size	0.16 x 0.12 x 0.05 mm^3	
Crystal system	Triclinic	
Space group	P$\bar{1}$	Z = 2
Unit cell dimensions	a = 9.4178(10) Å	α = 80.595(8)°.
	b = 11.8333(13) Å	β = 82.836(9)°.
	c = 13.3770(14) Å	ɣ = 78.513(9)°.
Volume	1434.7(3) Å^3	
Empirical formula	C36 H32 Pb V2	
Formula weight	773.69	
Density (calculated)	1.791 Mg/m^3	

168

Absorption coefficient	6.515 mm^{-1}
F(000)	752

Data collection:

Diffractometer type	Stoe IPDS-II
Wavelength	0.71073 Å
Temperature	193(2) K
Theta range for data collection	1.55 to 26.69°.
Index ranges	-11<=h<=11, -14<=k<=14, -16<=l<=16
Data collection software	Stoe Win-Expose
Cell refinement software	Stoe Win-Cell
Data reduction software	Stoe Win-Integrate
Reflections collected	19053
Independent reflections	6025 [R(int) = 0.0505]
Completeness to theta = 26.69°	99.5 %
Observed reflections	5477[I>2sigma(I)]
Reflections used for refinement	6025
Absorption correction	Gaussian
Max. and min. transmission	0.7365 and 0.4221
Largest diff. peak and hole	0.935 and -0.851 e.Å^{-3}
Solution	direct methods
Refinement	Full-matrix least-squares on F^2
Treatment of hydrogen atoms	located, isotropic refinement
Programs used	SHELXS-97 (Sheldrick, 1990)
	SHELXL-97 (Sheldrick, 1997)
	SHELXTL, STOE IPDS software
Data / restraints / parameters	6025 / 0 / 480
Goodness-of-fit on F^2	1.019
R index (all data)	wR2 = 0.0449
R index conventional [I>2sigma(I)]	R1 = 0.0202

9.10. Crystal data and structure refinement for (TVC)$_3$SnCl$_2$$^-$Li(THF)$_3$$^+$ (66$^{\cdots}$)

Crystal data

Habitus, colour	Plate, red violet	
Crystal size	0.60 x 0.30 x 0.12 mm^3	
Crystal system	Triclinic	
Space group	P$\bar{1}$	Z = 2
Unit cell dimensions	a = 11.6792(13) Å	α = 72.608(12)°.
	b = 13.139(2) Å	β = 70.347(9)°.
	c = 17.1370(19) Å	ɣ = 85.839(12)°.
Volume	2362.2(6) Å^3	
Empirical formula	C51.50 H61 Cl2 Li O3 Sn V3	
Formula weight	1077.35	

Density (calculated)	1.515 Mg/m^3
Absorption coefficient	1.253 mm^{-1}
F(000)	1100

Data collection:

Diffractometer type	Stoe IPDS-II
Wavelength	0.71073 Å
Temperature	193(2) K
Theta range for data collection	1.32 to 24.93°.
Index ranges	-13<=h<=13, -15<=k<=15, -20<=l<=20
Data collection software	Stoe Win-Expose
Cell refinement software	Stoe Win-Cell
Data reduction software	Stoe Win-Integrate

Solution and refinement:

Reflections collected	21625
Independent reflections	8185 [R(int) = 0.0417]
Completeness to theta = 24.93°	99.1 %
Observed reflections	7056[I>2sigma(I)]
Reflections used for refinement	8185
Absorption correction	Empirical from equivalent reflections
Max. and min. transmission	0.8642 and 0.5203
Largest diff. peak and hole	0.710 and -0.729 e.Å^{-3}
Solution	direct methods
Refinement	Full-matrix least-squares on F^2
Treatment of hydrogen atoms	Calculated positions, fixed isotropic U's
Programs used	SIR-92
	SHELXL-97 (Sheldrick, 1997)
	SHELXTL, STOE IPDS software
Data / restraints / parameters	8185 / 0 / 559
Goodness-of-fit on F^2	1.037
R index (all data)	wR2 = 0.0804
R index conventional [I>2sigma(I)]	R1 = 0.0295

9.11. Crystal data and structure refinement for Diphenyl([5]trovacenyl)silanol (67˙)

Crystal data

Habitus, colour	Plate, red	
Crystal size	0.50 x 0.10 x 0.06 mm^3	
Crystal system	Monoclinic	
Space group	Cc	Z = 8
Unit cell dimensions	a = 18.4655(14) Å	α = 90°.
	b = 10.0544(5) Å	β = 108.376(8)°.
	c = 23.7892(16) Å	γ = 90°.

Volume	4191.5(5) Å^3
Cell determination	8000 reflections
Empirical formula	C20 H23 O2 Si V
Formula weight	374.41
Density (calculated)	1.187 Mg/m^3
Absorption coefficient	0.538 mm^{-1}
F(000)	1568

Data collection:

Diffractometer type	Stoe IPDS
Wavelength	0.71073 Å
Temperature	193(2) K
Theta range for data collection	2.34 to 25.86°.
Index ranges	-22<=h<=22, -12<=k<=12, -29<=l<=27
Phi-range, increment	0-200, 1°
Expose time	8 min
Data collection software	Stoe Expose
Cell refinement software	Stoe Cell
Data reduction software	Stoe Integrate

Solution and refinement:

Reflections collected	15908
Independent reflections	7896 [R(int) = 0.0425]
Completeness to theta = 25.86°	99.5 %
Observed reflections	6607[I>2sigma(I)]
Reflections used for refinement	7896
Absorption correction	Empirical from equivalent reflections
Max. and min. transmission	0.9684 and 0.7747
Flack parameter (absolute struct.)	0.448(17) (inversion twin)
Largest diff. peak and hole	0.336 and -0.232 e.Å^{-3}
Solution	direct methods
Refinement	Full-matrix least-squares on F^2
Treatment of hydrogen atoms	located, isotropic refinement
Programs used	SHELXS-97 (Sheldrick, 1990)
	SHELXL-97 (Sheldrick, 1997)
	SHELXTL, STOE IPDS software
Data / restraints / parameters	7896 / 2 / 696
Goodness-of-fit on F^2	0.953
R index (all data)	wR2 = 0.0845
R index conventional [I>2sigma(I)] R1 = 0.0382	

9.12. Crystal data and structure refinement for [5]trovacenyl-1-(anti, syn)-7-hydroxybicyclo[2.2.1]hept-2-ene-7yl (72˙)

Crystal data

Habitus, colour	Narrow plate, violet	
Crystal size	0.42 x 0.15 x 0.06 mm^3	
Crystal system	Orthorhombic	
Space group	Pbca	Z = 8
Unit cell dimensions	a = 13.8026(16) Å	$\alpha = 90°$.
	b = 11.6433(9) Å	$\beta = 90°$.
	c = 18.5710(14) Å	$\gamma = 90°$.
Volume	2984.5(5) Å^3	
Cell determination	5000 reflections	
Empirical formula	C19 H20 O V	
Formula weight	315.29	
Density (calculated)	1.403 Mg/m^3	
Absorption coefficient	0.660 mm^{-1}	
F(000)	1320	

Data collection:

Diffractometer type	Stoe IPDS
Wavelength	0.71073 Å
Temperature	193(2) K
Theta range for data collection	2.54 to 25.90°.
Index ranges	-16<=h<=16, -14<=k<=12, -18<=l<=22
Phi-range, increment	0-150, 1.5°
Expose time	8 min.
Data collection software	Stoe Expose
Cell refinement software	Stoe Cell
Data reduction software	Stoe Integrate

Solution and refinement:

Reflections collected	16587
Independent reflections	2887 [R(int) = 0.0831]
Completeness to theta = 25.90°	99.4 %
Observed reflections	1555[I>2sigma(I)]
Reflections used for refinement	2887
Absorption correction	Empirical
Max. and min. transmission	0.9615 and 0.7689
Largest diff. peak and hole	0.320 and -0.237 e.Å^{-3}
Solution	direct methods
Refinement	Full-matrix least-squares on F^2
Treatment of hydrogen atoms	Located, isotropic refinement
Programs used	SHELXS-97 (Sheldrick, 1990)
	SHELXL-97 (Sheldrick, 1997)
	SHELXTL, STOE IPDS software
Data / restraints / parameters	2887 / 15 / 270

172

Goodness-of-fit on F^2 0.845

R index (all data)   wR2 = 0.0929

R index conventional [I>2sigma(I)]   R1 = 0.0391